2016-01-01

Application Of Uranium And Strontium Isotopes As Salinity And Paleo-Environmental Conditions Tracers:Insight From The Rio Grande River And Pedogenic Carbonates In Drylands Soils Of Southwest, USA.

Syprose Nyachoti
University of Texas at El Paso, nyachotimenge@gmail.com

APPLICATION OF URANIUM AND STRONTIUM ISOTOPES AS SALINITY AND PALEO-ENVIRONMENTAL CONDITIONS TRACERS: INSIGHT FROM THE RIO GRANDE RIVER AND PEDOGENIC CARBONATES IN DRYLAND SOILS OF SOUTHWEST, USA.

SYPROSE K. NYACHOTI

Doctoral Program in Geological Sciences

APPROVED:

Lin Ma, Ph.D., Chair

Thomas Gill, Ph.D.

Lixin Jin, Ph.D.

Richard Langford, Ph.D.

Craig C. Tweedie, Ph.D.

Charles H. Ambler, Ph.D.
Dean of the Graduate School

Dedication

To my
Parents: Mr. Justus Nyachoti Menge and Mrs. Sabina Moraa Nyachoti

APPLICATION OF URANIUM AND STRONTIUM ISOTOPES AS SALINITY AND PALEO-ENVIRONMENTAL CONDITIONS TRACERS: INSIGHT FROM THE RIO GRANDE RIVER AND PEDOGENIC CARBONATES IN DRYLAND SOILS OF SOUTHWEST, USA.

by

SYPROSE K. NYACHOTI, M.Sc.

DISSERTATION

Presented to the Faculty of the Graduate School of

The University of Texas at El Paso

in Partial Fulfillment

of the Requirements

for the Degree of

DOCTOR OF PHILOSOPHY

Department of Geological Sciences

THE UNIVERSITY OF TEXAS AT EL PASO

May 2016

Acknowledgements

I would like to express my appreciation and gratitude to my advisor, Dr. Lin Ma, for guidance, mentorship, financial support, and motivation to pursue a PhD program in the Geological Sciences Department at UTEP. I would also like to thank my committee members, Drs. Thomas Gill, Lixin Jin, Richard Langford, and Craig C. Tweedie for the friendly guidance and great support over these years. In a similar manner, I'd like to recognize Drs. Laura Serpa, Philip Goodell, and David Borrok for the contributions that each of them made towards my admission and induction into this program at the University of Texas at El Paso.

I will be forever grateful to Christine Cox for providing soil samples from agricultural sites near El Paso, Texas, Hernandez Hugo, Matthew Hiebing, Joe Collins, and Pereyra Yvette for field assistance. I am thankful to Sandra Garcia, Hernandez Hugo and Adam Ianno for laboratory assistance. I especially thank Carlos Montana for solving all computer related issues, Pam Hart and Kristen Gonzalez for paperwork related to assistantship and travel reimbursements. I would like to thank the staff of UTEP Geological Sciences Department, Graduate School, and Office of International Programs for their kind cooperation throughout my program. I wish to remember all the friends who have made this journey enjoyable with your company and caring support.

Lastly, I would like to thank my parents, siblings, and uncles who encouraged me to pursue a doctorate degree in the U.S.A, and provided continuous emotional support throughout this program. I share this degree and achievements with my lovely family.

Syprose Nyachoti

May 2016

Abstract

South New Mexico and west Texas regions of the northern Chihuahua Desert are characteristic of low annual rainfall and high potential evapotranspiration rates. Soils in these arid and semi-arid regions are abundant of pedogenic carbonates of various stages of development. Both surface and ground water resource in the area have high salt content; the Rio Grande river, which flows through the region is known for its high salinity downstream. Due to increasing population in cities of the region thus high food demand, irrigation activities along the river valley have enhanced crop productivity. High evapotranspiration rates and intense saline flood irrigation have caused excessive salt accumulation (e.g. pedogenic carbonates) in irrigated soils. Long term accumulation of pedogenic carbonates impair plant root and soil water infiltration, lower crop yield, and sequester carbon thus influencing carbon cycle and ultimately climate over time. It is important to monitor the chemistry of water in drylands and its impact on soil quality. This dissertation focuses on three main areas: (1) establishing factors that control formation rates of pedogenic carbonates in soils of the southwest USA, (2) reconstructing paleo-moisture information archived in pedogenic carbonates within the Jornada Basin, New Mexico and its environs, and (3) tracing salinity into the Lower Rio Grande river between Elephant Butte Reservoir, NM and El Paso, TX. Using major and minor element geochemistry (including carbon), U-series, strontium , and carbon isotopes, this study shows that: (1) Land management practices such as irrigation load high Ca^{2+} and HCO_3^- ions resulting in high pedogenic carbonate accumulation rate in irrigated soils (9±6 $gCaCO_3/m^2/yr$) along the Rio Grande valley compared to low rates in naturally forming carbonates at the Jornada Basin (2.5±1.0 to 3.5±1.5 $gCaCO_3/m^2/yr$), (2) Paleo-moisture conditions have varied between ~200 ka and 6 ka based on the pedogenic carbonate U-series chronology. Older carbonates at soil depth formed under moist

conditions while younger shallower carbonates precipitated in drier conditions, (3) significant salts are loaded into various sections of the lower Rio Grande River depending on the irrigation or non-irrigation season. Water released from Elephant Butte Reservoir dominated the river chemistry in the irrigation season. In the non-irrigation season, deep ground water salinity was distinct in the river a few kilometers after the reservoir while mixed anthropogenic salinity sources (e.g. shallow irrigation groundwater, agricultural drains, wastewater, and city effluents) were significant in the downstream locations near the Rio Grande at El Paso, TX. This work has demonstrated the effects of anthropogenic factors on water quality and carbon budgets in dryland areas.

Table of Contents

List of Tables

List of Figures

Chapter 1

1. Introduction

The southwest USA is dominated by arid and semi-arid climates characterized by deserts such as Chihuahua, Sonora, and Mojave. Future climate in this region is predicted to be drier partly due to increasing anthropogenic influence and changes in climatic factors (Fawcette et al., 2011; Borrok and Engle, 2014). Desertification has degraded water quality, influenced soil properties, and vegetation density in drylands (D'Odorico et al., 2013; Borrok and Engle, 2014). Low annual rainfall and high evapotranspiration rates in arid and semi-arid lands have increased water salinity and precipitation of salts in shallow soils. In addition, the growing population and associated land use activities (e.g. irrigation) have enhanced surface water and soil quality degradation. Irrigation is a common land management practice carried out in aridlands to boost crop productivity.

Saline irrigation water loads high concentrations of soluble ions (e.g. Ca^{2+} and HCO_3^-) and facilitates precipitation of secondary minerals such as pedogenic carbonates, gypsum and halite in soils (Cox, 2012). Over time these secondary carbonates accumulate in soils and impair water and plant root penetration, degrading soil quality and lowering crop yields. Therefore, it is important to monitor the chemistry of water in drylands and its impact on soil quality. Furthermore, water also serves other domestic, recreational, and municipal needs in drylands. Pedogenic carbonates also accumulate naturally in progressive morphological stages given low moisture content, Ca^{2+} and carbon influxes into soils (Gile et al., 1981; Capo and Chadwick, 1999). These carbonates record accumulative paleoenvironmental conditions during their formation thus providing history of past climatic oscillations and aiding in understanding the behavior of the earth systems relative to future climatic changes. Increasing drought,

desertification, and population growth in drylands under projected climate changes enhance the need to understand current hydrologic budgets and future plans to meet the water and food needs of the increasing arid-population as well as support ecosystems and other land-surface dynamics.

To address water quality, pedogenic carbonates and associated paleoclimate information, this dissertation focuses on three main areas: (1) assessing surface water salinity and quantifying salt loads into the Lower Rio Grande river, (2) establishing factors that control formation rates of pedogenic carbonates in soils of the southwest USA, and (3) reconstructing paleomoisture information archived in pedogenic carbonates within the Jornada Basin, New Mexico and its environs. The Rio Grande is the fifth longest river in the USA; it is fed by snowmelts in south Colorado and flows southward through New Mexico and Texas before emptying into the Gulf of Mexico. In addition to domestic and municipal purposes, the bulk of the river water is used to support agricultural activities through flood irrigation. Excess water from the farm that has been exposed to evaporation is drained back to the river thereby increasing salinity in downstream locations. Groundwater is occasionally used to supplement for irrigation purposes when the river discharge is low as a result of artificial flow control in the dams/reservoirs along the river course. Water is stored in the reservoirs mainly for irrigation purposes (usually May through August). In the non-irrigation seasons, the river is dry in part, but city and agricultural drains, ground water, and wastewater treatment plant effluents recharge some sections forming major part of base flow (Moore et al., 2008). This study monitors the spatial and temporal variations of salinity in the Lower Rio Grande river during the irrigation and non-irrigation seasons.

Soils along the Lower Rio Grande flood plains are seasonally irrigated to produce crops such as alfalfa, onions, pecans, and cotton. The saline irrigation water infiltrates and precipitates secondary minerals (e.g. pedogenic carbonates) at soil depths; these deposits impact soil

properties, soil sodicity, and soil salinity. In addition, deposition of carbonates in soils influences the carbon cycle and carbon budgets. For instance, precipitation of carbonates releases carbon dioxide to the atmosphere while sequestering carbon increases the inorganic soil carbon pool. To establish the implication of land management practice such as irrigation on global carbon cycles, we compare formation rates of carbonates in irrigated soils at El Paso, TX with those occurring naturally in soils at the Jornada Basin, NM.

Pedogenic carbonates form in soils by overprinting and/recrystallization resulting into thick caliche layers in the BK and K horizons (Gile et al., 1981). At the Jornada Basin mature stage III, IV, and V carbonates have been identified (Gile et al., 1981). Using stable C and O isotopes in the carbonates as well as their depth of occurrence in the soil profile, paleoenvironmental conditions in the basin and southwest USA have been reconstructed (Buck and Monger, 1999). The stable isotope and carbonate depth paleoclimate approaches have limitations; for instance, oxygen isotope signature may vary based on moisture source, temperature variations or evapotranspiration rates. The carbonate depths may vary as well depending on soil surface processes such as erosion. Recent studies have indicated that heavy radiogenic isotopes (e.g. ^{234}U and ^{238}U) incorporated in carbonates are good paleorainfall proxies (Maher et al., 2014). This is because pedogenic carbonates inherit ($^{234}U/^{238}U$) activity ratios in soil waters from which they precipitate (Oster et al., 2012). In this study, we use ($^{234}U/^{238}U$) activity ratios to detect variations in paleo-soil moisture quantities as recorded in stage V carbonates within the Jornada Basin.

Using major and minor element geochemistry (including carbon), U-series and strontium isotopes this study shows that: (1) significant salt are loaded into various sections of the Rio Grande River depending on the irrigation or non-irrigation season. Point deep ground water

salinity was dominant to the river after Elephant Butte Reservoir while non-point salinity sources from shallow groundwater used in irrigation, and city effluents were observed downstream, (2) Land management practices such as irrigation load high Ca^{2+} and HCO_3^- result in a three-fold carbonate precipitation rate increase in irrigated soils along the Rio Grande valley compared to naturally forming carbonates at the Jornada Basin, and (3) Older carbonates at soil depth in the Jornada Basin were formed in wetter conditions while shallow, younger carbonates formed in a drier environment. This work has quantified the soil inorganic carbon contents and their accumulation rates as well as assessing the effects of anthropogenic and climatic factors on carbon budgets in dryland areas of southwest USA.

References

Borrok, D. M. and Engle, M. A. (2014). The role of climate in increasing salt loads in dryland rivers. *Journal of Arid Environments 111,* 7-13.

Buck, B. J. and Monger, H. C. (1999). Stable isotopes and soil- geomorphology as indicators of Holocene climate change, northern Chihuahuan Desert. *Journal of Arid Environments* 43, 357–373.

Capo, R. C. and Chadwick, O. A. (1999). Sources of strontium and calcium in desert soil and calcrete. *Earth and Planetary Science Letters, 170*(1), 61-72.

Cox, C.L. (2012). Evaluation of Soil Sustainability Along the Rio Grande in West Texas: Changes in Salt Loading and Organic Nutrients Due to Farming Practices (M.S. Thesis). University of Texas at El Paso.

D'Odorico, P., Bhattachan, A., Davis, K. F., Ravi, S., & Runyan, C. W. (2013). Global desertification: drivers and feedbacks. *Advances in Water Resources*, *51*, 326-344.

Fawcett, P., Werne, J. P., Anderson, R., Heikoop, J., Brown, E., Berke, M., Smith, S., Goff, F., Hurley, L., Cisneros-Dozal, M., Schouten, S., Sinninghe Damste, J. S., Huang, Y., Toney, J., Fessenden, J., WoldeGabriel, G., Atudorei, V., Geissman, J., Allen, C. (2011). Extended megadroughts in the southwestern United States during Pleistocene interglacials. *Nature* 470, 518– 521.

Gile, L.H., Hawley, J.W., Grossman, R.B. (1981). Soils and geomorphology in the Basin and Range area of Southern New Mexico: Guidebook to the Desert Project. New Mexico Bureau of Mines and Mineral Resources., Socorro, NM, 222 .

Maher, K, Ibarra, D.E., Oster, J.L., Miller, D.M., Redwine, J.L., Reheis, M.C., Harden, J.W. (2014). Uranium isotopes in soils as a proxy for past infi ltration and precipitation across the western United States: *American Journal of Science* 314, 821–857, doi: 10 .2475 /04 .2014 .01

Moore, S.J., Bassett, R.L., Liu, B., Wolf, C.P., Doremus, D. (2008). Geochemical tracers to evaluate hydrogeologic controls on river salinization. *Ground Water*, 46(3), 489-501

Oster, J.L., Ibarra, D., Harris, C.R., Maher, K. (2012). Influence of eolian deposition and rainfall amounts on the U-isotopic composition of soil water and soil minerals: *Geochimica et Cosmochimica Acta*, 88, 146–166, doi: 10 .1016 /j .gca .2012 .04 .004.

Chapter 2

Insights into factors controlling formation rates of pedogenic carbonates: a combined geochemical and isotopic approach in dryland soils of the southwest USA

Syprose Nyachoti[1], Lixin Jin[1], Craig E. Tweedie[2], and Lin Ma[1],

[1]Department of Geological Sciences, University of Texas at El Paso, El Paso, TX 79968

[2]Department of Biology, University of Texas at El Paso, El Paso, TX 79968

2.1 Abstract

Recent studies have focused on natural accumulation of pedogenic carbonates in drylands; however, information on such carbonates remains scarce in arid, irrigated agricultural soils. This study aims to determine annual accumulation rates of pedogenic carbonates in intensively irrigated soils, and to define key linkages between flood irrigation, salt loading and soil-atmospheric CO_2 exchange in cultivated drylands of the southwestern United States. We use a combination of elemental chemistry (CaO contents, soil organic and inorganic carbon), mineralogy, and U-series (^{238}U-^{234}U-^{230}Th) disequilibrium dating technique specifically to: (1) investigate calcium and carbon fluxes of the carbonates, and (2) determine ages of pedogenic carbonates and their formation rates in soils. Sampling sites include an irrigated field (alfalfa; El Paso, western Texas) and a natural shrubland site (JPT1 and JPT2; Jornada Basin, southern New Mexico). Our results showed that high calcium and carbon in combination with other soluble elements are loaded into the irrigated soil through saline irrigation waters while dust and rainfall are important salt loads into Jornada soils. U-series activity ratios ($^{234}U/^{238}U$) and ($^{230}Th/^{238}U$) suggest external addition of U (and by inference other soluble ions) onto heavily ^{234}U-leached soils and consequent deposition in carbonate at depth at the studied soils. U-series carbonate ages in soils at alfalfa site were younger averaging at 7.3 ±5.0 ka compared to the Jornada site (28 ±11

to 34 ±14 ka). Depending on the Ca and carbon ion influxes and carbonate ages, alfalfa site indicated higher carbonate accumulation rates (9±6 $gCaCO_3/m^2/yr$) than the Jornada site (2.5±1.0 to 3.5±1.5 $gCaCO_3/m^2/yr$). This study demonstrates the effect of land use (e.g. irrigation) on rates of pedogenic carbonate accumulation and by inference formation of other secondary mineral deposits in dryland soils.

2.2 Introduction

Pedogenic carbonates are commonly formed as secondary phases in arid and semi-arid soils (e.g., Gile et al., 1981; Eswaran et al., 2000). This pool of soil inorganic carbon is estimated to contain 700 to 940 Pg C (1Pg = 10^{15}g), similar in size to carbon dioxide in the atmosphere and about two-thirds of the organic carbon in the soils (e.g., Schlesinger et al., 1982; Eswaran et al., 2000; Monger and Martinez-Rios, 2000; Serna-Perez, et al., 2006). Pedogenic carbonates precipitate because dissolved bicarbonate (HCO_3^-) and calcium (Ca^{2+}) reacts to form calcite ($CaCO_3$), carbon dioxide (CO_2) and water (H_2O):

$$2HCO_3^- + Ca^{2+} \rightarrow CaCO_3(s) + CO_2\,(g) + H_2O \qquad \text{Rxn (1)}$$

The precipitation of such secondary calcite minerals is entirely driven by the availability of Ca^{2+} and HCO_3^- in soil water; other factors which affect availability of these dissolved ion and soil moisture include local topography, rainfall amount, soil texture, and soil mineralogy (e.g., Lahann, 1978; Chadwick et al., 1989; Royer, 1999; Chiquet et al., 1999; Egli and Fitze, 2001; Hirmas et al., 2010; Laudicina et al., 2013). Understanding formation kinetics of pedogenic carbonates has great implications for studying the global C cycle, dating soils and geomorphic surfaces, and reconstructing paleo-environmental conditions (e.g., Cerling, 1984; Lal and Kimble, 2000b; Luo and Ku, 1991; Serna-Perez et al., 2006).

Pedogenic carbonates occur in various forms ranging from filaments to continuous hardpan calcrete depending on their stage of development. Six morphological stages (I-VI) that correlate with soil age have been identified (e.g., Gile et al., 1961;Machette, 1985; Birkeland et al., 1991; Monger et al., 1991; Violette et al., 2010). Dryland soils in the southwest USA including the Jornada Basin contain abundant carbonates which have provided key information for paleoclimate, paleovegetation, eolian processes, and geomorphic surface ages in southwestern New Mexico and western Texas (e.g., Gile and Grossman, 1979; Gile et al., 1981; Machette, 1985; Capo and Chadwick, 1999; Chiquet et al., 1999; Monger and Gallegos, 2000; Naiman et al., 2000; Deutz et al., 2002).

Climate and human-induced changes have heavily impacted dryland landscapes, thus deteriorating surface hydrological conditions, soil quality, and losses in ecosystem functions and services (e.g., Pimentel et al., 1995; Kummerer et al., 2010; D'Odorico et al., 2012). For example, soil salinization is a common problem of land degradation, especially in irrigated agricultural fields (e.g., Schoups et al., 2005). On a global scale, 4% of dryland surfaces (~ 2 million km^2) are currently managed as irrigated agriculture, and almost 20% of irrigated drylands (0.4 million km^2) are salt-affected, impacting crop growth and soil fertility (e.g., Ghassemi et al., 1995).

Dryland agriculture may have enhanced pedogenic carbonate development and soil C sequestration. High concentrations of calcium and bicarbonate ions in the irrigation water could lead to calcite saturation and precipitation in agricultural soils. This affects soil quality and agricultural productivity by reducing soil porosity thus impairing water infiltration and plant root penetration (e.g., Entry et al., 2004; Ontl and Schulte, 2012; Sanderman, 2012). However, few studies have focused on calcite deposition in these managed systems, even though irrigation

annually supply significant amounts of Ca^{2+} and HCO_3^- to these soils, and thus may dramatically alter carbon cycles (Suarez, 2000; Schlesinger, 2000; Sanderman, 2012).

Here, we compare carbonate formation rates in a soil profile at an irrigated agricultural alfalfa site in El Paso, Texas and two soil profiles (JPT1 and JPT2) at a natural site in the Jornada Basin, New Mexico. With low annual rainfall in drylands, irrigation is critical for realization of high crop yield. Irrigated farming in the Rio Grande valley with saline water from the Rio Grande River and local groundwater has prevailed for the past 100-200 years (e.g., Miyamoto, 2012; Ellis et al., 1993; Moore et al., 2008). Here, high evapotranspiration rates and intensive saline irrigation have collectively caused excessive salt accumulation including most soluble minerals halite and gypsum in soils (e.g., Cox, 2012). The non-cultivated site at the Jornada Basin on the other hand, contains voluminous naturally-occuring pedogenic carbonates, which allow us to compare their formation rates with agriculturally induced carbonates at alfalfa site. This study uses elemental chemistry, mineralogy, uranium-series isotopes, and published calcium carbonate loads into soils of southwest USA to: (1) establish calcium and carbon influxes in soil carbonates, (2) compute ages of pedogenic carbonates and their formation rates in these two natural and irrigated soils of southern New Mexico and west Texas.

2.3 Background information on U-series isotope dating of pedogenic carbonates

Pedogenic carbonates have successfully been dated using U-series isotope disequilibrium technique (e.g., Ku et al., 1979; Sharp et al., 2003; Ludwig and Paces, 2002). The U-series dating technique relies on the relationships between radioactive decay of the parent and ingrowth of the daughter isotopes in the U-series chain (e.g. ^{238}U, ^{234}U, and ^{230}Th). For example, ^{238}U ($t_{1/2}$ = ~4.5 Gyrs) decays to a relatively short-lived ^{234}U ($t_{1/2}$= ~246 kyrs) that subsequently decays to ^{230}Th

($t_{1/2}$ = 76 kyrs) (Cheng et al., 2000; Dickin, 1995). The upper limit of the U-series technique is around 500 ka (Ludwig, et al., 1992).

Assuming a rock system remains closed to U and Th for ~1Ma, activity of the parent nuclide will equal that of the daughter nuclide along U-series chain, a situation called secular equilibrium. Activity refers to the product of decay constant (λ) and number of a given radionuclide (N); therefore at secular equilibrium, $\lambda_{238}\ N_{238} = \lambda_{234}\ N_{234}$ and their activity ratios ($^{234}U/^{238}U$) (herein parenthesis of nuclide ratios indicate activity ratios) equal unity (Bourdon et al., 2003). In the event of chemical weathering, U-series isotopes are fractionated from each other by chemical and alpha recoil processes (e.g., Chabaux et al., 2008; Chabaux et al., 2003; Dosseto et al., 2008; Vigier et al., 2001). For example, due to high solubility of U in oxidizing environment and preferential leaching of ^{234}U into weathering fluids, the soil waters usually have high U concentrations and ($^{234}U/^{238}U$) ratios. On the other hand, low solubility of Th results in soil waters with very low Th concentrations and ($^{230}Th/^{238}U$) ratios (e.g., Langmuir and Herman, 1980). Precipitation of secondary minerals such as pedogenic carbonates from such soil waters effects in deposits with ($^{234}U/^{238}U$) greater than one but little or no ^{230}Th. Ideally any measurable ($^{230}Th/^{238}U$) in the carbonates is assumed to be radiogenic from the decay of ^{234}U over time (Andersen et al., 2008; Ivanovich and Harmon, 1992). However, pedogenic carbonates usually include U and Th from detrital silicate fractions, such inclusions must be corrected to avoid overestimation of the carbonate ages (e.g., Bischoff and Fitzpatrick, 1991; Edwards et al., 2003; Neymark, 2011).

The isochron technique is one of the methods employed in correction of detrital ^{230}Th in pedogenic carbonates (e.g., Edwards et al., 2003; Ku et al., 1979; Sharp et al., 2003). This correction method requires the use of cogenetic samples with similar initial concentrations of

$^{230}Th/^{232}Th$ ratios. Authigenic carbonates are almost impossible to separate from detrital component especially calcareous soils; therefore, cogenetic samples can be obtained from various bulk sample treatment techniques such as leachate/residue, leachate/leachate, and/or total sample dissolution methods (e.g., Bischoff and Fitzpatrick, 1991; Edwards et al., 2003; Neymark, 2011). Isochron detrital correction technique takes the following assumptions into consideration: 1) the pure carbonates precipitating from soil water have no detrital Th due to its low solubility, 2) there are only two isotopically homogeneous end members (detrital materials and authigenic carbonates) in a sample, and 3) the system remains closed to U and Th after formation of carbonates (Bischoff and Fitzpatrick, 1991; Luo and Ku, 1991). The ($^{230}Th/^{232}Th$), ($^{238}U/^{232}Th$), and ($^{234}U/^{238}U$) in cogenetic samples are used to construct 2D isochrons (Osmond et al., 1970; Rosholt, 1976) and to infer ($^{234}U/^{238}U$) and ($^{230}Th/^{238}U$) of the authigenic carbonate for age calculations (e.g., Ludwig, 2003).

2.4 Methodology

2.4.1 STUDY SITE DESCRIPTION

The study sites include an alfalfa field near El Paso, Texas (31.6729886°N, 106.2667956°W) and a natural shrubland at the Jornada Basin near Las Cruces, New Mexico (32.565500°N, 106.659800°W) (Fig. 1.1). Both sites are located within the Rio Grande valley, which comprises of basins surrounded by north-south trending mountains that formed during the tertiary Rio Grande tectonic event (e.g., Hawley and Kennedy, 2004), in the Chihuahua Desert region of the Basin and Range geomorphic province.

Agricultural soils in western Texas are developed on alluvium deposits of the Rio Grande valley and are classified as Entisols and Aridisols (e.g., Miyamoto and Chacon 2006). These floodplains belong to the Holocene Fillmore geomorphic surface (100 yrs to 7000 yrs B.P) in the

Hueco Basin (Gile et al., 1981). Field survey by soil pits and augered cores revealed that the top soils (<1 m depth) of the study area in general consist of a fine silty clay loam or clayey layer, which overlays a silty-loamy layer (~1 to 4 m depth) (e.g., Miyamoto, 2012).

Climate at El Paso, TX is semi-arid with low mean annual precipitation of ~25 cm and mean annual temperature of 18°C (Wainwright, 2006). The agricultural soils investigated in this study are cultivated for alfalfa and irrigated regularly during the growing seasons from April to October. During irrigation season, the field is flood-irrigated every two weeks with standing water for about one week. The main irrigation water is from Rio Grande River, an important upstream freshwater resource in the Southwest United States (e.g., Ellis et al., 1993). Rio Grande water becomes progressively more saline downstream from the headwater regions in the Colorado (e.g., Phillips et al., 2003; Hutchison, 2006; Hogan et al., 2007; Szynkiewicz et al., 2011) to southern New Mexico and western Texas. At El Paso, the salinity of the Rio Grande is about 800 to 2000 mg/l and varies with river discharges (e.g., Szynkiewicz et al., 2011; 2015). The river water is saturated with respect to calcite but under-saturated with respect to evaporite minerals such as gypsum and halite (e.g., Szynkiewicz et al., 2011).

The natural site of this study (Jornada Basin) is on Jornada Experimental Range (JER) operated by US Department of Agriculture as Long-Term Ecological Research sites (LTER), free of any agricultural activities (Serna-Perez et al., 2006). The JER is located in the basin floor and piedmont slopes, west of the San Andres mountains (e.g., Keller et al., 1990; Serna-Perez et al., 2006). The basin is filled with ~ 2000 m thick of marine and non-marine sediments (mostly piedmont alluvium, lacustrine materials) which are overlaid by ~150 m of late Tertiary and Quaternary ancestral Rio Grande and eolian deposits (Camp Rice Formation) (e.g., Gile et al., 1981; Mack et al., 1997; Monger, 2006). These young sediments include a mixture of clay, silt,

sand, and pebbles and contain <1% calcite (e.g., Gile et al., 1981). The sediments form the parent material of soils in the Jornada Basin (e.g., Gile et al., 1966; Seager et al., 1987; Mack and James, 1992; Monger and Gallegos, 2000). These soils are on the Jornada I geomorphic surface and contain well-developed mature petrocalcic horizons (caliche) with stage IV and V carbonates, which are either preserved in deep soil layers or exhumed by wind or water erosion (e.g., Gile et al., 1981; Machette, 1985). The estimated age of the Jornada I geomorphic surface range between 250 to 700 ka (e.g., Gile et al., 1981; Monger et al., 2009). The basin receives approximately 21-25 cm of precipitation each year, mostly during summer monsoon. The annual potential evapo-transpiration is approximately 220 cm and mean annual temperatures of about 16 °C (e.g., Gile et al., 1981). The vegetation at the Jornada basin has changed through time (e.g., Gibbens et al., 2005); it is currently dominated by C3 desert shrubs such as Mesquite (*Prosopis glandulosa*) and Creosotebush (*Larrea tridentata*) (e.g., Bergametti and Gillette, 2010; Gibbens et al., 2005; Serna-Perez et al., 2006).

2.4.2 SOIL SAMPLE COLLECTION

Soil samples were collected from a pit at the Alfalfa field as previously described by Cox (2012). Briefly, soil samples were collected at 10 cm interval on the wall of the pit until 60 cm depth, where a change of soil texture from silty- clayey to sandy soils was observed. Two pits (JPT1 and JPT2) of about 50 cm depths were dug at the Jornada Basin at approximately 5 m apart. JPT2 was located beneath a creosotebush shrub while JPT1was on a bare soil between shrubs. Soil samples were collected at 5 cm interval from land surface to the upper boundary of the caliche layer at each pit (~40 and 48 cm at JPT1 and JPT2 respectively). Caliche samples were also collected from the bottom of the two soil pits.

2.4.3 SOIL MAJOR ELEMENT CHEMISTRY AND MINERALOGY

For major element analysis, the soils were air dried, ground to pass through a 100-mesh sieve (<150µm), and digested using Li-metaborate fusion technique (Feldman, 1983). Specifically, 0.1 g ground soil powder and 1g lithium metaborate were weighed and mixed using a mixer mill (Spex sample prep 5100) before digestion in a muffle furnace at 900^0C for 15 min. The molten bead was then dissolved in 5% nitric acid, and the solution was diluted and analyzed for major elements using Perkin-Elmer Optima 5400 Inductively Coupled Plasma Optical Emission Spectrometer (ICP-OES) at the University of Texas at El Paso (UTEP). Twenty rock standards from NIST and USGS were similarly digested as the samples and used as calibration standards for major elements. A USGS reference rock material (W-2) was digested along with each batch of samples as a quality check. The difference in all major element concentrations on W-2 between measured and certified values were less than 10%.

Soil carbon (SC) contents, including soil organic carbon (SOC) and soil inorganic carbon (SIC) on the powdered soils were measured using a LECO SC632 carbon and sulfur determinator at UTEP. The SOC for a given soil sample was determined on SC632 after leaching off SIC with 10 ml of 10% v/v HCl. The SIC was then calculated as the difference between SC and SOC. Ore tailing, synthetic carbon, and calcium carbonate samples were used as check standards. Uncertainties on calcium carbonate standard were less than 10%.

The dominant minerals in soils were identified by a MiniFlex II X-ray diffractometer at UTEP. The powdered samples were scanned from 5^0 to 65^0 2θ at 30 kV voltage and 15 mA current with Cu-K_α radiation and scintillation counter detector. Diffraction patterns were collected at a sampling width of 0.020 and analyzed by peak matching with reference intensity ratios.

2.4.4 U-SERIES ISOTOPE MEASUREMENTS IN BULK SOILS AND PEDOGENIC CARBONATES

Leachate-residue and total sample digestion procedures were applied to bulk soils to obtain samples with various mixing ratios of detrital and pure carbonate end-members for U-series analysis. For each soil sample, three 100 mg aliquots were weighed and prepared as follows. The first aliquot was analyzed as a bulk soil after total digestion with combined HNO_3+HF+$HClO_4$ acids as well as H_3BO_3 + HCl for about 48 hrs. For the second aliquot, approximately 10 ml of 0.1M HCl were added and the mixture was allowed to settle for 30 min and then centrifuged. The acid leachate (HCl-L) and residue (HCl-R) were then separated into beakers. Lastly, 10 ml of de-ionized water (18.2MΩ) were added to the third aliquot and the mixture was allowed to settle for 10 min and centrifuged. The water suspended portion (H_2O-S) and residues (H_2O-R) were put into separate beakers. For two caliche samples from JPT1 and JPT2, five randomly selected points on the caliche were scraped off to obtain coeval samples for total sample digestion. All the bulk, leachates and residue samples were spiked with ^{233}U and ^{229}Th spikes prior to digestion in order to obtain ^{238}U and ^{232}Th concentrations by isotope dilution technique.

Uranium and Th in the digested samples were separated and purified from the matrix through an AG 1-X8 anion exchange resin (200-400 mesh) in a class-100 clean room. Isotopic ratios ($^{234}U/^{238}U$, $^{233}U/^{238}U$, $^{235}U/^{238}U$, $^{230}Th/^{232}Th$, and $^{229}Th/^{232}Th$) were measured using standard-sample bracketing method on the multi-collector inductively coupled plasma mass spectrometer at the University of Texas at El Paso. The NBL U145B solution was used as the U bracketing standard to correct for mass fractionation and ion counter gains for U isotope measurements. A $^{229\text{-}230\text{-}232}Th$ in-house standard calibrated against an IRMM 035 solution was used as the Th bracketing solution. U and Th concentrations were calculated using measured

$^{233}U/^{238}U$ and $^{229}Th/^{232}Th$ isotope ratios by the isotope dilution method, respectively. Activity ratios ($^{234}U/^{238}U$) and ($^{230}Th/^{232}Th$) were calculated from measured $^{234}U/^{238}U$ and $^{230}Th/^{232}Th$ isotope ratios. Accuracy was assessed by regularly analyzing the USGS W2 rock reference material. The measured average U and Th concentrations of W2 are: U = 0.503 ± 0.014 ppm (n = 8, 2σ) and Th = 2.148 ± 0.001 ppm (n = 7, 2σ), all within the reported values from other laboratories (Sims et al., 2008). Measured U-series activity ratios of the W-2 reference material were at secular equilibrium as expected. Uncertainties in ($^{234}U/^{238}U$) and ($^{230}Th/^{232}Th$) activity ratios were 5‰ (1σ) and 1% (1σ), respectively. U and Th concentrations in procedure blanks were negligible ~4 pg and ~100 pg respectively.

2.4.5 ^{14}C ANALYSIS OF PEDOGENIC CARBONATES

A soil sample from alfalfa site (alfalfa (40-43cm) and Jornada site (JPT2 (27-30cm)) were analyzed at the Center for Applied Isotope Studies at the University of Georgia for ^{14}C radiocarbon ages. These samples were chosen because their U-series ages lie within the limits of radiocarbon dating technique (<50 ka; Wang et al., 1996). For the analysis, carbon dioxide was released from pedogenic carbonates in the soil samples using phosphoric acid in a vacuum. The carbon dioxide was purified and converted to graphite following procedures detailed in Vogel et al. (1984). Graphite $^{14}C/^{13}C$ ratios were then measured using the CAIS 0.5 MeV accelerator mass spectrometer and compared to the ratio measured from the Oxalic Acid I (NBS SRM 4990). Apparent radiocarbon ages were reported in years before 1950 (years BP) after correcting for isotopic fractionation. The statistical and experimental errors were reported to one standard deviation.

2.5 Results

2.5.1 SOIL MINERALOGY AND MAJOR ELEMENT CHEMISTRY

The dominant minerals observed in all soils are quartz, calcite, feldspars and clays. Calcite is more abundant in the soils at the Jornada than the Alfalfa site, especially at greater depths (Table 1.1). The calcite/quartz abundance ratios (intensity ratios of calcite at peak 29.42° 2θ and quartz at peak 26.65° 2θ) increase with depth and show the highest values at about 30-40 cm depth of Jornada soil pits. Calcite/quartz ratios at the Alfalfa site are much lower and show little variation with depth (Fig. 1.2a). Consistent with these trends, SIC contents show similar depth profiles at these two sites (Fig. 1.2b). The high abundances of calcite and SIC at ~30-40 cm soil of the Jornada sites are consistent with the caliche layer observed in the field.

The SC contents at the Jornada site (3.0-9.1 wt% at JPT1 and 1.5- 6.6 wt% at JPT2) are higher than those at the Alfalfa site (0.6-1.7 wt %) (Table 1.1; Fig. 1.2c). The SC pool at the Alfalfa site is contributed roughly equally by SOC and SIC, while the SC pool at the Jornada site is dominated by SIC (Figs. 1.2b, c, d). The SOC contents in the Alfalfa site (0.07 to 0.82 wt %) increase in general toward the surface (Fig. 1.2d). The JPT2 soils have higher SOC contents than the JPTI soils, in agreement with the pit locations, where JPT2 is located right underneath a Creosotebush shrub while JPT1 is on bare soils between shrubs.

At the Jornada site, calcium oxide (CaO) concentrations range from 12.7 to 45 wt% at JPT1 and from 9.9 to 46.2 wt% at JPT2 (Table 1.1; Fig. 1.3). The highest CaO concentrations are observed at the deepest samples of JPT1 and JPT2 in the caliche layers. The CaO concentrations in the soils at the Alfalfa site are much lower, ranging from 2.9 to 5.4 wt%. Carbonate and silicate minerals, as well as evaporite minerals such as gypsum in dryland conditions can potentially contribute the CaO contents in soils. The measured SIC and CaO contents in these

soils were used to estimate the weight percentages of CaO contribution from calcite (based on stoichiometry of $CaCO_3$ and SIC content) vs. CaO contribution from silicates such as feldspars and evaporites (difference from total CaO and those from calcite). On average about 80% of the CaO in Alfalfa soils are as calcite, the percentages increase to 89 to 100% at JPT1. In contrast, at JPT2 profile, only 5 m from JPT1, about 50-65% of CaO are in calcite, with a higher contribution from silicate and evaporite minerals (Table 1.1; Figure 1.3).

2.5.2 U AND TH CONCENTRATIONS AND ACTIVITY RATIOS IN BULK SOILS

Uranium (U) concentrations in bulk soils range from 1.1 to 2.0 ppm (mg/kg) at JPT1 and 1.3 to 2.0 ppm at JPT2 respectively (Table 1.1). The thorium (Th) concentrations in bulk soils range from 2.3 to 8.7 ppm at JPT1, and 1.6 to 8.7 ppm at JPT2 (Table 1.1). The lowest U and Th concentrations at the Jornada site are observed in the caliche samples at the bottom of the soil pits. Both U and Th concentrations in these soil profiles increase in general toward the surface (Table 1.1). However, U/Th ratios in these two soil profiles decrease toward the surface (Figs. 1.4a, 1.4b). U and Th concentrations in bulk soils of the Alfalfa site are within the range of those from Jornada soils, but show much less variation with depth.

The ($^{234}U/^{238}U$) in bulk soils show distinct depth profiles for the Jornada and Alfalfa sites. At the Jornada site, ($^{234}U/^{238}U$) increase from 0.95 to 1.00 with increasing depth, and become significantly higher (1.18-1.30) at the caliche layer (Fig. 1.4c). At the Alfalfa site, ($^{234}U/^{238}U$) however, decrease from 1.02 to 0.97 with increasing depth (Fig. 1.4d).

($^{230}Th/^{238}U$) ratios in bulk soils at the Jornada site are greater than 1, with the exception of the bottom two caliche samples which indicate ($^{230}Th/^{238}U$) < 1 (0.75 to 0.92) (Fig. 1.4e). Similarly, ($^{230}Th/^{238}U$) ratios in bulk soils at the Alfalfa site are greater than 1, except for the

sample at 53 cm depth with ($^{230}Th/^{238}U$) of 0.75 (Fig. 1.4f). The ($^{230}Th/^{238}U$) ratios in bulk soils of all three profiles increase generally toward land surface (Figs. 1.4e, 1.4f).

2.5.3 U AND TH ACTIVITY RATIOS IN PEDOGENIC CARBONATES

The HCl leachates (HCl-L) of the bulk soils at both Alfalfa and Jornada sites show distinctively lower ($^{232}Th/^{238}U$) ratios and higher ($^{234}U/^{238}U$) ratios than their corresponding HCl residues (HCl-R) of the bulk soils (Table A1). Such an observation is consistent with the purpose of the leachate-residual procedure that the low strength acids (0.1 M HCl) preferentially leach carbonates with some addition of silicate minerals in bulk soils, while the residual is enriched in detrital silicate materials. The water-suspended portions (H_2O-S) of the bulk soils generally show higher ($^{232}Th/^{238}U$) ratios than the residual portions (H_2O-R). Such an observation suggests that the water-suspended portions are relatively enriched in detrital silicate fine particles such as clays than the residual portions (H_2O-R). Both the leachate-residue and water suspension-residue procedures have created sub-samples with various mixing ratios of the carbonate and detrital end-members as expected.

The two caliche samples collected from the bottom of the Jornada soil pits have ($^{234}U/^{238}U$) > ratios 1 and ($^{230}Th/^{238}U$) ratios <1 (Table 1.1), a typical U-series signature of "dirty" carbonates. Indeed, the relatively high ($^{232}Th/^{238}U$) ratios of these caliche samples indicate the presence of a significantly detrital component in these pedogenic carbonates.

2.5.4 ISOCHRONS IN DATING PEDOGENIC CARBONATES

The U-series isotope signatures of the ideal pure carbonate end-member in bulk soils and pedogenic carbonates were derived from the typical isochron diagrams (e.g. Rosholt type or Osmond type; Ludwig, 2003). For example, the Osmond type isochron diagrams ($^{230}Th/^{238}U$ vs.

$^{232}Th/^{238}U$ and $^{234}U/^{238}U$ vs. $^{232}Th/^{238}U$) for both Alfalfa and Jornada sites show strong linearity (R^2 = 0.52 to 0.99; Table A1) for all bulk soil samples (Fig. A1), except for the following samples: Alfalfa 60-63cm, JPT1 10-15 cm, and JPT2 0-7 cm. The isochron diagrams for the Jornada caliche samples also show strong linearity (Table A1; Fig. A1). The degree of linearity of the isochron diagrams is proxy to evaluate how valid the assumption for the U-series dating that the bulk soils and caliche samples are a mixture of one carbonate and one detrital end member. Isoplot III was used to calculate carbonate ages and $(^{234}U/^{238}U)_0$ (initial U isotopic composition at the time of carbonate formation) of pedogenic carbonates (Ludwig, 2003). The software calculates ages from radioactive decay equations using the measured and detrital corrected ($^{234}U/^{238}U$) and ($^{230}Th/^{238}U$) activity ratios, ^{234}U and ^{230}Th decay constants and the associated errors (Ludwig, 2003).

Pedogenic carbonate ages calculated from U-series range from 2.2 ± 1.7 ka to 15 ± 17 ka for soils at Alfalfa site (Fig. 1.5a; Table 1.1). Carbonates in JPT1 soils range from 14.5 ± 6.8 ka to 117 ± 26 ka and those in JPT2 soils range from 19.5 ± 7.5 ka to 100 ± 40 ka (Figs. 1.5b,c; Table 1.1). Very large uncertainties are observed in several carbonate ages (e.g. JPT2 0-7cm), probably due to the presence of multiple end members of detrital materials (which could explain poor linearity on the isochron diagrams). Large uncertainties are also observed for most of the bulk soils, which is expected as in general pedogenic carbonates in soil profiles lack the consistent and resolvable stratigraphy required to construct detailed time series and may only reflect time-integrated conditions over ~10-100 kyr timescales (e.g. the HCl leachates integrate carbonates formed at ~10-20cm depth interval over several kyrs). Despite the large uncertainties, ages of carbonates in bulk soils at JPT1 and JPT2 are greater than those of the Alfalfa profile. In addition, two caliche samples at the Jornada sites are much older than the carbonates in the bulk

profile (Fig. 1.5). Initial U activity ratios $(^{234}U/^{238}U)_0$ derived from the carbonate age calculations, increases towards land surface at the Alfalfa site, with values between 1.2±0.2 and 1.6±0.1 (Table 1.1). Carbonates at JPT1 and JPT2 soils show $(^{234}U/^{238}U)_0$ values ranging from 1.4±0.1 to 1.9±0.5 and 1.0±0.1 to 1.5±0.1 respectively (Table 1.1).

2.5.5 COMPARISON OF THE U- SERIES AND RADIOCARBON CARBONATE AGES

Apparent ^{14}C ages are reported for two bulk soil samples in Table 1.1. The Alfalfa 40-43 cm sample has an apparent ^{14}C age of 6.54 ± 0.03 ka, older than U-series age (2.2 ± 1.7 ka) calculated for the same sample (Table 1.1). The JPT2 27-30 cm sample yields a radiocarbon age of 8.36 ± 0.03 ka, younger than calculated U-series age (19.5 ± 7.5 ka) (Table 1.1). Since the ^{14}C ages from the carbonates were not corrected for the initial ^{14}C activity (e.g. ^{14}C activity in the initial soil water may be less than 100 percent modern C due to incorporation of dead carbon). The direct comparison of the apparent ^{14}C ages to the U-series ages is not justified. However, both the apparent ^{14}C ages and the U-series ages show that the JPT2 sample is older than the Alfalfa sample.

2.6 Discussion

2.6.1 BEHAVIOR OF U-SERIES ISOTOPES IN BULK SOILS

U-series isotope ratios in bulk soils reflect contributions from both pedogenic carbonates and detrital siliceous soils. During water-rock interaction, physical and chemical processes preferentially remove ^{234}U over ^{238}U from bulk siliceous soils, disturbing the secular equilibrium and causing variations in activity ratios of $(^{234}U/^{238}U)$ and $(^{230}Th/^{238}U)$ (e.g., Chabaux et al., 2003). Due to high solubility of U in oxidizing environment and preferential leaching of ^{234}U into weathering fluids, the soil waters usually have high U concentrations and $(^{234}U/^{238}U)$ ratios

greater than unity. Solubility of Th is low in similar environments, leading to low Th concentrations and ($^{230}Th/^{238}U$) ratios less than one in soil waters (Langmuir and Herman, 1980). As a result, in the bulk siliceous soils, the residual phase after water-rock interaction, ($^{234}U/^{238}U$) tends be lower than 1 and ($^{230}Th/^{238}U$) greater than 1. Precipitation of secondary minerals such as pedogenic carbonates should have similar isotopic signatures as those of soil waters (i.e., ($^{234}U/^{238}U$) >1 and ($^{230}Th/^{238}U$) <1). Both the secondary phases and the siliceous residues combine to control the mass balance of U-series isotopes in bulk soils.

The ($^{234}U/^{238}U$) ratios in the Jornada bulk soils are less than one and decrease toward the surface; ($^{230}Th/^{238}U$) values are >1 and increase with decreasing depth, and elemental U/Th ratios also decrease with decreasing depth (Fig. 1.4). Such trends are consistent with the expected mobility of U-series isotopes in siliceous soils during chemical weathering: preferential loss of ^{234}U and ^{238}U and accumulation of ^{230}Th and ^{232}Th in shallow soils. Thus, the U-series mass budget in these bulk soils is dominated by siliceous components with minor contribution from pedogenic carbonates. In contrast, the two caliche samples at depth (40 and 48 cm below land surface at JPT1 and JPT2) show distinct U-Th isotope ratios, with ($^{234}U/^{238}U$) values >1 and ($^{230}Th/^{238}U$) ratios <1. This agrees well with the high carbonate contents observed in the thick caliche layer, underneath the bulk soils and the carbonate is secondary in nature (Fig. 1.2).

Similar depth trends of ($^{230}Th/^{238}U$) and U/Th ratios are observed in the Alfalfa soils as the Jornada soils, suggesting U in Alfalfa soils is also contributed predominantly by the siliceous components, with minor addition of pedogenic carbonates. However, the ($^{234}U/^{238}U$) ratios of the Alfalfa soils increase toward the surface, showing an opposite trend to the Jornada soils. Such a difference suggests that U mass balance is controlled by more than chemical weathering at Alfalfa, and U is most likely added to soils from an external source characterized by higher

($^{234}U/^{238}U$) activity ratios. Indeed, the Alfalfa site is irrigated intensively with Rio Grande water as a part of agricultural practices. The Rio Grande water near the El Paso region has been shown to have high U concentrations (e.g., 3.3 to 5.6 ppb) and high ($^{234}U/^{238}U$) ratios of 1.6 to 2.2 (e.g., Szynkiewicz et al., 2015). After intensive water loss through evapotranspiration, irrigation water becomes even more concentrated, and oversaturated with respect to calcite in the soils, leading to precipitation of pedogenic carbonates in the agricultural fields (e.g., Cox, 2012). Dissolved U has high affinity for bicarbonate ions (e.g. forming uranyl carbonates) and tends to precipitate along with carbonates (e.g. review by Chabaux et al., 2003). Irrigation-induced U can be incorporated into secondary calcite, leading to higher ($^{234}U/^{238}U$) ratios in bulk soils. In addition to irrigation water, U from fertilizers in this region showed ($^{234}U/^{238}U$) ratios of ~1.0 (e.g., Szynkiewicz et al., 2015), also higher than the bulk soils at depth at the Alfalfa site, and could be another potential source of external U. Such external sources of U to Alfalfa soils may also be the reason that the ($^{230}Th/^{238}U$) ratios in the Alfalfa soils are systematically lower than the ratios in the Jornada bulk soils. In fact, the bulk Alfalfa soils at the 50-53 cm depth have ($^{230}Th/^{238}U$) ratios <1, similar to the two caliche samples of the Jornada site. These observations suggest the formation of pedogenic carbonates is important for U mass balance at the Alfalfa site: U is leached from bedrock or parent materials through chemical weathering and also added to by external sources (irrigation water and fertilizers), and incorporated into soil systems along with pedogenic carbonates.

2.6.2 PATTERNS AND RATES OF CALCITE ACCUMULATION IN NATURAL AND AGRICULTURAL SOIL PROFILES

2.6.2.1 Depth profiles of pedogenic carbonates

Quantification of soil mineralogy and elemental chemistry (CaO and C) all identified abundant soil carbonates (as calcite) at the natural (Jornada) and managed agricultural (Alfalfa)

sites (Figs. 1.2, 1.3). Because of the lack of primary calcite in parent sediments and bedrock at both sites, these soil carbonates are of pedogenic origin. The Jornada soils (JPT1 and JPT2) have much higher carbonate contents than the Alfalfa soils (Figs. 1.2, 1.3). At the bottom of the soil pits at Jornada, hard pans of caliche deposits were impossible to penetrate by auger or shovel. The only sample collected from the upper boundary of the thick caliche layer contain 4 to 8 wt% of SIC, or equivalent of 32 to 65 wt% of calcite in soils (Fig. 1.2b).

Carbonate concentrations at the Alfalfa site, lower than those of Jornada soils, are almost constant for the ~60 cm thick soil profile. No hard pans of caliche layers were observed in the field and the carbonates are present as fine particles in the soil matrix. The uniform distribution of the carbonates suggests that formation of carbonates occurred at all depths, without significant accumulation or redistribution at depth as observed in the natural systems. The Alfalfa soil profile changes from clayey loam soils at surface to more sandy soils at the bottom of the soil pit (e.g., Cox, 2012), and thus the increased drainage due to the change of soil texture may limit the formation of carbonates at depth.

2.6.2.2 Ages of pedogenic carbonates

Both isotopic systems and petrographic observations have been used to date pedogenic carbonates (e.g., Amundson et al., 1994; Ludwig and Paces, 2002; Candy et al., 2005; Pustovoyotov et al., 2007). In old soils, when pedogenic carbonates form continuous coatings on detrital clasts (e.g., Selleck and Baran, 2003), the calcite rind thickness is found to be positively correlated to soil age, even though the climate conditions differ among the sites (e.g., Amoroso, 2006). Ages of these carbonates in combination with other techniques were used to establish relative ages of the soil genesis and geomorphic surface. Ages of pedogenic carbonates within the Jornada Basin have been constrained using radiocarbon technique through the Desert Project

(e.g., Gile et al., 1981). Radiocarbon ages are useful to date materials that are younger than 30 ka. The U-series technique on the other hand, can date much older samples up to ~500 ka. Since late Pleistocene or older soils or formations are present within the Jornada basin, U-series technique is a more appropriate technique basin wide. In this study, U-Th isotope disequilibrium systems are utilized to date the pedogenic carbonates of different settings.

Ages of pedogenic carbonates show systematic differences for soils at the Jornada and Alfalfa sites (Fig. 1.5). The hard-pan caliche samples from the bottom of the Jornada soil pits have the oldest carbonate ages, 117 ± 26 ka and 100 ± 40 ka, respectively. This region is characterized as Jornada I geomorphic surface and its ages are placed at 250– 700 ka (Giles et al., 198; Monger et al., 2009). The carbonates at 40-50cm depth are the upper most boundary of the thick hardpan caliche layer and much younger than geomorphic surfaces. Such observations suggest that formation of pedogenic carbonates started at least ~100 kyrs ago and much older carbonates are expected in deeper caliche layers. These ages are consistent with the conceptual model that caliche layers grow upward and become younger towards land surface. Indeed, pedogenic carbonates in the topsoil columns (0- 50cm depths) are much younger at Jornada, with ages ranging from 15 ± 7 ka and 50 ± 21 ka. The shallowest soil samples at JPT1 and JPT2 have relatively large uncertainties in carbonate ages, probably due to the contribution of carbonate from multiple sources (dust vs. pedogenic origin, or multiple stages of carbonate formation). For Jornada soils, the carbonate ages tend to decrease slightly towards surface but the majority of the ages remain relatively constant with depth. We argue that the formation of the hardpan caliche layer plays an important role in controlling local hydrologic conditions and formation of the carbonates at shallower depths. Indeed, the continuous accumulation of calcite makes caliche relatively impermeable. Consequently, water is ponding on top of caliche layer, facilitating the

accumulation of pedogenic calcite in the above soil column. This will make caliche thicker and grow upwards with time.

Pedogenic carbonates in Alfalfa soils are much younger in comparison to the Jornada soils, with U-series ages observed between 2.2 ± 1.7 ka to 22.2 ± 8.1 ka. Consistent with their younger ages, the pedogenic carbonates are present as films and filaments in the soil matrix, which are typical features from early stages of carbonate development (e.g. Birkeland et al., 1991). The U-series isotope ratios of the bulk soils were modified by addition of U through irrigation water or/and fertilizers; similarly, young carbonates form after irrigation loads Ca^{2+} and bicarbonate to soils and leads to new calcite precipitation through Reaction 1. Indeed, the water used for irrigation in this region, both Rio Grande river and local groundwater, is near solubility equilibrium with calcite and becomes more super-saturated after extensive evapotranspiration in the agricultural fields (e.g., Cox, 2012). Soils developed on the Rio Grande floodplains in the late Holocene (2500 -1000yrs; Hall and Peterson, 2013) have been intensively cultivated for the last 200 years; so irrigation-induced pedogenic carbonates are extremely young (<200 years old) in comparison to the flood plains and Fillmore geomorphic surface ages (up to 7000 yrs). The continuous addition of irrigation-induced calcite lowers the average age of the bulk pedogenic carbonates. Thus, we argue that the young carbonate ages (e.g. ~2.2 ± 1.7 ka) observed at the Alfalfa site reflect mixing of naturally formed older carbonates (e.g. eolian materials or limestones) and irrigation-induced younger carbonates.

Carbonates in two soil samples were also dated by C-14 analyses. Interestingly, for one sample (Alfalfa 30-40cm), the ^{14}C-derived age is older than it U-series age, while for the other (JPT2 30-40cm), the ^{14}C-derived age is younger than its U-series age (Table 1.1). Possible reasons for such discrepancies could be: (1) ^{14}C age reported in this study is uncorrected for

initial ^{14}C activities in the soil water at the time of carbonate formation, and (2) the two dating methods may behave differently during mixing of carbonates with different ages. Both methods rely on the isotope decay, but C is a major component of calcite ($CaCO_3$), while in contrast, U co-precipitates with calcite as a minor element. Thus, the age of mixed pedogenic carbonates may be a linear function of relative fraction of old versus young carbonates for the C dating method. However for U, in addition to the variables mentioned above, two carbonate end-members may contain different amounts of U and thus the mixing between old and young carbonates is deviated from the linear line.

It is however important to note that both C-14 and U-series dating show that Jornada soils have much older carbonates than Alfalfa soils for the same depth, consistent with ages of their geomorphic landscapes. In addition, the radiocarbon dating is more accurate but limited to younger carbonates, while U-isotopes can extend to constrain the ages of much older soils. Indeed, the carbonates in caliche samples of JPT soil profiles were as old as 100 ka, beyond the dating limit of the ^{14}C method.

2.6.2.3 Pedogenic carbonate accumulation rates

The total amount of pedogenic carbonate accumulated at each site (M; g m^{-2}) is quantified by integrating over the entire soil profile sampled:

$$M = \sum_i (r_i l_i C_i) \qquad \text{Eq. (1)}$$

where ρ is soil bulk density (g cm^{-3}), l is the soil sampling interval (cm), and C is the pedogenic carbonate content (calculated from SIC; g g^{-1}) at depth interval *i*. The bulk density data used for calculating *M* are from Cox (2012) for the Alfalfa site and Monger et al. (2009) for the Jornada

sites. The average formation age of pedogenic carbonate for each site (t, yr) is the U-series age weighted by the mass of pedogenic carbonate at each depth and estimated as:

$$t = \sum_i (r_i l_i C_i t_i) / \sum_i (r_i l_i C_i) \quad \text{Eq. (2)}$$

The average age of pedogenic carbonate is ~7.3 ± 5.0 ka at Alfalfa, ~28 ± 11 ka at JPT1 and 34 ± 14 ka at JPT2 (the age uncertainty is the average uncertainty of each profile). The accumulation rate of pedogenic carbonate for a given site is thus calculated as ($gCaCO_3\ m^{-2}\ yr^{-1}$):

$$R = \frac{M}{t} \quad \text{Eq. (3)}$$

At Alfalfa pedogenic carbonate accumulates at 9 ± 6 g $CaCO_3\ m^{-2}\ yr^{-1}$, much higher than that in Jornada (3.5 ± 1.5 g $CaCO_3\ m^{-2}\ yr^{-1}$ at JPT1 and 2.5 ± 1.0 g $CaCO_3\ m^{-2}\ yr^{-1}$ at JPT2). According to Eq. (3), the uncertainty of *R* is mainly derived from the errors in quantifying t. Natural accumulation rates of pedogenic carbonates were estimated to range from <0.1 to 15 $gCaCO_3\ m^{-2}\ yr^{-1}$ in New Mexico and Utah (e.g., Gile et al., 1981; Machette, 1985; Monger and Gallegos, 2000), 1.0 to 3.5 $gCaCO_3\ m^{-2}\ yr^{-1}$ in the Mojave Desert (e.g., Schlesinger, 1985), 8.3 to 11 $gCaCO_3\ m^{-2}\ yr^{-1}$ in Saskatchewan, Canada (e.g., Eghbal and Southard, 1993; Landi et al., 2003). The rates estimated at Jornada are within the range of those for other natural systems.

This exercise reveals that much more pedogenic carbonate is deposited in Jornada, the natural site than in Alfalfa, the agricultural site, because of the much older geomorphic surface at Jornada. However, the accumulation rate of secondary calcite is much higher in Alfalfa than Jornada, probably accelerated by agricultural activities, i.e., flood irrigation as discussed below. This comparison is focused on the same depth range from the land surface for the natural and agricultural sites (top 40-50 cm). For the natural site, this rate is probably a good estimate of active carbonate formation for the entire soil profile, because the underlying caliche is closed to

water penetration. For the Alfalfa site, the calculated rate represents a minimum value given that soils below 70 cm were not sampled.

2.6.3 CALCIUM SOURCES IN THE JORNADA AND ALFALFA SOILS

According to Reaction 1, the precipitation of pedogenic carbonates is controlled by availability of Ca^{2+}, and dissolved inorganic carbon. Given that most of soils are covered by vegetation, even in dryland areas, in CO_2-open systems, soils thus have unlimited supply of dissolved inorganic carbon. Amount and rates of formation of pedogenic carbonates in soils of southwest USA vary greatly and are mostly controlled by Ca^{2+} input, amount of precipitation, and age of soils in which they occur (e.g., Gile et al., 1981; Machette, 1985). Below, we compiled and estimated the ranges of Ca fluxes from potential sources in natural and agricultural soils of the southwest region. Much of the data from the natural environments is gathered through USDA Desert Soil-Geomorphology Project (e.g., Gile et al., 1981; Monger et al., 2009). Major sources of Ca^{2+} into the soils include in-situ chemical weathering of soil minerals and atmospheric additions (dry and wet deposition). The emphasis for this study will be comparing these loads with those from agricultural practices (i.e., irrigation).

2.6.3.1 In-situ silicate and carbonate weathering in soils

Alfalfa and Jornada soils have developed on parent material with extremely low carbonate contents. Rio Grande ancestral deposits (Camp Rice Formation), parent sediments of the Alfalfa soils, contain only up to 1% $CaCO_3$ (e.g., Gile et al., 1981). The Jornada soils have developed also on the Camp Rice Formation, as well as rhyolitic alluvium from the mountains. The volcanic alluvial deposits contain approximately 0.16 to 3.95% CaO (e.g., Monger and Gallegos, 2000). Measurable Ca is observed in all the three soil profiles, mainly in the pedogenic calcite form with some addition from silicate minerals such as plagioclase, as observed by XRD.

Evaporite minerals such as gypsum are also present at trace levels as measured through soil-water extraction methods, but no such phases were detected by XRD. In this study, gypsum is considered as a secondary mineral with Ca sourced from dust or irrigation water as discussed below. Hence gypsum is not considered a separate Ca input flux here. Silicate weathering in the dryland soils is expected to be extremely slow, limited by both small amount of rainfall and relatively neutral and even alkaline soil water pH. Indeed, the rates of plagioclase dissolution are even smaller for the JPT1 soils, where less than 10% of CaO is from silicate minerals and the dissolution kinetics is further limited by mineral surfaces. Similarly, on the basis of mass balance and Sr isotope consideration, previous studies have also identified dissolution of silicate rocks as a minor contributor to the overall Ca in pedogenic carbonates of the Southwestern regions (e.g., Machette, 1985).

2.6.3.2 Atmospheric depositions (Dust and rainfall)

The Chihuhua desert of the southwest USA where this study is based is considered a dust "hot spot" (Baddock et al., 2011). Dryland landscapes are typically windy and dusty due to lower vegetation coverage, and thus dust-derived carbonates could be also important in soils (e.g., Chiquet et al., 2000). The atmospheric deposition and its contribution to soil carbonates have been vigorously investigated in the southwest USA (e.g., Gile et al., 1961; Grossman et al., 1995; Chiquet et al., 1999). Several studies have identified that Ca in pedogenic carbonates in arid to semi-arid soils of the southwest USA is mainly dust-derived (e.g., Gile et al., 1981; Naiman et al., 2000; Capo and Chadwick, 1999). A 10-year survey through the Desert Project in New Mexico trapped and analyzed dust samples, and estimated that dust loaded calcite at an average rate of 0.3 $gCaCO_3\ m^{-2}\ yr^{-1}$ (range: 0.2 to 0.4) and other types of water leachable Ca at an equivalent rate of 0.14 $gCaCO_3\ m^{-2}\ yr^{-1}$ (range: 0.10-0.17) (e.g., Gile and Grossman, 1979; Gile

et al., 1981; Monger and Gallegos, 2000). More build-up of pedogenic carbonates in soils has been also associated to Ca^{2+} dissolved in rainfall (e.g., Capo and Chadwick, 1999; Gile and Grossman, 1979; Monger and Gallegos, 2000). It was estimated Ca was added to the soils as rain, at an equivalent of 1.5 $gCaCO_3\ m^{-2}\ yr^{-1}$, making the total Ca input from atmospheric deposition at 1.9 $gCaCO_3\ m^{-2}\ yr^{-1}$ (e.g., Monger and Gallegos, 2000). The above estimates assume that carbon was made available by root respiration and microbial activities and was unlimited (e.g., Gile and Grossman, 1979).

2.6.3.3 Land management practices

Different from Jornada, Alfalfa site has been utilized as cropland. With limited rainfall, flood irrigation is one of common practices. Every year from April to October, the field is flood irrigated every two to three weeks, with standing water from the Rio Grande River. Salinity of the river water downstream at El Paso, TX near the alfalfa field ranges from 700 to 2000 mg/l, with its calcite saturation index at ~1.2 (e.g., Cox, 2012). Approximately 1.5 m of this water are released into the alfalfa farm every year, loading dissolved Ca at an equivalent rate of 200 $gCaCO_3\ m^{-2}\ yr^{-1}$ (e.g., Cox, 2012). The irrigation water becomes more concentrated, as standing water is continuously lost through evaporation and transpiration. As a result, evaporite salts precipitate, leading to elevated soil salinity and sodicity (e.g., Cox, 2012). Indeed, high abundance of halite, gypsum and calcite is observed in Alfalfa throughout the soil profiles (e.g., Cox, 2012). Again, the fluxes calculated above should be considered as the upper limits of Ca input from irrigation, as some of soil water drains into the agricultural canals and some recharges to the underlying groundwater aquifer, removing Ca away from the soil profiles (e.g., Cox, 2012).

In addition to irrigation, fertilizers are commonly used to increase crop yields in the region. Similarly, to mitigate the sodicity problems and improve the soil structure, gypsum and other Ca-bearing soluble minerals are usually supplied to the agricultural fields, where Ca^{2+} will replace Na^{+} in soils. Such practices are especially important for loamy to clayey soils, because these relatively impermeable soils tend to accumulate more salts and lead to more sodic conditions. At Alfalfa site, fertilizers were commonly applied but no Ca minerals were added in the last five years. We have no historical records of applying Ca minerals beyond the last five years. Future work on Sr isotopes is needed to evaluate the sources of Ca in pedogenic carbonates and the relative importance of fertilizers and Ca-minerals in overall Ca budgets in agricultural soils.

2.6.3.4 Summary

As discussed above, major Ca sources for pedogenic carbonates were identified and their magnitudes were compiled based on literature and our previous study (Cox, 2012). These bulk estimates suggest loading of Ca from dust and rainfall drives the formation of pedogenic carbonates in natural fields in the Chihuahua desert (e.g., Capo and Chadwick, 1999). Indeed, the annual loading from atmospheric inputs (10 years average at 1.9 $gCaCO_3\ m^{-2}\ yr^{-1}$) is similar to the formation rate of pedogenic carbonate in Jornada (2.5 to 3.5 $gCaCO_3\ m^{-2}\ yr^{-1}$ for up to 100 ka). In contrast, the Ca (and DIC) fluxes from agricultural practices were much larger, leading to calcite precipitation at much faster rates. This is consistent with relatively higher formation rates observed at Alfalfa than Jornada sites. However, the average formation rate at Alfalfa is still low compared to the Ca loading rate, due to the relatively short history of cultivation and flood irrigation.

2.6.4 BIOTIC CONTROL ON CALCITE FORMATION IN NATURAL SITES?

JPT2 soil pit was located underneath a Creosotebush shrub while JPT1 pit was dug in bare land, between Creosotebush bushes. JPT2 had slightly lower calcite contents compared to JPT1 (Figure 1.2a and 1.3c and 1.3d) for the same depth and the depth to caliche layer was also higher at JPT2 than that at JPT1. Depth distribution of pedogenic carbonates has been studied and modeled as functions of soil evolution and climate conditions (e.g., Marion and Schlesinger, 1994; Hirmas et al., 2010; Royer, 1999). JPT1 and JPT2 sites are only 5 m apart, thus we expect that the parent sediments, the soil ages, and dust and rainfall loadings are the same, except for the current land coverage. It is hard to correlate the different characteristics of pedogenic carbonates at JPT1 and JPT2 sites to their proximity to shrubs, because pedogenic carbonate accumulates in the soils over long timescales, during which types of vegetation have evolved due to climate changes (e.g., Monger et al., 2009; Kraimer and Monger, 2009). Even so, the impact of organic matter on pedogenic carbonate will be discussed below in context with observed differences in the Jornada soil pits.

Most of the studies on naturally occurring pedogenic carbonates assumed that carbon in the secondary calcite is supplied by soil organic matter and the carbon isotopes of such calcite are at equilibrium with soil respired CO_2 (e.g., Quade et al., 1989; Cerling et al., 1989; Monger et al., 2009). For example, microbes have been noted to boost pedogenic carbonate formation through respiration: some studies have reported precipitation of carbonates in their cultures (e.g., Monger et al., 1991). Other soil organisms fostering pedogenic carbonate formation such as termites have been found in high calcium environments (e.g. mounds and termite sheaths around plant remains) or contain carbonate crystals (e.g., Monger and Gallegos, 2000; Gutschick and

Snyder, 2006). When soil or atmospheric CO_2 is the only C source, then calcite precipitates according to the following reaction:

$$CO_2\ (g) + H_2O + Ca^{2+} \rightarrow CaCO_3(s) + 2H^+ \qquad \text{Rxn (2)}$$

Thus, biota can modify the precipitation of soil carbonates in complex ways including changing the water dynamics in soil profiles, increasing soil CO_2 levels through root and microbial activity, and lowering soil water pH through release of organic acids (e.g., Cerling, 1984; Landi et al., 2003; Kuzyakov and Damanski, 2000; Andrews and Schlesinger, 2001). Among all, the conditions that promote calcite formation are higher soil CO_2 concentrations, and water loss through transpiration that will drive supersaturation of soil solutions. In contrast, lowering the soil pH will prevent calcite from forming. If the difference between the two Jornada soil pits is significant, it is consistent with that the presence of shrub and its associated microecosystem slows down the pedogenic carbonate accumulation, implying that organic acids and thus the lower soil pH are important controls on the formation rates of secondary calcite.

In agricultural sites, DIC concentrations are high in irrigation water and theoretically provide all available bicarbonate ions to form calite. If so, soil derived CO_2 may become negligible in contributing to calcite formation. Instead, CO_2 is released to soils according to Reaction (1).

2.6.5 IMPLICATION OF DRYLAND IRRIGATION FOR GLOBAL CARBON CYCLES

Irrigation is an important land management practice in the arid to semi-arid zones. Its effects on pedogenic carbonate formation are not well constrained because the changes are gradual and can be observed only after a long time (e.g., Suarez, 2000). Depending on the chemistry of irrigation water and the amount of water leached to deeper soils, irrigation can either cause accumulation or dissolution of pedogenic carbonates (e.g., Sanderman, 2012;

Suarez, 2000). In addition to DIC, irrigation water supplies soluble cations (such as Ca^{2+}) which foster pedogenic carbonate formation (e.g., Lal and Kimble, 2000a; Sanderman, 2012). Irrigation increases soil CO_2 by precipitating carbonates and increasing biological activity (e.g., Sanderman, 2012; Suarez, 2000) thus influencing the carbon fluxes in soils.

Importantly, dryland area is expanding and already covers more than 40% of the terrestrial land surface on Earth. Drylands also host more than two billion people, with most living in developing countries (e.g., Grace et al., 2006; Wang et al., 2012). The combined increase in food demand and desertification has converted 4% of natural dryland to irrigated agriculture coverage (e.g., UNCCD, 2000). To date, however, few studies have quantified the production and emission of CO_2 during the development of pedogenic carbonates in agricultural drylands (e.g., Amundson and Lund, 1987; Lal and Kimble, 2000a; Wohlfahrt et al., 2008; Xie et al., 2009; Liu et al., 2012). One modeling study estimated that approximately 2.2 TgC yr^{-1} (1Tg = 10^{12}g) were released to the atmosphere from approximately 16 million ha of irrigated dryland fields in the western U.S. (e.g., Suarez, 2000), which is equivalent to a loss of soil CO_2 to the atmosphere at 14 gC m^{-2} yr^{-1}. The stoichiometry of Rxn (1) implies 14 gC m^{-2} yr^{-1} was also accumulated in pedogenic carbonates, which is one to two orders of magnitude higher than natural pedogenic carbonate accumulation rates (e.g., Eghbal and Southard, 1993; Landi et al., 2003). These findings suggest dryland agriculture has the potential to significantly alter land-atmosphere CO_2 flux over a large area of the Earth's surface. To date, representation of the potential shift in land-atmosphere CO_2 exchange associated with dryland agriculture has been poorly recognized and models forecasting the future state of the Earth System do not include such dynamics. Human land use activities such as irrigation, application of synthetic fertilizers, and afforestation influence soil organic carbon pool (e.g., Lal and Kimble., 2000b). Agricultural

soils in this region are also known to contain pedogenic carbonates. How these land use activities contribute to the soil inorganic carbon complex is not well documented and warrants future studies.

2.7 Conclusion

In this study, calcium oxides and soil carbon concentrations, mineralogy and U-series isotopes were combined to quantify the pedogenic carbonate inventory, pedogenic carbonate ages and formation rates at managed (Alfalfa site) and natural (Jornada; JPT1 and JPT2) soils of the southwestern United States. U-series dating technique indicated younger pedogenic carbonates in soils at Alfalfa site compared to carbonates at Jornada pit soils. However, the pedogenic carbonates formation rates at Alfalfa were higher compared to those at the Jornada soils. These elevated formation rates were supported by high fluxes of Ca and carbon induced by flood irrigation in the agricultural fields. Such carbonates enhanced through dryland agriculture alter land-atmosphere CO_2 shifts on the earth surface. The Jornada soils indicated different amounts of calcite for the same depth. The Jornada soil pit 1 (JPT1) indicated higher calcite content compared to the Jornada soil pit 2 (JPT2), which was dug near a Creosotebush. Eventhough, calcite content could not be directly associated with the current vegetation due to their accumulation over a long time; organic acids and low soil pH in the root zone may influence precipitation of pedogenic carbonates.

2.8 Acknowledgments

The authors wish to gratefully acknowledge Christine Cox for providing soil samples from an alfalfa agricultural site.

References

Amoroso, L. (2006). Age calibration of carbonate rind thickness in Late Pleistocene soils for surficial deposit age estimation, Southwest USA. *Quaternary Research* 65, 172-178.

Amundson, R.G. and Lund, L.J. (1987). The stable isotope chemistry of a native and irrigated Typic Natrargid in the San-Joaquin Valley of California. *Soil Science Society of America Journal* 51 (3), 761-67.

Amundson, R.G., Wang, Y., Chadwick, O.A., Trumbore, S., McFadden, L., McDonald, E., Wells, S., Deniro, M. (1994). Factors and processes governing the C-14 content of carbonate in desert soils. *Earth and Planetary Science Letters* 125, 385-402.

Andersen, M.B.Stirling, C.H., Potter, E.K., Halliday, A.N., Blake, S.G., McCulloch, M.T., Ayling, B.F., O'Leary, M. (2008). High-precision U-series measurements of more than 500,000 year old fossil corals. *Earth and Planetary Science Letters* 265 (1-2), 229-245.

Andrews, J.A. and Schlesinger, W.H. (2001). Soil CO_2 dynamics, acidification, and chemical weathering in a temperate forest with experiment CO_2 enrichment. *Global Biogeochemical Cycles* 15,149-162.

Baddock, M. C., Gill, T. E., Bullard, J. E., Acosta, M. D., Rivera Rivera, N. I. (2011). Geomorphology of the Chihuahuan Desert based on potential dust emissions. *Journal of Maps 7*(1), 249-259.

Bergametti, G. and Gillette, D.A. (2010). Aeolian sediment fluxes measured over various plant/soil complexes in the Chihuahuan desert. *Journal of Geophysical Research-Earth Surface*, 115. F03044, doi:10.1029/2009JF001543

Birkeland, P.W., Machette, M.N., Haller, K.M. (1991). Soils as a tool for applied Quaternary geology [Utah Geological and Mineral Survey Misc. Pub. 91-3]. Salt Lake City: Utah Department of Natural Resources.

Bischoff, J.L. and Fitzpatrick, J.A.(1991). U-Series Dating of Impure Carbonates - an Isochron Technique Using Total-Sample Dissolution. *Geochimica Et Cosmochimica Acta*, 55(2), 543-554.

Bourdon, B., Turner, S., Henderson, G. M., Lundstrom, C. C. (2003). Introduction to U-series geochemistry. *Reviews in Mineralogy and Geochemistry, 52*(1), 1-21.

Candy, I., Black, S., Sellword, B.W. (2005). U-series isochron dating of immature and mature calcretes as a basis for constructing Quaternary landform chronologies for the Sorbas basin, southern Spain. *Quaternary Research* 64, 100-111.

Capo, R.C. and Chadwick, O.A. (1999). Sources of strontium and calcium in desert soil and calcrete. *Earth and Planetary Science Letters* 170 (1-2), 61-72.

Cerling, T.E. 1984. The Stable Isotopic Composition of Modern Soil Carbonate and Its Relationship to Climate. *Earth and Planetary Science Letters* 71(2), 229-240.

Cerling, T.E., Quade, J., Wang, Y., Bowman, J.R. (1989). Carbon isotopes in soils and palaeosols as paleoecologic indicators. *Nature* 341, 138-139.

Chabaux, F., Bourdon, B., Riotte, J. (2008). U-series geochemistry in weathering profiles, river waters and lakes. *Radioactivity in the Environment* 13, 49-104.

Chabaux, F., Riotte, J., Dequincey. O. (2003). U-Th-Ra fractionation during weathering and river transport. *Reviews in Mineralogy and Geochemistry* 52, 533–576.

Chadwick, O.A., Sowers, J.M., Amundson, R.G. (1989). Morphology of calcite crystals in clast coatings from four soils in the Mojave Desert region. *Soil Science Society of America Journal* 52, 211-219.

Cheng, H., Edwards, R.L., Hoff, J., Gallup, C.D., Richards, D.A., Asmerom, Y. (2000). The half-lives of uranium-234 and thorium-230. *Chemical Geology* 169, 17-33.

Chiquet, A., Colin, F., Hamelin, B., Michard, A., Nahon, D. (2000) Chemical mass balance of calcrete genesis on the Toledo granite (Spain). *Chemical Geology* 170, 19-35.

Chiquet, A., Michard, A., Nahon, D., Hamelin, B. (1999). Atmospheric input vs insitu weathering in the genesis of calcretes: An Sr isotope study at Galvez (Central Spain). *Geochimica et Coscochimica Acta* 63, 311-323.

Cox, C.L. (2012). Evaluation of Soil Sustainability Along the Rio Grande in West Texas: Changes in Salt Loading and Organic Nutrients Due to Farming Practices (M.S. Thesis). University of Texas at El Paso.

Deutz, P., Montanez, I.P., Monger, C.H. (2002). Morphology and Stable and Radiogenic Isotope Composition of Pedogenic Carbonates in Late Quaternary Relict Soils, New Mexico, U.S.A.: An Integrated Record of Pedogenic Overprinting. *Journal of Sedimentary Research* 72 (6), 809-822.

Dickin, A.P. (1995). Radiogenic Isotope Geology. Cambridge University Press, Cambridge. 490.

D'Odorico, P., Bhattachan, A., Davis, K., Ravi, S., Runyan, C. (2012). Global desertification: drivers and feedbacks. *Advances in Water Resources* 51, 326-344.

Dosseto, A., Turner, S.P., Chappell, J. (2008). The evolution of weathering profiles through time: New insights from uranium-series isotopes. *Earth and Planetary Science Letters* 274, 359–371.

Edwards, R.L., Gallup, C.D., Cheng, H. (2003). Uranium-series Dating of Marine and Lacustrine Carbonates. *Reviews in Mineralogy and Geochemistry*, 52: 363-405.

Eghbal, M.K. and Southard, R.J. (1993). Stratigraphy and genesis of Durorthids and Haplargids on dissected alluvial fans, western Mojave Desert, California. *Geoderma* 59, 151-174.

Egli, M.and Fitze, P. (2001). Quantitative aspects of carbonate leaching of soils with differing ages and climates. *Catena* 46, 35-62.

Ellis, S.R., Levings, G.W., Carter, L.F., Richey, S.F., Radell, M.J. (1993). Rio Grande Valley, Colorado, New Mexico, and Texas. *Journal of the America Water Resources Association* 29 (4), 617–646.

Entry, J.A., Sojka, R.E., Shewmaker, G.E. (2004). Irrigation increases inorganic carbon in agricultural soils. *Environmental Management*, 33: S309-S317.

Eswaran, H., Reich, P. F., Kimble, J. M., Beinroth, F. H., Padmanabhan, E., Moncharoen, P. (2000). Global carbon stocks. . In: J.M.K. R. Lal and B.A. Stewart. (Editors), Global Climate Change and Pedogenic Carbonates. CRC/Lewis Press, Boca Raton, Fla, 15–26.

Feldman, C. (1983). Behavior of Trace Refractory Minerals in the Lithium Metaborate Fusion-Acid Dissolution Procedure. *Analytical Chemistry* 55(14), 2451-2453.

Ghassemi, F., Jakeman, A.J., Nix, H.A. (1995). Salinisation of Land and Water Resources: Human Causes, Extent, Management and Case Studies, University of New South Wales Press, Sydney and CAB International, Wallingford.

Gibbens, R.P., McNeely, R.P., Havstad, K.M., Beck, R.F. and Nolen, B. (2005). Vegetation changes in the Jornada Basin from 1858 to 1998. *Journal of Arid Environments* 61(4), 651-668.

Gile, L.H. (1961). A classification of ca horizons in the soils of a desert region, Dona Ana County, New Mexico. *Soil Science Society of America Proceedings* 25, 52–61.

Gile, L.H. and Grossman, R.B. (1979). The Desert Project soil monograph: Soils and landscapes of a desert region astride the Rio Grande Valley near Las Cruces, New Mexico. Lincoln, NE: U.S. Department of Agriculture, Soil Conservation Service.

Gile, L.H., Hawley, J.W., Grossman, R.B. (1981). Soils and geomorphology in the Basin and Range area of Southern New Mexico: Guidebook to the Desert Project. New Mexico Bureau of Mines and Mineral Resources., Socorro, NM, 222

Gile, L.H., Peterson, F.F., Grossman, R.B. (1966). Morphological and genetic sequences of carbonate accumulation in desert soils. *Soil Science* 101, 347–360.

Grace, J., Jose, J.S., Meir, P., Miranda, H.S., Montes, R.A. (2006) Productivity and carbon fluxes of tropical savannas, *Journal of Biogeography* 33, 387–400.

Grossman, R. B., Ahrens, R. J., Gile, L. H., Montoya, C. E., & Chadwick, O. A. (1995). Areal evaluation of organic and carbonate carbon in a desert area of southern New Mexico. In R. Lal, J. Kimble, E. Levine, & B. A. Steward (Eds.), Soils and global change (pp. 81–92). Boca Raton, FL: CRC Press, Inc.

Gutschick, V. P., & Snyder, K. A. (2006). Water and energy balances within the Jornada Basin. Structure and Function of a Chihuahuan Desert Ecosystem, The Jornada Basin long-term ecological research site. Oxford University Press, New York, 176-188.

Hall, S. A. and Peterson, J. A. (2013). Floodplain construction of the Rio Grande at El Paso, Texas, USA: response to Holocene climate change.*Quaternary Science Reviews 65*, 102-119.

Hawley, J.W. and Kennedy, J.F. (2004). Creation of a Digital Hydrogeologic Framework Model of the Mesilla Basin and Southern del Muerto Basin, New Mexico Water Resources Research Institute Technical, Las Cruces, New Mexico.

Hirmas, D.R., Amrhein, C., Graham, R.C. (2010). Spatial and process-based modeling of soil inorganic carbon storage in an arid piedmont. *Geoderma* 154, 486-494.

Hogan, F.M., Phillips, F.M., Mills, S.K., Hendrickx, J.M.H., Ruiz, J., Chesley, J.T. and Asmerom, Y. (2007). Geologic origins of salinization in semi-arid river: the role of sedimentary basin brines. *Geology* 35, 1063–1066.

Hutchison, W. R. (2006). Groundwater management in El Paso, Texas. Universal-Publishers.

Ivanovich, M. and Harmon, R.S. (1992). Uranium-series disequilibrium: Applications to earth, marine, and environmental sciences. Clarendon Press, Oxford University Press.

Keller, G.R., Morgan, P., Seager, W.R. (1990). Crustal Structure, Gravity-Anomalies and Heat-Flow in the Southern Rio-Grande Rift and their Relationship to Extensional Tectonics. *Tectonophysics* 174(1-2), 21-37.

Kraimer, R.A. and Monger, H.C. (2009) Carbon isotopic subsets of soil carbonate- A particle size comparison of limestone and igneous parent materials. *Geoderma* 150, 1-9.

Ku, T.L., Bull, W.B., S.T., F., Knauss, K.G. (1979). Th^{230}-U^{234} dating of pedogenic carbonates in gravelly desert soils of Vidal Valley, southeastern California. *Geological Society of America Bulletin* 90(11), 1063-1073.

Kummerer, K., Held, M., Pimentel, D. (2010). Sustainable use of soils and time. *Journal of Soil and Water Conservation* 65, 141-149.

Kuzyakov, Y. and Domanski, G. (2000) Carbon input by plants into soil. Review. Journal of Plant Nutrition and Soil Science 163, 421-431.

Lahann, R.W. (1978). A chemical model for calcite crystal growth and morphology control. *Journal of Sedimentary Petrology*. 48, 337-344.

Lal, R. and Kimble., J.M. (2000a). Pedogenic carbonates and the global carbon cycle. In: R. Lal, J.M. Kimble, H. Eswaran and B.A. Stewart (Editors), Global climate change and pedogenic carbonates. Lewis Publishers, Boca Raton, 1-14.

Lal, R. and Kimble, J.M.(2000b). Inorganic carbon and the global C cycle: Research and development priorities. Global Climate Change and Pedogenic Carbonates. CRC/Lewis Publishers, Boca Raton, Florida, 291-302.

Landi, A., Mermut, A.R., Anderson, D.W. (2003) Origin and rate of pedogenic carbonate accumulation in Saskatchewan soils, Canada. *Geoderma* 117, 143-156.

Langmuir, D. and Herman, J.S. (1980). The Mobility of Thorium in Natural-Waters at Low-Temperatures. *Geochimica Et Cosmochimica Acta* 44(11), 1753-1766.

Laudicina, V.A., Scalenghe, R., Piscoiotta, A., Parello, F., Dazzi, C. (2013). Pedogenic carbonates and carbon pools in gypsiferous soils of a semiarid Mediterranean environment in south Italy. *Geoderma* 192, 31-38.

Liu, R., Li, Y., Wang, Q.X. (2012). Variations in water and CO_2 fluxes over a saline desert in western China. *Hydrological Process* 26, 513–522.

Ludwig, K.R. and Paces, J.B. (2002) U-series dating of pedogenic silica and carbonate, Crater Flat. Nevada. *Geochimica et Cosmochimica Acta* 66, 487–506.

Ludwig, K.R. (2003). Mathematical-statistical treatment of data nd errors for Th-230/U geochronology. Uranium-Series Geochemistry, *Reviews in Minerology and Geochemistry* 52, 631-656.

Ludwig K. R., Simmons K. R., Szabo B. J., Winograd I. J., Landwehr J. M., Riggs A. C., Hoffman R. J. (1992). Mass-spectrometric ^{230}Th-^{234}U-^{238}U dating of the Devils Hole calcite vein. *Science* 258,
284–287.

Luo, S.D. and Ku, T.L. (1991). U-Series Isochron Dating - A Generalized-Method Employing Total-Sample Dissolution. *Geochimica Et Cosmochimica Acta* 55(2), 555-564.

Machette, M.N. (1985). Calcic soils of the southwestern United States. *Geological Society of America* 203, 1–21.

Mack, G.H. and James, W.C. (1992). Calcic paleosols of the Plio-Pleistocene Camp Rice and Palomas Formations, southern Rio Grande rift, USA. *Sedimentary Geology* 77(1-2), 89-109.

Mack, G.H., Love, D.W., Seager, W.R. (1997). Spillover models for axial rivers in regions of continental extension: the Rio Mimbres and Rio Grande in the southern Rio Grande rift, USA. *Sedimentology* 44(4), 637-652.

Marion, G.M. and Schlesinger, W.H. (1994) Quantitative modeling of soil forming process in desert: the CALDEP and CALGYP models. In: Bryant, R.B. and Arnold, R.W. (Eds.), Quantitative modeling of soil forming processes. *SSSA special publication* 39, 129-145.

Miyamoto, S. (2012). Salinization of Irrigated Urban Soils: A Case Study of El Paso, Texas. Texas A&M University, Texas Water Resources Institute, 434

Miyamoto, S. and Chacon, A. (2006). Soil salinity of urban turf areas irrigated with saline water. II. Soil factors. *Landscape & Urban Planning*, 77:28-38.

Monger, H.C., (2006). Regional Setting of the Jornada Basin In: K. Havstad, l.F. Huenneke and W.H. Schlesinger (Editors), Structure and Function of Chihuahuan desert Ecosystem: The Jornada Basin Long-Term Ecological Research Site The Long-Term Ecological Research Network Series. Oxford University Press, 492

Monger, H.C., Daugherty, L.A., Lindemann, W.C., Liddell, C.M. (1991). Microbial Precipitation of Pedogenic Calcite. *Geology* 19(10), 997-1000.

Monger, H.C. and Gallegos, R.A. (2000). Biotic and abiotic processes and rates of pedogenic carbonate accumulation in the southwestern United States-relationship to atmospheric CO2 sequestration. In Global Climate Change and Pedogenic Carbonates. CRC/Lewis Press, Boca Raton, Fla, 273-289.

Monger, C.H., Gile, L.H., Hawley, J.W. and Grossman, R.B. (2009). The Desert Project-An Analysis of Aridland Soil-Geomorphologic Processess, New Mexico State University, Las Cruces, NM.

Monger, H. C.and Martinez-Rios, J. J. (2000). Inorganic carbon sequestration in grazing lands. The potential of US grazing lands to sequester carbon and mitigate the greenhouse effect. CRC/Lewis Publisher, Boca Raton, FL, 87-118.

Moore, S.J., Bassett, R.L., Liu, B., Wolf, C.P., Doremus, D. (2008). Geochemical tracers to evaluate hydrogeologic controls on river salinization. *Ground Water* 46(3), 489-501.

Naiman, Z., Quade, J., Patchett, P.J. (2000). Isotopic evidence for eolian recycling of pedogenic carbonate and variations in carbonate dust sources throughout the southwest United States. *Geochimica Et Cosmochimica Acta*, 64 (18), 3099-3109.

Neymark, L.A. (2011). Potential effects of alpha-recoil on uranium-series dating of calcrete. *Chemical Geology* 282(3-4), 98-112.

Ontl, T.A. and Schulte, L.A. (2012). Soil Carbon Storage. *Nature Education Knowledge* 3(10), 35.

Osmond, J.K., May, J.P., Tanner, W.F. (1970). Age of the Cap Kennedy barrier-and-lagoon complex. *Journal of Geophysics Research* 75, 5459-5468.

Phillips, F.M., Hogan, J., Mills, S., Hendrickx, M.H. (2003). Environmental tracers applied to quantify causes of salinity in arid-region rivers: Preliminary results from the Rio Grande, southwestern USA. In Alsharha, A.S. and Wood, W.W. Eds., Water resources perspective: evaluation, management, and policy: Developments in water science, V50, Amsterdam, Elsevier *Science*, 327-334.

Pimentel, D., Harvey, C., Resosudarmo, P., Sinclair, K., Kurz, D., McNair, M., Crist, S., Shpritz, L., Fitton, L, Saffouri, R., Blair, R. (1995). Environmental and Economic costs of soil erosion and conservation benefits. *Science* 267 (5201), 1117-1123.

Pustovoytov, K., Schmidt, K., Taubald, H. (2007). Evidence for Holocene environmental changes in the northern fertile Crescent provided by pedogenic carbonate coatings. *Quaternary Research* 67, 315-327.

Quade, J., Cerling, T.E., Bowman, J.R. (1989) Systematic variations in the carbon and oxygen isotopic composition of pedogenic carbonate along elevation transects in the southern Great Basin, United States. *Geological Society of America Bulletin* 101, 464-375.

Rosholt, J.N. (1976). $^{230}Th/^{234}U$ dating of travertine and caliche rinds. *GSA abstracts with Programs*. 8: 1076.

Royer, D.L. (1999). Depth to pedogenic carbonate horizon as a paleoprecipitation indicator? *Geology* 27, 1123-1126.

Sanderman, J. (2012). Can management induced changes in the carbonate system drive soil carbon sequestration? A review with particular focus on Australia. Agriculture, *Ecosystems and Environment*, 155: 70-77.

Schlesinger, W.H. (1982). Carbon storage in the caliche of arid soils: a case study from Arizona. *Soil Science*, 133: 247-255.

Schlesinger, W.H. (1985). The formation of caliche in soils of Mojave Desert, California. *Geochimica Et Cosmochimica Acta* 49, 57-66.

Schlesinger, W.H. (2000). Carbon sequestration in soils: some cautions amidst optimism. *Agriculture, Ecosystems and Environment* 82, 121-127.

Schoups, G., Hopmans, J.W., Young, C.A., Vrugt, J.A., Wanllender, W.W., Tanji, K.K. (2005). Sustainability of irrigated agriculture in the San Joaquin Valley, California. *Proceedings of the National academy of science of the United States of America* 102 (43), 15352-15356.

Seager, W.R., Hawley, J.W., Kottolowski, F.E. and Kelley, S.A. (1987). Geology of east half of Las Cruces and northeast El Paso 1^0 x 2^0 sheets, New Mexico, New Mexico, Bureau of Mines & Mineral Resources, Geologic Map 57.

Selleck, B. and Baran, J. (2003) Petrology and stable isotope geochemistry of Holocene and

Pleistocene calcite cement in kame terrace gravel, central New York State. *Northeastern Geology and Environmental Science* 25(3), 186-196

Serna-Perez, A., Monger, H.C., Herrick, J.E. and Murray, L., 2006. Carbon dioxide emissions from exhumed petrocalcic horizons. *Soil Science Society of America Journal* 70(3), 795-805.

Sharp, W.D., Ludwig, K.R., Chadwick, O.A., Amundson, R., Glaser, L.L. (2003). Dating fluvial terraces by the ^{230}Th/U on pedogenic carbonate, Wind River Basin, Wyoming. *Quaternary Research* 59, 139–150.

Sims K.W.W., Gill, J.B., Dosseto, A., Hoffmann, D.L., Lundstrom, C.C., Williams, R.W., Ball, L., Tollstrup, D., Turner, S., Pyrtulak, J., Glessner, J.G., Standish, J.J., Elliott, T. (2008). An Inter-Laboratory Assessment of the Thorium Isotopic Composition of Synthetic and Rock Reference Materials. *Geostandards and Geoanalytical Research* 32(1), 65-91.

Suarez, D. L. (2000). Impact of Agriculture on CO_2 as Affected by Changes in Inorganic Carbon', in Lal, R., Kimble, J. M., Eswaran, H., and Stewart, B. A. (eds.), Global Climate Change and Pedogenic Carbonates, CRC/Lewis Publishers, Boca Raton, FL, 257–272.

Szykiewicz, A., Wither, J., Modelska, M., Borrok, D.M., Pratt, LM. (2011). Anthropogenic sulfate loads in the Rio Grande, New Mexico (USA). *Chemical Geology* 283, 194-209.

Szynkiewicz, A., Borrok, D.M., Skrzypek, G., Rearick, MS. (2015). Isotopic studies of the Upper and Middle Rio Grande.Part1-Importance of sulfide weathering in the riverine sulfate budget. *Chemical Geology* 411, 323-335.

UNCCD. (2000). Assessment of the status of land degradation in arid, semi-arid and dry sub-humid areas. United Nations Convention to Combat Desertification, Bonn.

Vigier, N., Bourdon B., Turner S., Allegre, C.J. (2001). Erosion timescales derived from U-decay series measurements in rivers. *Earth and Planetary Science Letters* 193, 485–499.

Violette, A., Riotte, J., Braun, J., Oliva, P., Marechal, J., Sekhar, M., Jeandel, C., Subramanian, S., Prunier, J., Barbiero, L. and Dupre, B. (2010). Formation and preservation of pedogenic carbonates in Southern Indian, links with paleo-monsoon and pedological conditions: Clues from Sr isotopes, U-Th series and REEs. *Geochimica et Cosmochimica Acta* 74, 7059-7085.

Vogel, J.S., Southen, J.R., Nelson, D.E., Brown, T.A. (1984). Performance of catalytically condensed carbon for use in accelerator mass spectrometry. *Nuclear Instruments and Methods* 223, 289-293.

Wainwright, J. (2006). Climate and climatological variations in the Jornada Basin. In: Havstad K, Huenneke L, Schlesinger W (eds) Structure and function of the Chihuahuan Desert ecosystem. Oxford University Press, Oxford, 44–80

Wang, Y., Amundson, R., Trumbore, S. (1996). Radiocarbon dating of soil organic matter. *Quaternary Research 45*(3), 282-288.

Wang, L, D'Odorico, P., Evans, J.P., Eldridge, D.J., McCabe, M.F., Caylor, K.K., King, E.G. (2012). Dryland ecohydrology and climate change: critical issues and technical advances. *Hydrology and Earth System Sciences* 16, 2585-2603.

Wohlfahrt, G., Fenstermaker, L.F., Arnone, J.A. (2008). Large annual net ecosystem CO_2 uptake of a Mojave Desert ecosystem. *Global Change Biology* 14, 1475–1487.

Xie J., Li Y., Zhai C., Li C., Lan Z. (2009): CO_2 absorption by alkaline soils and its implication to the global carbon cycle. *Environmental Geology* 56, 953-961.

Table 1.1: Mineralogy, carbon contents, major element, U-series isotope concentrations and activity ratios, and calculated U-series ages for pedogenic carbonate in Alfalfa and Jornada (JPT1 and JPT 2) samples

Sample name	**Depth**	**Calcite/ Quartz[a]**	**SC**	**SOC**	**SIC[b]**	**CaO**	**U[c]**	**Th[c]**	**$(^{234}U/^{238}U)^{c}_{bulk}$**	**$(^{230}Th/^{238}U)^{c}_{bulk}$**	**$(^{234}U/^{238}U)_{initial}$**	**$CaCO_3$ Age (U-series dating)[d]**	**Average carbonate ages in profile**	**Accumulation rate of pedogenic carbonate (gCaCO3 m^{-2} yr^{-1})**	**$CaCO_3$ Age (^{14}C dating)**
	(cm)		(wt%)	(wt%)	(wt%)	(wt%)	ppm	ppm				(ka)	(ka)		(ka)
Alfalfa samples															
0-3cm	1.5	0.23	1.67	0.82	0.85	4.83	2.31	8.09	1.01	1.21	1.49±0.06	15±17	7.3±5.0	9±6	
10-13cm	11.5	0.16	1.48	0.57	0.91	4.93	2.53	9.58	1.00	1.03	1.52±0.08	6.5±8.7			
20-23cm	21.5	0.33	1.38	0.49	0.89	4.79	2.33	7.66	1.01	1.08	1.59±0.11	9.1±8.6			
30-33cm	31.5	0.18	1.33	0.50	0.83	4.69	2.45	8.07	1.00	1.04	1.32±0.14	5.1 ±5.7			
40-43cm	41.5	0.22	1.31	0.39	0.93	5.35	2.46	7.73	1.00	1.08	1.47±0.06	2.2 ±1.7			6.54±0.03
50-53cm	51.5	0.16	0.94	0.18	0.76	4.45	2.12	6.58	0.98	0.75	1.25±0.09	2.9±1.9			
60-63cm	61.5	0.10	0.57	0.07	0.50	2.87	1.94	6.24	0.97	1.00	1.23±0.24	22.2±8.1			
JPTI samples															
0-10cm	5.0	0.36	2.96	0.42	2.54	12.75	1.94	8.91	0.95	1.23	1.89±0.51	44±32	28±11	3.5±1.5	
10-15cm	12.5	0.40	3.52	0.52	2.99	13.89	2.04	6.41	0.97	1.21	1.50±0.09	17.1±6			
15-20cm	17.5	0.85	4.94	0.48	4.45	20.29	1.89	6.17	1.00	1.20	1.46±0.09	30±11			
25-30cm	27.5	0.81	4.37	0.49	3.88	20.07	1.95	6.40	1.00	1.19	1.64±0.13	14.5±6.8			
40cm	40.0	3.99	9.11	0.38	8.73	45.57	1.14	2.35	1.18	0.92	1.40±0.11	117±26			
JPTII samples															
0-7cm	3.5	0.35	1.51	0.41	1.10	9.92	1.95	8.72	0.96	1.54	1.38±0.09	68±110	34±14	2.5±1.0	
7-10cm	8.5	0.39	2.60	0.57	2.03	15.69	1.76	6.32	0.97	1.18	1.03±0.06	29±13			
27-30cm	28.5	0.52	2.43	0.59	1.84	13.80	1.95	6.10	0.99	1.18	1.50±0.08	19.5±7.5			8.36±0.03
37-40cm	38.5	0.44	2.64	0.78	1.86	14.73	1.84	7.00	0.99	1.18	1.40±0.07	50±21			
48cm	48.0	2.72	5.82	0.43	5.39	46.2	1.30	1.56	1.30	0.75	1.32±0.08	100±40			

a: XRD Maximum intensity peak ratio of calcite (29.42^0)to quartz (26.65^0)

b: Calculated SIC =SC-SOC

c: Uncertainty for U and Th concentrations and ($^{234}U/^{238}U$) and ($^{230}Th/^{238}U$) is 1%

d: See appendix table and figures for detailed U-series age calculation in pedogenic carbonates

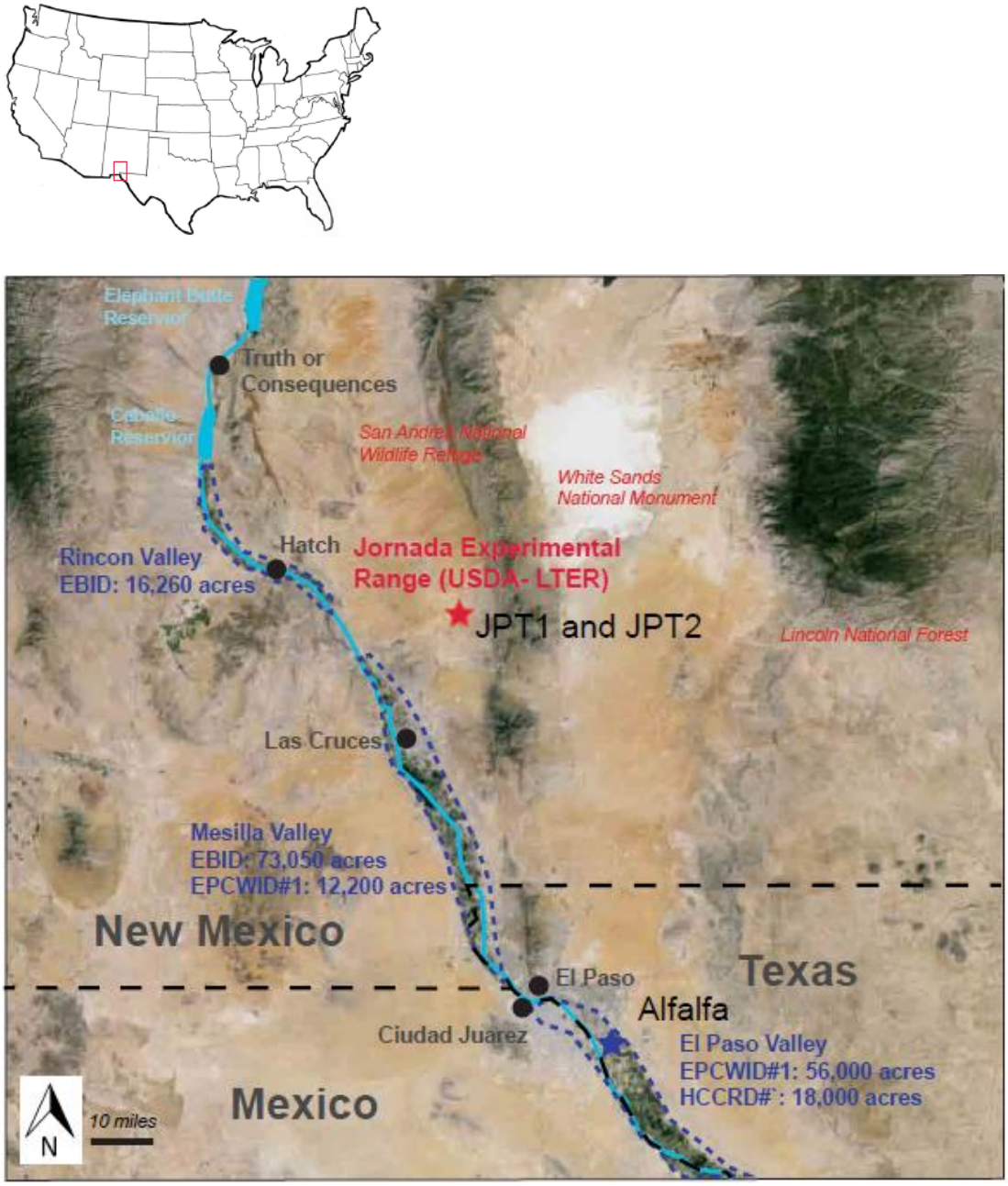

Figure 1.1: Location map showing the studied soil sites: 1) near El Paso, TX (alfalfa, blue star), and 2) the Jornada Experimental Range (USDA-LTER) in New Mexico (JPT1 and JPT2, red star).

The irrigation districts along the Rio Grande valley and the total acreage of the irrigated drylands in this region are also shown. EBID: Elephant Butte Irrigation District; EPCWID: El Paso County Water Improvement District; HCCRD: Hudspeth County Conservation and Reclamation District. (www.ebid-nm.org; www.epcwid1.org)

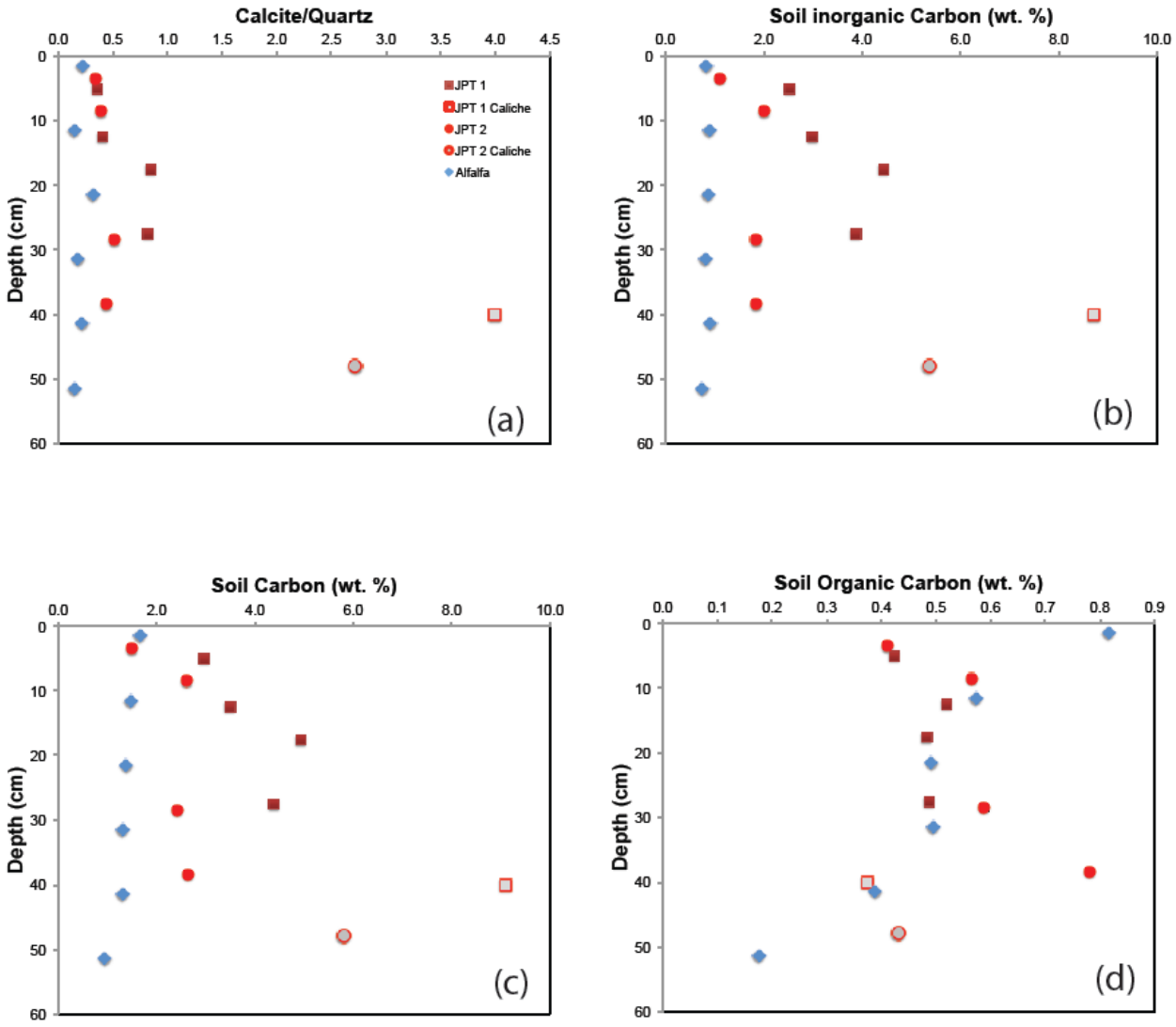

Figure 1.2: a) Measured calcite/quartz ratios; b) soil inorganic carbon contents; c) soil total carbon contents; and soil organic carbon contents in bulk soil samples from Alfalfa (El Paso, TX) and JPT 1 and JPT2 (Jornada Basin, NM).

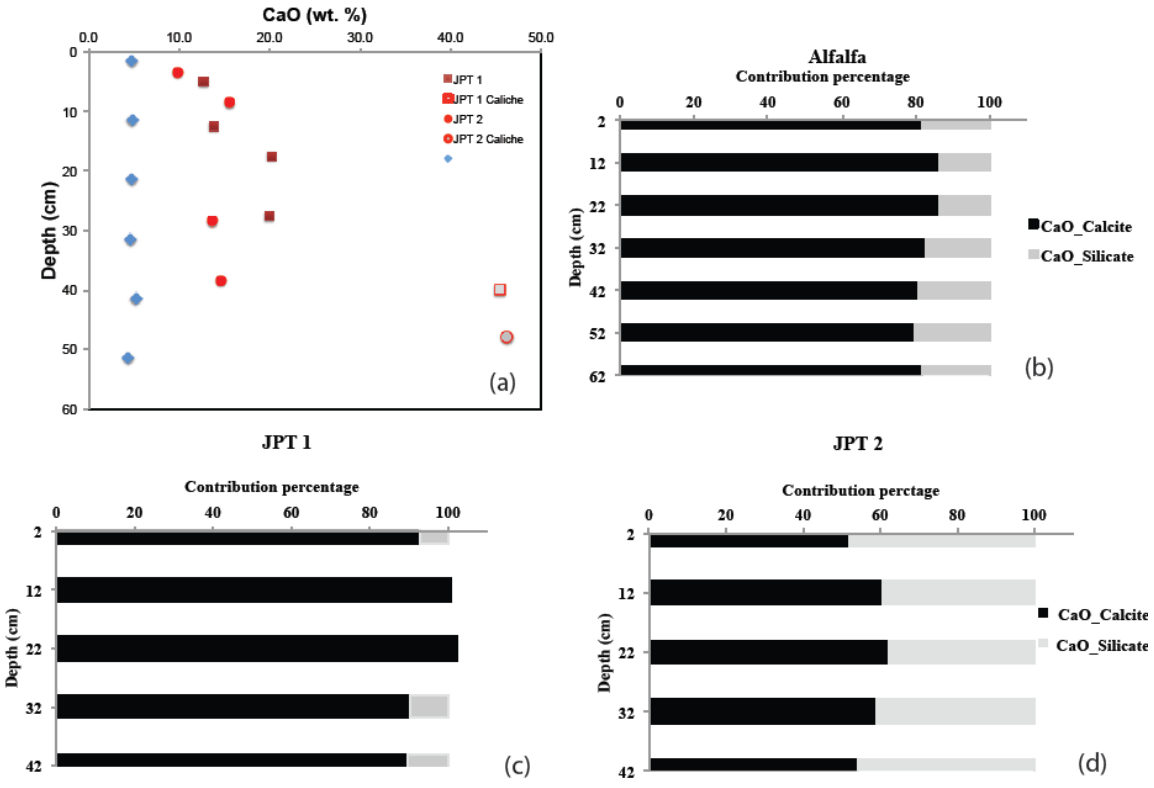

Figure 1.3: a) Measured CaO contents (wt%) in bulk samples from Alfalfa (El Paso, TX) and JPT 1 and JPT2 (Jornada Basin, NM); b) Contribution percentage of CaO from calcite vs silicates in Alfalfa soils; c) and d) Contribution percentage of CaO from calcite vs silicates in Jornada soils.

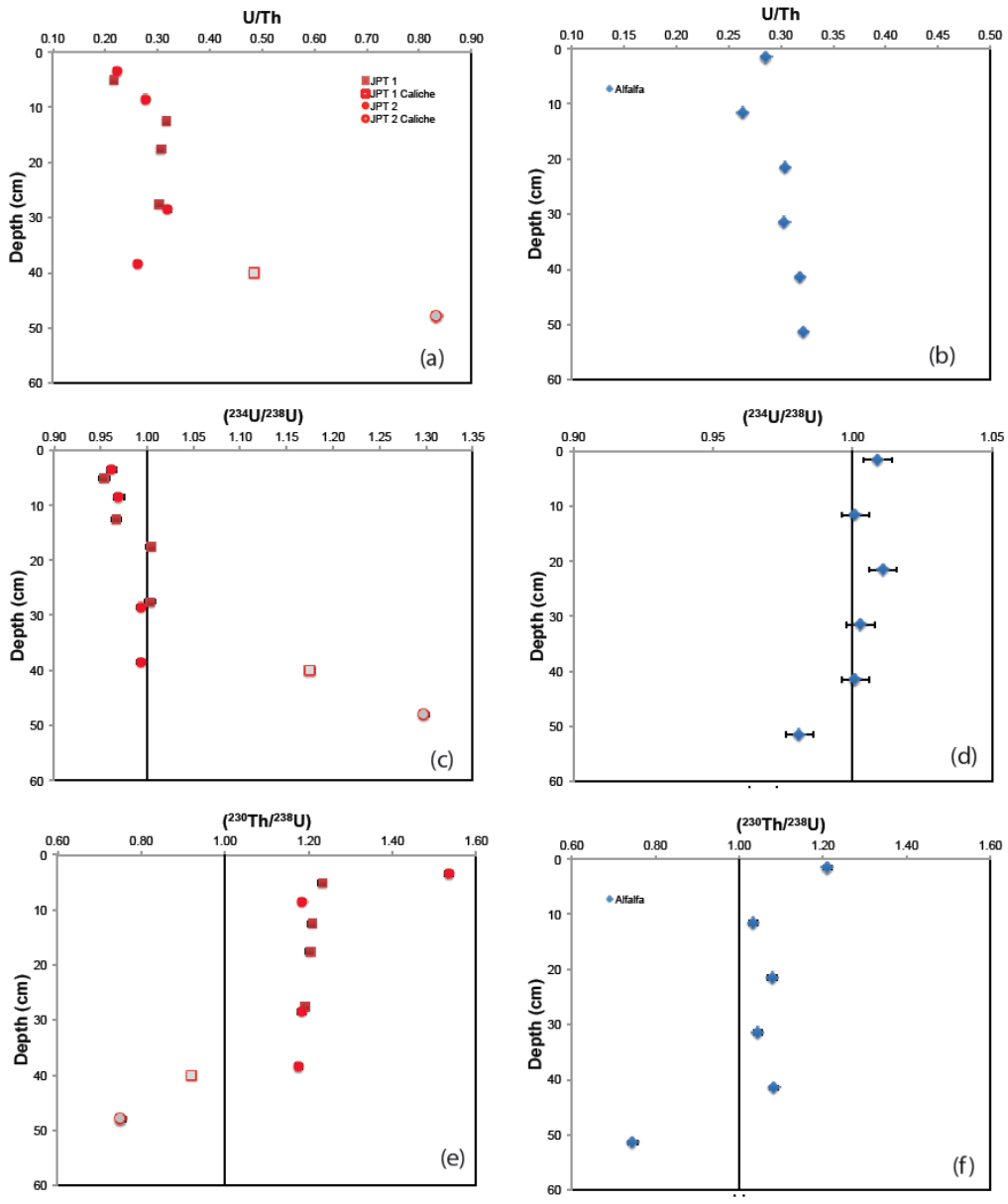

Figure 1.4: Measured U/Th element ratios, ($^{234}U/^{238}U$) and ($^{230}Th/^{238}U$) activity ratio in bulk soil samples and caliche samples from Alfalfa (El Paso, TX) and JPT 1 and JPT2 (Jornada Basin, NM).

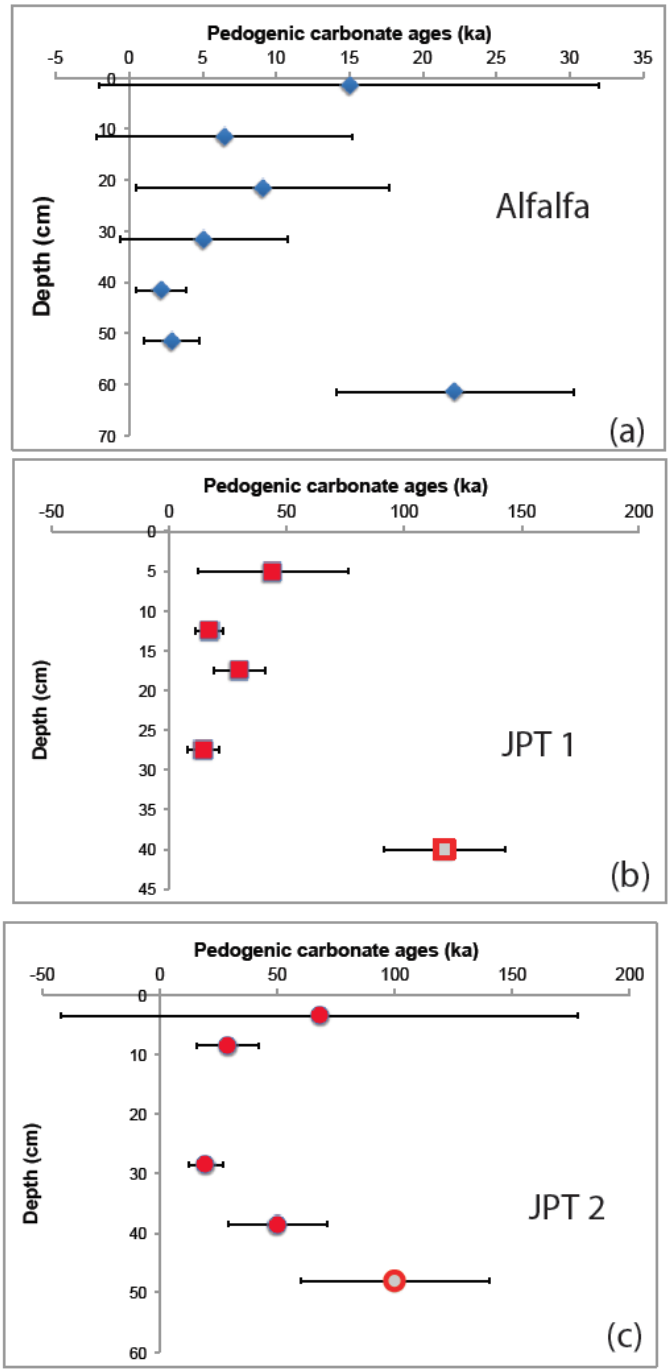

Figure 1.5: Calculated U-series ages for pedogenic carbonates in bulk soils from Alfalfa (El Paso, TX) and for pedogenic carbonates in bulk soils (closed symbols) and in hardpan caliche (open symbols) in JPT 1 and JPT2 (Jornada Basin, NM).

Chapter 3

Paleo-environmental conditions of the Jornada Basin, New Mexico: insight from U and SR isotopes in pedogenic carbonates at the La Mesa geomorphic surface

Syprose Nyachoti[1*], Lin Ma[1],Thomas E. Gill[1], and Curtis Monger[2]

[1]Department of Geological Sciences, University of Texas at El Paso, El Paso, TX 79968,
*sknyachoti@miners.utep.edu

[2]Department of Plant and Environmental Sciences, New Mexico State University, Las Cruces, NM 88003

3.1 Abstract

In this chapter we explored the application of U isotopes in pedogenic carbonates, in combination with more traditional Sr and C isotopes, as paleo-environmental tracers. In a thick petrocalcic horizon of the La Mesa geomorphic surface soils within the Jornada Basin (New Mexico, USA), we determined: (1) Ca and C sources in the carbonates using Sr and $\delta^{13}C_{OC}$ and $\delta^{13}C_{CaCO3}$ isotopes, (2) estimated pedo-carbonate U-series ages and associated initial U activity ratios $(^{234}U/^{238})_0$. Major element concentrations, U and Sr isotope compositions were also determined in modern dust and bulk soils collected from the study area. The $\delta^{13}C_{CaCO3}$ isotopes suggest the carbonates at the Jornada Basin are of pedogenic origin. While soluble fractions of shallow carbonates within the profile indicated $^{87}Sr/^{86}Sr$ ratios of 0.7086–0.7091, similar to those of local modern dust, carbonates at depth indicated more radiogenic $^{87}Sr/^{86}Sr$ ratios of 0.7112. This suggests that atmospheric dust sources were significant Ca and Sr contributors to the shallow carbonates while carbonates at depth had a different source of Ca. The pedo-carbonate U-series ages range between ~200 ka and 6 ka and decrease towards the soil surface, despite

large uncertainties. Pedogenic carbonates are influenced by overprinting, dissolution and re-precipitation processes; therefore, these U-series ages presented here should be considered as an average timescale of cumulative climatic record. High $(^{234}U/^{238}U)_0$ ratios averaging at 1.41 in shallower carbonates suggest drier climate during their formation as opposed to lower $(^{234}U/^{238}U)_0$ ratios averaging at 1.12 in carbonates at depth, which formed in more moist environments in the past. Increase of $\delta^{13}C_{OC}$ isotopes from pedo-carbonates at depth to shallower carbonates suggests a change of vegetation (from C3 to C4 plants) through time depending on moisture availability. Consistent with low $(^{234}U/^{238}U)_0$ ratios, lighter $\delta^{13}C_{OC}$ isotopes in pedogenic carbonates at depth imply existence of C3 plants, which thrive in wetter environments. Heavier $\delta^{13}C_{OC}$ isotopes in shallower carbonates suggest existence of C4 plants that grow in warmer and drier conditions. Similarly, coinciding of $^{87}Sr/^{86}Sr$ ratios in shallow carbonates and modern dust suggests formation of these carbonates in less moist environment unlike the carbonates at depth. In addition to traditional C and Sr isotopes of pedogenic carbonates that have long been used to study paleo-environmental conditions, this study provides a new isotope system (U-series) that can be used to reconstruct paleo-moisture conditions and carbonate formation timescales for soil carbonates in desert environments.

3.2 Introduction

Formation of carbonates in Bk or K horizons of soil profiles is dependent on soil moisture availability, calcium and carbon fluxes (Machette, 1985; Tanner, 2010). In the presence of soil water and CO_2, bicarbonate and calcium ions are leached down the soil profile and precipitate carbonates at depth (Lal and Kimble, 2000a; Monger et al., 2015). Pedogenic carbonates form progressively into various morphological stages in a range of climatic zones (e.g. sub-humid and temperate climate areas; Gile et al., 1981; Sobecki and Wilding 1983;

Machette, 1985), but their dominant presence in soils generally signifies low annual rainfall environments, characteristic of semi-arid to arid climate (Birkeland, 1999; Eswaran et al., 2000; Monger et al., 2006; Violette et al., 2010).

In the soils of the Jornada Basin, pedogenic carbonates have previously been associated with atmospheric sources such as carbonate dust and/or dissolved Ca^{2+} (Gile and Grossman, 1979; Gile et al., 1981; Monger and Gallegos, 2000; Dart et al., 2012; McFadden, 2013). Biotic (e.g. role of microorganisms, plant roots, and animals) and abiotic (e.g. weathering of silicate and carbonate rocks) processes have also added carbonates into soils (Jaillard et al., 1991; Liu et al., 2007; Monger et al., 2009, 2015; Verreechia et al., 2011). Calcified root hairs, termite galleries, and communities/cultures of some microorganisms in soils provide evidence for the role of plants, termites, and microorganisms in pedogenic carbonate production (Monger, 2002; Liu et al., 2007; Mujinya et al., 2011). Silicate and carbonate weathering processes on earth systems result in sequestration of carbonates in arid to semiarid soils and groundwaters (Monger et al., 2015). The dissolved Ca^{2+} and DIC in groundwater could precipitate in soils following groundwater upwelling processes (Monger et al., 2015; Mack et al., 2012). Precise information on soil water, calcium pathways and carbon sequestration potential aids in understanding the sources, kinetics and formation mechanisms of pedogenic carbonates in non-calcareous soils (Mack et al., 2012; Monger et al., 2015). This information is also necessary in interpretation of paleo-environmental conditions during formation of pedogenic carbonates.

Pedogenic carbonates have extensively been studied to reconstruct precipitation, vegetation types, atmospheric circulation patterns, temperatures, and atmospheric pCO_2 in the geological past (Cerling and Quade, 1993; Retallack, 1994, 2005; Caudill et al., 1996; Monger et al., 1998; Ekart et al., 1999; Alonso-Zarza, 2003; Dworkin et al., 2005). Increasing drought,

desertification and population growth in drylands under projected future climate changes have enhanced the need to understand water demands and budgets in ecosystem functions and land-surface dynamics. Therefore, reconstructed Quaternary climatic information from pedogenic carbonates in drylands could aid in modeling of earth system response to future climatic oscillations.

Pedogenic carbonates are suitable paleoclimate indicators because they accumulate in soils over long periods of geologic time scales and record information of different climatic regimes. Stable isotope compositions (C and O) in pedogenic carbonates as well as depths of their occurrence within the soil profile have revealed useful information on rainfall quantities, moisture sources, temperatures, and vegetation types that prevailed during their formation (Cerling, 1984; Mack et al., 1994; Retallack, 1994; 2005; Buck and Monger, 1999; Duetz et al., 2002; Monger et al., 2009; Candy, 2002). For example, the carbon incorporated in the carbonates can be traced back to paleosoil CO_2 thus reflecting types of soil organic matter and changes in vegetation over time (Quade and Cerling, 1995; Cerling, 1999; Rao et al., 2007; Catoni et al., 2011). There are a few challenges associated with using C and O isotopes in pedogenic carbonates as paleoclimate indicators. For instance erosion of soil profiles, sediment compaction, burial diagenesis, evaporation of soil pore water, impermeability of older plugged horizons, imprinting of carbonates, and soil order and permeability properties may influence the depth ages, and stable isotopic composition of carbonates and therefore paleoclimatic interpretation (Driese and Mora, 1993; Royer, 1999; Tabor et al., 2006; Nordt et al., 2006; Durand et al., 2007). Despite these challenges, pedogenic carbonates fill a paleoclimatic proxy void in areas where other recording systems are absent. Uranium co-precipitated with calcium in pedogenic carbonates and its isotopes could be used to rebuild paleo-environmental conditions. Carbonates

record the initial uranium isotopic composition dissolved in soil water used in their formation; these uranium isotopic compositions are useful in reconstructing relative paleo-moisture thus paleo-rainfall quantities (Robinson et al., 2004a; Oster et al., 2012; Maher et al., 2014).

Soils of the Jornada Basin, New Mexico, USA contain pedogenic carbonates of different morphological stages (Gile et al., 1981). Within the Jornada Experimental Range, soils of the La Mesa geomorphic surface contain mature stage V pedogenic carbonates (Gile, 2002). Similar to other mature petrocalcic horizons in aridisols, these carbonates contain information about past climate (Brock and Buck 2009). They are therefore suitable for investigating climatic changes through time in this region. In this study we combined C, Sr, and U isotopes to determine controls and rates of pedogenic carbonate accumulation at the La Mesa geomorphic surface in the Jornada Basin, and reconstructed paleo-environmental conditions during the Quartenary period.

3.3 Background information

3.3.1 SOURCES OF PEDOGENIC CARBONATES IN SOILS

Strontium isotopes ($^{87}Sr/^{86}Sr$) in pedogenic carbonates of arid and semiarid soils have been widely used as a tracer of Ca sources (Capo et al., 1998; Capo and Chadwick, 1999; Chiquet et al., 1999; Naiman et al., 2000; Van Der Hoven and Quade, 2002). This is because Sr behaves geochemically as Ca and substitutes it in Ca-bearing mineral crystals such as pedogenic carbonates. $^{87}Sr/^{86}Sr$ ratios show minimal fractionation in surface and subsurface processes, reflecting the Sr signature of source material (Capo et al., 1998, Capo and Chadwick, 1999, Paces and Wurster 2014). Indeed, the $^{87}Sr/^{86}Sr$ ratios in carbonate deposits such as speleothems have been found to remain unchanged for thousands of years because of their low Rb/Sr ratios and much longer halflife of ^{87}Rb (Frumkin and Stein, 2004).

Sources of carbon incorporated in the pedogenic carbonates can be traced using stable carbon isotopes. This is because various carbon reservoirs in the surface and near surface environments have distinct carbon isotope compositions. For example, the $\delta^{13}C_{CO2}$ values in atmospheric range from -6‰ to -8‰ (Mermut et al., 2000), marine carbonates have $\delta^{13}C$ values near 0‰ (West et al., 1988), and soil CO_2 show variant $\delta^{13}C$ values depending on prevailing vegetation type (Cerling, 1999). Stable carbon isotopes in pedogenic carbonates are characteristic of soil CO_2 dissolved in soil water from which they initially precipitated (Buck and Monger, 1999). Soil CO_2 is produced through biological processes (such as organic matter decomposition and plant root respiration) and diffuses to atmosphere at the land-atmosphere interface (Nortdt et al., 1996; Mermut et al., 2000). The $\delta^{13}C$ of soil gas CO_2 depend on the vegetative photosynthesis pathway: C4 plants results in enriched $\delta^{13}C$ values (-10 to -14‰) compared to C3 plants (-20 to -35‰) (Cerling, 1999; O'Leary, 1981; Nord et al., 1996; Monger et al., 1998; Buck and Monger, 1999; Mermut et al., 2000; Kraimer and Monger, 2009). Proportions of C3 and C4 vary depending on prevailing climatic conditions (Rao et al., 2007; Zhou and Chafetz, 2010). In addition to C4 plants (e.g. grasslands) and C3 plants (e.g. shrubs), CAM plants (e.g. Cacti) are commonly at the Jornada Basin; their $\delta^{13}C$ values range between the values between C4 and C3 plants. Establishing the paleo-vegetation as recorded in pedogenic carbonates aid in inferring paleo-environmental conditions at the time of carbonate formation.

3.3.2 U-SERIES ISOTOPES IN PEDOGENIC CARBONATES AS A DATING TOOL AND PALEO-RAINFALL/ MOISTURE INDICATOR

Uranium occurs naturally in rocks and is released into soil water systems through weathering and external sources such as transported dust. The solubility of uranium depends on the redox conditions of the environment; for instance under oxic conditions (e.g. surface and near surface environment), U^{6+} is more soluble than U^{4+}, which dominates in reducing environments

(Chabaux et al., 2003). Uranium has three naturally occurring isotopes: ^{238}U ($t_{1/2}$ = 4.46 Gy), ^{235}U ($t_{1/2}$ = 700 Ma) and ^{234}U ($t_{1/2}$= 248 kys) (Cheng et al., 2000). The ^{234}U is naturally of low abundance, produced through alpha decay of ^{238}U via two short lived daughters (^{234}Pa ($t_{1/2}$ = 1.18minute); ^{234}Th ($t_{1/2}$ = 24.1days). Alpha recoil processes control the release of ^{234}U into water systems (Chabaux et al., 2003; Robinson et al., 2004a). During this process, ^{234}U is preferentially released from rock into water systems in two ways depending on the position of ^{238}U relative to the mineral surface; (1) indirectly through release of ^{234}Th which later decays to ^{234}U, and (2) direct release of ^{234}U from alpha recoil tracks (Fleischer, 1980). For this reason, water systems become enriched with ^{234}U indicating activity ratios ($^{234}U/^{238}U$) (here after parenthesis refer to activity ratios) greater than 1 while the weathered rock remains depleted of ^{234}U. Activity refers to the product of the decay constant (λ) and the number of radionuclei (N) (e.g. activity = $\lambda_{238}N_{238}$). When the activity of a daughter nucleus is equal to that of the parent, their ratio is equal to 1 (e.g. ($^{234}U/^{238}U$) = 1). Such a system is considered to be in secular equilibrium and can be observed in old unweathred rocks (~1Ma) within a closed system (Bourdon et al., 2003).

Secondary minerals that precipitate from soil waters such as pedogenic carbonates inherit the dissolved ($^{234}U/^{238}U$) ratios from soil waters, which are usually greater than one (disequilibrium) (Chabaux et al., 2003). Over time as the pedogenic carbonates age, excess ^{234}U decay to ^{230}Th approaching secular equilibrium values. The decay towards equilibrium allows for U-series dating technique and calculation of the initial uranium activity ratios (hereafter abbreviated as ($^{234}U/^{238}U$) $_0$) in soil water from which the carbonates formed. Determining ages of pedogenic carbonates using the U-series dating technique requires correction for detrital U and Th, which contaminate carbonates during precipitation (Ludwig, 2003). Isochron and single

sample detrital correction techniques are commonly employed in order to get detrital-free ($^{230}Th/^{238}U$) and ($^{234}U/^{238}U$) activity ratios required in age calculation (Ludwig, 2003).

The ($^{234}U/^{238}U$) in soil water are controlled by a number of factors including U distribution in parent material and alpha recoil processes due to open system behavior as well as dust composition and grain size (Oster et al., 2012). Soil water in arid soils is mainly supplied by rainfall; variations in annual precipitation regulate the ($^{234}U/^{238}U$) in soil water and consequently ($^{234}U/^{238}U$) in secondary minerals such as pedogenic carbonates (Oster et al., 2012). Assuming constant evaporation rates, high rainfall results into low ($^{234}U/^{238}U$) in soil waters due to complete rock dissolution, thus reduced selective loss of ^{234}U. Low rainfall, on the other hand results to high ($^{234}U/^{238}U$) in soil waters due to preferential release of ^{234}U into weathering fluids by enhanced alpha recoils. The calculated ($^{234}U/^{238}U$) in pedogenic carbonates could be a potential proxy for paleo-precipitation in the southwest USA and other arid and semi-arid regions.

3.4 Methods

3.4.1 SITE DESCRIPTION

The Jornada Basin is an intermontane basin east of the Rio Grande River in the southeastern Basin and Range province of New Mexico, USA. The Basin is surrounded by north-south trending block faulted mountains (San Andres and Organ) on the east and Dona Ana and Caballo Mountains to the west (Figure 2.1); these mountains formed during the Rio Grande rift tectonic events in the mid-Tertiary (Seager et al., 1984; Mack et al., 1998; Hawley, 1981). Common rocks on the mountain ranges include Palezoic sedimentary rocks (mainly fosilliferous limestones, sandstone, and shale) and Precambrian metamorphic rocks intruded by Tertiary volcanic and plutonic rocks (Mack et al., 1998; Monger et al., 2006). Exposed rocks on the

mountain flanks are eroded and washed downslope filling the basin floor; these mountaneous alluvium overlay the Pliocene-Pleistocene river sediments (Mack et al., 1993). The Jornada Basin is part of the Chihuahuan desert. According to the National Climatic Data Center between 1981 and 2010, the area received an annual average precipitation of ~ 29 cm about half of which falls during the summer North American Monsoon and winter storms originating from the Pacific Ocean (Wainwright, 2006). Mean annual temperatures of about 15^0C and high evaporation rates (~220 cm/yr) are recorded at the basin; however, during summer mean maximum daily temperatures rise to 25^0C (Gile and Grossman, 1979; Gile et al., 1981).

Our sampling sites are located in the Jornada Experimental Range (JER) within the basin floor (Figure 2.1). The La Mesa geomorphic surface within JER (referred to as La Mesa_JER) is the oldest surface overlying fluvial sediments that were deposited between 5-0.8 Ma, when the ancestral Rio Grande ran through the Jornada Basin (Gile et al., 1981; Mack et al., 2006; 2012). Fluvial sediments underlying the La Mesa surface belong to mainly the Camp Rice Formation consisting of materials ranging from conglomerate to mudstones derived from upstream (Mack et al., 1993). The La Mesa geomorphic surface occurs on an alluvial plain, which is heavily wind eroded indicating deflation and depositional features oriented in the prevailing west-southwest wind direction (Monger et al., 2006). The geomorphic surface is estimated to be of late Pliocene to middle Pleistocene in age (Gile et al., 1981; Gile, 2002); its soils that contain stage V pedogenic carbonates are estimated to be about 1.6 Ma (Mack et al., 1993; 1996). The Camp Rice Formation constitutes the parent material of soils at the La Mesa geomorphic surface (Mack et al., 1993). Similar to soil petrocalcic horizons on the Upper and Lower La Mesa geomorphic surface at the Mesilla Basin, these mature carbonates have been associated to wet and dry

atmospheric deposition processes since fluvial Camp Rice Formation sediments contain minimal carbonates (<1% $CaCO_3$) (Gile et al., 1981; Capo and Chadwick, 1999).

The Jornada Basin and its desert environs have been considered significant dust sources in the North America (Monger, 2006; Rivera Rivera et al., 2010). Though sources of aeolian sediments may vary depending on soil moisture, wind speed, threshold wind velocity, and land surface type (Gillete, 1999), previous works have considered playas, bare (unvegetated) soils, and agricultural soils significant dust sources within the Chihuahua desert (Gillette and Chen, 2001; Rivera Rivera et al., 2010). Aeolian sediment production and transport in relation to the prevailing vegetation communities at JER have been previously investigated (Bergametti and Gillette, 2010; Floyd and Gill, 2011; Alvarez et al., 2012). Vegetation at the Chihuahua desert including JER has gradually transformed over the past ~20,000 kys to recent 100 yrs from grassland to shrubland dominated plant communities probably due to climate changes and land uses (Van Devender, 1995; Monger, 2003; Snyder and Tartowski, 2006; Weems and Monger, 2012). Current plant communities at JER include five major vegetation types: mesquite (*Prosopis glandulosa*), tarbush (*Flourensia cernua),* black grama grass (*Bouteloua eriopoda*), creosotebush (*Larrea tridentata*), and playa grasslands (Gibbens et al., 2005; Bergametti and Gillette, 2010). Areas dominated by mesquite shrubs were reported to contribute the highest aeolian sediment fluxes by Bergametti and Gillette (2010). Aeolian dust samples collected from areas dominated by tarbush, mesquite, grassland, and playa in 2005-2006 (Floyd and Gill, 2011), are investigated in this study (Figure 2.1).

Regions dominated by mesquite (sites M-Well and M-Rabb) and grama grass (G-IBPE) occur on alluvial plains of the Jornada geomorphic surface. As indicated earlier this is a wind-worked zone and surface soils are mainly sandy (Monger et al., 2006; Bergametti and Gillette,

2010; Floyd and Gill, 2011). The area dominated with tarbush vegetation occurs on alluvial flats covered with silty-clayey surface soils (Bergametti and Gillette, 2010). Grain sizes of aeolian sediments emitted from this area (sites T-East and T-Tyl samples) were greater than 50 μm (sand-sized) on the ground surface to ≤ 20 cm above ground, but finer for samples collected at 50-100 cm heights (Floyd and Gill, 2011). Topographically, small playas within the Jornada Basin occur on alluvial flats with silty-clayey surface soils (Bergametti and Gillette, 2010). Dust emitted within the playa sites (P-Tobo and P-Coli samples, Figure 2.1) indicated abundant finer particles at equivalent heights compared to dust collected from grassland, mesquite, and some tarbush vegetation dominated areas (Floyd and Gill, 2011).

3.4.2 SOIL PROFILE DESCRIPTION

A soil profile in a pre-excavated trench at La Mesa geomorphic surface within the Jornada Basin (La Mesa_JER) was sampled for this study. The topsoil consists of unconsolidated sandy-loamy sediments, which are underlain by stage V pedogenic carbonates (Robins et al., 2015). The boundary of the topsoil and petrocalcic layer is irregular (Figure 2.2). The sharp boundary is characterized by brittle to massively indurated, smooth micritic carbonate laminae (Robins et al., 2015). The topsoil contains filament (root-like structures) of stage I carbonates, a soil sample (H1) was collected at ~40 cm depth below ground surface. Previous studies have shown that the hard pan underlying the young alluvium in the La Mesa_JER show evidence of pedofeatures (e.g. ooids and pisoids), brecciation, dissolution pipes, and insignificant erosion (Robins et al., 2015). On a vertical profile, two caliche samples at 60 cm (H2) and 200 cm (H3) depths from ground surface were sampled for analysis (Figure 2.2). In some cases, the upper soil horizon is pierced into the petrocalcic horizon indicating possible surficial disturbance by erosion, sedimentation, or rooting and bioturbation. For instance, approximately 3 m laterally

away from H2 the profile is shallower with the lower boundary of the topsoil lower than H2 (Figure 2.2). A caliche sample (H4) right along this boundary was collected to test the lateral variability of the pedogenic carbonates.

3.4.3 SOIL AND CALICHE SAMPLE PREPARATION

The soil sample (H1) was air-dried and pulverized to pass through 100μm sieve. Hand samples of H2, H3, and H4 were saw-cut to expose a fresher surface then drilled along different lamina (Figure 2.3). The lamina are thought to have formed from infiltrating soil waters which are impaired from draining down the soil profile due to underlying plugged horizons (Gile et al., 1981). Three laminae in each caliche hand sample were sampled and labeled as A, B, and C, where A is bottommost while C is the upper or outermost laminae. Assuming new growth of pedogenic carbonates on top of old units, lamina A is expected to have deposited earlier than lamina B which in turn is anticipated to be older than lamina C. Approximately 100 mg of the drilled samples along each lamina of all caliche samples were separately homogenized and stored in plastic bags.

3.4.4 DUST SAMPLE COLLECTION AND PREPARATION

Modern dust samples collected from the Jornada Basin between 2005 and 2006 were investigated in this study (Figure 2.1); details of dust collection criteria were discussed in the works of Bergametti and Gillette, (2010) and Floyd and Gill, (2011). Briefly, at least five Big Spring Number Eight (BSNE) dust samplers at 5, 10, 20, 50, and 100 cm above ground were placed on towers at various sites at the Jornada Experimental Range. Sample sites were chosen based on the dominant vegetation and the need to assess the effect of vegetation on dust mass fluxes (Bergametti and Gillette, (2010). Labels of dust samples therefore, were based on the

dominant vegetation at the sampling spot (Bergametti and Gillette, 2010; Floyd and Gill, 2011). Based on proximity to the La Mesa soil profile, only dust samples from seven sites collected above the saltation zone (50 and 100 cm) were considered due to the likelihood of farther transport distance. The dust- sized particles (≤50μm) would dissolve completely in strong acids; therefore, only visible organic materials (e.g. leaves) were removed before sample weighing.

3.4.5 LABORATORY ANALYTICAL PROCEDURES

Major and trace element concentrations, Sr and U-series isotope analyses were conducted on dust, soils, and caliche/pedogenic carbonate samples from the La Mesa_JER as described below. Using the measured U-series isotope, carbonate ages and initial uranium activity ratios were calculated. The soil sample (H1) and some caliche samples (H2A, H2C, H3C, and H3A) were sent to the Jozef Stefan Institute of Slovenia for carbon isotope analysis.

3.4.5.1 Elemental chemistry in dust

Major and minor element concentrations of dust were measured using Perkin-Elmer Optima 5400 Inductively Coupled Plasma Optical Emission Spectrometer at the University of Texas at El Paso. The samples were digested using Li-metaborate fusion technique as described by Feldman, (1983). Fine dust samples and lithium metaborate were weighed in the ratio of 1:10 into a plastic vial. The two were mixed using a mixer mill (Spex sample prep 5100) before being fused in a muffle furnace at 900^0C for 15 min forming a red bead. The bead was dissolved in 5% nitric acid in readiness for measurements. For quality check, twenty calibration rock standards and a USGS reference rock material (W-2) were digested alongside the samples, relative errors of element concentrations on W2 measurements were less than 10%.

3.4.5.2 Strontium isotopic analyses

Approximately 50 mg of dust and 100 mg of powered soil and caliche samples were weighed in two portions. One portion (the bulk) was wholly digested in HF and HNO_3 followed by HCl and boric acids attack. The remaining portion was leached with 1N acetic acid for 30 minutes. Residues were separated from the supernatant and acid-digested in two steps similar to bulk samples while the leachates were evaporated to dryness. The digested bulk, residues and leachate samples were re-dissolved in 3.5N HNO_3 and passed through Sr-Spec resin to separate Sr from the matrix. In addition, a marine carbonate sample collected at Tortugas "A" mountains south of the Jornada Basin was drilled on one spot and digested in a similar way as bulk samples. The purified samples were then analyzed for $^{87}Sr/^{86}Sr$ isotopes on the Multi Collector Inductively Coupled Plasma Mass Spectrometry (MC-ICPMS) using standard-sample bracketing method. The Sr isotope standard SRM 987 yielded average $^{87}Sr/^{86}Sr$ ratios of 0.710235± 0.000005 (2SD, n=32). For quality control purposes BCR2 rock standards were treated as bulk samples indicating measured average $^{87}Sr/^{86}Sr$ ratios of 0.70502±0.00001 (2SD), n=9) which were within the values reported in literature (Jweda et al., 2015). Sr blanks were negligible pico-gram scales (~80 pg).

3.4.5.3 U and Th concentrations and U-series isotopic composition analyses

3.4.5.3.1 Sample digestion

Bulk samples of dust were digested using total sample dissolution (TSD). Soil and caliche samples were digested using both TSD or acid-leachate techniques (L/R) in order to obtain coeval subsamples with presumably various mixing ratios of detrital and pure carbonate end-members for U-series analysis. Three portions of ~100 mg of the soils and caliche samples

and one 100 mg portion of dust samples were weighed into separate beakers. Dust samples as well as the first aliquot of soil and caliche were digested in acids (HNO_3 and HF followed by HCl and H_3BO_3) as bulk samples after spiking them with either ^{233}U or ^{229}Th separate spikes or a combined ^{233}U-^{229}Th spike. The second and third aliquots of soil and caliche samples were leached with 1N HCl and 1N AcOH acids respectively and allowed to settle for 30 minutes. The HCl leachate (HCl-L) and residue (HCl-R) as well as the acetic acid leachate (AcOH-L) and residue (AcOH-R) were separated into beakers. Like the bulk samples, all the leachates and residues were spiked prior to evaporation in order to obtain ^{238}U and ^{232}Th concentrations by isotope dilution technique. The residues were digested with strong acids as bulk sample while the leachates were dissolved in 7.5N HNO_3 in readiness for column chemistry.

3.4.5.3.2 Column separation, purification, and isotope analysis

Column chemistry aimed at separation and purification of U and Th was performed through AG 1-X8 anion exchange resin (200-400 mesh) in a class-100 cleanroom. First U and Th were separated from the sample matrix through a 2 ml resin. Second, U was separated from Th through a 0.6 ml resin by eluting U with 7.5 N HNO_3 and Th with 6 N HCl. Third, U and Th were purified separately and eluted through 0.6 ml and 0.15 ml resin respectively. The pure U and Th samples were measured for $^{234}U/^{238}U$, $^{233}U/^{238}U$, $^{238}U/^{235}U$, $^{230}Th/^{232}Th$, and $^{229}Th/^{232}Th$ isotopic ratios using the standard-sample bracketing method on a MC-ICP-MS.

3.4.5.3.3 U and Th concentration and U-series activity ratio calculations

Uranium concentrations were calculated from the weight and concentration of the ^{233}U artificial spike and the weight of the sample. Uranium activity ratios ($^{234}U/^{238}U$) were calculated from ion count gain and mass fractionation corrected $^{234}U/^{238}U$ isotope ratios as well as ^{234}U and

^{238}U half-lives after Cheng et al. (2000). Thorium concentrations were calculated from the gain fractionation corrected ^{229}Th/^{232}Th ratios, concentration of ^{229}Th spike, weight of the sample, and atomic weight of ^{229}Th and ^{232}Th isotopes. A BCR2 reference rock material from USGS was regularly assessed for accuracy. The reference material showed average U concentrations of 1.689 ± 0.018 ppm; n = 25, (2σ) and Th concentrations of 5.86 ± 0.07 ppm; n = 10, (2σ), these concentrations were consistent with those reported from other laboratories (Sims et al., 2008). Calculated (^{234}U/^{238}U) of the BCR2 were at equilibrium values indicating averages of 1.002 ± 0.005; n = 25, (2σ) and (^{230}Th /^{232}Th) gain fractionation corrected ratios averaged at 4.895± 0.011x 10^{-6}; n = 10, (2σ). All these ratios were within the errors reported from other laboratories (Sims et al., 2008). Procedure blanks were negligible, ~4 pg and ~100 pg for uranium and thorium respectively.

3.4.5.3.4 Pedogenic carbonate ages and initial (^{234}U/^{238}U)$_0$ determination

U-series dating technique of secondary minerals (e.g. pedogenic carbonates) assumes that secondary carbonate deposits are uranium-rich and thorium-free at the time of formation because of their chemical behaviors (Chabaux et al., 2003). Uranium is soluble in water under oxidative environments, and co-precipitates with other soluble elements such as Ca in pedogenic carbonates while the insoluble Th tends to adsorb on insoluble particles (Chabaux et al., 2003). Such a chemical fractionation would result in extremely low Th/U elemental ratios in the pedogenic carbonates. In a closed system, radioactive ^{234}U decays to ^{230}Th over time yielding high ^{230}Th/^{234}U or ^{230}Th/^{238}U isotope ratios which are applicable in U-Th dating technique (see section 3.3.2). Since ^{230}Th is also radioactive, the time required to reach equilibrium with its parent isotope allows us determine the ages of the carbonates and initial (^{234}U/^{238}U) activity ratios using mathematical equations based on radioactive decay. Because pedogenic carbonates

form in soils that contain other minerals such as clays, these carbonates contain abundant detritus material, which inpact U-series dating method. The detrital component in the carbonates results in erroneous ages and must be taken into account. Different correction methods which aim at determining the proportion of ^{230}Th, ^{234}U, and ^{238}U in the pure (authigenic) carbonate have been employed (Kaufman, 1993). In this study we explore single sample and isochron detrital correction techniques.

The single sample point detrital Th correction technique was performed on 9 bulk samples prepared by TSD method. This technique corrects for ^{230}Th using the measured (^{230}Th/^{238}U), (^{232}Th/^{238}U), and assumed initial (^{230}Th/^{232}Th) (Kaufman, 1993; Ibarra et al., 2014). The chosen initial (^{230}Th/^{232}Th) depends on Th concentration in a sample, usually the ratio is assumed to be equal to (^{230}Th/^{232}Th) ratios of continental crust (Polyak and Asmeron, 2001; Ibarra et al., 2014). Because acid residues of local soil better represent the detrital component on a local soil profile scale, this study employs measured (^{230}Th/^{232}Th) of H1 acid residues (HCl_R and AcOH_R) as initial ratios for detrital correction. The results were compared to those obtained when (^{230}Th/^{232}Th) of continental crust (~0.87) are used in detrital correction (Equation 2). The detrital corrected U- series activity ratios and their associated errors were used for age calculation and initial U activity ratios on Isoplot 3.75 (Ludwig 2012). The equation governing the detrital correction of single sample point is from Kaufman, 1993

$$\left(\frac{^{230}\mathrm{Th}}{^{238}\mathrm{U}}\right)_{A}=\left[\left(\frac{^{230}\mathrm{Th}}{^{238}\mathrm{U}}\right)_{M}-\left(\frac{^{232}\mathrm{Th}}{^{238}\mathrm{U}}\right)_{M}*\left(\frac{^{230}\mathrm{Th}}{^{232}\mathrm{Th}}\right)_{0}\left(e^{-\lambda_{230}t}\right)\right] \qquad (2)$$

Where A is the detrital free/authigenic (^{230}Th/^{238}U) activity ratio, M indicates the measured (^{230}Th/^{238}U) and (^{232}Th/^{238}U) activity ratios, Zero signify the assumed initial (^{230}Th/^{232}Th) ratios, and t is the uncorrected period inclusive of detrital Th (cf. Ibarra, 2013).

Isochron detrital correction method assumes presence of an isotopically homogeneous mixture of single types of detrital and pure carbonate end members in a sample. The method requires a set of coeval samples in order to obtain mixing ratios of detrital and pure carbonate end members. Activity of ^{230}Th, ^{234}U, ^{238}U, and ^{232}Th in the coeval subsamples (e.g. Bulk, HCl-L, HCl-R, AcOH-L, and AcOH-R) were measured and normalized by either ^{232}Th or ^{238}U and plotted in MATLAB to define two types of 2D isochrons: Rosholt-type [(^{234}U/^{232}Th), (^{230}Th/^{232}Th) vs (^{238}U/^{232}Th)] and Osmond-type [(^{234}U/^{238}U), (^{230}Th/^{238}U) vs (^{232}Th/^{238}U)]. The isochrons define a straight line whose slope (in the Rosholt-type) and intercepts (in the Osmond-type) result in (^{230}Th/^{238}U) and (^{234}U/^{238}U) in authigenic carbonate end-member (Fig. A2). The errors of these pure carbonate activity ratios were calculated using a MATLAB code, whose procedures are based on the works of York et al. (2004). These corrected activity ratios and their errors are used for age calculations using ISOPLOT 3.75 (Ludwig, 2012). For the 3D isochrons, measured (^{230}Th/^{238}U), (^{234}U/^{238}U), and (^{232}Th/^{238}U) and their errors for the coeval subsamples, were directly plugged into ISOPLOT 3.75 software for initial $(^{234}U/^{238}U)_0$ activity ratios and ages calculations. The ISOPLOT 3.75 software calculations are based on mathematical radioactive decay equations adopted from Kafman, (1993) and Ibarra, (2013)

$$\left(\frac{^{234}U}{^{238}U}\right)_t = \left[\left(1-e^{-\lambda_{230}t}\right)+\left(\frac{^{234}U}{^{238}U}\right)_0\right] \qquad (3)$$

$$\left(\frac{^{230}Th}{^{238}U}\right)_t = \left[\left(\frac{\lambda_{230}}{\lambda_{230}-\lambda_{234}}\right)\left(\frac{^{234}U}{^{238}U}\right)0\left(e^{-\lambda_{234}t}-e^{-\lambda_{230}t}\right)+\left(1+\frac{\left(\lambda_{234}e^{-\lambda_{234}t}-\lambda_{230}e^{-\lambda_{234}t}\right)}{\lambda_{230}-\lambda_{234}}\right)\right] \qquad (4)$$

Where λ_{230} and λ_{234} denotes decay constants of ^{230}Th and ^{234}U respectively, t is the age of the mineral, (^{230}Th/^{238}U) t and (^{234}U/^{238}U) t are measured or detrital corrected activity ratios (cf Ibarra, 2013).

3.4.5.4 Carbon isotope analysis

The organic and inorganic C isotopes of H1, H2, and H3 (lamina A and C) were conducted at the Jozef Stefan Institute of Slovenia. Procedures used in these analyses are outlined in Jin et al. (2009). Briefly, carbonate minerals were removed from the samples with 1M HCl in order to determine organic C isotopes. The samples were then washed in distilled water, oven dried at 60^0C and aliquots of about 8 mg weighed into tin capsules. The capsules were combusted in readiness for organic C isotope determination. For inorganic C isotopic composition, about 8 mg of the raw sample was weighed into capped vessels. The vessels were flushed with helium and the samples were treated with H_3PO_4 for 24hrs at 25^0C to release CO_2. The combusted capsules and released CO_2 were analyzed for organic C and inorganic C isotope composition on the Europa Scientific 20-20 continuous flow Isotope Ratio Mass Spectrometer. IAEA-CH7 was used as a reference material for organic C isotope measurements while NBS 18 and NBS 19 were reference materials for inorganic C isotope determination.

3.5 Results

Elemental concentrations, carbon isotope compositions ($\delta^{13}C$), U-series activity ratios, and $^{87}Sr/^{86}Sr$ isotopic ratios in dust, soils and caliche samples, as well as U-series carbonate ages and their associated $(^{234}U/^{238}U)_0$ are presented below.

3.5.1 MAJOR AND MINOR ELEMENT OXIDE CONCENTRATIONS IN DUST

Major and minor element oxide concentrations in dust samples are given in Table 2.1. The most dominant major element was SiO_2 ranging from 54.9- 85.7wt% in dust collected at 50 cm height above ground (Table 2.1; Figure 2.4a) and 55.3-87.6wt% at 100 cm (Table 2.1; Figure 2.4b). The second dominant major element was Al_2O_3 showing values of 6.1-14.3 wt% at 50 cm

(Table 2.1; Figure 2.4a) and 5.9-12.6 wt% at 100 cm (Table 2.1; Figure 2.4b). Other major elements showed values less than 5 wt% in the following order of decreasing dominance Fe_2O_3> K_2O> CaO> MgO> Na_2O> TiO_2 in all the sites (Figure 2.4a and 2.4b). P-Coli, a playa site was generally depleted of SiO_2 and enriched in Al_2O_3 in dust samples collected at both 50 cm and 100 cm above ground level.

Barium concentrations in dust samples were higher than Zr concentrations, which in turn were higher than Sr (Figure 2.4c and 2.4d). Dust collected at 50 cm, showed concentrations ranging from 468.5 to 584.2 ppm for Ba, 193.0 to 406.1ppm for Zr, and 142.3 and 230.9 ppm for Sr (Table 2.1; Figure 2.4c). M-Well was depleted in both Zr and Sr compared to other sites. These trace elements were higher in dust collected at 100 cm above ground compared to dust collected at 50 cm. Ba concentrations ranged between 497 and 653 ppm, 140- 633 ppm for Zr, and Sr showed values between 137 and 221 ppm (Table 2.1; Figure 2.4d). Dust collected at G-IBPE4 site indicated lower Zr and Sr concentration. Uranium concentrations in dust collected at 50 and 100 cm heights above ground from two sites (T-TYL and T-East) ranged from 1.45 to 2.13 ppm (Table 2.1). Their Th concentrations showed values between 6.66 and 9.31 ppm at 50 and 100 cm respectively (Table 2.1). Both U and Th concentrations were lower in dust collected at 50 cm height compared to dust collected at 100 cm above ground, likely due to the contribution of small amount of saltating sand grains at 50 cm.

3.5.2 URANIUM AND TH CONCENTRATIONS IN BULK SOIL AND CALICHE SAMPLES

The bulk soil (H1) indicated U and Th concentrations of 1.59 and 6.02 ppm respectively (Table 2.2 and 2.5). Samples drilled on three spots along a lamina and dissolved by TDS indicated U concentrations ranging from 2.04 to 3.66 ppm in H3C, 1.12-1.24 ppm in H2B, 1.34-1.64 ppm in H2C, 0.49-0.62 ppm in H4B, and 0.46-0.54 ppm in H4C (Table 2.2 and 2.4). H3

bulk caliche samples showed the highest U concentrations while H4 indicated the lowest concentrations. Thorium concentrations indicated values ranging from 2.12 to 2.84 ppm in H3C, 1.80-2.46 ppm in H2B, 1.94-2.04 ppm in H2C, 0.95-1.17 ppm in H4B, and 1.21-1.68 ppm in H4C (Table 2.2 and 2.4).

3.5.3 URANIUM AND TH CONCENTRATIONS IN PEDOGENIC CARBONATES

Both acetic acid and HCl leachates of H1 soil sample showed lower U and Th concentrations compared to their corresponding residue subsamples (Table 2.5). This is because there were only little carbonates in the bulk soils and U and Th in these soils lies in the silicate residuals. All caliche leachate (HCl_L and AcOH_L) subsamples indicated low Th concentrations as opposed to their residues, which indicated high Th concentrations (Table 2.5). This is consistent with the behavior of Th to adsorb on insoluble particles. Leachates of H2A and H3A indicated low U concentrations while their residues showed higher concentrations suggesting that more U resided in the detrital-siliceous portion of the sample. On the contrary, H2C and H3C leachates indicated high U concentrations, but low U concentrations in their residues (Table 2.5). This is consistent with chemical fractionation behavior of U and Th in soil water environment and subsequent precipitation of secondary minerals in soils.

3.5.4 ISOTOPIC COMPOSITIONS

3.5.4.1 Strontium isotopic composition

Soluble dust fractions (acetic acid leachates) showed low $^{87}Sr/^{86}Sr$ ratios ranging from 0.7086 to 0.7091. The residue fractions and bulk dust samples indicated more radiogenic signature ranging from 0.7119 to 0.7225 and 0.7126 to 0.7184 respectively (Table 2.3). The $^{87}Sr/^{86}Sr$ ratios of leachates, residues, and bulk subsamples in soils differ significantly: while H1

leachate showed the lowest $^{87}Sr/^{86}Sr$ ratios of 0.7086, the residues and bulk subsamples indicated higher radiogenic $^{87}Sr/^{86}Sr$ ratios of 0.7250 and 0.7227 respectively (Table 2.3). The H1 leachate $^{87}Sr/^{86}Sr$ ratios are similar to those observed in leachate/soluble fractions of modern dust (Figure 2.5a).

The caliche samples showed distinct $^{87}Sr/^{86}Sr$ ratios at depth in the profile. H3 sample had $^{87}Sr/^{86}Sr$ ratios of 0.7112 in the soluble fraction, 0.7135 to 0.7156 in the residue fraction, and 0.7115 in the bulk/whole sample (Table 2.3). Shallower H2 sample showed $^{87}Sr/^{86}Sr$ ratios of 0.7085 in the soluble fraction while the residue portion and bulk indicated values ranging from 0.7138 to 0.7190 and 0.7101 to 0.7123 respectively. H4 sample indicated $^{87}Sr/^{86}Sr$ ratios ranging from 0.7091 to 0.7102 in soluble fraction, 0.7202 in residue portion and 0.7098-0.7107 in the bulk sample respectively (Table 2.3). The $^{87}Sr/^{86}Sr$ ratios of H3, H4B, and H4A soluble fractions are more radiogenic compared to H2 and H4C leachate fractions. The H2 and H4C leachate fractions have $^{87}Sr/^{86}Sr$ ratios similar to H1 and modern dust soluble portions (Figure 2.5a).

3.5.4.2 U-series isotopic composition in bulk dust, soil, and caliche samples

The ($^{234}U/^{238}U$) in bulk dust samples at 50 and 100 cm were close to unity indicating values between 0.94 and 0.98 while the ($^{230}Th/^{238}U$) showed high values between 4.21 and 4.45 (Table 2.1). U-series activity ratios ($^{234}U/^{238}U$) and ($^{230}Th/^{238}U$) in H1 bulk samples showed values of 0.91 and 0.77 respectively (Table 2.2). The bulk caliche samples showed ($^{234}U/^{238}U$) ranging from 0.97 to 1.08 in H3, 1.13-1.19 in H4, and 1.21-1.34 in H2 (Table 2.2). The ($^{234}U/^{238}U$) ratios increased from caliche at depth (H3) to shallower carbonates indicating the highest ($^{234}U/^{238}U$) at H2. Caliche sample at H2 indicated the lowest ($^{230}Th/^{238}U$) of 0.52-0.70 while H3 and H4 showed ratios close to one (0.96 - 0.98; 0.95-1.02 respectively) (Table 2.2). High ($^{232}Th/^{238}U$) ratios at H2 sample are characteristic of "dirty" carbonates due to inclusion of

detrital materials into the sample (Table 2.2). Activity ratios varied within the lamina of each hand sample; H2, H3, and H4 showed a general increasing ($^{234}U/^{238}U$) trend from inner (A) to outer (C) lamina. On the other hand, ($^{230}Th/^{238}U$) activity ratios generally increased to the outer lamina in H2, but remained fairly constant in H3 and H4 samples (Table 2.2).

3.5.4.3 U-series isotopic composition in pedogenic carbonates

H1 leachate subsamples indicated lower ($^{230}Th/^{238}U$) and higher ($^{234}U/^{238}U$) unlike their residues, which indicated higher ($^{230}Th/^{238}U$) and lower ($^{234}U/^{238}U$) (Table 2.5). The observed activity ratios in the soil leachates are consistent with selective leaching of uranium in carbonates and other minerals with weak acids from bulk soils. All caliche leachate subsamples indicated higher ($^{234}U/^{238}U$), but lower ($^{234}U/^{238}U$) in the residue subsamples as expected; again, due to preferential leaching of carbonates characteristic of higher uranium activity ratios. H2A and H2C leachate subsamples indicated lower ($^{230}Th/^{238}U$) and higher ($^{230}Th/^{238}U$) in their residues while leachate subsamples of H3A and H3C at depth indicated higher ($^{230}Th/^{238}U$) and lower ($^{230}Th/^{238}U$) in the residue subsamples (Table 2.5). High ($^{230}Th/^{238}U$) in H3 leachate indicate suspension of detrital silicate material in the supernatant fluid and H2 caliche samples are characteristic of "dirty carbonates".

3.5.5 PEDOGENIC CARBONATE AGES AND $(^{234}U/^{238}U)_0$ RATIOS

Uranium series ages of pedogenic carbonate and $(^{234}U/^{238}U)_0$ are given in Tables 2.2, 2.4, and 2.5. These ages were obtained after detrital U and Th correction by either single sample or isochron (2D or 3D) techniques. Carbonate ages derived from measured activity ratios (uncorrected for detrital U and Th) were also computed for comparison purposes; these ages were older than those calculated from detrital- corrected activity ratios (Table 2.2).

3.5.5.1 Single sample correction technique-derived carbonate ages

The carbonate ages obtained after detrital Th correction using the single sample correction technique are given in Table 2.2. The $^{230}Th/^{232}Th$ ratio of the upper continental crust and measured ($^{230}Th/^{232}Th$) of HCl_R and AcOH_R in H1 soil sample were used in computing detrital free activity ratios. However, only carbonate ages obtained after correction with ($^{230}Th/^{232}Th$) ratios in acetic acid H1 soil residue are discussed here because of the assumption that the weak acetic acid does not release much Th into leachate phase. Other carbonate ages due to correction from Th-ratios in HCl soil residue and upper continental crust are presented in table 2.2. H3 carbonates yielded U-series ages ranging from 145.7 ± 3.6 to 99.8 ± 1.9 ka (2σ) and $(^{234}U/^{238}U)_0$ between 0.95 and 1.11 (±7‰, 2σ). H4 carbonates yielded ages between 20.59 ± 0.3 to 71.6 ± 1.1 ka (2σ) and $(^{234}U/^{238}U)_0$ between 1.15 and 1.21 (±7‰, 2σ). H2 carbonates were young indicating ages ranging from 8.67 ± 0.1 to 5.94 ± 0.068 ka (2σ) with higher $(^{234}U/^{238}U)_0$ between 1.21 and 1.35 (±7‰, 2σ). The carbonate ages are oldest at H3 (deepest sample) and youngest at H2, the $(^{234}U/^{238}U)_0$ increase from H3 to H2 (Table 2.2). The calcareous soils (H1) did not yield any reliable age (Table 2.2).

3.5.5.2 Isochron-derived carbonate ages

As described in section 3.1.5.3.1, coeval samples were obtained by digesting drilled subsamples by either TSD or acid-leachate/residue techniques. Three subsamples drilled along a given lamina of the caliche sample were digested by TSD to obtain coeval samples of respective caliche samples (Table 2.4). For example, H4 caliche sample was drilled along lamina C to obtain three subsamples (H4C, H4C2, and H4C3) for TSD. Similar three coeval subsamples were obtained from H4B, H2C, H2B, and H3C (Table 2.4). H2C and H3C subsamples were also

treated with acid leachate/residue technique to obtain five coeval subsamples, which included the Bulk, HCl-L, HCl-R, AcOH-L, and AcOH-R (Table 2.4).

2D (Rosholt and Osmond) isochron ages of either 3 or 5 coeval subsamples are summarized in table 2.4. Three subsample of H3C yielded 2D age of 194±37 ka and $(^{234}U/^{238}U)_0$ of 1.21± 0.092 (Osmold) and 182 ± 38 ka and $(^{234}U/^{238}U)_0$ of 1.23± 0.11 (Rosholt). H2B subsample yielded 2D age of 56.1± 7.5 ka and $(^{234}U/^{238}U)_0$ of 1.54± 0.087 (Osmold) and 57.2 ± 7.1 ka and $(^{234}U/^{238}U)_0$ of 1.54± 0.081(Rosholt) (Table 2.4). H2C subsample yielded 2D age of 58± 24 ka and $(^{234}U/^{238}U)_0$ of 1.37± 0.091 (Osmold) and 60 ± 27 ka and $(^{234}U/^{238}U)_0$ of 1.37± 0.1(Rosholt). H4C subsample yielded 2D age of 116.2± 7.3 ka and $(^{234}U/^{238}U)_0$ of 1.58± 0.045 (Osmold) and 118 ± 9.9 ka and $(^{234}U/^{238}U)_0$ of 1.57± 0.059 (Rosholt). H4B subsample did not yield any age or initial activity ratios (Table 2.4). Recalculating the ages with five subsample H3C yielded 2D age of 87 ± 41ka and $(^{234}U/^{238}U)_0$ of 1.33 ± 0.1 (Osmold) and 64 ± 24ka and $(^{234}U/^{238}U)_0$ of 1.24 ± 0.064 (Rosholt). Five subsamples of H2C yielded 2D age of 10.9± 4.4 ka and $(^{234}U/^{238}U)_0$ of 1.60± 0.026 (Osmold) and 10 ± 1.3ka and $(^{234}U/^{238}U)_0$ of 1.60 ± 0.008 (Rosholt) (Table 2.4). The standard error on the carbonate ages is 2σ and the activity ratio is ~7‰.

The 3D isochrons yielded single carbonate ages on 5 subsamples of selected caliche samples (H2A, H2C, H3A, and H3C). H2A subsample yielded a carbonate age of 20 ± 10ka and $(^{234}U/^{238}U)_0$ of 1.73 ± 0.12 while H2C subsample yielded a carbonate age of 10 ± 3.2ka and $(^{234}U/^{238}U)_0$ of 1.6± 0.064 (Table 2.5). The H3A and H3C carbonates yielded unreliable ages lower than their associated calculated errors, the samples however, showed $(^{234}U/^{238}U)_0$ of 1.7 ± 1.2 and 2.4 ± 1.1 respectively (Table 2.5). H1 subsamples yielded no reliable age but indicated $(^{234}U/^{238}U)_0$ of 1.02 ± 0.33 (Table 2.5).

In summary, samples that yielded no ages or carbonate ages with negative values and huge errors were not used in timing paleo-moisture events at the Jornada Basin. Only meaningful carbonate ages obtained by single sample point correction (using H1 AcOH_R), 2D and 3D Osmond isochron technique were used in the following section to elucidate temporal variability of paleohydrologic conditions in the Jornada Basin.

3.5.6 STABLE CARBON ISOTOPE COMPOSITION

The stable carbon isotope compositions of the inorganic carbon portion ($\delta^{13}C_{CaCO3}$) were enriched showing values between -3.72 and -1.82‰ compared to $\delta^{13}C_{OC}$ values, which indicated values from-23.32 to -20.28‰ (Table 2.5).

3.6 Discussion

3.6.1 LOCAL SOURCES OF MODERN DUST AND ITS EFFECTS ON SOILS

Aeolian activities modify land surfaces through dust deposition and/or wind erosion processes. Dust deposition on arid and island land surfaces improves the fertility of soils and may alter soil texture (Creamean et al., 2013; Chadwick et al., 1999; Reynolds et al., 2001; Ravi et al., 2011; Aciego et al., 2015). Impact of wind activity on landscapes depends on vegetation coverage, wind speed, soil moisture, and supply and grain size of erodible particles (Gillette and Monger, 2006; Alvarez et al., 2012). Low vegetation cover and strong winds in the desert southwest USA including the Jornada Basin have enhanced local dust production and transportation (Rivera et al., 2009, 2010; Gillette and Monger, 2006; Reynolds et al., 2003; Floyd and Gill, 2011).

3.6.1.1 Evidence from elemental chemistry

Low vegetation cover and strong winds in the desert southwest USA including the Jornada Basin have enhanced local dust production and transportation (Rivera et al., 2009, 2010; Gillette and Monger, 2006; Reynolds et al., 2003; Floyd and Gill, 2011; Tong et al., 2012). Reheis et al., (2009) reported similarity in dust geochemistry and surface soil chemistry in another portion of the southwest USA. Modern dust at the Jornada Basin indicated high SiO_2 > Al_2O_3 > Fe_2O_3 and K_2O concentrations (Figure 2.4a and 2.4b). These high concentrations observed in dust compositions are commonly attributed to minerals such as quartz, aluminosilicates, and clays abundant in the earth's crustal material (Upadhyay et al., 2015) and typical of aeolian dusts. Concentrations of CaO, MgO, and Na_2O in dust (Figure 2.4a and 2.4b) can be accounted for by wind erosion of weathered depleted soils and/or evaporite salts. Infiltrating soil waters leach these elements to greater depths and precipitate in secondary minerals such as pedogenic carbonates. Calcium for instance, accumulates in the Jornada soils from the atmosphere through wet and dry deposition and consequently precipitates in pedogenic carbonates at soil depths (Gile et al., 1981; Capo and Chadwick, 1999; Monger and Gallegos, 2000). Such elemental additions to soils occur alongside other soluble ions such as Na, Sr, and Ba.

Generally, Th concentrations were higher than U in the bulk dust, however both of these concentrations were lower in dust collected at 50 cm compared to that sampled at 100 cm above ground (Table 2.1). High Th concentration could be sourced from surface soil, which tends to accumulate Th among other immobile elements. Due to differences in solubility of U and Th in oxidative environments thus their mobility in soils, the insoluble Th tends to accumulate in surface soils while the soluble U is leached and deposited at depth in soil carbonates (chapter 2).

Wind erosion of such soils results in higher Th content in local dust relative to U concentrations. Elemental dust composition is partially attributed to dust particle sizes and adsorbed minerals. The samples collected much closer to the ground (e.g. 50 cm) are more likely to contain some saltating particles, which are predominantly pure quartz grains. These quartz grains contain no trace elements and have a smaller proportional surface area coated by clays or other materials, which are more likely to result in a lower overall concentration of minor elements. Finer suspended particles at 100 cm on the other hand, are more likely to be mineralogically diverse including clay minerals, oxides and other aluminosilicate minerals which bear any and all trace elements including Th, U, Sr, etc (Rojo et al., 2008). Such a dust compositional and grain size variability could explain the higher concentrations of Th and U in dust collected at 100 cm relative to that of 50 cm height above ground at the Jornada Basin. In coherence with quartz mineralogy, high SiO_2 content was observed in some dust samples (M-Rabb, M-well, and T-Tyl) collected at 50 cm relative to their corresponding dust at 100 cm (Table 2.1). Indeed, dust at 100 cm confirms high concentrations of Sr, Ba, and Zr trace elements consistent with high adsorption capacity of trace elements on finer silt-clayey materials in suspended dust (Table 2.1).

3.6.1.2 Evidence from strontium isotope composition

Due to the similarity in geochemical behavior between Sr and Ca, strontium isotopes ($^{87}Sr/^{86}Sr$) have been extensively used to fingerprint calcium sources in various surface and near-surface environments (Capo et al., 1998). Matching of $^{87}Sr/^{86}Sr$ ratios in soluble fraction of dust, soils, shallow carbonates (H2 and H4C), and Paleozoic marine carbonates ("A" mountain carbonates) provide further evidence of local sources of dust within the Jornada Basin (Figure 2.5a). The $^{87}Sr/^{86}Sr$ ratios of ~0.7089 observed in the soluble fraction of dust, soils and shallow carbonates suggests that atmospherically derived Sr has contributed significantly to the

formation of these shallow carbonates (Figure 2.5a). Similarity of $^{87}Sr/^{86}Sr$ ratios of the Paleozoic carbonates in Tortugas "A" mountain south of the Jornada Experimental Range (Figure 2.1) with those of leachable soils and dust within JER also provide evidence of wind activity in the area. Because similar Paleozoic carbonates are exposed at mountain flanks of San Andres and Robledo Mountains, occasional weathering, runoff and wind erosion of exposed carbonate rocks could account for many of the Sr sources in JER. Additionally, coincidence of $^{87}Sr/^{86}Sr$ ratios in the soluble fraction of the playa-site dust with those of the shallow carbonates suggest that evaporite minerals (e.g. gypsum, halite and carbonates) associated with desiccation of paleo-lakes are potential sources of Sr, Ca, Na, and other soluble elements in the basin (Gile, 2002). Some soils in alluvial flats/plains in the Jornada Basin have been found to contain gypsum (Gile, 2002; Monger, 2006). Gypsum is a component of dust-emitting soils in the Chihuahua Desert (Buck and Van Hoesen, 2002: Buck and Hoesen, 2005; Peinado, 2013) and the White Sands, in the Tularosa Basin directly to the northeast, is a prodigious dust source (White et al., 2015). This gypsum is also found within the Permian Yeso formation, which is exposed at San Andres and Caballo mountains (Mack and Suguio, 1991). Our findings are consistent with previous studies of the southwest USA that have attributed salt-loads into desert soils to atmospheric input from local sources (Monger and Gallegos, 2000; Gile et al., 1981; Capo and Chadwick, 1999; Reheis, 2006; Reheis and Urban, 2011; Floyd and Gill, 2011; White et al., 2015). Floyd and Gill, (2011) examined mass fluxes and particle size distributions of dust within the Jornada Basin indicating that playa sites are significant dust producers in the basin. Capo and Chadwick (1999) showed that both atmospheric wet (rain) and dry (dust) deposition mechanisms add Sr and other soluble elements to soils near Las Cruces, NM. Simple mixing calculations using equation 5 (cf. Naiman et al., 2000) and $^{87}Sr/^{86}Sr$ ratios of the Camp Rice formation (the

parent material of the Jornada Basin soils; 0.7165; Capo and Chadwick, 1999) indicated that about 98% of Sr (hence Ca) is derived from the atmosphere.

$$X \left(\frac{^{87}Sr}{^{86}Sr}\right)_{dust} + (1-X) \left(\frac{^{87}Sr}{^{86}Sr}\right)_{parent\ material} = \left(\frac{^{87}Sr}{^{86}Sr}\right)_{soil\ carbonates} \quad (5)$$

Soluble fractions of other carbonates (e.g. H3, H4A, H4B) in the soil profile at the La Mesa_JER indicated more radiogenic $^{87}Sr/^{86}Sr$ ratios (>0.7100) compared to shallow carbonates (Table 2.3; Figure 2.5a). Such high $^{87}Sr/^{86}Sr$ ratios are associated with weathering of silicate rocks in terrestrial environments (Capo et al., 1998). Similarity of ionic radii between K and Rb allows for substitution of these two elements in potassium rich silicate minerals. The mineral incorporated Rb has two isotopes, ^{87}Rb and ^{85}Rb; over time, the radioactive ^{87}Rb decays to ^{87}Sr. In the event of weathering, high radiogenic $^{87}Sr/^{86}Sr$ ratios dissolve in weathering fluids and ultimately precipitate in secondary minerals such as pedogenic carbonates at soil depths. The Camp Rice Formation and local soil silicates near Las Cruces have $^{87}Sr/^{86}Sr$ ratios between 0.7131 and 0.7173 (Capo and Chadwick, 1999). Since the ancestral Rio Grande river sediments form part of soil parent material at the La Mesa_JER, we would expect a positive correlation of $^{87}Sr/^{86}Sr$ ratios between the residue and soluble fractions if the soils and parent material were significant Sr sources (Figure 2.5b). Probably a more radiogenic material must have supplied Sr during the formation of the carbonates at depth. Using Sr, C and O isotopes, Mark et al. (2012) suggested that secondary minerals in the Jornada Basin (e.g. opal and calcite) precipitated from a mixture of deep upwelling geothermal fluids and shallow meteoric groundwater. Such deep groundwater flowing through old granitic formations is characteristic of radiogenic $^{87}Sr/^{86}Sr$ ratios. Another possible source of high $^{87}Sr/^{86}Sr$ ratios in these carbonates is the heterogeneous nature the basin fills (sediments), which is a wide combination of river and mountain alluvium. This implies that a more radiogenic $^{87}Sr/^{86}Sr$ ratios material could be local or externally sourced

through distant riverine alluvium or exogenic dust. The precise source of radiogenic Sr signature in carbonates at depth (e.g. H3 and lamina A and B of H4) and possible heterogeneity of Sr isotopes in the basin remains open for investigation.

3.6.2 EVIDENCE FROM U-SERIES ISOTOPIC COMPOSITION

While ($^{230}Th/^{238}U$) show high ratios of 4.21-4.47 in dust, ($^{234}U/^{238}U$) indicated low values of 0.94-0.97, closer to the equilibrium value (~1) (Table 2.1); these activity ratios indicated no significant difference between dust collected at 50 cm and 100 cm. The high ($^{230}Th/^{238}U$) could be explained by the likelihood of ^{230}Th adsorbing onto insoluble grain coatings released as dust particles unlike U, which tends to be more soluble in water. Another explanation for the observed activity ratios could be the isotope composition of source dust such as weathered, wind-eroded soil surface materials. During chemical weathering of rocks and soil minerals, ^{234}U is preferentially lost into weathering fluids by alpha recoil processes resulting in ^{234}U depleted and ^{230}Th enriched mineral phases (Chabaux et al., 2003). Weathered siliceous products therefore indicate ($^{234}U/^{238}U$) less than unity and ($^{230}Th/^{238}U$) greater than one. The H1 soils in the Jornada Basin indicate ($^{230}Th/^{238}U$) of 0.77 and ($^{234}U/^{238}U$) of 0.91 (Table 2.2). H1 soils contained filaments of stage I carbonates which may result in lower ($^{230}Th/^{238}U$) ratios due to averaging effect. Because ^{238}U has a higher solubility in soil water compared to ^{230}Th, secondary carbonates are characteristic of lower ($^{230}Th/^{238}U$) ratios. Bulk soil analysis of soils containing pedogenic carbonates (e.g. H1 soils) results in averaging lower ($^{230}Th/^{238}U$) ratios. Even though H1 soil sample indicated low ($^{230}Th/^{238}U$) (less than one), soils from another area in the Jornada Basin have generally indicated ($^{230}Th/^{238}U$) >1 and ($^{234}U/^{238}U$) <1 in surface soils (see chapter 2) suggesting selective loss of U to greater depths and accumulation of Th in shallower soils. However, other studies have documented mobility of Th in soil profiles (Taboada et al., 2006).

Because clay illuviation processes are unlikely due to low annual rainfall, differences of ($^{230}Th/^{238}U$) between dust and soils could be accounted for by differences in grain-size fractions. H1 soils were courser in texture (sandy-loamy) compared to dust (silty-clayey), finer dust particles are likely to contain more ^{230}Th compared to the soils. This is consistent with Taboada et al. (2006) study that showed higher concentrations of Th in finer gain particles.

Higher ($^{230}Th/^{238}U$) in dust could also be explained by external distant–derived foreign dust. This is because much smaller particles in dust are likely to be suspended longer in the atmosphere and transported over vast areas (Prospero, 1999). Similarity in ($^{234}U/^{238}U$) between Jornada soils and dust confirm the locally sourced dust material. Previous studies have proposed radionuclide fractionation in long distance travelling dust; daughter nuclides are suggested to be lost from dust into coarser particles due to gravitational settling (Biscaye et al., 1997; Aciego et al., 2015). If this were the case at the Jornada Basin, we would expect higher ($^{234}U/^{238}U$) in dust collected at 50 cm relative to that at 100 cm. Close-range activity ratios in the dust collected at the two heights despite differences in their particle sizes suggest that Jornada Basin dust does not travel significant distances as evidenced from $^{87}Sr/^{86}Sr$ ratios. Local sources frequently emit significant amounts of dust in the northern Chihuahuan Desert (Lee et al., 2009; Rivera Rivera et al., 2010; Baddock et al., 2011; Bullard et al., 2011).

3.6.2.1 Carbonate ages at the La Mesa geomorphic surface in the Jornada Basin

Presence of Bk horizons with stage V pedogenic carbonates at the La Mesa geomorphic surface suggests stability of landscape in the Jornada Basin for the last 1.6 Ma (Gile et al., 1981; Monger et al., 1998; Amundson et al., 1994; Gile, 2002). Pedogenic carbonates have progressively accumulated in soils since the Pleistocene Epoch; because precipitation process of the carbonates is thought to be affected by dissolution and re-precipitation, the carbonate tend to

vary in ages on micro and macroscales (Monger et al., 1998; Gile et al., 1981; Duetz et al., 2002). Therefore, carbonate ages obtained in this study most likely characterize averages for several periods of carbonate crystal growth within a large carbonate sample.

Determination of pedogenic carbonates allows interpretation of paleo-environmental conditions when the carbonates formed. Correlation of geomorphic positions/mapping units, Carbon-14, volcanic rocks (e.g. pumice) dating, and magnetostratigraphy have also provided useful age information on geomorphic surfaces, soils, and pedogenic carbonates of the southern Rio Grande rift (Gile et al., 1981, Buck and Monger, 1999; Mack et al., 2006). These dating techniques have different challenges; for instance, carbon-14 technique is suitable for material ranging ~30-40 ka. Co-precipitation of radioactive U with Ca^{2+} in the carbonate minerals have allowed us determine ages of such deposits using U-series dating technique, which provides reliable ages for relatively older formations of up to ~ 350 to 500 ka (St Pierre et al., 2012; Ku et al., 1979; Ludwig and Paces, 2002; Sharp et al., 2003; Pustovoyotov et al., 2007).

As mentioned earlier, incorporated detrital siliceous-derived U and Th into precipitating carbonates must be rectified in order to obtain meaningful carbonate ages. Failure to correct for detrital U or Th contamination in carbonates yields overestimated old ages (Ludwig 2003; Blisniuk et al., 2012). For this reason uncorrected carbonate ages for the caliche samples at the La Mesa_JER in table 2 are not discussed further. However, we note that the uncorrected ages mark the upper-most age limits of the carbonates. Most of the corrected ages of the thick caliche deposit at the La Mesa_JER become progressively younger towards the land surface (Table 2.4; Figure 2.6). This is consistent with carbonate stratigraphy in which carbonates grow upward from older layers at the bottom (Duetz et al., 2002). The obtained single sample U-series ages for H2, H4, and H3 relied on an assumed initial ($^{230}Th/^{232}Th$) (Table 2.2). Both HCl and AcOH acids

leach out carbonates and other soluble minerals from the bulk caliche samples leaving behind the insoluble siliceous component; all acid caliche leachates indicated higher ($^{234}U/^{238}U$) as expected (Table 2.5). However, HCl is a stronger acid relative to acetic acid, it can dissolve some residual detrital material therefore increasing the ($^{230}Th/^{232}Th$); using such high initial ($^{230}Th/^{232}Th$) for single sample correction method may results in overcorrection of detrital component yielding younger ages (Linge et al., 2009). For example, the single sample carbonate ages obtained after detrital correction with initial ($^{230}Th/^{232}Th$) of the H1 HCl_R were about 4-14% younger than those reported after assuming initial ($^{230}Th/^{232}Th$) of the upper continental crust and H1 AcOH_R fraction (Table 2.2). These carbonate ages were not thus considered for temporal variations of the paleoclimate conditions in the region. The initial ($^{230}Th/^{232}Th$) of the upper continental crust and that of H1 AcOH_R fraction were similar suggesting that bulk earth siliceous component dominate the detrital phase. ^{230}Th detrital correction using these activity ratios yielded close-ranged carbonate ages between ~145 and 5 ka (mid-Pleistocene- mid Holocene Epoch) (Tables 2.2; Figure 2.6). Shallower carbonates (H4C and H2) formed between the Last Glacial Maxima (LGM; ~20 ka) and mid- Holocene (~6000yrs) while the older H3 carbonates formed in the Pleistocene (~150-50 ka) epoch (Figure 2.6). These ages imply that the thick caliche at the La Mesa_JER formed at least by the mid-Holocene.

Carbonate ages obtained using the isochron techniques resulted in older carbonate ages compared to single sample detrital corrected ages of the same samples (Tables 2.2, 2.4, and 2.5). Because pedogenic carbonates are likely to have different mixing proportions of cogenetic detritus and carbonate samples, isochron correction techniques enable extrapolation of the isotope compositions of detritus and authigenic components of a sample (Torfstein et al., 2013). Isochrons therefore give a better estimate of authigenic carbonate isotope composition as

compared to the single sample correction technique, which relies on the assumed initial ($^{230}Th/^{232}Th$). Either Rosholt-type or Osmond-type isochrons give similar detrital-corrected ($^{230}Th/^{238}U$) and ($^{234}U/^{238}U$). However, Rosholt-type isochrons result in highly correlated ($r^2 = 1$) points of ($^{234}U/^{232}Th$) and ($^{230}Th/^{232}Th$) with ($^{238}U/^{232}Th$) that are expected for older crustal materials (Ludwig, 2003). Ludwig, (2003) explores the drawbacks associated with isochrons in which Rosholt-type of isochron are suitable for high ^{232}Th samples and Osmond-type isochrons fit for low ^{232}Th samples. Thorium concentrations range between 1 and 3 ppm in the caliche samples (Tables 2.2, 2.4, and 2.5), which are about 2 magnitudes lower than the average concentration expected in continental crust (Toboada et al., 2006). Due to such low ^{232}Th concentrations in caliche samples, only Osmond-derived ages were considered for paleoclimate interpretation. Ludwig, (2003) further explains that the ^{230}Th, ^{234}U, and ^{238}U isotopes relate with each other in a complex way rendering both 2D paired isochrons statistically erroneous. As a result, 3D Osmond isochrons, which involve plotting ^{232}Th, ^{230}Th, and ^{234}U normalized by ^{238}U on a 3D space to obtain authigenic ($^{230}Th/^{238}U$) and ($^{234}U/^{238}U$) are recommended (Ludwig, 2003). Only H2 samples yielded reliable carbonate ages following these 3D calculations, H1and H3 yielded ages with huge errors (Table 2.5). An effort to reduce the errors on corrected carbonate ages of H1 and H3 samples by reducing the number of subsamples from five to three was not fruitful (Table A2). Possible explanation for the unreliable H1 and H3 carbonates could be multiple detrital U and Th incorporated in the carbonates due to open system behavior (Chabaux et al., 2003) or multiple sources of carbonates.

Lateral variability in carbonate ages between H2 and H4 are distinct; H4, which occur at shallower depths than H2 yielded older ages (Table 2.2). This may suggest that younger carbonates above H4 might have been eroded away or deflated exposing older carbonates prior

to sandy-loamy eolian sediment deposition. The sharp boundary between the cemented caliche top layer and H1 soil could be related to an unconformity (Figure 2.2); erosion of upper soil profile has previously been proposed in the Jornada Basin (Monger et al., 1998). Because lamina A and C are the first and last layers to be deposited in a given caliche hand sample respectively, we would expect the carbonate ages to decrease as follows A>B>C if upward growth is the main formation mechanism. Variability in carbonate ages between the lamina of one hand sample can be explained by dissolution and re-precipitation processes common on reworked carbonates or inclusion of carbonate crystals of wide ranges of ages within one hand sample. Variations of uranium concentrations and ($^{234}U/^{238}U$) ratios are indicative of open system behavior, which normally affects the U- series chronometer. Nevertheless, based on paleomagnetic data and pumice dating, soils of the La Mesa_JER geomorphic surface in the Jornada Basin have been found to be between 1.6 and 0.78 Ma (Gile et al., 1981, Gile, 2002; Mack et al., 1996). The amount of pedogenic carbonates in La Mesa_JER soils range between 858 and 1861 kg/m^2 with accumulation rates of 1.2 kg/m^2/1000yrs (Gile, 2002). Because pedogenic carbonates form after stabilization of the sediments and soils, they are expected to be younger than the host material. Indeed the exposed caliche indicated the expected carbonate younger ages (194 - 5ka) compared to the La Mesa geomorphic surface age; however, possible older carbonates could be interfered to locate beyond the 200m depths.

3.6.3 PALEO-SOIL MOISTURE CONDITIONS IN THE JORNADA BASIN

3.6.3.1 Evidence from uranium activity ratios ($^{234}U/^{238}U)_0$

Paleohydrologic conditions within the Jornada Basin have varied through geologic time as deduced from the ($^{234}U/^{238}U)_0$ activity ratios. The ($^{234}U/^{238}U)_0$ indicate the uranium isotopic composition in soil water from which pedogenic carbonates precipitated (Maher et al., 2006.

2014; Oster et al., 2012). Variation of $(^{234}U/^{238}U)_0$ in soil water depends on changes of U in dust or water input, U distribution in rocks, or open system behavior (Oster et al., 2012). The $(^{234}U/^{238}U)_0$ of carbonates at La Mesa_JER range between 0.95 ± 0.01 and 1.73± 0.12 (Table 2.2, 2.4, and 2.5), these initial U activity ratios vary with the method used in sample treatment, but overall they show lower values in older carbonates and increase from the inner to the outer lamina of the carbonates (Table 2.2; Figure 2.6). Since it is challenging to ascertain the distribution of U concentration and $(^{234}U/^{238}U)$ in the parent material (Camp Rice Formation in this case) and paleodust, we interpret the observed variation of $(^{234}U/^{238}U)_0$ as a mixture of different U isotopic compositions in soil water characteristic of carbonate generation.

Soil moisture (thus rainfall amounts) controls weathering processes and thus mobility of soluble ions including U and controls $(^{234}U/^{238}U)$ isotope fractionation in soils (Chabaux et al., 2003; Pelt et al., 2008). Due to rock dissolution during chemical weathering processes, fractionation of U isotopes likely results in lower measured $(^{234}U/^{238}U)$ in soil water. Physical weathering on the other hand, exposes fresh mineral surfaces, which enhances U isotope fractionation by alpha recoil processes; this results in high $(^{234}U/^{238}U)$ in soil water. Lower $(^{234}U/^{238}U)_0$ observed in H3 carbonates could suggest higher rainfall at the time of formation, which leads to rock dissolution or water flowing through ^{234}U-depleted soils. Another explanation of the low $(^{234}U/^{238}U)_0$ in the H3 carbonates is old deep geothermal fluids upwelling to soils through faults. Because these old deep fluids are characteristic of low $(^{234}U/^{238}U)$ ratios, carbonate precipitates from such waters are characteristic of low $(^{234}U/^{238}U)_0$. Mack et al. (2012) has shown that meteoric water in combination with geothermal water have resulted in precipitation of secondary minerals in soils within southern Rio Grande Rift, NM. The $^{87}Sr/^{86}Sr$ ratios show that modern dust is a major cation source for H2 and H4C carbonates suggesting

relatively constant dust chemical composition since their formation, thus ($^{234}U/^{238}U$) of modern dust (~1; Table 2.1) alone cannot explain the high ($^{234}U/^{238}U)_0$ of 1.21 ± 0.01 to 1.73± 0.12 in the carbonates (Table 2.2, 2.4, and 2.4). Higher ($^{234}U/^{238}U)_0$ in soil water at the time of H2 and H4C formation could suggest lower rainfall, which resulted in higher preferential loss of ^{234}U and subsequent deposition in carbonates.

3.6.3.2 Evidence from stable carbon isotopes ($\delta^{13}C_{OC}$)

Interpretation of $\delta^{13}C$ values in pedogenic carbonates is complex due to multiple carbon sources in the soil/root zone (Cook and Herczeg, 2012). However, enrichment of $\delta^{13}C_{CaCO3}$ in pedogenic carbonates compared to $\delta^{13}C_{OC}$ values provides evidence of authigenic carbonates (Table 2.5). These $\delta^{13}C_{CaCO3}$ values are consistent with ^{13}C values in the pedogenic carbonates reported at various locations within the Jornada Basin (Liu, 2002; Serna-Perez et al., 2006). The $\delta^{13}C_{OC}$ in pedogenic carbonates are controlled by soil CO_2 during carbonate precipitation; soil CO_2 is in turn a mixture of atmospheric CO_2 and soil respired CO_2 from plants and heterotrophic respiration (Catoni et al., 2011; Cerling, 1999). Monger et al. (1998) discusses factors which affect interpretation of $\delta^{13}C$ in pedogenic carbonates as paleo-environmental indicators. In their study, they related variations in $\delta^{13}C_{OC}$ within soil profiles to changes in respiration rates and vegetation types (Monger et al., 1998). In this light, we note a slight enrichment of the $\delta^{13}C_{OC}$ of pedogenic carbonates (-23 to -20.3‰) towards land surface (Table 2.5). This enrichment could probably be associated with: (1) changes in vegetation type, (2) change in mixing of atmospheric CO_2 with soil CO_2, and (3) variations in land stability and plant density. Cole and Monger, (1994) has previously associated variations in $\delta^{13}C_{OC}$ in paleosols within Chihuahua, New Mexico to vegetation changes and climatic factors. We note that $\delta^{13}C_{OC}$ values are within the

ranges documented for C3 dominated plants (Cerling, 1999); therefore, if change in vegetation types is a vital factor accounting for $\delta^{13}C_{OC}$ enrichment, then changes were gradual or minimal at the time of carbonate formation.

The lowest $\delta^{13}C_{OC}$ values in H3 carbonates suggest high respiration rates thus increased plant density. High plant biomass infers high precipitation thus relative high relative paleo-moisture environments; moreover, the inferred C3 vegetation performs best under cooler and more humid conditions (Cerling and Quade, 1993). Such an interpretation is consistent with low $(^{234}U/^{238}U)_0$ which implied formation of H3 carbonates in moister conditions. A slight shift towards enriched $\delta^{13}C_{OC}$ in H2 carbonates probably suggests decrease in respiration rates thus low plant density due to drier conditions. Alternatively, the shift could also imply intrusion of C4 plants, which grow on hotter and drier conditions relative to cooler wetter climate (Cerling and Quade, 1993). The C4 vegetation may have shifted to CAM, C4, and C3 vegetation currently found at the Jornada Basin. Pedogenic carbonates in H1 soils were the most enriched (Table 4) providing further evidence of warm and drier periods during the of Holocene Epoch that has shifted C3 shrubs to higher elevation. Oxygen isotopes in pedogenic carbonates would better constrain the effect of meteoric water on pedogenic carbonate formation (Cerling 1984; Cerling and Quade, 1993, Amundson, 1996, Monger et al., 1998). However, previous studies of soil pedons in the vicinity of the Jornada Basin did not show significant shifts in $\delta^{18}O$ values with depth and various geomorphic surfaces (Monger et al., 1998).

3.6.3.3 Evidence from strontium isotopes ($^{87}Sr/^{86}Sr$)

Due to low Rb/Sr ratios in pedogenic carbonates, the $(^{87}Sr/^{86}Sr)$ ratios incorporated in the carbonates are stable and can be used to fingerprint calcium sources in soil water from which they precipitated. Shallow carbonates at our study area showed $(^{87}Sr/^{86}Sr)$ ratios similar to the

local modern dust (Figure 2.5); because production of dust is associated to low annual rainfall (Prospero et al., 2002) thus low soil moisture, shallower pedogenic carbonates may have formed in drier conditions similar to todays' climate. More radiogenic ($^{87}Sr/^{86}Sr$) ratios in pedogenic carbonates at depth have a different source probably groundwater which weather older granitic rocks. Chemical weathering requires relative high moisture implying that carbonates at depth could have formed in more wet environments. Mack et al. (2012) shows that shallow meteoric groundwater or upwelling geothermal fluids have contributed significantly to precipitation of secondary minerals such as opal and calcite in the Jornada Basin.

3.6.4 COMPARISON OF PALEO-MOISTURE CONDITIONS OF THE JORNADA BASIN WITH OTHER PALEOCLIMATE INFORMATION OF THE SOUTHWEST USA

Determination of pedogenic carbonates ages in Quaternary formations provides timing of various climatic events. This study considers the climatic record of the late Pleistocene to mid Holocene as indicated by ages of the pedogenic carbonate at the La Mesa_JER. This period involves a series of glacial and interglacial cycles generally known for wet Pleistocene and drier Holocene (Asmeron et al., 2010; Wagner et al., 2010; Feng et al., 2014; Wong et al., 2015). This period encloses a wide range of major climatic events characterized by rapid temperature and moisture changes at the global or regional scales such as Last Glacial Maxima (LGM; ~20 ka), Heinrich stadial I (H1; 18-14 ka), warmer-drier BΦlling – AllerΦd (BA; 14.7 – 12.9 ka), and cool- wet Younger Dryas (YD; ~12.9 -11.5 ka) (Ballenger et al., 2011; Briles et al., 2012). Such climatic changes have been reconstructed from proxy data in southwest North America based on physical evidence (pluvial lakes), biotic evidence (packrat middens, fossil pollen, paleontology, stable C isotopes of organic matter, paleosols, and pedogenic carbonates), and soil-geomorphic evidence (alluvial and dune stratigraphy, pedogenic carbonates; speleothems; groundwater

deposits) (Monger, 2003; Pigati et al., 2008; Ballenger et al., 2011; Wong, et al., 2015). We relate proxy records within the Jornada Basin, New Mexico and the general southwest region with $(^{234}U/^{238}U)_{0,}$ $^{87}Sr/^{86}Sr$, and $\delta^{13}C_{OC}$ values in order to provide an overview of paleo-moisture conditions within the Jornada Basin between 194 ± 37 and 6 ka.

Timing of paleoclimate record of the southwest USA region beyond the carbon-14 age limits (≤ 40ka) are inadequate; however, our U-series ages and isotopic data suggest more moist conditions in the Jornada Basin around 194 ± 37ka. Bradbury, (1997) has shown evidence of moist climates (overflowing lake systems) in the south west USA between 180-110ka due to dominance of freshwater planktic diatoms in sediments from the Pleistocene Owens lake, California. Because H3 carbonates yielded ages >100ka we suggest that these carbonates formed in wet conditions/high effective moisture in soil environments as evidenced from low $(^{234}U/^{238}U)_{0,}$ high $^{87}Sr/^{86}Sr$, and depleted $\delta^{13}C_{OC}$ values (Figure 2.6). Variations of $(^{234}U/^{238}U)_{0}$ in H3 carbonates (e.g. H3C>H3B and H3A; Table 2.2) could suggest that even within a dominant wet period there were warmer and low moisture events during which some carbonates formed.

H2 carbonates formed over a wide period of time spanning from ~60 ka to mid-Holocene (Figure 2.6); this is a period of known alternating dry and wet stages within the southwest USA and northern Mexico (Bradbury, 1997; Pigati et al., 2008; Metcalfe et al., 2002; Holmgren et al., 2003, 2007; Ballenger et al., 2011). While variations in the $(^{234}U/^{238}U)_{0}$ ratios in H2 carbonates generally agree with periodic dry and moist phases in the southwest, differences in timing of climate events between the carbonate lamina represent time-integrated climatic record consistent with poor stratigraphy and diachronous nature of pedogenic carbonates. Reconstruction of paleovegetation using packrat middens, fossil pollen, and stable C isotope proxies in the vicinity of the Jornada Basin has provided clues of prevailing climatic conditions prior to significant

anthropogenic influence. For instance existence of woodlands and C4 grasses in the American southwest between 42 and 10 ka suggest wet conditions (Van Devender, 1990; Betancourt et al., 2001; Holmgren et al., 2003, 2007; Monger, 2003; Ballenger et al., 2011). Paleo-lake highstands between 20 and 10 ka and expansion of lakes in the late Pleistocene to early Holocene suggest high moisture conditions in the southwest region (Metcalfe et al., 1997; Krider, 1998; Phillips et al., 1992; Allen and Anderson, 2000; Castiglia and Fawcett, 2006). Similarly, paleoclimate reconstruction using pollen and algae in lake sediments cores as well as vegetation suggest high moisture events in the southwest North America during the late Pleistocene-early Holocene Epoch (Davis, 1999; Mensing, 2001). Previous studies have related high moisture events during the late Pleistocene to early Holocene in the southwest USA to southward deflection of polar jet stream and insolation variability (Cooperative Holocene Mapping Project Members, 1988; Davis 1999). Other studies have indicated alternating wetter and drier conditions in the late Pleistocene. For instance based on studies of groundwater deposits, reconstructed high water table (hence effective moisture) was reported in southeast Arizona between 50-30 ka (Pigati et al., 2008). Fluctuations of the water table were consistent with major climatic events recording lower moisture contents during the BΦlling – AllerΦd (~14.7 – 12.9 ka) but higher moisture events during the Younger Dryas (Pigati et al., 2008). Similarly stable O isotopes in speleothems from New Mexico and Arizona have revealed wet conditions due to winter and summer precipitations between 56-11 ka (Polyak et al., 2004; Brook et al., 2006; Asmeron et al., 2010; Wagner et al 2010; Feng et al., 2014). The summer precipitations were associated with drier BΦlling – AllerΦd while the winter precipitations were linked to wetter Younger Dryas. We associate high $(^{234}U/^{238}U)_0$ and enriched $\delta^{13}C_{OC}$ in H2 carbonates to deposition during a drier phase. However,

variations of $(^{234}U/^{238}U)_0$ within H2 carbonates suggest fluctuations in soil moisture (hence rainfall) quantities during this period implying oscillations of wet and dry climate.

The mid Holocene is generally associated with warmer and drier conditions in southwest North America based on paleovegetation studies and other proxy records (Holmgren et al., 2003; 2007; Wong et al., 2015). Dry phases have been recorded at the Jornada Basin at about 10,000 ±3000yrs B.P in the early Holocene transition period (Monger, 2003; Gile et al., 1981; Cole and Monger 1994; Hawley, 1993; Monger et al., 1998; Buck and Monger, 1999). Consistent with these dry spells, enriched $\delta^{13}C_{OC}$ values in pedogenic carbonates of Holocene soils (H1) show evidence of aridity. Age range of H2 carbonates span between Pleistocene to early-mid Holocene (Figure 2.6), variations in associated $(^{234}U/^{238}U)_0$ suggests that transition from Pleistocene to early-mid Holocene was not completely dry, short wet spells occurred within the prevailing dry period in which the carbonates formed. For example, based on variations of paleo-lake levels, significantly wet conditions have been reported in the northern Mexico, a part of Chihuahua Desert during the early-late Holocene (Castiglia and Fawcett, 2006). Based on Packrat midden found in Durango New Mexico, Van Devender, (1990) reported a wet climate in the mid-Holocene Epoch. Similarly significant wet climatic intervals during the mid-Holocene have been reconstructed within the southwest North America such as Estancia Basin, New Mexico, Mono lake, California, (Davis, 1999; Menking and Anderson, 2003; Polyak et al., 2001; Hall et al., 2013). Moist conditions in the mid-Holocene have been associated with monsoon activities and southward shifts of winter storm tracks (Van Devender, 1990; Castiglia and Fawcett, 2006).

3.7 Conclusion

Stage V pedogenic carbonates at the La Mesa geomorphic surface in the Jornada Basin have recorded relative paleo-moisture average quantities through geologic time. Initial uranium

activity ratios {($^{234}U/^{238}U)_0$,}, $^{87}Sr/^{86}Sr$ ratios, and $\delta^{13}C_{OC}$ values in the carbonates show that paleo-moisture conditions continuously varied on long-term scale (between 200 and 6 ka) and within short time intervals. Young shallower carbonates formed during drier conditions while older carbonates at depth precipitated under wetter and moist environment. However even within dominating respective moisture conditions, opposite paleo-precipitation regimes occurred over, which carbonates were deposited. Similar to variability of paleo-moisture conditions with depth along a soil profile, carbonate sources varied in the shallow and deeper carbonates. The $^{87}Sr/^{86}Sr$ ratios in soluble carbonate fractions suggest that atmospheric local dust was a significant contributor of Ca and Sr to shallower carbonates while carbonates at depth precipitated from a more radiogenic source. We speculate that the carbonates at depth could have precipitated from soil waters with higher $^{87}Sr/^{86}Sr$ ratios probably from weathering of older igneous material, radiogenic dust or from upwelling deep groundwater.

3.8 Recommendations

Only four points on a soil profile at the La Mesa geomorphic surface, Jornada Basin were considered for this study. Even though our paleohydrologic conditions are generally consistent with some paleoclimatic proxy indicators, additional $(^{234}U/^{238}U)_0$ in pedogenic carbonates in various parts of the in the basin need to be computed to better constrain paleomoisture conditions of the region.

References

Aciego, S. M., Aarons, S. M., Sims, K. W. (2015). The uranium-isotopic composition of Saharan dust collected over the central Atlantic Ocean *Aeolian Research, 17*, 61-66.

Amundson, R., Chadwick, O., Kendall, C., Wang, Y., DeNiro, M. (1996). Isotopic evidence for shifts in atmospheric circulation patterns during the late Quaternary in mid-North America. *Geology*, 24, 23-26.

Amundson, R.G., Wang, Y., Chadwick, O.A., Trumbore, S., McFadden, L., McDonald, E., Wells, S., Deniro, M. (1994). Factors and processes governing the C-14 content of carbonate in desert soils. *Earth and Planetary Science Letters*, 125, 385-402.
Allen, B. D. and Anderson, R. Y. (2000). A continuous, high-resolution record of late Pleistocene climate variability from the Estancia basin, New Mexico. *Geological Society of America Bulletin*, *112*(9), 1444-1458.

Alonso-Zarza, A.M. (2003). Palaeoenvironmental significance of palustrine carbonates and calcretes in the geological record. *Earth-Science Reviews*, 60, 261–298.

Alvarez, L. J., Epstein, H. E., Li, J., Okin, G. S. (2012). Aeolian process effects on vegetation communities in an arid grassland ecosystem. *Ecology and evolution*, *2*(4), 809-821.

Asmerom, Y., Polyak, V.J., Burns, S.J. (2010). Variable winter moisture in the Southwestern United States linked to rapid glacial climate shifts. *Nature Geoscience* 3, 114-117.

Baddock, M. C., Gill, T. E., Bullard, J. E., Acosta, M. D., Rivera Rivera, N. I. (2011). Geomorphology of the Chihuahuan Desert based on potential dust emissions. *Journal of Maps*, *7*(1), 249-259.

Ballenger, J.A.M., Holliday, V.T., Kowler, A.L., Reitze, W.T., Prasciunas, M.M., Miller, D.S., Windingstad, J.D. (2011). Evidence for Younger Dryas global climate oscillation and human response in the American Southwest. *Quaternery. International* 242, 502–519.

Bergametti, G. and Gillette, D. A. (2010). Aeolian sediment fluxes measured over various plant/soil complexes in the Chihuahuan desert. *Journal of Geophysical Research* 115, F03044, doi:10.1029/2009JF001543

Betancourt, J.L., Rylander, K.A., Pen˜alba C., McVickar, J.L. (2001). Late Quaternary vegetation history of Rough Canyon, south-central New Mexico, USA. *Palaeogeography, Palaeoclimatology, Palaeoecology*, 165 (1), 71–95.

Blisniuk, K., Oskin, M., Fletcher, K., Rockwell, T., Sharp, W. (2012). Assessing the reliability of U-series and 10 Be dating techniques on alluvial fans in the Anza Borrego Desert, California. *Quaternary Geochronology*, *13*, 26-41.

Birkeland, P.W. (1999). Soils and Geomorphology. Oxford University Press, New York, 430

Biscaye, P. E., Grousset, F. E., Revel, M., Van der Gaast, S., Zielinski, G. A., Vaars, A., Kukla, G. (1997). Asian provenance of glacial dust (stage 2) in the Greenland Ice Sheet Project 2 ice core, Summit, Greenland. *Journal of Geophysical Research: Oceans*, *102*(C12), 26765-26781.

Bourdon, B., Turner, S., Henderson, G. M., Lundstrom, C. C. (2003). Introduction to U-series geochemistry. *Reviews in Mineralogy and Geochemistry*, *52*(1), 1-21.

Bradbury, J. P. (1997). A diatom record of climate and hydrology for the past 200 ka from Owens Lake, California with comparison to other Great Basin records. *Quaternary Science Reviews, 16*(2), 203-219.

Briles, C.E., Whitlock, C., Meltzer, D. (2012). Last glacial-interglacial environments in the southern Rocky Mountains, USA and implications for Younger Dryas-age human occupation. *Quaternary Research* 77, 96–103.

Brock, A. L. and Buck, B. J. (2009). Polygenetic development of the Mormon Mesa, NV petrocalcic horizons: geomorphic and paleoenvironmental interpretations. *Catena, 77*(1), 65-75.

Brook, G. A., Ellwood, B. B., Railsback, L. B., Cowart, J. B. (2006). A 164 ka record of environmental change in the American Southwest from a Carlsbad Cavern speleothem. *Palaeogeography, Palaeoclimatology, Palaeoecology 237*(2), 483-507.

Buck, B. J. and Monger, H. C. (1999). Stable isotopes and soil- geomorphology as indicators of Holocene climate change, northern Chihuahuan Desert. *Journal of Arid Environments* 43, 357–373.

Buck, B. J. and Van Hoesen, J.G. (2002). Snowball morphology and SEM analysis of pedogenic gypsum, southern New Mexico. *Journal of Arid Environments* 51, 469–487

Buck, B. J. and Van Hoesen, J. G. (2005). Assessing the applicability of isotopic analysis of pedogenic gypsum as a paleoclimate indicator, Southern New Mexico. *Journal of arid environments 60*(1), 99-114.

Bullard, J. E., Sandy, P. H., Matthew, C. B., Nick, D., Thomas, E. G., Grant, M., Youbin, S. (2011). Preferential dust sources: A geomorphological classification designed for use in global dust-cycle models. *Journal of Geophysical Research: Earth Surface* 116, F04034, doi:10. 1029/2011JF002061

Candy, I. (2002). Formation of a rhizogenic calcrete during a glacial stage (Oxygen Isotope Stage 12): its palaeoenvironmental and stratigraphic significance. *Proceedings of the Geologists' Association,* 113, 259 – 270

Capo, R. C. and Chadwick, O. A. (1999). Sources of strontium and calcium in desert soil and calcrete. *Earth and Planetary Science Letters*, *170*(1), 61-72.

Capo, R. C., Stewart, B. W., Chadwick, O. A. (1998). Strontium isotopes as tracers of ecosystem processes: theory and methods. *Geoderma, 82*(1), 197-225

Castiglia, P. J. and Fawcett, P. J. (2006). Large Holocene lakes and climate change in the Chihuahuan Desert. *Geology*, *34*(2), 113-116.

Catoni, M., Monger, H. C. M., Bonifacio, E. (2011). Pedogenic carbonate $\delta^{13}C$ and environmental precipitation conditions. *EQA-International Journal of Environmental Quality*, *7*(7), 17-24.

Caudill, M.R., Driese, S.G., Mora, C.I. (1996). Preservation of a paleo-Vertisol and an estimate of late Mississippian paleoprecipitation. *Journal of Sedimentary Research* 66A, 58–70.

Cerling, T. E. (1984). The stable isotopic composition of modern soil carbonate and its relationship to climate. *Earth Planetary Science Letters* 71, 229–240.

Cerling, (1999), Stable carbon isotopes in palaeosol carbonates, in M. Thiry, R.S.-C., ed., Palaeoweathering, palaeosurfaces and related continental deposits. *Special Publication of the International Association of Sedimentologists* 27, 43-60.

Cerling, T.E.and Quade, J. (1993). Stable carbon and oxygen isotopes in soil carbonates. In: Swart, P.K, Lohmann, K.C., McKenzie, J., Savin, S. (Eds), Climate Change in Continental Isotopic Records. *American Geophysical Union, Monograph 78,* 217–231.

Chabaux, F., Riotte, J., Dequincey, O. (2003). U-Th-Ra fractionation during weathering and river transport. *Reviews in Mineralogy and Geochemistry 52*(1), 533-576.

Chadwick, O.A., Derry, L.A., Vitousek, P.M., Huebert, B.J., Hedin, L.O. (1999). Changing sources of nutrients during four million years of ecosystem development. *Nature,* 397 (6719), 491–497.

Cheng, H., Edwards, R. L., Hoff, J., Gallup, C. D., Richards, D. A., Asmerom, Y. (2000). The half-lives of uranium-234 and thorium-230. *Chemical Geology*, *169*(1), 17-33.

Chiquet, A., Michard, A., Nahon, D., Hamelin, B. (1999). Atmospheric input vs in situ weathering in the genesis of calcretes: an Sr isotope study at Gálvez (Central Spain). *Geochimica et Cosmochimica Acta 63*(3), 311-323.

Cole, D. R. and Monger, H. C. (1994). Influence of atmospheric CO_2 on the decline of C4 plants during the last deglaciation. *Nature 368*, 533-536.

Cook, P. G. and Herczeg A. L. (Eds.). (2000). Environmental tracers in subsurface hydrology. Kluwer Academic Publishers, Boston, Massachusetts, USA

Cooperative Holocene Mapping Project Members (1988). Climatic changes of the last 18,000 years: Observations and model simulations: *Science* 241, 1043–1052.

Creamean, J. M., Suski, K. J., Rosenfeld, D., Cazorla, A., DeMott, P. J., Sullivan, R. C., Tomlinson, J. M. (2013). Dust and biological aerosols from the Sahara and Asia influence precipitation in the western US. *Science*, *339*(6127), 1572-1578.

Dart, R. C., Barovich, K. M., Hill, S. M., Chittleborough, D. J. (2012). Sr-isotopes as a tracer of Ca sources and mobility in profiles hosting regolith carbonates from southern Australia. *Australian Journal of Earth Sciences, 59*(3), 373-382.

Davis, O. K. (1999). Pollen analysis of a late-glacial and Holocene sediment core from Mono Lake, Mono County, California. *Quaternary Research 52*(2), 243-249.

Deutz, P., Montanez, I.P., Monger, C.H. (2002). Morphology and Stable and Radiogenic Isotope Composition of Pedogenic Carbonates in Late Quaternary Relict Soils, New Mexico, U.S.A.: An Integrated Record of Pedogenic Overprinting. *Journal of Sedimentary Research*, 72(6), 809-822.

Driese, S.G. and Mora, C.K. (1993). Physico-chemical environment of pedogenic carbonate formation in Devonian vertic paleosols, central Appalachians, USA. *Sedimentology* 40, 199–216.

Durand, N., Gunnell, Y., Curmi, P., Ahmad, S. M. (2007). Pedogenic carbonates on Precambrian silicate rocks in South India: Origin and paleoclimatic significance. *Quaternary International*, *162*, 35-49.

Dworkin, S.I., Nordt, L., Atchley, S. (2005). Determining terrestrial paleotemperatures using the oxygen isotopic composition of pedogenic carbonate. *Earth Planetary Science Letters*, 237 (1–2), 56–68.

Ekart, D.D., Cerling, T.E., Montanez, I.P., Tabor, N.J. (1999). A 400-million year carbon isotope record of pedogenic carbonate: implications for paleoatmospheric carbon dioxide. *American Journal of Science*, 299, 805–827.

Eswaran, H., Reich, P. F., Kimble, J. M., Beinroth, F. H., Padmanabhan, E., Moncharoen, P. (2000). Global carbon stocks. . In: J.M.K. R. Lal and B.A. Stewart. (Editors), Global Climate Change and Pedogenic Carbonates. CRC/Lewis Press, Boca Raton, Fla, 15–26.

Feldman, C. (1983). Behavior of traces of refractory minerals in the lithium metaborate fusion-acid dissolution procedure. *Analytical Chemistry 55*(14), 2451-2453.

Feng, W., Hardt, B. F., Banner, J. L., Meyer, K. J., James, E. W., Musgrove, M., ... Min, A. (2014). Changing amounts and sources of moisture in the US southwest since the Last Glacial Maximum in response to global climate change. *Earth and Planetary Science Letters 401*, 47-56.

Fleischer, R. L. (1980). Isotopic Disequilibrium of Uranium: Alpha-Recoil Damage and Preferential Solution Effects. *Science*, 207, 979

Floyd, K. W. and Gill, T. E. (2011). The association of land cover with aeolian sediment production at Jornada Basin, New Mexico, USA. *Aeolian Research 3*(1), 55-66.

Frumkin, A. and Stein, M. (2004). The Sahara–East Mediterranean dust and climate connection revealed by strontium and uranium isotopes in a Jerusalem speleothem. *Earth and Planetary Science Letters*, *217*(3), 451-464.

Gibbens, R. P., McNeely, R. P., Havstad, K. M., Beck, R. F., Nolen, B. (2005). Vegetation changes in the Jornada Basin from 1858 to 1998. *Journal of Arid Environments* 61, 651– 668.

Gile, L. H. (2002). Lake Jornada, an early-middle Pleistocene lake in the Jornada del Muerto Basin, southern New Mexico. *New Mexico Geology 24*(1), 3-14.

Gile, L. H. and Grossman, R. B. (1979). The desert project soil monograph: Soils and landscapes of a desert region astride the Rio Grande Valley near Las Cruces, New Mexico. Washington, DC: US Department of Agriculture, Soil Conservation Service.

Gile, L.H., Hawley, J.W., Grossman, R.B. (1981). Soils and geomorphology in the Basin and Range area of Southern New Mexico: Guidebook to the Desert Project. New Mexico Bureau of Mines and Mineral Resources., Socorro, NM, 222 .

Gillette, D. A. (1999). A qualitative geophysical explanation for hot spot dust emitting source regions. *Contributions to Atmospheric Physics 72*(1), 67-77.

Gillette, D. A. and Chen, W. (2001). Particle production and aeolian transport from a "supply-limited" source area in the Chihuahuan desert, New Mexico, United States. *Journal of Geophysical Research: Atmospheres 106*(D6), 5267-5278.

Gillette, D.and Monger, H.C., 2006. Eolian processes on the Jornada Basin. In: Havstad, K.M., Huenneke, L.F., Schlesinger, W.H. (Eds.), Structure and function of a Chihuahuan Desert ecosystem: the Jornada Basin long-term ecological research site. Oxford University Press, Oxford, New York, 189–210.

Hall, S. A. and Penner, W. L. (2013). Stable carbon isotopes, C 3–C 4 vegetation, and 12,800 years of climate change in central New Mexico, USA.*Palaeogeography, Palaeoclimatology, Palaeoecology*, *369*, 272-281.

Hawley, J. W. (1981). Pleistocene and Pliocene history of the international boundary area, southern New Mexico. *Hoffer, J-. M., Hoffer, RL (eds.), Geology of the border*, 26-32.

Hawley, J.W. (1993). Geomorphic Setting and Late Quaternary History of Pluvial-Lake Basins in the Southern New Mexico Region. New Mexico Bureau of Mines and Mineral Resources. Open-file Report 391.

Hellstrom, J. C. (2006). U-Th dating of speleothems with high initial ^{230}Th using stratigraphical constraint. *Quaternary Geochronology* 1, 289-295

Holmgren, C. A., Norris, J. and Betancourt, J. L. (2007). Inferences about winter temperatures and summer rains from the late Quaternary record of C4 perennial grasses and C3 desert shrubs in the northern Chihuahuan Desert. *Journal of Quaternary Science*, 22, 141–161. ISSN 0267-8179.

Holmgren, C.A., Peñalba, M.C., Rylander, K.A., Betancourt, J.L. (2003). A 16,000 14C yr B.P. packrat midden series from the USAeMexico borderlands. *Quaternary Research* 60, 319-329.

Ibarra, D. E. (2013). Applying Uranium-series Isotope Geochemistry and Geochronology to Great Basin Pleistocene Paleohydrology (Doctoral dissertation, Stanford University).

Ibarra, D. E., Egger, A. E., Weaver, K. L., Harris, C. R., & Maher, K. (2014). Rise and fall of late Pleistocene pluvial lakes in response to reduced evaporation and precipitation: Evidence from Lake Surprise, California.*Geological Society of America Bulletin*, B31014-1.

Jaillard, B., Guyon, A., Maurin, A. F. (1991). Structure and composition of calcified roots, and their identification in calcareous soils. *Geoderma* 50, 197–210.

Jin, L., Ogrinc, N., Hamilton, S. K., Szramek, K., Kanduc, T., Walter, L. M. (2009). Inorganic carbon isotope systematics in soil profiles undergoing silicate and carbonate weathering (Southern Michigan, USA). *Chemical Geology 264*(1), 139-153

Kaufman, A. (1993). An evaluation of several methods for determining ^{230}ThU ages in impure carbonates. *Geochimica et Cosmochimica Acta 57*(10), 2303-2317.

Krider, P. R. (1998). Paleoclimatic significance of late Quaternary lacustrine and alluvial stratigraphy, Animas Valley, New Mexico. *Quaternary Research 50*(3), 283-289.

Ku, T.L., Bull, W.B., S.T., F., Knauss, K.G. (1979). Th^{230}-U^{234} dating of pedogenic carbonates in gravelly desert soils of Vidal Valley, southeastern California. *Geological Society of America Bulletin*, 90(11), 1063-1073.

Lal, R. and Kimble, J.M. (2000a). Pedogenic carbonates and the global carbon cycle. In: R. Lal, J.M. Kimble, H. Eswaran and B.A. Stewart (Editors), Global climate change and pedogenic carbonates. Lewis Publishers, Boca Raton, 1-14.

Lee, J. A., Thomas, E. G., Kevin, R. M., Miguel, D. A., Adriana, E. P. (2009). Land use/land cover and point sources of the 15 December 2003 dust storm in southwestern North America. *Geomorphology*, 105 (1), 18-27.

Linge, H., Baker, A., Andersson, C., Lauritzen, S. E. (2009). Variability in luminescent lamination and initial ^{230} Th/^{232} Th activity ratios in a late Holocene stalagmite from northern Norway. *Quaternary Geochronology 4*(3), 181-192.

Liu, X. (2002). Calcium carbonate in subterranean termite foraging galleries in the northern Chihuahuan Desert. Ph.D. dissertation. New Mexico State University, Las Cruces

Liu, X., Monger, H. C., Whitford, W. G. (2007). Calcium carbonate in termite galleries – biomineralization or upward transport? *Biogeochemistry* 82, 241–250.

Ludwig, K. R. (2003). Mathematical–statistical treatment of data and errors for 230Th/U geochronology. *Reviews in Mineralogy and Geochemistry 52*(1), 631-656.

Ludwig, K. R. (2012). Isoplot 3.75: A geochronology toolkit for Microsoft Excel. *Berkeley Geochronology Center, Spec. Publ*, *5*.

Ludwig, K.R. and Paces, J.B. (2002) U-series dating of pedogenic silica and carbonate, Crater Flat. Nevada. *Geochimica et Cosmochimica Acta* 66, 487–506.

Machette, M.N. (1985). Calcic soils of the southwestern United States. *Geological Society of America,* 203, 1–21.

Mack, G. H., Giordano, T. H., Cole, D. R., James, W. C., Salyards, S. L. (1994). Stable oxygen and carbon isotopes of pedogenic carbonate as indicators of Plio-Pleistocene paleoclimate in the southern Rio Grande Rift, south-central New Mexico. *American Journal of Science 294*(5), 621-640.

Mack, G. H., Jones, M. C., Tabor, N. J., Ramos, F. C., Scott, S. R., Witcher, J. C. (2012). Mixed Geothermal and Shallow Meteoric Origin of Opal and Calcite Beds In Pliocene–Lower Pleistocene Axial–Fluvial Strata, Southern Rio Grande Rift, Rincon Hills, New Mexico, USA. *Journal of Sedimentary Research 82*(8), 616-631.

Mack, G. H., McIntosh, W. C., Leeder, M. R., Monger, H. C. (1996). Plio-Pleistocene pumice floods in the ancestral Rio Grande, southern Rio Grande rift, USA. *Sedimentary Geology 103*(1), 1-8.

Mack, G. H., Salyards, S. L., McIntosh, W. C., Leeder, M. R. (1998). Reversal magnetostratigraphy and radioisotopic geochronology of the Plio-Pleistocene Camp Rice and Palomas Formations, southern Rio Grande rift.*Guidebook 49*, 229-236.

Mack, G.H., Salyards, S.L., James, W.C. (1993). Magnetostratigraphy of the Plio-Pleistocene Camp Rice and Palomas Formations in the Rio Grande rift of southern New Mexico. *American Journal of Science 293,* 49-77.

Mack, G. H., Seager, W. R., Leeder, M. R., Perez-Arlucea, M., Salyards, S. L. (2006). Pliocene and Quaternary history of the Rio Grande, the axial river of the southern Rio Grande rift, New Mexico, USA. *Earth-Science Reviews 79*(1), 141-162.

Mack, G.H. and Suguio, K. (1991). Depositional environments of the Yeso formation (Middle Permian), southern Caballo Mountains. *New Mexico Geology* 13, 45–47.

Maher, K, Ibarra, D.E., Oster, J.L., Miller, D.M., Redwine, J.L., Reheis, M.C., Harden, J.W. (2014). Uranium isotopes in soils as a proxy for past infi ltration and precipitation across the western United States: *American Journal of Science* 314, 821–857, doi: 10 .2475 /04 .2014 .01

Maher, K., Steefel, C. I., DePaolo, D. J., Viani, B. E. (2006). The mineral dissolution rate conundrum: Insights from reactive transport modeling of U isotopes and pore fluid chemistry in marine sediments. *Geochimica et Cosmochimica Acta 70*(2), 337-363.

McFadden, L. D. (2013). Strongly dust-influenced soils and what they tell us about landscape dynamics in vegetated aridlands of the southwestern United States. *Geological Society of America Special Papers 500*, 501-532.

Menking, K.M. and Anderson, R.Y. (2003). Contributions of La Nin˜a and El Nin˜o to middle Holocene drought and late Holocene moisture in the American southwest. *Geology* 31, 937–940

Mensing, S. A. (2001). Late-glacial and early Holocene vegetation and climate change near Owens Lake, eastern California. *Quaternary Research 55*(1), 57-65.

Mermut, A. R., Amundson, R., Cerling, T. E. (2000). The use of stable isotopes in studying carbonate dynamics in soils. *Global climate change and pedogenic carbonates*, 65-85.

Metcalfe, S.E., Bimpson, A., Courtice, A.J., O'Hara, S.L., Taylor, D.M. (1997). Climate change at the monsoon/westerly boundary in northern Mexico. *Journal of Paleolimnology* 17, 155–171.

Metcalfe, S., Say, A., Black, S., McCulloch, R., & O'Hara, S. (2002). Wet conditions during the last glaciation in the Chihuahuan Desert, Alta Babicora Basin, Mexico. *Quaternary Research*, *57*(1), 91-101.

Monger, H. C. (2002). Pedogenic carbonate: links between biotic and abiotic $CaCO_3$. In 17. World congress of soil science, Bangkok (Thailand), *14-21 Aug 2002*.

Monger, H.C. (2003). Millennial-scale climate variability and ecosystem response at the Jornada LTER site. In: Greenland, D., Goodin, D.G., Smith, R.C. (Eds.), Climate Variability and Ecosystem Response at Long-Term Ecological Research Sites. Oxford University Press, London, 341–369.

Monger, H. C. (2006). Soil development in the Jornada Basin. *Structure and function of a Chihuahuan Desert ecosystem: The Jornada Basin Long Term Ecological Research site. Oxford Univ. Press, New York*, 81-106.

Monger, H.C., Cole, D.R., Buck, B.J., Gallegos, R.A. (2009). Scale and the isotopic record of C4 plants in pedogenic carbonate: from the biome to the rhizosphere. *Ecology* 90 (6), 1498-1511.

Monger, H.C., Cole, D.R., Gish, J.W., Giordano, T.H. (1998). Stable carbon and oxygen isotopes in Quaternary soil carbonates as indicators of ecogeomorphic changes in the northern Chihuahuan Desert, USA. *Geoderma* 82(1-3),137-172

Monger, H. C. and Gallegos, R. A. (2000). Biotic and abiotic processes and rates of pedogenic carbonate accumulation in the southwestern United States—relationship to atmospheric CO2 sequestration. Global climate change and pedogenic carbonates. CRC, Boca Raton, Fla, 273-289.

Monger, H. C., Kraimer, R. A., Cole, D. R., Wang, X., Wang, J. (2015). Sequestration of inorganic carbon in soil and groundwater. *Geology*, *43*(5), 375-378.

Monger, H.C., Mack, H.G., Nolen, A. B., Gile, H.L. (2006). Regional Setting of the Jornada Basin. In: Havstad, K., Huenneke, l.F., Schlesinger, W.H. (Eds.), Structure and Function of Chihuahuan desert Ecosystem: The Jornada Basin Long-Term Ecological Research Site. Oxford University Press, 492.

Mujinya, B. B., Mees, F., Boeckx, P., Bodé, S., Baert, G., Erens, H., Delefortrie, S., Verdoodt, A., Ngongo, M., Van Ranst, E. (2011). The origin of carbonates in termite mounds of the Lubumbashi area, DR Congo. *Geoderma 165*(1), 95-105.

Naiman, Z., Quade, J., Patchett, P. J. (2000). Isotopic evidence for eolian recycling of pedogenic carbonate and variations in carbonate dust sources throughout the southwest United States. *Geochimica et Cosmochimica Acta 64*(18), 3099-3109.

Nordt, L., Orosz, M., Driese, S., Tubbs, J. (2006). Vertisol carbonate properties in relation to mean annual precipitation: implications for paleoprecipitation estimates. *The Journal of geology*, *114*(4), 501-510.

Nordt, L.C., Wilding, L.P., Hallmark, T.C., Jacob, J.S. (1996). Stable carbon isotope composition of pedogenic carbonates and their use in studying pedogenesis. In: Boutton, T.W., Yamasaki, S. (Eds.), Mass Spectrometry of Soils. Marcel Dekker, New York, 133–154.

O'Leary, M. H. (1981). Carbon isotope fractionation in plants. *Phytochemistry*, *20*(4), 553-567.

Oster, J.L., Ibarra, D., Harris, C.R., Maher, K. (2012). Influence of eolian deposition and rainfall amounts on the U-isotopic composition of soil water and soil minerals: *Geochimica et Cosmochimica Acta*, 88, 146–166, doi: 10 .1016 /j .gca .2012 .04 .004.

Paces, J. B. and Wurster, F. C. (2014). Natural uranium and strontium isotope tracers of water sources and surface water–groundwater interactions in arid wetlands–Pahranagat Valley, Nevada, USA. *Journal of Hydrology*, *517*, 213-225.

Peinado, P. (2013). "Geochemical characterization of mineral dust sources in the Chihuahuan Desert and southern High Plains regions." Ph.D. Dissertation, Environmental Science and Engineering, University of Texas- El Paso.

Pelt, E., Chabaux, F., Innocent, C., Navarre-Sitchler, A. K., Sak, P. B., Brantley, S. L. (2008). Uranium–thorium chronometry of weathering rinds: rock alteration rate and paleo-isotopic record of weathering fluids. *Earth and Planetary Science Letters 276*(1), 98-105.

Phillips, F.M., Campbell, A.R., Kruger, C., Johnson, P., Roberts, R., Keyes, E. (1992). A reconstruction of the response of the water balance in western United States lake basins to climatic change: Las Cruces, New Mexico Water Resources Research Institute Report 269, 167

Pigati, J.S., Bright, J.E., Shanahan, T.M., Mahan, S.A. (2008). Late Pleistocene paleohydrology near the boundary of the Sonoran and Chihuahuan deserts, southeastern Arizona, USA. *Quaternary Science Reviews* 28 (3-4), 286-300.

Polyak, V. J. and Asmerom, Y. (2001). Late Holocene climate and cultural changes in the southwestern United States. *Science 294*(5540), 148-151.

Polyak, V.J., Rasmussen, J.B.T., Asmerom, Y. (2004). Prolonged wet period in the southwestern United states through the Younger Dryas. *Geology* 32 (1), 5-8.

Prospero, J. M. (1999). Long-range transport of mineral dust in the global atmosphere: Impact of African dust on the environment of the southeastern United States. *Proceedings of the National Academy of Sciences 96*(7), 3396-3403.

Prospero, J. M., Ginoux, P., Torres, O., Nicholson, S. E., Gill, T. E. (2002), Environmental characterization of global sources of atmospheric soil dust identified with the NIMBUS 7 Total Ozone Mapping Spectrometer (TOMS) absorbing aerosol product. *Reviews of Geophysics* 40(1), 1002, doi:10.1029/2000RG000095

Pustovoytov, K., Schmidt, K., Taubald, H. (2007). Evidence for Holocene environmental changes in the northern fertile Crescent provided by pedogenic carbonate coatings. *Quaternary Research* 67, 315-327.

Quade, J. and Cerling, T.E. (1995). Expansion of C4 grasses in the late Miocene of northern Pakistan: evidence from stable isotopes in paleosols. Palaeogeography Palaeoclimatology Palaeoecology 115, 91-116

Rao, Z., Zhu, Z., Zhang, J. (2007). Different climatic controls of soil δ 13Corg in three mid-latitude regions of the Northern Hemisphere since the Last Glacial period. *Chinese Science Bulletin 52*(2), 259-266.

Ravi, S., D'Odorico, P., Breshears, D. D., Field, J. P., Goudie, A. S., Huxman, T. E., ... & Van Pelt, S. (2011). Aeolian processes and the biosphere. *Reviews of Geophysics 49*(3), 1-45

Reheis, M.C. (2006). A 16-year record of eolian dust in southern Nevada and California, USA: controls on dust generation and accumulation. *Journal of Arid Environments* 67, 487–520

Reheis, M. C., Budahn, J. R., Lamothe, P. J., Reynolds, R. L. (2009). Compositions of modern dust and surface sediments in the Desert Southwest, United States, Journal of Geophysical Research 114, F01028, doi:10.1029/2008JF001009.

Reheis, M. C. and Urban, F. E. (2011). Regional and climatic controls on seasonal dust deposition in the southwestern US. *Aeolian Research 3*(1), 3-21.

Retallack, G.J. (1994). The environmental factor approach to the interpretation of palaeosols. In: Amundson, R., Harden, J., Singer, M. (Eds), Factors of Soil Formation: A Fiftieth Anniversary Retrospective. Soil Science Society of America, Madison, Wisconsin, 31–64.

Retallack, G.J. (2005). Pedogenic carbonate proxies for amount and seasonality of precipitation in paleosols. *Geology* 33, 333–336.
Reynolds, R., Belnap, J., Reheis, M., Lamothe, P., Luiszer, F. (2001). Aeolian dust in Colorado Plateau soils: nutrient inputs and recent change in source. *Proceedings of the National Academy of Sciences USA 98* (13), 7123–7127.

Reynolds, R., Reheis, M., Hinkley, T., Tigges, R., Clow, G., Lamothe, P., Yount, J. et al. (2003). Dust emission and deposition in southwestern United States—integrated field, remote sensing, and modeling studies to evaluate response to climatic variability and land use. Desertification in the third millennium. Swets and Zeitlinger (Balkema) Publishers, The Netherland, 271-282.

Rivera, N. I. R., Gill, T. E., Bleiweiss, M. P., & Hand, J. L. (2010). Source characteristics of hazardous Chihuahuan Desert dust outbreaks.*Atmospheric environment* 44(20), 2457-2468.

Rivera, N. I. R., Gill, T. E., Gebhart, K. A., Hand, J. L., Bleiweiss, M. P., Fitzgerald, R. M. (2009). Wind modeling of Chihuahuan Desert dust outbreaks. *Atmospheric Environment 43*(2), 347-354.

Robins, C. R., Deurlington, A., Buck, B. J., Brock-Hon, A. L. (2015). Micromorphology and formation of pedogenic ooids in calcic soils and petrocalcic horizons. *Geoderma 251*, 10-23.

Robinson L. F., Henderson, G. M., Hall, L., Matthews, I. (2004a). Climatic control of riverine and Seawater uranium-isotope ratios. *Science,* 305(5685), 851-854.

Rojo, L., Gill, T. E., Gillette, D. A. (2008). Particle size/composition relationships of wind-eroding sediments, Owens (dry) Lake, California, USA. *X-Ray Spectrometry 37*(2), 111-115.

Royer, D.L. (1999). Depth to pedogenic carbonate horizon as a paleoprecipitation indicator?: *Geology*, 27, 1123-1126.

Seager, W. R., Shafiqullah, M., Hawley, J. W., & Marvin, R. (1984). New K-Ar dates from basalts and the evolution of the southern Rio Grande rift.*Geological Society of America Bulletin* *95*(1), 87-99.

Serna-Pérez, A., Monger, H. C., Herrick, J. E., & Murray, L. (2006). Carbon dioxide emissions from exhumed petrocalcic horizons. *Soil Science Society of America Journal 70*(3), 795-805.

Sharp, W.D., Ludwig, K.R., Chadwick, O.A., Amundson, R., Glaser, L.L. (2003). Dating fluvial terraces by the ^{230}Th/U on pedogenic carbonate, Wind River Basin, Wyoming. *Quaternary Research* 59, 139–150.

Sobecki, T. M. and Wilding, L. M. (1983). Formation of calcic and argillic horizons in selected soils of the Texas coast prairie. *Soil science society of America Journal* 47, 707 – 715

Snyder, K. A. and Tartowski, S. L. (2006). Multi-scale temporal variation in water availability: implications for vegetation dynamics in arid and semi-arid ecosystems. *Journal of Arid Environments 65*(2), 219-234.

St Pierre, E., Zhao, J.-X., Feng, Y.-X., Reed, E. (2012). U-series dating of soda straw stalactites from excavated deposits: method development and application to Blanche Cave, Naracoorte, South Australia. *Journal of Archaeological Science* 39, 922-930.

Taboada, T., Cortizas, A. M., García, C., García-Rodeja, E. (2006). Uranium and thorium in weathering and pedogenetic profiles developed on granitic rocks from NW Spain. *Science of the total environment 356*(1), 192-206.

Tabor, N.J., Montanez, I.P., Kelso, K.A., Currie, B.S., Shippman, T.A. (2006.) A late Triassic soil catena: landscape controls on paleosol morphology across the Carnian–Age Ischigualasto–Villa Union Basin, Northwestern Argentina. In: Alonso-Zarza, A.M., Tanner, L.H. (Eds.), Paleoenvironmental Record and Applications of Calcretes and Palustrine Carbonates. *Geological Society of America Special Paper*, 416, 17–41.

Tanner, L. (2010). Continental carbonates as indicators of paleoclimate. *Developments in sedimentology*, 62, 181 – 188. ISSN 0070-4571, DOI 10.1016/S0070-4571 (09) 06204-9

Tong, D. Q., Dan, M., Wang, T., Lee, P. (2012). Long-term dust climatology in the western United States reconstructed from routine aerosol ground monitoring. *Atmospheric Chemistry and Physics 12*(11), 5189-5205.

Torfstein, A., Goldstein, S. L., Stein, M., Enzel, Y. (2013). Impacts of abrupt climate changes in the Levant from Last Glacial Dead Sea levels. *Quaternary Science Reviews*, *69*, 1-7.

Upadhyay, N., Clements, A.L., Fraser, M.P., Sundblom, M., Solomon, P., Herckes, P (2015). Size_Differentiated chemical composition of Re-Suspended soil dust from the desert southwest United States. *Aerosol and air quality Research* 15, 387-398

Van Devender, T.R. (1990). Late Quaternary vegetation and climate of the Chihuahuan desert, United States and Mexico. In: Betancourt, J.L., Van Devender, T.R., Martin, P.S. (Eds.), Packrat Middens - the Last 40,000 Years of Biotic Change. University of Arizona Press, Tucson, 104-133.

Van Devender, T.R. (1995). Desert grassland history: changing climates, evolution, biogeography and community dynamics. In: McClaran, M.P., Van Devender, T.R. (Eds.), The Desert Grassland. University of Arizona Press, Tucson, AZ, USA, 68–99.

Van der Hoven, S. J. and Quade, J. (2002). Tracing spatial and temporal variations in the sources of calcium in pedogenic carbonates in a semiarid environment. *Geoderma 108*(3), 259-276.

Verrecchia, E. P. (2011). Pedogenic carbonates. *Encyclopedia of Geobiology*, 721-725.

Violette, A., Riotte, J., Braun, J., Oliva, P., Marechal, J., Sekhar, M., Jeandel, C., Subramanian, S., Prunier, J., Barbiero, L., Dupre, B. (2010) Formation and preservation of pedogenic carbonates in Southern Indian, links with paleo-monsoon and pedological conditions: Clues from Sr isotopes, U-Th series and REEs. *Geochimica et Cosmochimica Acta* 74, 7059-7085.
Wagner, J.D.M., Cole, J.E., Beck, J.W., Patchett, P.J., Henderson, G.M., Barnett, H.R. (2010). Moisture variability in the Southwestern United States linked to abrupt Glacial climate change. *Nature Geoscience* 3, 110-113

Wainwright, J. (2006), Climate and climatological variations in the Jornada Experimental Range, in Structure and Function of a Chihuahuan Desert Ecosystem: The Jornada Basin Long-Term Ecological Research Site, edited by K. M. Havstad, L. F. Huenneke, and W. H. Schlesinger, , Oxford Univ. Press, New York. 44 – 80

Weems, S. L. and Monger, H. C. (2012). Banded vegetation-dune development during the Medieval Warm Period and 20th century, Chihuahuan Desert, New Mexico, USA. *Ecosphere* 3(3), 21. http://dx.doi.org/10.1890/ ES11-00194.1

West, L. T., Drees, L. R., Wilding, L. P., Rabenhorst, M. C. (1988). Differentiation of pedogenic and lithogenic carbonate forms in Texas. *Geoderma 43*(2), 271-287.

White, W H., Nicole P. H., Krystyna, T., Sinan, Y., Randy, S. R., Thomas, E. G., Lixin ,J. (2015). Regional transport of a chemically distinctive dust: Gypsum from White Sands, New Mexico (USA). *Aeolian Research* 16, 1-10.

Wong, C. I., Banner, J. L., Musgrove, M. (2015). Holocene climate variability in Texas, USA: An integration of existing paleoclimate data and modeling with a new, high-resolution speleothem record. *Quaternary Science Reviews 127*, 155-173.

York, D., Evensen, N. M., Lo´pez Martinez, M., and De Basabe Del- gado, J. (2004). Unified equations for the slope, intercept, and standard errors of the best straight line. American Journal of Physics, 72(3), 367–375.

Zhou, J. and Chafetz, H.S. (2010). Pedogenic carbonates in Texas: Stable isotope distributions and their implications. *Journal of Sedimentary Research* 80, 137–150.

Tables

Table 2.1. Major and minor element oxide concentrations, $^{87}Sr/^{86}Sr$ ratios, ($^{234}U/^{238}U$), and ($^{230}Th/^{238}U$) of mordern dust at the Jornada Experimental Range.

Dust sample	Height	Na_2O	K_2O	MgO	CaO	SiO_2	Al_2O_3	Fe_3O_2	TiO_2	P_2O_5	Sr	Ba	Zr	$^{87}Sr/^{86}Sr$	$^{87}Sr/^{86}Sr$	$^{87}Sr/^{86}Sr$	U	Th	($^{234}U/^{238}U$)	($^{230}Th/^{238}U$)
	(cm)	Wt (%)	Wt (%)	Wt (%)	Wt (%)	Wt (%)	Wt (%)	Wt (%)	Wt (%)	Wt (%)	ppm	ppm	ppm	Soluble fraction	Residue fraction	Bulk	ppm	ppm		
M-Rabb	50	0.3	2.1	0.9	0.7	85.7	6.6	2.1	0.3	0.2	130	547	251.	0.7087± 0.00000235	0.7165± 0.00000796	-	-	-	-	-
M-well	50	0.6	1.9	0.9	0.9	84.5	6.7	1.8	0.3	0.2	142	517	193	0.7091± 0.00000470	0.7225± 0.00000582	-	-	-	-	-
G-IBPE4	50	0.2	1.6	0.8	0.8	72.2	6.1	1.7	0.3	0.1	127	584	210	0.7087± 0.00000655	0.7190± 0.0000081	-	-	-	-	-
P-Tobo	50	0.8	2.0	1.3	1.4	72.0	9.7	2.6	0.5	0.1	193	469	368	0.7088± 0.00000199	0.7147± 0.00000413	-	-	-	-	-
P-Coli	50	0.6	2.3	2.3	1.6	54.9	14.3	5.0	0.6	0.1	171	531	260	0.7086± 0.00000915	0.7119± 0.00000556	-	-	-	-	-
T-TYL	50	1.0	2.5	1.2	1.7	78.8	8.5	2.3	0.4	0.1	163	544	300	0.7087± 0.00000457	0.7190± 0.00000348	0.7184± 0.00000466	1.55	7.04	0.969	4.316
T-East	50	1.3	2.5	1.6	1.6	71.6	11.0	3.5	0.6	0.2	231	582	406	0.7088± 0.00000898	0.7134± 0.00000486	0.7141± 0.00000498	1.45	6.66	0.959	4.452
M-Rabb	100	0.8	2.2	1.2	1.2	78.1	9.5	3.4	0.6	0.1	198	598	633	0.7088± 0.00000639	0.7151± 0.00000673	-	-	-	-	-
M-well	100	0.7	2.0	1.0	1.1	79.8	8.0	2.6	0.5	0.2	176	497	365	0.7090± 0.00000986	0.7164± 0.00000492	-	-	-	-	-
G-IBPE4	100	0.5	1.8	0.8	0.7	87.6	5.9	1.7	0.3	0.0	137	525	140	0.7088± 0.00000938	0.722± 0.0000071	-	-	-	-	-
P-Tobo	100	0.9	2.2	1.4	1.8	77.9	9.3	3.1	0.5	0.1	215	620	420	0.7088± 0.00000104	0.715± 0.00000552	-	-	-	-	-
P-Coli	100	0.7	2.1	1.8	2.9	55.3	12.6	3.8	0.6	0.2	221	516	323	0.7087± 0.00000556	0.7119± 0.00000513	-	-	-	-	-
T-TYL	100	1.0	2.3	1.4	2.9	74.2	9.4	3.1	0.6	0.1	208	575	390	0.7088± 0.00000541	0.7158± 0.00000576	0.7170± 0.00000522	1.95	8.71	0.942	4.211
T-East	100	1.5	2.8	1.1	1.6	78.2	9.9	2.4	0.4	0.2	207	653	257	0.7089± 0.00000389	0.7127± 0.00000386	0.7126±0.00000522	2.13	9.31	0.978	4.447

The dashes means not measured

Table 2.2. Uranium and thorium concentrations, activity ratios, and single sample detrital corrected- derived ages for soil (H1) and caliche (H2-H4).

									Upper Continental crust corrected			H1 HCl soil residue (HCl_R)			H1 Acetic acid soil Residue (AcOH_R)		
Sample	**Depth**	**U**	**^{232}Th**	**(^{232}Th/^{238}U)**	**(^{230}Th/^{238}U)$_M$**	**(^{234}U/^{238}U)**	**Uncorrected Age***	**(^{234}U/^{238}U)$_0$***	**(^{230}Th/^{238}U)$_{Cal\_UCC}$**	**Corrected age****	**(^{234}U/^{238}U)$_0$ ****	**(^{230}Th/^{238}U)$_{Cal\_Hcl\ soil\ R}$**	**Corrected age*****	**(^{234}U/^{238}U)$_0$ *****	**(^{230}Th/^{238}U)$_{cal\_Acetic\ acid\_soil\ R}$**	**Corrected age******	**(^{234}U/^{238}U)$_0$ ******
	(cm)	**ppm**	**ppm**				**ka**		**0.87**	**ka**		**0.917**	**ka**		**0.886**	**ka**	
H1	40	1.59±0.02	6.02±0.06	1.24±0.01	0.77±0.01	0.91±0.005	219±13	0.84±0.01	-0.31	Negative age	0.9189±0.004	-0.37	Negative age	0.92±0.004	-0.33	Negative age	0.92±0.004
H2C	60	1.34±0.01	1.94±0.02	0.48±0.01	0.524±0.01	1.34±0.007	52.7±1.1	1.40±0.008	0.12±0.001	9.34±0.11	1.35±0.007	0.09±0.0009	7.39±0.09	1.35±0.007	0.10±0.001	8.67±0.1	1.35±0.007
H2B	60	1.13±0.01	2.46±0.02	0.71±0.01	0.70±0.01	1.21±0.007	90.2±2.3	1.27±0.007	0.08±0.0008	7.026±0.08	1.22±0.007	0.04±0.0004	3.87±0.04	1.21±0.006	0.06±0.0006	5.94±0.07	1.21±0.006
H2A	60	1.00±0.01	2.57±0.03	0.844±0.01	0.68±0.01	1.25±0.006	82.7±2	1.31±0.008	-0.05	Negative age	1.24±0.006	-0.09	Negative age	1.24±0.006	-0.06	Negative age	1.24±0.006
H3C	200	3.66±0.04	2.76±0.03	0.25±0.003	0.98±0.02	1.079±0.005	244±15	1.16±0.01	0.770±0.008	132.6±2.9	1.12±0.007	0.76±0.008	128.9±2.8	1.11±0.007	0.77±0.008	131.3±2.9	1.11±0.007
H3B	200	2.39±0.02	2.13±0.02	0.29±0.003	0.97±0.02	0.97±0.005	No age	No Ratio	0.716±0.007	147.8±3.7	0.95±0.008	0.702±0.007	141.9±3.4	0.95±0.008	0.71±0.007	145.7±3.6	0.95±0.008
H3A	200	1.81±0.02	2.39±0.02	0.43±0.01	0.98±0.02	0.995±0.005	465±140	0.99±0.02	0.60±0.006	101.7±1.9	0.99±0.007	0.58±0.006	96.2±1.8	0.99±0.007	0.60±0.006	99.8±1.9	0.99±0.007
H4C	40	0.46±0.004	1.20±0.01	0.86±0.01	0.97±0.02	1.20±0.006	165.2±6.2	1.31±0.009	0.221±0.002	22.09±0.27	1.21±0.006	0.18±0.002	17.74±0.2	1.21±0.006	0.21±0.002	20.59±0.3	1.21±0.006

H4B	40	0.60±0.01	0.95±0.01	0.52±0.01	1.02±0.02	1.15±0.006	216±11	1.27±0.01	0.568±0.006	73.1±1.2	1.18±0.007	0.54±0.005	68.8±1.1	1.18±0.007	0.56±0.006	71.6±1.1	1.18±0.007
H4A	40	0.65±0.01	1.20±0.01	0.61±0.01	0.95±0.02	1.13±0.006	183.8±7.8	1.23±0.009	0.42±0.004	49.97±0.71	1.15±0.007	0.39±0.004	45.79±0.6	1.15±0.006	0.41±0.004	48.53±0.7	1.15±0.006

Table 2.3. $^{87}Sr/^{86}Sr$ ratios in the bulk, soluble and residue fraction for soil (H1) and caliche (H2-H4) samples.

Sample	**Depth**	**$^{87}Sr/^{86}Sr$**	**$^{87}Sr/^{86}Sr$**	**$^{87}Sr/^{86}Sr$**
	(cm)	**Soluble fraction**	**Residue fraction**	**Bulk**
H1	40	0.7086±0.00000323	0.725±0.00000452	0.723±0.00000432
H2C	60	0.7089±0.00000475	0.714±0.00000348	0.7101±0.00000307
H2B	60	0.7090±0.00000472	0.719±0.00000367	0.7123±0.00000303
H2A	60	0.7089±0.00000744	0.720±0.00000382	0.7120±0.00000364
H3C	200	0.7111±0.00000673	0.714±0.00005676	0.7115±0.00000426
H3B	200	0.7112±0.00000425	0.716±0.00000295	0.7115±0.00000382
H3A	200	0.7112±0.00000387	0.714±0.00000532	0.7114±0.00000399
H4C	40	0.7091±0.00000291	N/M	0.7098±0.00000501
H4B	40	0.7101±5.41E-06	N/M	0.7104±0.00000390
H4A	40	0.7102±0.00000397	0.720±0.00000469	0.7107±0.00000468

N/M = Not measured

Table 2.4. Measured U and Th concentrations and activity ratios for 3 and 5 subsamples as well as 2D Osmond and Rosholt-derived age.

				Measured concentrations		Measured activity ratios			R^2 for 2D Osmond isochrons		Osmond isochron carbonate activity ratios		Osmond isochron derived ages		Rosholt isochron carbonate activity ratios		Rosholt isochron derived ages	
Sample name	**Lamina**	**Sub-sample ID**	**Sample treatment**	^{238}U	^{232}Th	$(^{234}U/^{238}U)m$	$(^{230}Th/^{238}U)m$	$(^{232}Th/^{238}U)m$	R^2 $(^{230}Th/^{238}U)$ Vs $(^{232}Th/^{238}U)$	R^2 $(^{234}U/^{238}U)$ Vs $(^{232}Th/^{238}U)$	$(^{230}Th/^{238}U)^*$	$(^{234}U/^{238}U)^*$	Age (ka)	$(^{234}U/^{238}U)_0$	$(^{230}Th/^{238}U)^{**}$	$(^{234}U/^{238}U)^{**}$	Age (ka)	$(^{234}U/^{238}U)_0$
H4	H4C	H4C	TSD	0.46± 0.005	1.21± 0.01	1.186±0.006	0.967± 0.015	0.857± 0.010	0.09	0.97	0.97± 0.02	1.42± 0.04	116.2± 7.3	1.58± 0.05	0.97± 0.03	1.41± 0.05	118± 9.9	1.57± 0.06
		H4C2		0.55± 0.005	1.57± 0.02	1.177±0.006	0.958± 0.015	0.943± 0.011										
		H4C3		0.48± 0.005	1.68± 0.02	1.112±0.006	0.962± 0.015	1.151± 0.014										
H4	H4B	H4B	TSD	0.598 ±0.006	0.95± 0.01	1.147±0.006	1.021± 0.016	0.521± 0.006	0.51	0.9	1.14± 0.09	0.88± 0.08	No age	No ratio	1.11± 0.13	0.90± 0.11	No age	No ratio
		H4B2		0.50± 0.005	1.17± 0.01	1.259±0.006	0.986± 0.016	0.767± 0.009										
		H4B3		0.62± 0.006	1.12± 0.01	1.144±0.006	1.051± 0.017	0.594± 0.007										
H2	H2C	H2C	TSD	1.34± 0.01	1.94± 0.02	1.340±0.007	0.524± 0.008	0.475± 0.006	0.05	0.07	0.56±0.17	1.32±0.08	58±24	1.38± 0.09	0.57± 0.19	1.31± 0.09	60± 27	1.37± 0.1
		H2C2		1.45± 0.01	2.04± 0.02	1.355±0.007	0.492± 0.008	0.459± 0.006										
		H2C3		1.64± 0.02	2.03± 0.02	1.341±0.007	0.521± 0.008	0.404± 0.005										
H2	H2B	H2B	TSD	1.13± 0.01	2.45± 0.02	1.211±0.006	0.697± 0.011	0.714± 0.009	0.54	0.82	0.60±0.05	1.46±0.08	56.1±7.5	1.54± 0.09	0.61± 0.05	1.46± 0.07	57.2 ±7.1	1.54± 0.08
		H2B2		1.17± 0.01	2.41± 0.02	1.262±0.006	0.666± 0.011	0.677± 0.008										

		H2B3		1.24±0.01	1.80±0.02	1.304±0.007	0.660±0.011	0.474±0.006										
H3	H3C	H3C	TSD	3.66±0.04	2.84±0.03	1.079±0.005	0.991±0.016	0.253±0.003	0.94	0.42	0.95±0.01	1.12±0.07	194±37	1.21±0.09	0.95±0.01	1.14±0.08	182±38	1.23±0.11
		H3C2		2.24±0.02	2.12±0.02	1.034±0.005	1.005±0.016	0.310±0.004										
		H3C3		2.04±0.02	2.51±0.03	1.043±0.005	1.015±0.016	0.402±0.005										
H2	H2C	H2C Bulk	L/R	1.42±0.01	1.85±0.02	1.365±0.007	0.506±0.008	0.426±0.005	0.96	0.98	0.15±0.06	1.58±0.02	10.9±4.4	1.60±0.02	0.14±0.02	1.58±0.01	10±1.3	1.59±0.01
		H2C HCl R		0.49±0.005	1.39±0.02	1.120±0.006	0.889±0.014	0.932±0.011										
		H2C AcO H R		0.73±0.007	1.69±0.02	1.133±0.006	0.926±0.015	0.758±0.009										
		H2C HCl L		0.90±0.009	0.36±0.004	1.516±0.008	0.273±0.004	0.131±0.002										
		H2C AcO H L		0.85±0.009	0.29±0.003	1.515±0.008	0.231±0.004	0.113±0.001										
H3	H3C	H3C Bulk	L/R	1.67±0.02	2.86±0.03	0.980±0.005	0.978±0.016	0.562±0.007	0.2	0.76	0.71±0.22	1.26±0.08	87±41	1.33±0.1	0.55±0.15	1.2033±0.01	64±24	1.24±0.06
		H3C HCl R		0.88±0.009	1.65±0.02	0.884±0.004	0.882±0.014	0.610±0.007										
		H3C AcO H R		0.91±0.009	1.86±0.02	0.883±0.004	0.900±0.014	0.668±0.008										
		H3C HCl L		0.91±0.008	1.07±0.01	1.094±0.005	1.122±0.018	0.452±0.005										
		H3C AcO H L		1.15±0.01	0.81±0.01	1.097±0.005	0.689±0.011	0.229±0.003										

Table 2.5: Measured U and Th concentrations and activity ratios for five subsamples (bulk, acid residues and leachates) and 3D Osmond -derived ages.
The organic and inorganic stable carbon isotopic composition in pedogenic carbonates aew also shown.

Sample name	Subsample ID	^{238}U	±2σ	^{232}Th	±2σ	($^{230}Th/^{232}Th$)	±2σ	($^{230}Th/^{238}U$)	±2σ	($^{234}U/^{238}U$)	±2σ	($^{232}Th/^{238}U$)	±2σ	Age (ka)	±2σ	($^{234}U/^{238}U$)0	±2σ	δ13C $_{OC}$(VPDB)	δ13C $_{CaCO3}$(VPDB)
H1	H1 Bulk	1.585	0.016	6.017	0.060	0.620	0.006	0.770	0.012	0.911	0.005	1.242	0.015	-62	160	1.02	0.33	-20.92	-2.95
	H1 HCl R	0.956	0.010	4.227	0.042	0.917	0.009	1.327	0.021	0.915	0.005	1.447	0.017						
	H1AcOH R	0.684	0.007	4.301	0.043	0.886	0.009	1.825	0.029	0.913	0.005	2.059	0.025						
	H1 HCl L	0.043	0.000	0.173	0.002	0.897	0.009	1.192	0.019	1.098	0.005	1.328	0.016						
	H1 AcOH L	0.055	0.001	0.284	0.003	0.840	0.008	1.426	0.023	0.997	0.005	1.697	0.020						
H2A	H2A Bulk	0.989	0.010	2.547	0.025	0.887	0.009	0.747	0.012	1.192	0.006	0.843	0.010	20	10	1.73	0.12	-22.27	-3.72
	H2A HCl R	0.719	0.007	2.837	0.028	0.734	0.007	0.949	0.015	1.005	0.005	1.292	0.016						
	H2A AcOH R	0.692	0.007	2.052	0.021	0.945	0.009	0.916	0.015	1.015	0.005	0.970	0.012						
	H2A HCl L	0.393	0.004	0.411	0.004	1.411	0.014	0.484	0.008	1.483	0.007	0.343	0.004						
	H2A AcOH L	0.352	0.004	0.343	0.003	1.473	0.015	0.470	0.008	1.500	0.007	0.319	0.004						
H2C	H2C Bulk	1.421	0.014	1.849	0.018	1.188	0.012	0.506	0.008	1.365	0.007	0.426	0.005	10	3.2	1.6	0.06	-20.28	-3.55
	H2C HCl R	0.488	0.005	1.390	0.014	0.953	0.010	0.889	0.014	1.120	0.006	0.932	0.011						
	H2C AcOH R	0.729	0.007	1.688	0.017	1.223	0.012	0.926	0.015	1.133	0.006	0.758	0.009						
	H2C HCl L	0.900	0.009	0.360	0.004	2.080	0.021	0.273	0.004	1.516	0.008	0.131	0.002						
	H2C AcOH L	0.352	0.004	0.294	0.003	2.050	0.020	0.231	0.004	1.515	0.008	0.113	0.001						

H3A	H3A Bulk	2.068	0.021	2.394	0.024	2.636	0.026	0.999	0.016	1.016	0.005	0.379	0.005	472	640	1.7	1.2	-23.32	-1.82
	H3A HCl R	1.026	0.010	1.706	0.017	1.679	0.017	0.914	0.015	0.955	0.005	0.544	0.007						
	H3A AcOH R	1.203	0.012	1.833	0.018	1.917	0.019	0.956	0.015	0.987	0.005	0.499	0.006						
	H3A HCl L	0.920	0.009	0.805	0.008	3.826	0.038	1.096	0.018	1.080	0.005	0.287	0.003						
	H3A AcOH L	0.831	0.008	0.571	0.006	4.838	0.048	1.088	0.017	1.080	0.005	0.225	0.003						
H3C	H3C Bulk	1.667	0.017	2.864	0.017	1.738	0.017	0.978	0.016	0.980	0.005	0.562	0.007	283	300	2.4	1.1	-23.08	-2.23
	H3C HCl R	0.884	0.009	1.647	0.017	1.447	0.014	0.882	0.014	0.884	0.004	0.610	0.007						
	H3C AcOH R	0.910	0.009	1.857	0.017	1.348	0.013	0.900	0.014	0.883	0.004	0.668	0.008						
	H3C HCl L	0.771	0.008	1.065	0.017	2.480	0.025	1.122	0.018	1.094	0.005	0.452	0.005						
	H3C AcOH L	1.154	0.012	0.806	0.017	3.014	0.030	0.689	0.011	1.097	0.005	0.229	0.003						

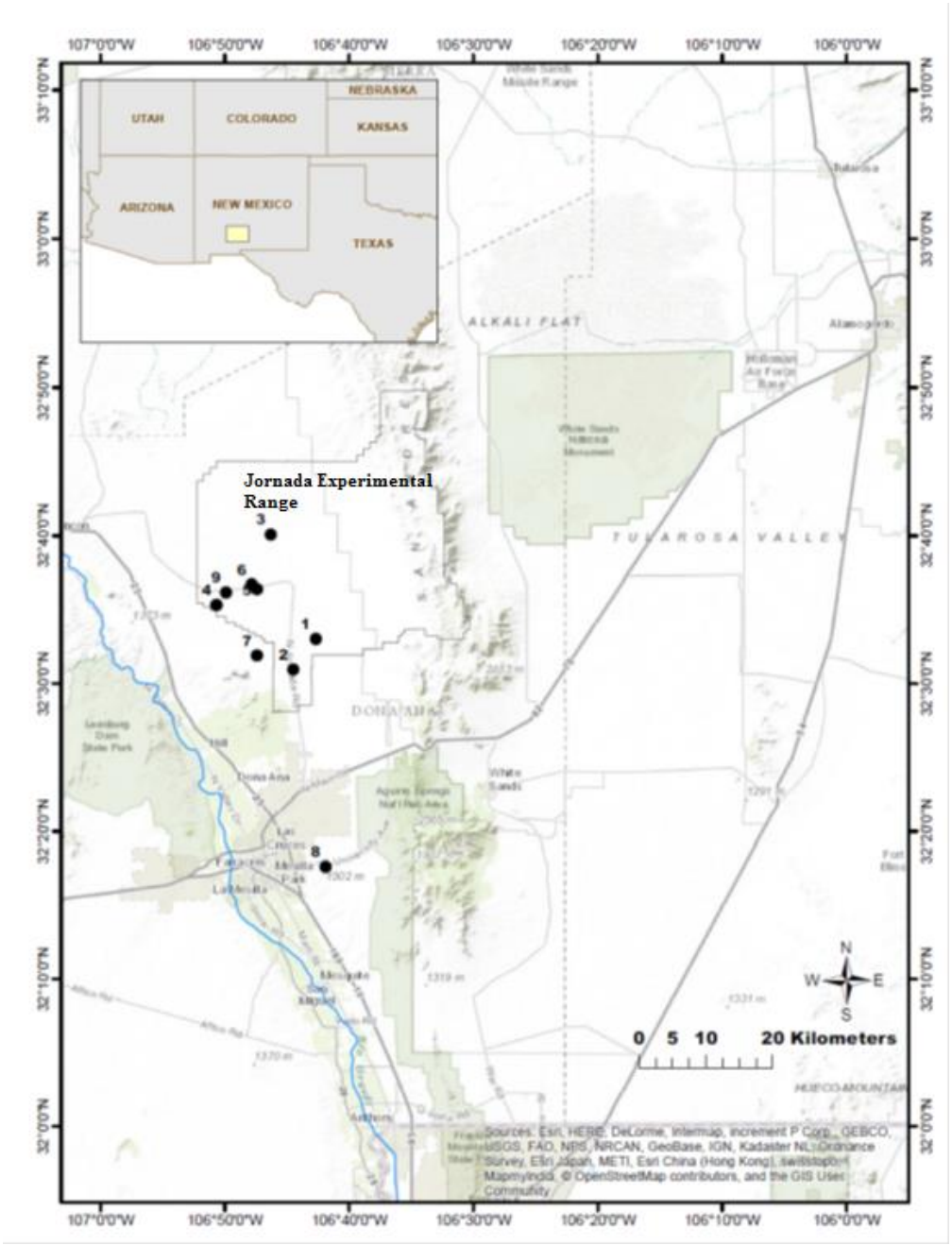

Figure 2.1: Location map showing a studied soil profile at Jornada Experimental Range (Mesa_JER (9)).
Sites where modern dust (T-East (1), T-tyl (2), P_Tobo (3), G_IBPE (4), M-Well (5), M-Rabb (6), and P_Coli (7)) and marine carbonate from the Tortugas mountains (A-Mts (8)) were sampled are also shown.

Figure 2.2: An exposed trench at the La Mesa geomorphic surface within the Jornada Basin containing approximately 150 cm of thick horizon of stage V pedogenic carbonates/caliche.
H1 is a soil sampled at 40cm from surface; H2 and H3 are caliche samples collected at 60 cm, 200cm respectively from surface. H4 is a caliche sample at 40cm from surface and 3m laterally away from H2 caliche.

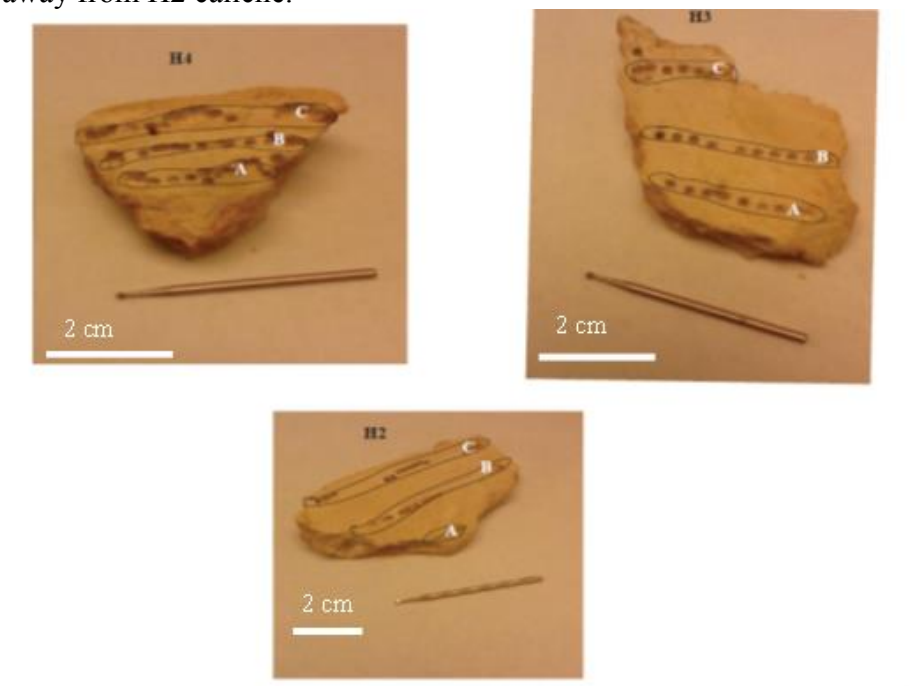

Figure 2.3: Saw-cut caliche samples of H4, H2 and H3 showing drilled lamina A, B, and C.
A is the innermost lamina, B is the middle, and C is the outermost lamina

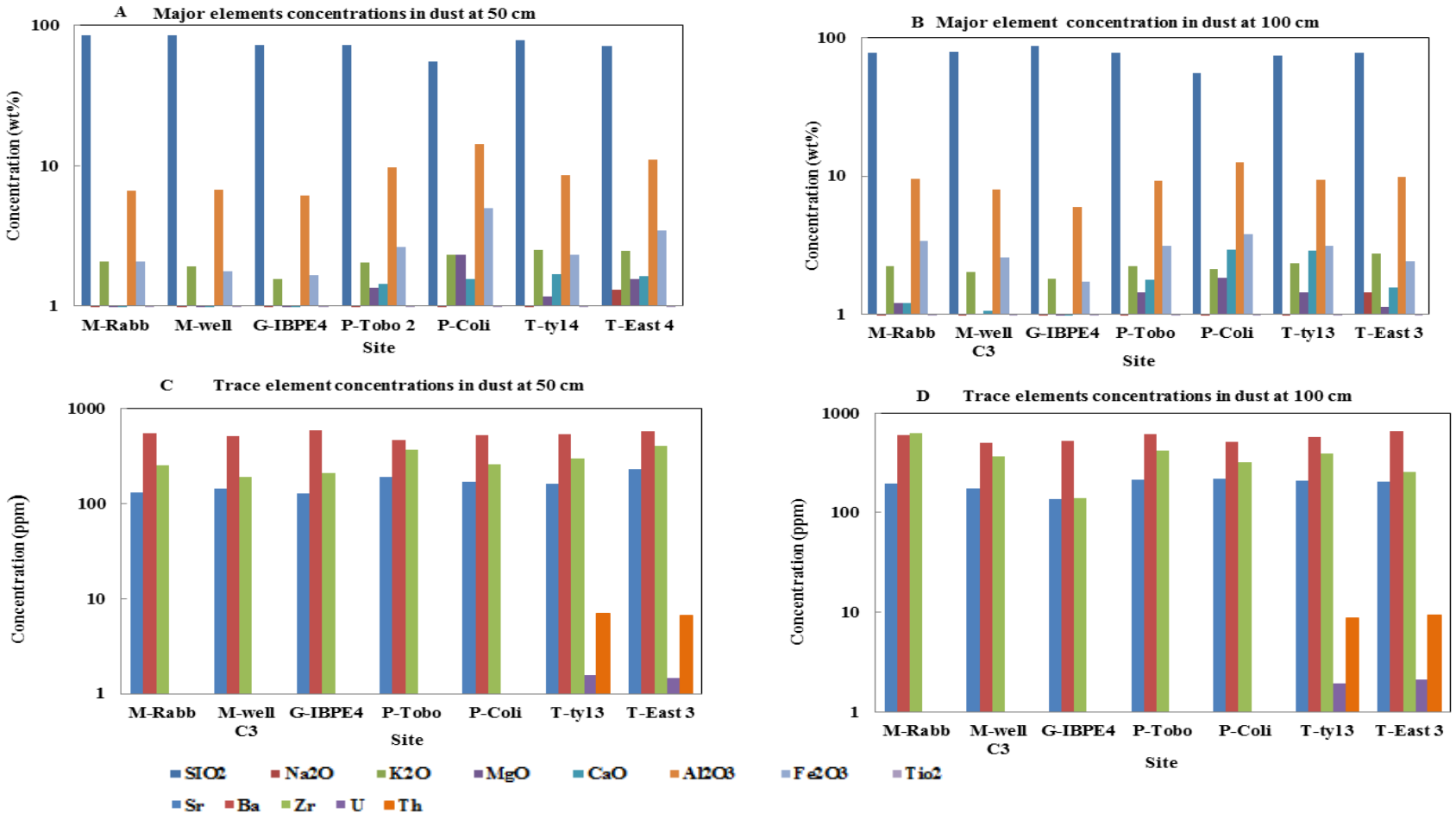

Figure 2.4: Major element concentrations (wt. %) in modern dust at 50 cm (a) and at 100 cm (b). SiO_2 and Al_2O_3 concentrations are dominant at both heights. Trace elements concentrations (ppm) in dust at 50 cm (c) and 100 cm (d). The y-axis is in log scale.

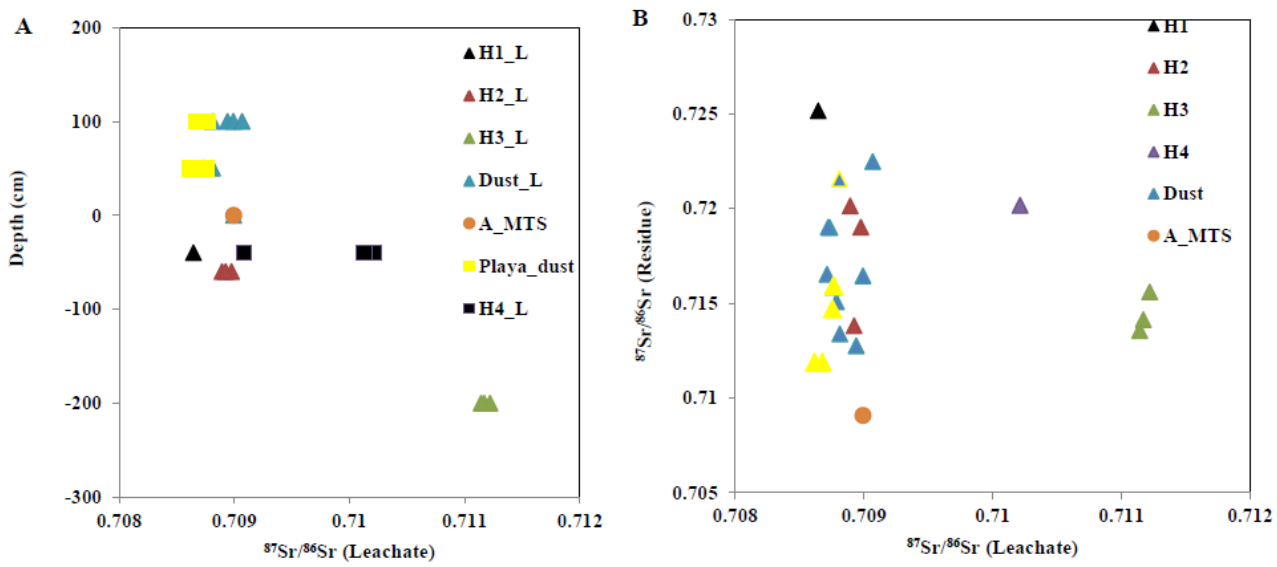

Figure 2.5: (a) $^{87}Sr/^{86}Sr$ ratios of soluble fraction in dust and soil as well as caliche along a soil profile.
Ratios of shallower carbonates are similar to those of modern dust (including playa dust) and carbonates at "A" mountains. H4B, H4A, and H3 carbonates show slightly high radiogenic $^{87}Sr/^{86}Sr$ ratios. (b) Comparison of $^{87}Sr/^{86}Sr$ ratios of soluble and residue fractions of dust and the carbonates, the residues are more radiogenic than the leachates, except for the "A" mountain carbonates.

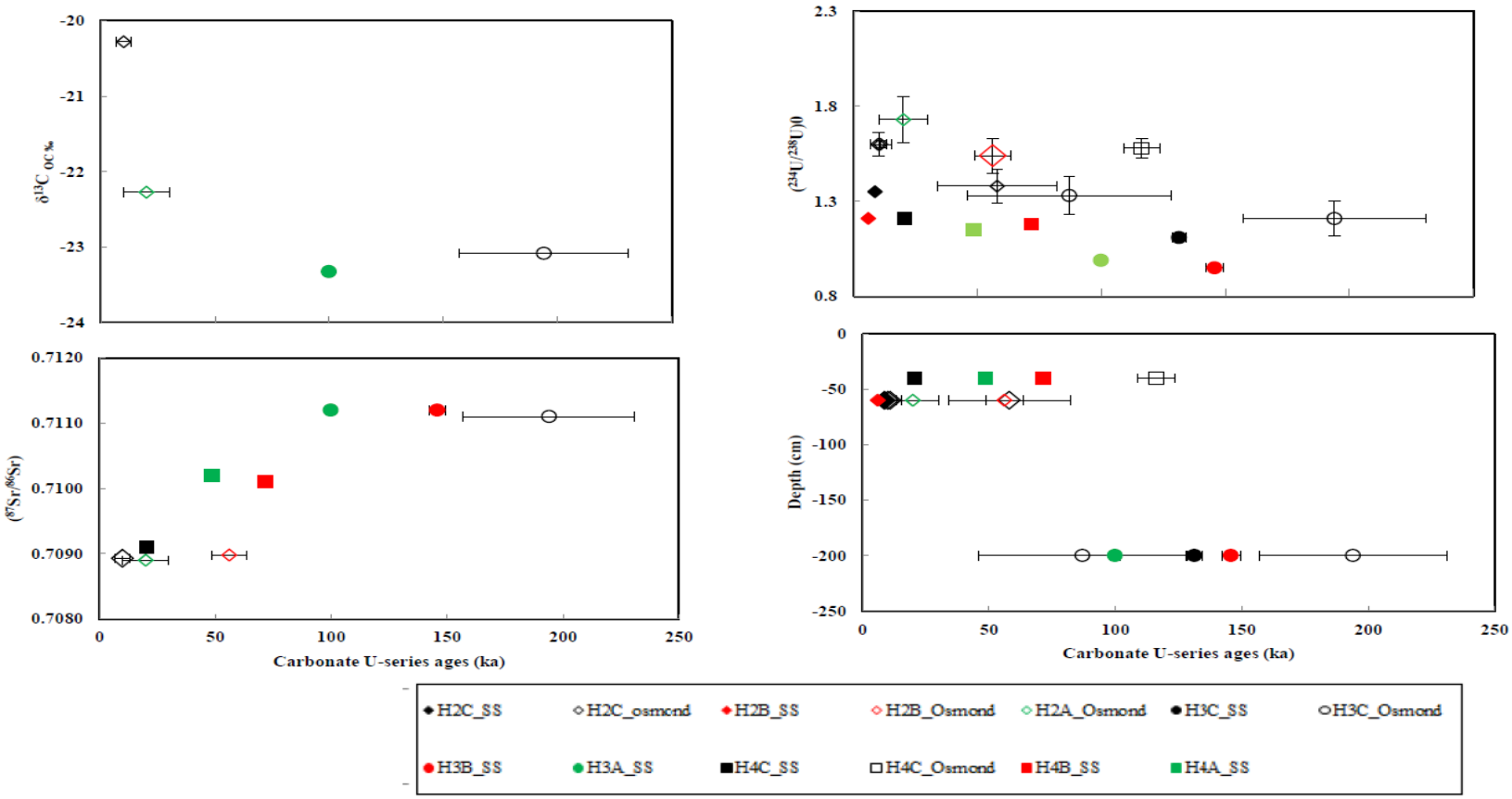

Figure 2.6: Temporal variation of $\delta^{13}C_{OC}$, $(^{234}U/^{238}U)_0$, $^{87}Sr/^{86}Sr$ of pedogenic carbonates at various depths at the La Mesa _JER. Solid fill symbols represent carbonate ages obtained from authigenic U-series activity ratios after single sample (SS) detrital correction method. Unfilled symbols represent calculated carbonate ages from authigenic U-series activity ratios following detrital correction on 2D Osmond isochrons

Chapter 4

Tracing salinity sources in the Lower Rio Grande River using U and Sr isotopes

Nyachoti, S.K[1*], Lin Ma[1], Anna Szynkiewicz[2], Lixin Jin[1], and Jennifer McIntosh[3]
[1]Department of Geological Sciences, University of Texas at El Paso, El Paso, TX 79968
[2]Department of Earth and Planetary Sciences, the University of Tennessee, Knoxville, TN 37996
[3]Department of Hydrology and Water Resources, the University of Arizona, Tucson, AZ 85721
sknyachoti@miners.utep.edu

4.1 Abstract

Major and minor element concentrations, U and Sr isotopic ratios were analyzed in river water, groundwater wells, and urban drains along the Lower Rio Grande River between Elephant Butte reservoir, NM and El Paso, TX during the irrigation and non-irrigation seasons of 2014-2015. Additionally, various types of archived water samples (river, groundwater, wastewater, agricultural drains, and city drains) collected in 2009-2010 in this region were analyzed in order to identify possible salinity end-members and elucidate processes that are responsible for salt addition into the Rio Grande. Our results indicated that salinity end-members in the Lower Rio Grande region include: deep groundwater, shallow groundwater, agricultural return flows, and urban drains; their contributions to the Rio Grande vary both spatially and temporally. During the irrigation season the water released from the Elephant Butte reservoir dominates the river water chemistry; however, additional salinity sources were identified at many locations along the river. During the non-irrigation season, salinity from deep groundwater is readily identified in the area immediately below the Elephant Butte reservoir; the contributions of anthropogenic salt-loads from agricultural and urban activities increases significantly in downstream locations toward El Paso, TX. Moreover, temporal variations of [U], uranium activity ratios ($^{234}U/^{238}U$),

[Sr], and $^{87}Sr/^{86}Sr$ ratios in the Rio Grande at Canutillo, TX and agricultural drains suggest addition of fertilizer-derived salinity to the river. Other factors such as dilution effect, evapoconcentration, dissolution, and precipitation reactions were also inferred to influence river chemistry. This study demonstrates the potential of using ($^{234}U/^{238}U$) values to fingerprint deep groundwater, surface and near-surface water sources, and anthropogenic salinity sources. Uranium activity ratios in combination with more traditional tracers such as $^{87}Sr/^{86}Sr$ ratios are very useful tools in fingerprinting salinity sources within the Lower Rio Grande.

4.2 Introduction

Good water quality is essential for domestic, industrial and agricultural purposes on both local and global scales. Populations in arid and semiarid areas often utilize poor quality surface and ground waters, which are generally characterized by elevated concentrations of dissolved salts (Ghassemi et al., 1995; Moore et al., 2008; Sheng, 2013). For this reason, sources of river salinization in many arid and semiarid zones are of growing worldwide concern. The Rio Grande is a major river flowing in the arid and semiarid southwest USA and northern Mexico; it provides water for irrigation, industrial, municipal, and recreational purposes along its course (Ellis et al., 1993; Hogan, 2013). Salinity of the Rio Grande increases from ~40 mg/L in upstream waters near Colorado to ~2000 mg/L in downstream locations near El Paso, TX when the river discharge is low (Moore and Anderholm, 2002; Philip et al., 2003; Hogan et al., 2007). Recent studies have shown that climatic factors (e.g. precipitation quantities and evaporation rates), geological factors (e.g. upwelling of groundwater), and human impacts (e.g. agricultural activities, groundwater pumping, and urban effluents) contribute to the Rio Grande salinity

(Mills, 2003; Hogan et al., 2007; Moore et al., 2008; Moore and Anderholm, 2002; Szynkiewicz et al., 2011; 2015).

Most of the Rio Grande water (approximately 90%) is used for irrigation (Ellis et al., 1993; Moore and Anderholm, 2002). During the irrigation season, water is diverted from the river into farms via canals and returned back to the river through agricultural drains (agricultural return flows). In the non-irrigation season, local shallow groundwater is used to supplement for irrigation and municipal, industrial and domestic water needs (Sheng, 2013). In addition to flood irrigation with saline river and shallow groundwaters, other agricultural practices (e.g. fertilizers and pesticides application) have increased crop yield, but impacted water quality (Szynkiewicz et al., 2011). Due to increasing agricultural activities and growing population in cities within the Lower Rio Grande valley, anthropogenic-derived salts (both agricultural and city effluents) are likely a dominant salinity factor in this region. Using stable sulfur isotope compositions, Szynkiewicz et al. (2011) showed that dissolved sulfates in the Lower Rio Grande river are fertilizer-derived rather than geologically sourced. They also observed high nitrate concentrations in the Lower Rio Grande at Canutillo, TX mainly sourced from agriculture.

Some recent studies have characterized salinity sources of the Rio Grande using water chemistry, stable isotopes (e.g. $\delta^{11}B$, $\delta^{34}S$, $\delta^{18}O$, and $\delta^{2}H$), and radiogenic isotopes (e.g. $^{87}Sr/^{86}Sr$ and $\delta^{234}U$) (Hogan et al., 2007; Moore et al., 2008, Szynkiewicz et al., 2011). Near surface processes such as evaporation, change of redox conditions, and microbial activities modify major elemental concentrations and light isotope composition, often resulting in complex data (Paces and Wurster, 2014). However, radiogenic isotopes are more conservative and could easily distinguish natural and anthropogenic salinity sources. For example, strontium and uranium isotopes have been applied in hydrology (Osmond and Cowart, 1992; Osmond and Ivanovich,

1992; Frost and Toner, 2004; Negrel et al., 2004; Vitvar et al., 2005; Paces and Wurster, 2014); but, few studies have systematically used uranium isotopes to fingerprint salinity sources and investigate spatial and temporal uranium variability in rivers (Riote and Chabaux, 1999; Riotte et al., 2003; Hogan et al., 2007; Uralbekov et al., 2014; Szynkiewicz et al., 2015). Particularly, only few studies have focused on distinguishing and quantifying spatial and temporal anthropogenic contamination in the Lower Rio Grande using uranium isotopes (i.e. Hogan et al., 2007; Szynkiewicz et al., 2015).

We use major and minor element chemistry, U and Sr isotopes in various types of water samples collected along the Lower Rio Grande river starting from Elephant Butte, NM to El Paso, TX (Figure 3.1a and 3.1b) to investigate both natural and anthropogenic factors impacting water salinity. We assess the spatial and temporal variability of these geochemical signatures and identify sources of salt loads into the Lower Rio Grande.

4.3 Background information

4.3.1 URANIUM ISOTOPES IN WATER SYSTEMS

Uranium naturally occurs in rocks as a trace element (at parts per million level) (Herring, 2013). Solubility of uranium in water depends on reducing /oxidizing conditions of the environment; U (VI) is more soluble than U (IV) under oxic conditions (Duff et al., 1999; Finch and Murakami, 1999; Bourdon et al., 2003). Weathering processes release uranium to water flowing through rocks and soils and control its concentration and isotopic composition (Osmond and Cowart, 1976; Chabaux et al., 2008; Robinson et al., 2004; Vigier et al., 2005).

Uranium is a radioactive element and has three isotopes that occur in nature: ^{238}U ($t_{1/2}$ = 4.468 Gy), ^{235}U ($t_{1/2}$ = 700 Ma), and ^{234}U ($t_{1/2}$ = 245 ky (Cheng et al., 2000a). The ^{234}U is a daughter nuclide of the ^{238}U decay process. High abundant ^{238}U decays to ^{234}U via two

intermediate short-lived radiogenic daughters (^{234}Th, $t_{1/2}$ = 24.1d and ^{234}Pa, $t_{1/2}$ = 6.69 h) through an energetic alpha recoil process, which distorts the mineral crystals (Fleischer, 1980). Because of low abundance of ^{234}U, the ratio of (^{234}U/^{238}U) nuclides is normally converted to activity ratios to define their association in large numbers (Bourdon et al., 2003; Hanson, 2011). Activity is referred to as the product of the decay constant and the number of a given radioactive nuclei within the decay chain (Bourdon et al., 2003). When the activity of the parent radioactive nuclei equals to the activity of the radiogenic daughter, the activity ratio of these two isotopes equal one. This situation is termed as secular equilibrium and is observed in old rocks (≥1Ma) in a closed system (e.g. (^{234}U/^{238}U) = 1; Luo et al., 2000). At secular equilibrium, the decay rate of radiogenic product (^{234}U) is equal to its production rate from ^{238}U (Bourdon et al., 2003). In the event of water-rock interaction, ^{234}U is fractionated from its parent ^{238}U into the fluid phase via alpha recoil processes resulting to ^{234}U depleted solid phases and ^{234}U enriched waters (Chabaux et al., 2003, 2008; Depaolo et al., 2006). Due to this preferential leaching of ^{234}U nuclide, water tends to have high activity ratios (^{234}U/^{238}U) > 1 (parentheses here refer to activity ratios) (Chabaux et al., 2003; Henderson and Anderson, 2003; Grzymko et al., 2007).

The (^{234}U/^{238}U) ratios derived from natural sources into water systems may be influenced by factors such as lithology (type of rock and dissolution mechanism, mineral-surface area, uranium concentration in the rock, Wood et al., 2004; Bagard et al., 2008), climate (amount of precipitation and temperatures, Robinson et al., 2004; Depaolo et al., 2006), and water residence times in aquifers (Osmond and Cowart, 1976; Drever, 1997; Chabaux et al., 2003). High solubility of U in oxic environments and fractionation of ^{234}U from its parent (^{238}U) due to alpha recoil processes have triggered the application of U isotopes in hydrology (Osmond and Ivanovich, 1992; Chabaux et al., 2003). Uranium isotopes have been used in tracing water and

salinity sources into rivers, fingerprinting flow paths of groundwater, identifying mixing of ground and surface waters, and estimating weathering and erosion rates (Kraemer and Brabets, 2012; Granet et al., 2010; Ma et al., 2010; Sardinha et al., 2010). These isotopes have been previously suggested to trace salinity into the Rio Grande River (Hogan et al., 2007). Recently, Skynzkwiez et al. (2015) applied uranium isotopes to distinguish salt loads from shallow and deep ground waters into the Rio Grande; this is due to differences in U solubility and alpha recoil rates in the near-surface and deep aquifer settings. Overall, most natural uranium sources from weathering show higher uranium isotope disequilibria ($^{234}U/^{238}U>>1$) in deep groundwater aquifers than shallow aquifers.

Uranium isotopes can also distinguish anthropogenic salinity sources in water systems (Kubiak and Muchula, 2014). Anthropogenic U sources indicate ($^{234}U/^{238}U$) close to secular equilibrium (($^{234}U/^{238}U$) = 1) since no preferential separation of ^{234}U over ^{238}U occurs. This is due to dissolution of phosphate fertilizers (e.g. N.P.K) in the irrigation fields, resulting to high uranium concentrations and ($^{234}U/^{238}U$) around secular equilibrium characteristic of phosphate ores (e.g. typically old apatite rocks) used in fertilizer processing (Zielinski et al., 1997, 2000, 2006; Kratz and Schnug 2006; Bituh et al., 2009).

4.3.2 STRONTIUM ISOTOPES IN WATER SYSTEMS

Strontium is an ideal salinity tracer in water systems because: (1) it is highly soluble and remains conservative during transport, and (2) mass-dependent fractionation in Sr isotopes ($^{87}Sr/^{86}Sr$) is minimal due to small mass difference (Paces and Wurster, 2014). Strontium has been used to identify water sources, flow paths, and salinity sources as well as suspended materials in rivers (Douglas et al., 1995; Semhi et al., 2000; Grosbois et al., 2000; Hogan et al., 2007; Moore et al., 2008; Paces and Wurster, 2014). Like other soluble divalent

alkali- earth element in rocks, strontium is released into water systems naturally through chemical weathering. Strontium has four abundant isotopes; three stable ^{88}Sr, ^{86}Sr, ^{84}Sr isotopes and one radiogenic isotope ^{87}Sr (Faure, 1977). The $^{87}Sr/^{86}Sr$ isotope ratios in water are mainly controlled by type and age of the source rock along its flow paths (Blum et al., 1998; Capo et al., 1998; Shand et al., 2009). This is because different rock types have varying Rb/Sr ratio, which change with rock age (Capo et al., 1998; Shand et al., 2009). Rubidium isotope, (^{87}Rb, $t_{1/2}$ = $4.8x10^{10}$yrs) undergoes a beta decay to ^{87}Sr in rocks, therefore older and Rb-enriched rocks (e.g. igneous rocks) tend to have much higher $^{87}Sr/^{86}Sr$ ratios (Shand et al., 2009). Evaporite or carbonate rocks generally have lower $^{87}Sr/^{86}Sr$ ratios because of lower Rb/Sr ratios due to the substitution of Ca by stable Sr in the carbonate mineral, thus contributing lower non-radiogenic $^{87}Sr/^{86}Sr$ ratios in water systems (Capo et al., 1998). Marine carbonates (e.g. limestones) with different formation ages have characteristic $^{87}Sr/^{86}Sr$ ratios derived from seawater at their formation time (McArthur et al., 2001; McArthur and Howarth, 2004). $^{87}Sr/^{86}Sr$ ratios can hence distinguish salinity from different rock lithologies along river flow paths.

Strontium can also be added into rivers through anthropogenic sources. Athropogenic salinity sources such as waste waste water and fertilizer-derived salts are characteristic of low $^{87}Sr/^{86}Sr$ ratios, but high Sr concentrations (Moore et al., 2008; Christian et al., 2011).

4.3.3 RIO GRANDE WATERSHED

The Rio Grande is the fourth longest river system in the USA; the source water for Rio Grande is from snow melts in south central Colorado, flowing southward through New Mexico, Texas and discharging into the Gulf of Mexico (Keller and Baldridge, 1999; Parcher et al., 2010). It serves as an international border between Texas and Mexico. The river flows within the Basin and Range province of the Rio Grande rift; a crustal extension feature that started about 30

Ma ago (Keller and Cather 1994). The river can be divided into three drainage area; the Upper, Middle and Lower Rio Grande (Hogan et al., 2007). In this study, we consider the Lower Rio Grande to start at Elephant Butte reservoir, NM to El Paso, TX (Figure 3.1a and 3.1b). This section of the river flows on the Engle, Palomas, and Mesilla basins before reaching El Paso, TX. These basins trend from north to south and are generally filled with Cenozoic deposits of the Santa Fe Formation (Seager et al., 1984; Mack et al., 1998). The formations include; (1) alluvial fans and piedmont-derived sediments from erosion of exposed Precambrian igneous and Paleozoic sedimentary rocks on mountain ranges and (2) ancestral Rio Grande fluvial deposits (Keller and Cather, 1994; Keller and Baldridge, 1999). Groundwater in the basins is normally recharged by runoffs from the mountains, leakages from Rio Grande river, agricultural canals and drains, and interflows from neighboring aquifers (Ellis et al 1993; Hogan, 2013).

The Lower Rio Grande river flows through arid to semi-arid zones of south west North America. This region receive an annual rainfall of about 20 cm/yr during summer and experiences high evaporation rates approximately 250 to 300 cm/yr near El Paso, TX (Wainwright, 2006). The river flow discharge in the Lower Rio Grande is mainly controlled from Elephant Butte reservoir in central/southern New Mexico. Water is usually released from the reservoirs during the irrigation seasons (normally from April to July) and supplied to several network of agricultural drains and canals for irrigation purposes. Excess water from irrigation farms is channeled back to the river through agricultural drains. Other water management systems include city drains, wastewater effluents, and groundwater pumping. Unlike the upper Rio Grande section, this portion of the river does not have tributaries joining the river. Occasionally surface runoffs during the summer monsoon rainfall contribute to the Rio Grande

at different points along its drainage. The river discharge generally decreases downstream due to diversions to farms for irrigation, evaporation, and river leakages to groundwater (Hogan, 2013).

Water quality of the Rio Grande deteriorates downstream due to high salt load from natural and anthropogenic sources (Philips et al., 2003; Hogan et al., 2007; Moore et al., 2008; Szynkiewicz et al., 2011). The water chemistry of the Lower Rio Grande river shows large variations associated with discharge, for instance high river flow results in dilution of dissolved salts while low river discharge is associated with high concentrations of the dissolved salts.

4.4 Methods

4.4.1 SAMPLE COLLECTION

In 2014, grab surface water samples were collected monthly from the Rio Grande at various locations starting from Elephant Butte, NM (site1; starting point, 0 km) through the Rio Grande at 237 (site 15; 215 km) in El Paso, TX during the irrigation (May-July) and non-irrigation (August-November) seasons (Figure 3.1b). Field measurements including temperature, pH, TDS, and NO_3 were conducted using the YSI professional plus instrument. About 1000 ml water samples were collected in pre-cleaned HPDE plastic bottle in the field. Approximately 250 ml of these water samples were filtered through 0.45 μm filters in the laboratory and stored into two equal proportions in clean 125 ml HPDE plastic bottles. Five drops of pure concentrated nitric acid were added to one of the filtered 125 ml sample for cation and isotopic analyses while the other portion was left untreated and stored for anion analysis. In September 2014, city drains (Sunset (site 16; 206 km) and Racetrack (site 17; 213 km) that recharge the river near El Paso, TX were sampled. In February 2015, groundwater samples were also collected from irrigation

pumping wells (site 18-23; 78-176 km) in the Mesilla Basin, New Mexico. These samples were filtered and treated as the river water.

Most of the Rio Grande river locations were dry during the non-irrigation season due to controlled water flow from the reservoir, water loss by evaporation and infiltration processes. As such, dissolved salts in the river water accumulate on the riverbed sediments. In order to mimic the chemistry of the river water at dry locations along the river during the non-irrigation season, we considered leaching river sediment with deionized water. The sediments were collected from the middle riverbed or riverbanks at 0-20 cm depth from several locations along the river; these sediments were mainly of clay and sandy texture. In the laboratory, approximately 100 g of river sediments and deionized water were weighed and placed in the ultrasonic bath for about 90 minutes. The mixture was allowed to settle for 24 hrs before decanting and vacuum filtering the supernatant through a 0.45 μm filter. The filtrate was divided into two equal portions; 5-7 drops of concentrated nitric acid were added to one portion for cation analysis while the other portion was left untreated for anion analysis.

4.4.2 SELECTION OF SAMPLES FOR U AND SR ISOTOPE ANALYSES

Because May and July 2014 were the start and end months of irrigation season in the Lower Rio Grande respectively, river samples collected in June were selected to represent the irrigation season for detailed U and Sr isotopic analyses. Closure of Elephant Butte reservoir gates in August 2014 marked the beginning of the non-irrigation season. With reduced river base flow over time, November water samples were chosen to represent the non-irrigation season. Some sites along the river were completely dry in November, and only nine sites including the reservoir were analyzed in this study. Other water samples selected for isotope analyses included: (1) river water samples from the Lower Rio Grande at Williamsburg (site 2, ~ 18 km),

Road 359 (site 9, ~ 150 km), Racetrack (site 14, ~213 km), and Road 237 (site 15, ~215 km) of all the sampled months, (2) groundwater from irrigation wells at the Mesilla Basin and city drains in El Paso, TX, and (3) archived water samples periodically collected between 2009 and 2010. Site numbers, field and laboratory procedures of the archived samples have been presented in Szynkiewicz et al. (2015). Specifically, we analyzed waters from the Rio Grande at Canutillo, TX (site 13,), agricultural drains (e.g. Vado R189: site 46, ~ 183 km; Westside: site 47, ~206 km; Newmexas: site 48, 209 km; Faben: site 53, 276 km; and Tornillo: site 54, ~284 km;), city drains (e.g. Montoya: site 50, ~ 211 km), El Paso treatment wastewater sample (site 58, ~217 km), deep groundwater (Tor C: site 77, ~16 km and Faben artesian wells: sites 87, ~276 km and site 88, ~274 km), and domestic groundwater wells (e.g. Vinton (170 Hemway Rd and 140 Hemway Rd: sites 83, ~ 145 km and site 84, ~ 143 km). These archived samples were analyzed for isotopic composition in order to identify salinity end members into the Lower Rio Grande.

4.4.3 LABORATORY ANALYTICAL TECHNIQUES

4.4.3.1 Major and minor ion concentration analyses

Approximately 1 ml of each acidified water sample was diluted with 10 ml distilled water (~18.2MΩ) and measured for major cation concentrations on the Perkin Elmer 5300DV Inductively Coupled Plasma-Optical Emission Spectrometer in the Department of Geological Sciences at the University of Texas at El Paso. Precision and accuracy were checked using multi-element atomic adsorption water reference standards from NIST and U.S. Geological Survey. Errors were less than 10% on all major elements concentrations. The non-acidified water samples along with calibration water standards were analyzed for anion concentrations on the Dionex Ion Chromatography (ICS-2100) at the University of Texas at El Paso. A water standard was analyzed for quality assurance; errors on standard measurements were within 10%.

Alkalinity was determined by titration on the Mettler Toledo DL 15 Titrator except for groundwater samples, which were calculated by mass balances.

4.4.3.2 Uranium concentrations and isotope ($^{234}U/^{238}U$) analyses

Approximately 25 ml of each water sample were spiked with about 60 mg of artificial ^{233}U spike in order to determine uranium concentrations [U] by isotope dilution technique. The samples were evaporated to dryness in a class 100-clean room in preparation for ion exchange chromatography. Samples were then dissolved in 7.5 N HNO_3 and passed through a resin (AG 1-X8 anion exchange resin (200-400 mesh)) in two steps for separation and purification of uranium. Purified samples were analyzed for $^{234}U/^{238}U$, $^{233}U/^{238}U$, and $^{235}U/^{238}U$ isotopic ratios on Nu Instruments ^{TM} Multi-Collector Inductively Coupled Plasma Mass Spectrometer (MC-ICP-MS) at the University of Texas at El Paso. The samples were analyzed by standard-sample bracketing method using uranium standard (NBL145B) in order to correct for mass dependent fractionation and Faraday-ion counter gain variations. The $^{234}U/^{238}U$ isotope ratios were corrected with ion counter gain and mass fractionation during the instrument analysis. The ($^{234}U/^{238}U$) activity ratios were calculated from the $^{234}U/^{238}U$ isotope ratios assuming decay half-lives of 2.4525×10^5 yr and 4.468×10^9 yr for U^{234} and U^{238} respectively (Cheng et al., 2000a). Uranium concentrations were calculated from weight and concentrations of the spike as well as ion counter gain and mass fractionation corrected $^{233}U/^{238}U$ isotope ratios.

For quality assurance purposes, about 200 mg of rock standard (W2) was spiked with ^{233}U reference material and digested in HNO_3-HF then followed by HCl-H_3BO_3 to dissolve all silicates and fluorides in the samples (Pelt et al., 2008;Granet et al., 2007; Dequincey et al., 2002). The W2 standard showed values (U = 0.503 ± 0.014 ppm; n = 8, (2σ) and ($^{234}U/^{238}U$) = 1.005±0.0045 (2σ)) consistent with those reported from other laboratories (Sims et al., 2008).

Procedure blanks for U were also spiked with artificial ^{233}U evaporated and analyzed as water samples. The blank values were negligible (~7 pg).

4.4.3.3 Strontium isotope composition ($^{87}Sr/^{86}Sr$) analysis

About 25 ml of water samples were evaporated to dryness, the dry samples were re-dissolved in 3.5 N HNO_3 then separated and purified through Sr-Spec resin. The purified samples and strontium standard (SRM 987) were measured for $^{87}Sr/^{86}Sr$ ratios on MC-ICP-MS using the standard-sample bracketing method. About 200 mg of rock standard BCR2 was acid-digested in HNO_3-HF and HCl-H_3BO_3 then separated through Sr-Spec resin. $^{87}Sr/^{86}Sr$ ratios in BCR2 reported values of 0.705019 ±4 (2σ) consistent with averages reported in other studies (Raczek et al., 2003). Blanks indicated significantly negligible Sr concentrations (~82 pg).

4.4.3.4 Geochemical modeling

Using Geochemical Workbench software version 10.0 (Bethke and Yeakel, 2015), the pH, TDS, temperature, and major ion concentrations of river water, city drains, and groundwater of the Lower Rio Grande were used to calculate mineral saturation indices and water types. The saturation indices were of minerals that are likely to influence water chemistry by dissolution and precipitation processes such as calcite ($CaCO_3$), dolomite ($CaMg(CO_3)_2$, gypsum ($CaSO_4.2H_2O$), halite (NaCl), and Thenardite ($NaSO_4$). Saturation indices (SI) are reported as log Q/K (where Q is actual composition of mineral in a fluid and K is equilibrium composition of a given mineral). When SI = 0, the mineral is at equilibrium; when SI<0 or SI>0, the mineral is under-saturated or oversaturated in water respectively.

4.5 Results

Field site information and sample field measurements along the Lower Rio Grande river, city drains and irrigation groundwater wells for the 2014-2015 sampling season are presented in Table 3.1. Major and minor element concentrations, U and Sr isotopic compositions, water types, and saturation indices of the river water, groundwater, agricultural return flows, city drains, and wastewaters are presented in Table 3.2, 3.3, 3.4, and 3.5. The concentrations of major and minor element concentrations in water leachates of the Lower Rio Grande river sediments are shown in Table 3.6.

4.5.1 MAJOR AND MINOR ELEMENT CONCENTRATIONS

The total dissolved solids (TDS) concentrations of the river water were lower in the irrigation season (600-776 mg/L) compared to the non-irrigation season (564.7-3283 mg/L) (Table 3.2; Figure 3.2a and 3.2b). While TDS concentrations slightly increased downstream in the irrigation season (Figure 3.2b), higher TDS in the non-irrigation season indicated spike concentrations in the Rio Grande at Williamsburg (site 2, ~18 km), Rio Grande at Road 359 (site 9, ~ 150 km), Rio Grande at Racetrack (site 14, ~ 213 km), and Rio Grande at Road 237 (site 15, ~ 215 km) (Figure 3.2a). Similar trends were observed in the major and minor element concentrations of the river water. In the irrigation season, low and narrow-ranged concentrations were observed for K (9.38-14.63 mg/L), Na (96.26-143.03 mg/L), Mg (13.04-16.82 mg/L), Ca (61.14-82.89 mg/L), Sr (0.83-1.02 mg/L), NO_3 (0.08-2.94 mg/L), Cl (80.56-199.45 mg/L), SO_4 (90.83-217.57 mg/L), Br (0.12-2.77 mg/L), and HCO_3 (2.06-3.35 meq/kg) (Table 3.2). These concentrations remain generally low and fairly constant from Elephant Butte reservoir to downstream locations at El Paso, TX (Figure 3.3a and 3.3b). May samples indicated slightly higher K, Ca, and Cl concentrations and lower SO_4 concentrations compared to respective

concentrations in June and July river water samples (Figure 3.3a and 3.3b). In contrast, high and wide-ranged concentrations were observed in the non-irrigation season for K (9.19-30.22 mg/L), Mg (13.96-40.47 mg/L), Na (95.25-853.47 mg/L), Ca (38.47-164.19 mg/L), Sr (0.74-3.15 mg/L), NO_3 (0.05-164 mg/L), Cl (83.67-829.67 mg/L), SO_4 (159.23-973.06 mg/L), Br (0.08-3.65 mg/L), and HCO_3 (0.35-6.59 meq/kg) (Table 3.2). Variation of these concentrations from Elephant Butte to downstream locations showed spike high concentrations of Na, K, Ca, Sr, Mg, Cl, and HCO_3 in the Rio Grande at Williamsburg (site 2, ~18 km) and Rio Grande at Road 237. High SO_4, Br, and low NO_3 concentrations were detected in the Rio Grande at Road 237 (site 15, ~215 km), but low SO_4, NO_3, and Br concentrations were observed in the Rio Grande at Williamsburg (Figure 3.3a and 3.3b). TDS concentrations in the river water were found to correlate well with concentrations of Mg, Na, Sr, Ca, Si, HCO_3, SO_4, and Cl in the non-irrigation season (Figure 3.4).

The irrigation groundwater wells showed TDS ranging from 780 to 1600 ppm and chloride concentrations between 119.4 and 781.3 mg/L, SO_4 (207.04-741.7 mg/L), NO_3 (11.89-29.64 mg/L), Br (2.2-3.1 mg/L), K (7.16-12.57 mg/L), Mg (19.83-45.47 mg/L), Na (86.26-222.23 mg/L), Ca (151.73-278.50 mg/L), Sr (1.41-3.1 mg/L), and Si (13.51-15.18 mg/L) (Table 3.2). While these concentrations remained similar to water samples within the mid-section of the river (~150-200 km), Ca, Mg, Sr, Si, and Br concentrations were notably high (Figure 3.3a). Among these irrigation groundwater wells, groundwater well#1 near New Mexico Road 391 (GW1_NM391; site 18, ~ 78 km) showed high concentrations of Cl, PO_4, Na, and K while GW3_NM28 (site 20, ~ 159 km) indicated low concentrations of TDS, Na, Sr, Mg, Ca, and Cl. Both of these irrigation groundwater wells indicated lower SO_4 concentrations compared to the other wells (Table 3.2; Figure 3.3a and 3.3b). City drains discharging to the Rio Grande river in

El Paso, TX showed considerably high TDS concentrations (2795 - 4095 mg/L) and variable Cl levels (716.6-1258.8 mg/L). A similar variability was observed for SO_4 (877.27-1192.80 mg/L), Br (2.55-3.35 mg/L), HCO_3 (6.02-6.74 meq/kg), K (11.14-11.95 mg/L), Mg (40.76-46.23 mg/L), Na (768.84-1306.61 mg/L), Ca (156.87-200.71 mg/L), Si (20.65-20.93 mg/L), and Sr (2.51-2.17 mg/L) concentrations (Table 3.2). The range of Ca, Na, Mg, Si, Sr, SO_4, Cl, HCO_3, and Br concentrations in the city drains match those downstream locations in the Rio Grande at Road 237 (site 15, ~215 km) (Table 3.2; Figure 3.3a and 3.3b).

Uranium concentrations [U] of the river water were fairly constant in the irrigation season (3.07-3.42 ppb) compared to the non-irrigation season (0.55-5.87 ppb), which showed alternating high and low values downstream (Table 3.4; Figure 3.8a). Significant high [U] were observed in the Rio Grande at Percha dam (site 3, ~53 km), Rio Grande at Road187/1 (site 4, ~62 km), and the Rio Grande at Road 237(site 15, ~215 km) during the non-irrigation season. However, low uranium values were noted in the mid-river section between 100 and 200 km in the same season (Figure 3.8a). Temporal variability of [U] and strontium concentrations [Sr] in the Rio Grande at Williamsburg (site 2, ~18 km), Canutillo (site 13, ~197 km), and Road 237 (site 15, ~215 km) showed lower [U] and [Sr] during the irrigation season compared to respective higher concentrations of the non-irrigation season. In contrast, the Rio Grande at Road 359 (site 9, ~150 km) and Racetrack (site 14, ~213 km) showed fairly constant [Sr] in either season except for November samples, which indicated very low values; Uranium concentrations were higher at these two sites during the irrigation season compared to the non-irrigation season (Figure 3.9a, 3.9c, 4a, 4c). Uranium verses HCO_3 concentrations were positively correlated for the river water; however, a contrasting trend was observed between uranium and Br concentrations (Figure 3.7a).

Higher [U] were observed in the irrigation groundwater wells (1.6 to 13 ppb) and domestic groundwater wells (3.5-13ppb) compared to artesian wells (0.01-3.4 ppb) (Tables 3.4 and 3.5). Generally, uranium levels in groundwater were lower compared to concentrations in the river water, except for the irrigation well (GW2_NM185; site 19, ~159 km) and the domestic well (Hemway Rd.170; site 83, ~145 km), which indicated high concentrations of about 13 ppb (Figure 3.8a). Agricultural drains contained up to 12 ppb of uranium concentrations, these concentrations increased considerably from Vado drains to Tornillo drains in the downstream locations (Table 3.5; Figure 3.8a). Detailed evaluation of [U] and [Sr] in Tornillo drains suggested higher concentrations of these elements during the irrigation and non-irrigation seasons compared to the river water (Figure 4b and 4d). Similarly, city drains showed significant increase of uranium concentration from Sunset drain (site 16, ~207 km; 0.7 ppb) to Racetrack drain (site 17, ~217 km; 3.59 ppb) (Table 4a); these uranium concentrations were comparable to the Rio Grande at Road 237 (site 15, ~215 km) (Figure 3.8a). High uranium concentrations (~15 ppb) were observed in wastewater discharging to the river in El Paso, TX (Table 3.5; Figure 3.8a).

4.5.2 WATER TYPES AND MINERAL SATURATION INDICES

Saturation indices (SI) and water types determined by Geochemical Workbench software for the river water, groundwater and city drains are presented in Table 3.3. The river water showed Na-Cl and Na-SO_4 water types during the irrigation season while the non-irrigation season river indicated Na-Cl, Na-SO_4, and $NaHCO_3$ water types (Table 3.3; Figure 3.5a-3.5e). Water types in most of the investigated river sites during the non-irrigation season were similar to those of irrigation groundwater wells (Na-SO_4, Ca-SO_4, and Ca-Cl types) and artesian wells (Na-Cl water type) (Figure 3.5f). However, the Rio Grande at Percha dam (site 3, ~53 km) and

the Rio Grande at Road 185 (site 7, ~ 112 km) showed $NaHCO_3$ water types for November samples (Table 3.3; Figure 3.5e). The Rio Grande at Road 237 (site 15, ~215 km) showed Na-Cl water type as did the city drain and El Paso wastewater samples (Figure 3.5f).

Saturation indices in the Lower Rio Grande river water was saturated (SI >0) with calcite and dolomite while gypsum, halite, and thenardite were undersaturated (SI <0) during the investigated seasons (Table 3.3; Figure 3.6a-3.6d). Dolomite and calcite SI notably increased downstream from Elephant Butte to El Paso, TX (Figure 3.6a and 3.6b).

4.5.3 URANIUM AND SR ISOTOPE COMPOSITIONS

River water of the irrigation season showed a narrow range of ($^{234}U/^{238}U$) and $^{87}Sr/^{86}Sr$ ratios of 1.75 to 1.79 and 0.7099 to 0.7103 respectively, compared to the respective ratios of the non-irrigation season (Figure 3.8b and 3.8d). The river water of the non-irrigation season showed large ($^{234}U/^{238}U$) and $^{87}Sr/^{86}Sr$ ratio variations with the highest average values in the Rio Grande at Williamsburg (site 2, ~18 km; 2.31 and 0.7145, respectively) compared to low values in the Rio Grande at Road 237 (site 15, 215 km; 1.53 and 0.7097, respectively) (Table 3.4). Contrary to the Rio Grande at Canutillo (site 13, ~197 km, Road 359 (site 9, ~150 km) and Road 237 (site 15,~215 km) that showed low ($^{234}U/^{238}U$) and $^{87}Sr/^{86}Sr$ ratios in the non-irrigation season, the Rio Grande at Williamsburg (site 2; ~18 km) and Canutillo (site 13, ~ 197 km) showed higher ($^{234}U/^{238}U$) and $^{87}Sr/^{86}Sr$ ratios during the non-irrigation season (Figure 3.9b, 3.9d, 4b, and 4d).

The ($^{234}U/^{238}U$) values and $^{87}Sr/^{86}Sr$ ratios were higher in the irrigation groundwater wells (site 18-23; 1.28-2.71 and 0.7093-0.7111 respectively) while lower ratios were more common in domestic groundwater wells (site 1.18-1.27 and 0.7100-0.7106 respectively) (Table 3.4 and 3.5). Artesian wells indicated higher $^{87}Sr/^{86}Sr$ ratios at Truth or Consequences (0.7203) and lower $^{87}Sr/^{86}Sr$ ratios of 0.7091 in the Faben area (Table 3.5). While the $^{87}Sr/^{86}Sr$ ratios of groundwater

showed values similar to the river water, ($^{234}U/^{238}U$) ratios in most groundwater wells were lower than river water except for GW3-NM28 (site 20, ~159 km) and Tor C wells. Significantly high ($^{234}U/^{238}U$) and low $^{87}Sr/^{86}Sr$ ratios were observed in GW3-NM28 irrigation groundwater well. Deep groundwater from Tor C artesian well showed higher $^{87}Sr/^{86}Sr$ and ($^{234}U/^{238}U$) ratios. Indeed, high ($^{234}U/^{238}U$) ratios were previously reported in deep saline groundwater in Szynkiewicz et al. (2015).

The ($^{234}U/^{238}U$) and $^{87}Sr/^{86}Sr$ ratios varied over a narrow range (from 1.52-1.56 and 0.7096-0.7098 respectively) in city drains while corresponding ratios in agricultural drains varied over a much wider range (1.31-1.72 and 0.7091-0.7106 respectively) (Table 3.4 and Table 3.5). El Paso wastewater sample showed ($^{234}U/^{238}U$) of 1.6 and $^{87}Sr/^{86}Sr$ ratios of 0.7088 (Table 3.5). While city drains and wastewater samples indicated low close-ranged ($^{234}U/^{238}U$) values, these ratios slightly decreased in agricultural drains from upstream Vado drains (site 46, ~183 km) to downstream Tornillo drains (site 54, ~284 km (Figure 3.9b and 3.9d). Temporal evaluation of Tornillo agricultural drains indicated low and constant ($^{234}U/^{238}U$) and $^{87}Sr/^{86}Sr$ ratios during both the irrigation and non-irrigation seasons compared to river water in the Rio Grande at Canutillo except for one agricultural drain sample of November 2010 (Figure 4c, 4d, 4.1b, and 4.1d); this sample had very low $^{87}Sr/^{86}Sr$ ratios. $^{87}Sr/^{86}Sr$ ratios in the river water, groundwater, agricultural and city drains in the downstream locations near El Paso showed large overlaps among the range of values, except for El Paso wastewater sample which indicated distinctly lower $^{87}Sr/^{86}Sr$ ratios (Figure 3.9d).

4.5.4 ELEMENTAL RATIOS IN WATER AND SEDIMENT LEACHATES

Major element concentrations of river sediment water leachates are presented in Table 3.6. To minimize the effect of concentration and dilution effects in the samples, elemental molar

ratios normalized with conservative elements (e.g. Cl and Na) were calculated. River sediment water leachates of the Rio Grande at Road 391(site 5, ~ 76 km), Road 154 (site 6, ~ 86 km), Road US70 (site 8, ~ 144 km), Road189 (site 11, ~ 173 km), Road 259/Canutillo (site 13, ~ 197 km), and Road 237 (site 15, ~ 215 km) showed elevated SO_4/Cl ratios compared to the river water, groundwater, agricultural return flows, city drains, and wastewater (Figure 4.2a). A similar pattern was observed for Na/Cl, NO_3/Cl, and K/Na in river sediment water leachates for samples collected between 150-200 km downstream; however, NO_3/Cl and K/Na in river water at the Rio Grande at Road 359 (site 9, ~150 km) were measurably high (Figure 4.1b, 4.1d, 4.1f). Low and fairly constant SO_4/Cl ratios were observed in river water collected at the start of the irrigation season (May 2014). River water of the non-irrigation season (August and November 2014) had higher SO_4/Cl ratios except the Rio Grande at Williamsburg (site 2, ~18 km), which indicated notably low SO_4/Cl ratios. The SO_4/Cl ratios in river water during non-irrigation season matched reasonably well with similar values in city drains, agricultural drains, wastewater, and groundwater except the sample from Tor C well, which indicated significantly low SO_4/Cl ratios (Figure 4.1a). The SO_4/Cl ratios were positively correlated with Na/Cl molar ratios in sediment water leachates, river water, groundwater and city drains; a similar relationship was observed for the SO_4/Cl verses Ca/Cl (Figure 4.2g and 4.2h).

Only two river sediment water leachates collected at about 210 km downstream showed similarly high Br/Cl molar ratios as irrigation groundwater wells (Figure 4.1c). Other sediment water leachates between 70 and 200 km had low fairly uniform Br/Cl ratios. On the contrary, irrigation groundwater wells showed elevated Ca/Na ratios, as did most river sediment water leachates between 70-200 km; these ratios were significantly higher compared to river water, city

drains, wastewater, artesian and domestic wells as well as river sediment water leachates collected at about 210 km downstream during the irrigation season (Figure 4.1e).

The Ca/Na verses Mg/Na ratios positively correlated well for river sediment leachates, groundwaters, river water of non-irrigation season, wastewater, agricultural drains, and city drains; these samples show ratios intermediate between silicate and evaporite lithology (Figure 4.1b). However, in the irrigation season no correlation between Ca/Na and Mg/Na ratios is depicted, river water samples show values similar to silicate lithology (Figure 4.2a). A similar pattern is observed in the correlation of Ca/Na verses HCO_3/Na, except that in the irrigation season, river waters ratios between silicate and evaporite lithology while during the non-irrigation season: river water, groundwaters, wastewater, agricultural drains, and city drains show similar values as evaporite lithology (Figure 4.2c and 4.2d). No correlation was observed when plotting $^{87}Sr/^{86}Sr$ ratios verses Ca/Na molar ratios; however, a negative correlation between ($^{234}U/^{238}U$) and Ca/Na ratios was observed (Figure 4.2e and 4.2f). While river water from Rio Grande at Road 237 (site 15, ~215 km) and Racetrack (site 14, ~213 km), wastewater, agricultural drains, domestic groundwater wells showed similar ($^{234}U/^{238}U$) values, artesian wells and irrigation groundwater wells showed distinct ratios.

4.6 Discussion

4.6.1 Spatio-temporal variations of natural and anthropogenic salts in the Lower Rio Grande

High salt content in dryland river waters impairs its usage for agricultural and domestic purposes (Hogan et al., 2007; Borrok and Engle, 2014). Previous studies have identified that the salinity of the Rio Grande in the arid and semiarid southwest USA is contributed by both natural sources (e.g. saline groundwater) and anthropogenic factors (e.g. agricultural return flows, city drains, wastewater effluents)(Hogan et al., 2007; Moore et al., 2008; Szynkiewicz et al., 2011,

2015; Borrok and Engle, 2014). Irrigation activities using high salinity water results in precipitation of secondary mineral (e.g. pedogenic carbonates) in managed agricultural soils (Suarez, 2000; Bughio et al., 2016).

Our results indicate that both natural and anthropogenic salinity sources into the Lower Rio Grande river vary over time and space. Dissolved ions including Mg, Na, Sr, Ca, Si, HCO_3, SO_4, and Cl were identified as the major contributors of the total dissolved solids (TDS) in the Lower Rio Grande river (Figure 3.4). TDS levels changed significantly along the river depending on the river discharge (Figure 3.2a). For instance, in the irrigation season when the river discharge is high due to opening of the Elephant Butte reservoir gates, uniform and fairly constant major and minor element concentrations, water types and isotope compositions (($^{234}U/^{238}U$) and $^{87}Sr/^{86}Sr$ ratios) were observed in the river. Such fairly uniform trends imply dominance of reservoir water and dilution processes in the river (Figure 3.2b and 3.3a and 3.3b, 3.8a to 3.8d). However, slight increases noted in these parameters downstream near El Paso, TX during the irrigation season are indicative of salt addition. Increasing [U], [Sr], but decreasing ($^{234}U/^{238}U$) and $^{87}Sr/^{86}Sr$ ratios in the Rio Grande at Road 359 (site 9; ~150 km) during the irrigation season are indicative of anthropogenic salt loads probably from agricultural return flows or urban wastewater (Figure 3.9a to 3.9d). Waste effluents and fertilizer-derived salts are characteristic of low ($^{234}U/^{238}U$) and $^{87}Sr/^{86}Sr$ ratios (Antich et al., 2000; Christian et al., 2011; Borylo et al., 2009; Szynkiewicz et al., 2015). Decreasing [U], [Sr], and fairly constant ($^{234}U/^{238}U$), and $^{87}Sr/^{86}Sr$ ratios in the Rio Grande at Racetrack (site 14; ~213 km) during the irrigation season show evidence of mixed salinity such as shallow groundwater and anthropogenic sources to the river (Figure 3.9a to 3.9d). One way geologically sourced salts mix with anthropogenic salinity is through agricultural and city drains, which have been reported to

be deep enough to interconnect shallow water table or flow over salt flats (Walton et al., 1999; Szynkiewicz et al., 2015).

In the non-irrigation season, Elephant Butte reservoir is normally closed thus decreasing the river discharge; some sites along the river are typically dry. The river base flow is mainly composed of deep groundwater, shallow groundwater, agricultural return flows, and urban drains. Consistent with Moore et al. (2008)'s study, these water sources were identified as salinity end-members to the Rio Grande (Figure 3.2a; Figure 4.3). Notably high Mg, Ca, Sr, Na, K, and Cl concentrations in the Rio Grande at Williamsburg (site 2, ~ 18 km) suggest addition of high saline water such as deep groundwater to the river (Figure 3.3a and 3.3b). Particularly low SO_4 and U concentrations and significantly high ($^{234}U/^{238}U$) and $^{87}Sr/^{86}Sr$ ratios at this site are characteristic of deep ground water salinity (Figure 3.3b; Figure 3.8b and 3.8d). Temporal evaluation of [U], [Sr], ($^{234}U/^{238}U$), and $^{87}Sr/^{86}Sr$ ratios in the Rio Grande at Williamsburg suggest addition of distinctive saline deep ground water to the river during the non-irrigation season (Figures 3.9a- 3.9d). The U and Sr (concentration and isotopic) values observed in the Rio Grande at Williamsburg were similar to groundwater from artesian wells at T or C (low [U] of 3.40 ppb; high ($^{234}U/^{238}U$) of 2.66; $^{87}Sr/^{86}Sr$ ratios ~0.7203) (Table 3.5; Figure 3.8a, 3.8b, 3.8d; Szynkiewicz et al., 2015). This confirms loading of salts from deep groundwater to surface waters particularly during the non-irrigation season. Our explanation is consistent with previous studies that identified geothermal salt contribution along the Rio Grande (e.g. at the T or C area) either directly through deep groundwater upwelling, mixing with shallow groundwater or spa and mineral baths discharge to the river (Witcher et al., 2004; Lacey, 2006; Hogan et al., 2007; Szynkiewicz et al., 2011).

Chemistry of the river base flow suggest that salt contribution from deep groundwater diminishes downstream while anthropogenic salt-loads from agricultural and urban drains generally increased significantly toward El Paso, TX. However, cycling of salts from shallow groundwater, agricultural return flows, and wastewater effluents were implicated in the river due to interconnection of surface and near surface waters (Walton et al., 1999). For example, similarity of Ca, Mg, Sr, Si, and Br concentrations as well as $^{87}Sr/^{86}Sr$ ratios in both the river water of the mid-river section and irrigation groundwater wells suggests mixing or addition of shallow groundwaters to surface waters (Figure 3.3a, 3.3b, 3.8d). Additionally, high Br/Cl ratios in the irrigation groundwater wells probably account for the intermediate to high Br concentrations in the river water of the mid-river section (Figure 3.3b and 4.1c). Gradually increasing ($^{234}U/^{238}U$) values in the river water of the mid river section could be explained by addition of groundwaters with distinctively high ($^{234}U/^{238}U$) ratios (Figure 3.8b). Despite lower ($^{234}U/^{238}U$) ratios in the irrigation groundwater wells compared to the river water in the mid river section, distinctively high ($^{234}U/^{238}U$) values were observed at GW3_NM 28 irrigation well (site 20, ~ 159 km) (Figure 3.8b). Variations of U concentrations and activity ratios in shallow groundwater could be associated with changes of lithology and/or mixing processes between deep geothermal water and anthropogenic salinity (Figure 3.8a and 3.8b). Previous studies on uranium signature in river systems have linked elevated ($^{234}U/^{238}U$) ratios in river waters with groundwater input (Riotte and Chabaux, 1999; Durand et al., 2005; Camacho et al., 2010). The chemistry of the Rio Grande at Road 154 (site 6; ~86 km) was specifically influenced with shallow groundwater especially during the non-irrigation season. The Rio Grande at Road 154 showed ($^{234}U/^{238}U$) and $^{87}Sr/^{86}Sr$ ratios similar to irrigation groundwater well (GW1_NM391; site 18; ~78 km) suggesting a link of salinity in the surface and near surface waters systems

(Figure 3.8b). This is consistent with the common practice of using shallow groundwaters to supplement for irrigation needs during the non-irrigation season and channeling excess irrigation water to the river through drains (Moore et al., 2008; Szynkiewicz et al., 2011, 2015). Other studies have also suggested that groundwater salinity adds to the river within the Mesilla Basin directly through upwelling processes over a faulted system or indirectly through intersection with agricultural drains (Witcher et al., 2004).

Additions of urban effluents were prominent in the Rio Grande at Road 359 (site 9; ~150 km) and downstream locations in the Rio Grande at Road 237 (site 15; ~215 km) during the non-irrigation season. River water and sediment water leachates of the Rio Grande at Road 359 indicated high NO_3/Cl and K/Na molar ratios during the non-irrigation season (Figure 4.1d and 4.1f). Because irrigation groundwater wells in the region showed lower NO_3/Cl and K/Na molar ratios (Figure 4.1d and 4.1f), we associate the elevated molar ratios in the river to localized anthropogenic sources. High NO_3 and K concentrations have previously been documented in waste effluents near Las Cruces, NM (Szynkiewicz et al., 2015) and fertilizers used in crop farming within the Mesilla irrigation district (Szynkiewicz et al., 2011). However, temporal evaluation of water in the Rio Grande at Road 359 showed low [U] and high ($^{234}U/^{238}U$) ratios during the non-irrigation season (Figure 3.9a and 3.9b), this suggest addition of characteristically high ($^{234}U/^{238}U$) ratio waters (e.g. groundwater) to the river. Additionally high Ca/Na molar ratios in river water of non-irrigation season as well as sediment leachates in mid-river section could be associated to geological sources because shallow ground waters indicated similar ratios (Figure 4.1e). Further downstream, chemistry of the Rio Grande at Road 237, city drains, agricultural drains (e.g. New Mexas and Westside) and El Paso wastewater effluents overlap during the non-irrigation season. These waters indicated similar values of TDS, major and minor

element concentrations (e.g. Na, Mg, Si, Ca, Sr, SO_4, Cl, and Br), Na-Cl water type, ($^{234}U/^{238}U$), and $^{87}Sr/^{86}Sr$ ratios (Figures 3.2a, 3.3a, 3.3b 3.8a, 3.8b, 3.9b, 4.3). Matching of these geochemical signatures in these waters suggest loading of anthropogenic salinity to the river. The network of city drains, agricultural drains and wastewater effluent around the Rio Grande at Road 237 (site 15, ~ 215 km) allow for cycling of anthropogenic salinity in the downstream locations. For example, New Mexas and Westside agricultural drains join the Montoya city drain that discharge to the river about a kilometer upstream of the Rio Grande at Road 237. Sunset and Racetrack city drains are sections of the Montoya drain. Montoya drain has been proposed to flow over salt flats with evaporate minerals (USACE, 2013; Szynkiewicz et al., 2015). This suggests that in addition to anthropogenic salinity, Montoya drain load geologically sourced salts to the Rio Grande at Road 237 (site 15, ~ 215 km). Moreover, river water in the Rio Grande at Road 237, city drains, and El Paso wastewater effluents show Mg/Na and HCO_3/Na molar ratios similar to water flowing through evaporite lithology (Figure 4.2b and 4.2d). Clearly, river water in the Rio Grande at Road 359 (site 9, ~150 km) and Road 237 (site 15, ~ 215 km) is influenced by both anthropogenic and lithological salinity.

4.6.2 EFFECT OF AGRICULTURAL RETURN FLOWS ON THE RIVER CHEMISTRY

Repeated usage of the Lower Rio Grande river water in irrigation activities has degraded water quality in the downstream river locations. Because of high evapotranspiration rates, water infiltration processes, salt addition from fertilizers, and soluble soil minerals, agricultural return flows are characteristic of high salinity. Detailed temporal evaluation and comparison of archived river water and agricultural return flows was performed in this study. Tornillo agricultural drains showed high [U] and [Sr] probably due to fertilizer related salts (Figure 4a and 4c). Consistent with U and Sr signature in fertilizers, agricultural drains showed low

($^{234}U/^{238}U$) and $^{87}Sr/^{86}Sr$ ratios compared to the Rio Grande at Canutillo (site 13; ~197 km) (Figure 4b and 4d). Agricultural drains showed increasing [U] and decreasing ($^{234}U/^{238}U$) ratios from Vado (site 46; ~ 183 km) to Faben agricultural drains (site 53; ~ 276 km), which indicated highest [U] and lowest ($^{234}U/^{238}U$) ratios (Figure 3.8a and 3.8b). This suggests increasing fertilizer-derived salinity in the downstream locations. Anthropogenic salinity decreases the river water ($^{234}U/^{238}U$) and $^{87}Sr/^{86}Sr$ ratio signatures due to mixing processes. The Rio Grande at Canutillo indicated lower [U] and [Sr] but high ($^{234}U/^{238}U$) and $^{87}Sr/^{86}Sr$ ratios compared to the agricultural drains. While the ($^{234}U/^{238}U$) and $^{87}Sr/^{86}Sr$ ratios in Tornillo agricultural drains remained fairly constant during investigated seasons, the Rio Grande at Canutillo indicated lower ($^{234}U/^{238}U$) and $^{87}Sr/^{86}Sr$ ratios in the irrigation season compared to the non-irrigation season. These lower ratios in the river water could be linked to fertilizer-derived salts loaded to the rivers through drains. High ($^{234}U/^{238}U$) and $^{87}Sr/^{86}Sr$ ratios in the river water in the non-irrigation season could be associated to geological salts loaded to the river through shallow ground water that supplements for irrigation (Figure 4). This explanation is consistent with Szynkiewicz et al. (2015)'s study who linked ($^{234}U/^{238}U$) ratios in the Lower Rio Grande to shallow groundwater rather than deep groundwater.

4.6.3 OTHER PROCESSES AFFECTING THE WATER CHEMISTRY IN THE RIVER

In addition to salt addition, mixing of water sources, precipitation and dissolution of minerals, as well as ion adsorption processes influence the concentrations and behavior of dissolved loads in the river water (Yuan and Miyamoto, 2005). Plots of Mg/Na, HCO_3/Na, and ($^{234}U/^{238}U$) ratios verses Ca/Na molar ratios suggest mixing of water flowing through siliceous and evaporite lithology in the Lower Rio Grande (Figure 4.2a- 4.2e). Minimal salt contribution from carbonate lithology is also implicated in the plot of Mg/Na verses Ca/Na molar ratios

(Figure 4.2b). One way to identify chemical signature due to lithological influence in rivers is by correlation of measured elemental molar ratios and isotope compositions (Gaillardet et al., 1999; Riote and Chabaux, 1999; Chabaux et al., 2001; Millot et al., 2002). Lithological salt contribution to the river water is mainly through weathering processes; however, deep and shallow groundwaters conveyed to the river through surface runoff (irrigation drains) or direct upwelling processes on fault zones add salts to rivers. Deep groundwater from artesian wells (T or C and Faben area) showed low Mg/Na and HCO_3/Na molar ratios compared to higher ratios in irrigation groundwater wells; all other investigated samples indicated intermediate values (Figure 4.2b and 4.2d). This may suggest mixing of deep and shallow groundwater-derived salts in river water of the non-irrigation season, city and agricultural drains, and domestic groundwater. Although $^{87}Sr/^{86}Sr$ ratios in the investigated samples were similar except for Tor C artesian wells (Figure 4.2f, 4.3), a plot of ($^{234}U/^{238}U$) versus Ca/Na molar ratios and $^{87}Sr/^{86}Sr$ ratios provide further evidence of mixing processes between deep groundwater and shallow groundwater/agricultural drains. Consistent with this interpretation of mixing processes, distinct water types were observed in the deep groundwater from artesian wells and irrigation groundwater wells while the other samples showed intermediary water types (Figure 3.5g). Indistinguishable $^{87}Sr/^{86}Sr$ ratios in the Lower Rio Grande water, wastewater, agricultural drains, domestic groundwater well, and city drains could suggest mixing and cycling of salts between surface and subsurface water sources (Figure 4.2e, 4.2f, 4.3).

Precipitation reactions in water systems remove dissolved ions from solution while dissolution of minerals releases ions into solvents thus increasing TDS. The Lower Rio Grande river water is oversaturation with dolomite and calcite (SI>0) suggesting precipitation of these minerals while undersaturation of gypsum, halite and thenardite minerals (SI<0) imply

dissolution processes (Figure 3.6c and 3.6d). Positive correlation of bicarbonates and uranium concentrations suggest similar behavior of these two elements; for example, precipitation/reactions of these two elements in the Lower Rio Grande (Figure 3.7a). At optimum pH dissolved uranium has been reported to complex with carbonates to form uranyl carbonates in water systems (Kelly et al., 2003). Consistent with dissolution of the undersaturated minerals, concentrations of Ca, SO_4, Na, and Cl were noted to increase with TDS in the river water of the non-irrigation season (Figure 3.4).

The Lower Rio Grande river is thought to be a losing stream recharging shallow groundwater aquifers (Walton and Ohlmacher, 2000). Infiltration of river water through porous sediments and high evaporation rates result in adsorption of some minerals/ions on the river sediments. Positive correlation of SO_4/Cl with Ca/Cl and Na/Cl in river sediment water leachates suggest that dissolved Ca, SO_4, Na, and Cl ions in river water adsorb on river sediments or precipitate gypsum, halite and/or thenardite minerals on riverbed following infiltration or evaporation processes (Figure 4.2g, and 4.2h). The river sediment water leachates indicated high Ca/Na molar ratios (Figure 4.1e). Ca and Na ions on river sediment leachates could be associated with evaporite minerals such as gypsum and halite on river sediments. Both Na and Cl ions in solution are considered conservative and are expected to maintain 1:1 Na/Cl ratios. If the observed Na/Cl ratios in river sediment water leachates were due to dissolution of halite adsorbed on riverbed, we would expect constant ratios downstream. High Na/Cl ratios of some river sediment water leachates could be explained by adsorption of Na ions on clays (Figure 4.1b). High K/Na molar ratios in the river sediment water leachates could be accounted for by either anthropogenic salinity such as fertilizer or wastewater effluents or adsorption on clay river sediments (Figure 4.1f). High SO_4/Cl in the river sediment water leachates could also be

accounted for by dissolution of gypsum on the riverbed. With exception of high Br/Cl ratios in river sediment water leachates from the Rio Grande at Canutillo and Road 237, other sediments water leachates showed lower Br/Cl ratios (Figure 4.1c). This suggests that Cl ions were adsorbed more on the sediments as opposed to Br ions or the river water characteristically low in Br content compared to Cl concentrations. High Br/Cl ratios in sediment leachates Rio Grande at Canutillo (site 13, ~ 197 km) and Road 237 (site 15, ~215 km) are associated with shallow ground water and anthropogenic salinity respectively. These adsorbed ions influence the chemistry of the river water at the beginning of the next irrigation season. For example, river water samples of May 2014 (starting month of irrigation season) recorded higher Cl concentration compared to other irrigation months (June and July, 2014). We linked these high Cl values to dissolution of halite on the riverbed following the non-irrigation season of the year 2013.

4.7 Conclusion

Dissolved load of the Lower Rio Grande river between Elephant Butte Reservoir and El Paso, TX is significantly controlled by river discharge. The Reservoir water dominated the chemistry of the river during the irrigation season while water sources such as deep and shallow groundwater, agricultural drains, city drains, and wastewaters constitute the river base flow and significantly load salts to the river in the non-irrigation season. The Rio Grande at Williamsburg (site 2, ~18 km) showed distinctively high ($^{234}U/^{238}U$) and $^{87}Sr/^{86}Sr$ ratios characteristic of deep groundwater salinity. Other locations downstream (e.g. the Rio Grande at Road 237 (site 15, ~ 215 km) were influenced with anthropogenic salinity through irrigation pumping, city drains and wastewater effluents. In addition to natural and anthropogenic salt loading to the Lower Rio

Grande, mixing, salt precipitations, mineral dissolution and river sediment adsorption processes were found to control the chemistry of the Lower Rio Grande River.

4.8 Acknowledgements

The National Science Foundation under grant number: EAR-1349091 to Lin Ma supported this work. We thank Adam Ianno, Hugo Hernandez, Mathew Hiebing, Yvette Pereyra, and Julio Ceniceros for help with 2014-2015 water sampling exercise and laboratory analyses.

References

Antich, N., Canals, A., Soler, A., Darbyshire, D. P. F., Spiro, B. F. (2000). The isotope composition of dissolved strontium as a tracer of pollution in the Llobregat River, northeast Spain. In Tracers and Modelling in Hydrogeology; Dassargues, A., Ed.; International Association of Hydrological Sciences: Oxfordshire, 207-212.

Bagard, M.L., Chabaux, F., Pokrovsky, O.S., Prokushkin, A.S., Viers, J., Dupre, B. (2008) Temporal variations of chemical weathering fluxes in boreal rivers under permafrost conditions: examples of the Nizhnaya Tunguska watershed (Central Siberia). EGU General Assembly 2008, EGU, Washinton, DC. Geophysical Research Abstracts 10:EGU2008-A-04760

Bethke, C.M. and Yeakel, S. (2015). The Geochemist's Workbench Release 10.0: Reaction Modeling Guide. Aqueous Solutions, LLC, Champaign, Illinois.

Bourdon, B., Turner, S., Henderson, G.M., Lundstrom, C.C. (2003). Introduction to U-series geochemistry. *Reviews in Mineralogy and Geochemistry* 52, 1–21.

Borrok, D. M. and Engle, M. A. (2014). The role of climate in increasing salt loads in dryland rivers. *Journal of Arid Environments 111*, 7-13.

Boryło, A., Nowicki, W., Skwarzec, B. (2009). Isotopes of polonium (^{210}Po) and uranium (^{234}U and ^{238}U) in the industrialised area of Wiślinka (North Poland). *International Journal of Environmental and Analytical Chemistry 89*(8-12), 677-685.

Bituh, T., Marovic, G., Franic, Z., Sencar, J., Bronzovic, M. (2009). Radioactive contamination in Croatia by phosphate fertilizer production.*Journal of hazardous materials 162*(2), 1199-1203.

Blum, J. D., Gazis, C. A., Jacobson, A. D., Chamberlain, C. P. (1998). Carbonate versus silicate weathering in the Raikhot watershed within the High Himalayan Crystalline Series. *Geology 26*(5), 411-414.

Bughio, M. A., Wang, P., Meng, F., Qing, C., Kuzyakov, Y., Wang, X., Junejo, S. A. (2016). Neoformation of pedogenic carbonates by irrigation and fertilization and their contribution to carbon sequestration in soil. *Geoderma 262*, 12-19.

Capo, R.C., Stewart, B.W., Chadwick, O.A. (1998). Strontium isotopes as tracers of ecosystem processes: theory and methods. *Geoderma* 82, 197–225.

Camacho, A., Devesa, R., Vallés, I., Serrano, I., Soler, J., Blázquez, S., Ortega, X., Matia, L. (2010). Distribution of uranium isotopes in surface water of the Llobregat river basin (Northeast Spain). *Journal of environmental radioactivity*, *101*(12), 1048-1054.

Chabaux, F., Riotte, J., Dequincey, O. (2003). U–Th–Ra fractionation during weathering and river transport. In: Bourbon, B., Henderson, G.M., Lundstrom, C.C., Turner, S.P. (Eds.), Uranium-Series Geochemistry. The Mineralogical Society of America. 533–576.

Chabaux, F., Bourdon, B., Riotte, J., (2008). U-series geochemistry in weathering profiles, river waters and lakes. *Radioactivity in the environment* 13, 49–104.

Chabaux, F., Riotte, J., Clauer, N., France-Lanord, C. (2001). Isotopic tracing of the dissolved U fluxes of Himalayan rivers: implications for present and past U budgets of the Ganges-Brahmaputra system. *Geochimica et Cosmochimica Acta*, *65*(19), 3201-3217.

Cheng, H., Edwards, R.L., Hoff, J., Gallup, C.D., Richards, D.A., Asmeron, Y., 2000a. The half-lives of uranium-234 and thorium- 230. *Chemical Geology* 169, 17–33.

Christian, L. N., Banner, J. L., Mack, L. E. (2011). Sr isotopes as tracers of anthropogenic influences on stream water in the Austin, Texas, area.*Chemical Geology 282*(3), 84-97.

Douglas, G. B., Gray, C. M., Hart, B. T., Beckett, R. (1995). A strontium isotopic investigation of the origin of suspended particulate matter (SPM) in the Murray-Darling River system, Australia. *Geochimica et Cosmochimica Acta*. 59, 3799–3815.

DePaolo, D.J., Maher, K., Christensen, J.N., McManus, J. (2006). Sediment transport time measured with U-series isotopes: results from ODP North Atlantic drift site 984. *Earth and Planetary Science Letters* 248, 394–410

Dequincey, O., Chabaux, F., Clauer, N., Sigmarsson, O., Liewig, N., Leprun, J.C., (2002). Chemical mobilizations in laterites : evidence from trace elements and ^{238}U–^{234}U– ^{230}Th disequilibria. *Geochimica et Cosmochimica Acta* 66, 1197–1210.

Duff, M., Hunter, D., Bertsch, P., Amrhein, C. (1999). Factors influencing uranium reduction and solubility in evaporation pond sediments. *Biogeochemistry* 45(1), 95–114

Durand, S., Chabaux, F., Rihs, S., Duringer, P., Elsass, P. (2005). U isotope ratios as tracers of groundwater inputs into surface waters: example of the Upper Rhine hydrosystem. *Chemical Geology 220*(1), 1-19.

Drever, J.I. (1997). The Geochemistry of Natural Waters. 3rd ed. Prentice-Hall, Englewood Cliffs, NJ.

Ellis, S.R., Levings, G.W., Carter, L.F., Richey, S.F., Radell, M.J. (1993). Rio Grande Valley, Colorado, New Mexico, and Texas: *Water Resources Bulletin* 29, 617–646.

Faure, G. (1977). Principles of Isotope Geology. John Wiley & Sons.

Fleischer, R.L. (1980). Isotopic disequilibrium of uranium: alpha-recoil damage and preferential solution effects. *Science* 207, 979–981.

Finch, R. and Murakami, T. (1999). Systematics and paragenesis of uranium minerals. *Reviews in Mineralogy* 38, 91-180.

Frost, C.D. and Toner, R. (2004). Strontium isotopic identification of water–rock interaction and ground water mixing. *Ground water* 42 (3), 418–432.

Gaillardet, J., Dupre´, B., Louvat, P., Alle`gre, C.J. (1999). Global silicate weathering and CO2 consumption rates deduced from the chemistry of large rivers. *Chemical Geology* 159, 3 – 30.

Ghassemi, F., Jakeman, A.J., Nix, H.A. (1995). Salinisation of land and water resources: Human causes, extent, management and case studies: Wallingford, UK, CAB International, 544 p.

Granet, M., Chabaux, F., Stille, P., France-Lanord, C., Pelt, E., 2007. Time-scales of sedimentary transfer and weathering processes from U-series nuclides: clues from the Himalayan rivers. *Earth and Planetary Science Letters* 261, 389–406.

Granet M., Chabaux F., Stille P., Dosseto A., France-Lanord C., Blaes E. (2010) U-series disequilibia in suspended river sediments and implication for sediment transfer time in alluvial plains: the case of the Himalayan rivers. *Geochimica et Cosmochimica Acta* 74, 2851–2865.

Grosbois, C., Négrel, P., Fouillac, C., Grimaud, D. (2000). Chemical and isotopic characterization of the dissolved load of the Loire river. *Chemical Geology* 170, 179–201.

Grzymko, T.J., Marcantonio, F., McKee, B.A., Stewart, C.M. (2007). Temporal Variability of Uranium Concentrations and 234U/238U Activity Ratios in the Mississippi River and Its Tributaries. *Chemical Geology* 243, 344–356.

Hanson, B. (2011). Isotopic and Geochemical Investigation Into the Origin of Elevated Uranium Concentrations in Treasure Valley Ground and Surface Waters, Idaho (Doctoral dissertation, Boise State University).

Henderson, G.M. and Anderson, R. (2003). The U-series toolbox for paleoceanography. In: Bourbon, B., Henderson, G.M., Lundstrom, C.C., Turner, S.P. (Eds.), Uranium-Series Geochemistry. The Mineralogical Society of America, 493–531.

Hogan, J. F., Phillips, F. M., Mills, S. K., Hendrickx, J. M., Ruiz, J., Chesley, J. T., Asmerom, Y. (2007). Geologic origins of salinization in a semi-arid river: The role of sedimentary basin brines. *Geology 35*(12), 1063-1066.
Herring, J. S. (2013). Uranium and thorium resources. In *Nuclear Energy* Springer New York. 463-490.

Hogan, J. F. (2013). Water quantity and quality challenges from Elephant Butte to Amistad. *Ecosphere* 4(1),9. http://dx.doi.org/10.1890/ES12-00302.1

Lacey, H.F. (2006). Quantification and Characterization of Chloride Sources in the Rio Grande. New Mexico Institute of Mining and Technology. M.S. Thesis.

Luo, S., Ku, T., Roback, R., Murrell, M., McLing, T.L. (2000). In-situ Radionuclide Transport and Preferential Groundwater Flows at INEEL (Idaho): Decay-series Disequilibrium Studies. *Geochimica et Cosmochimica Acta* 64 (5), 867–881.

Keller, G.R. and Baldridge, W.S. (1999). The Rio Grande rift: A geological and geophysical overview. *Rocky Mountain Geology* 34, 121–130, doi:10.2113/34.1.121.

Keller, G. R. and Cather, S. M. (1994). Basins of the Rio Grande Rift: structure, stratigraphy, and tectonic setting. Special Paper 291. Geological Society of America, Boulder, Colorado, USA.

Kelly, S. D., Newville, M. G., Cheng, L., Kemner, K. M., Sutton, S. R., Fenter, P., Sturchio, N.C.,Spötl, C. (2003). Uranyl incorporation in natural calcite.*Environmental science & technology*, *37*(7), 1284-1287.

Kraemer, T. F. and Brabets, T. P. (2012). Uranium isotopes (234U/238U) in rivers of the Yukon Basin (Alaska and Canada) as an aid in identifying water sources, with implications for monitoring hydrologic change in arctic regions.*Hydrogeology Journal 20*(3), 469-481.

Kubiak, J. and Machula, S. (2014). Concentration of uranium in waters of the biggest lakes of the Tywa river drainage basin. *Journal of Ecological Engineering 15*(3) , 56-63.

Kratz, S. and Schnug, E. (2006). Rock phosphates and P fertilizers as sources of U contamination in agricultural soils. In Uranium in the environment . Springer Berlin Heidelberg. 57-67.

Ma L., Chabaux F., Pelt E., Blaes E., Jin L., Brantley S. L. (2010) Regolith production rates calculated with uranium-series isotopes at Susquehanna/Shale Hills Critical Zone Observatory. *Earth and Planetary Science Letters* 297, 211–225

Mack, G. H., Salyards, S. L., McIntosh, W. C., Leeder, M. R. (1998). Reversal magnetostratigraphy and radioisotopic geochronology of the Plio-Pleistocene Camp Rice and Palomas Formations, southern Rio Grande rift.*Guidebook 49*, 229-236.

McArthur, J.M. and Howarth, R.J .(2004). Strontium isotope stratigraphy. In: Gradstein, F.M., Ogg, J.G., Smith, A.G. (Eds.), A Geological Timescale 2004. Cambridge University Press, Cambridge, 96–105

McArthur, J.M., Howarth, R.J., Bailey, T.R. (2001). Strontium isotope stratigraphy: LOWESS Version 3: Best fit to the marine Sr isotope curve for 0–509 Ma and accompanying look-up table for deriving numerical age. *Journal of Geology*, 109, 155–170, doi:10.1086/319243.

Millot, R., Gaillardet, J., Dupré, B., Allègre, C. J. (2002). The global control of silicate weathering rates and the coupling with physical erosion: new insights from rivers of the Canadian Shield. *Earth and Planetary Science Letters*, *196*(1), 83-98.

Moore, S.J. and Anderholm, S.K. (2002). Spatial and temporal variations in streamfl ow, dissolved solids, nutrients, and suspended sediment in the Rio Grande Valley study unit, Colorado, New Mexico, and Texas, 1993–1995: U.S. Geological Survey Water-Resources Investigations Report 02–4224, 58 .

Moore, S.J., Bassett, R.L., Liu, B., Wolf, C.P., Doremus, D. (2008). Geochemical tracers to evaluate hydrogeologic controls on river salinization. *Ground Water*, 46(3), 489-501.

Mills, S.K. (2003). Quantifying Salinization of the Rio Grande Using Environmental Tracers. (M.S. Thesis) New Mexico Institute of Mining and Technology, 397

Négrel, P., Giraud, E. P., Widory, D. (2004). Strontium isotope geochemistry of alluvial groundwater: a tracer for groundwater resources characterisation. *Hydrology and Earth System Sciences Discussions 8*(5), 959-972.

Osmond, J. K. and Ivanovich, M. (1992). Uranium series mobilization and surface hydrology. In (M. Ivanovich & R. S. Harmon, Eds) Uranium Series Disequilibrium, Applications to Earth, Marine, and Environmental Sciences, Clarendon Press, Oxford, 259–289.

Osmond, J.K. and Cowart, J.B. (1976) The theory and uses of natural uranium isotopic variations in hydrology. *Atomic Energy Review* 14, 621–679

Osmond, J.K., Cowart, J.B., 1992. Groundwater. In: Ivanovich, M., Harmon, R. (Eds.). Uranium Series Disequilibrium: Application to Environmental Problems. 2nd ed.. Clarendon Press, Oxford, 290-333.

Paces, J.B. and Wurster, F.C.(2014). Natural uranium and strontium isotope tracers of water sources and surface water–groundwater interactions in arid wetlands—Pahranagat Valley, Nevada, USA. *Journal of Hydrology* 517, 213–225.

Pelt, E., Chabaux, F., Innocent, C., Navarre-Sitchler, A.K., Sak, P.B., Brantley, S.L. (2008). Uranium–thorium chronometry of weathering rinds: rock alteration rate and paleo-isotopic record of weathering fluids. *Earth and Planetary Sciences Letters* 276, 98–105.

Phillips, F.M., Hogan, J., Mills, S., Hendricks, J.M.H. (2003). Environmental tracers applied to quantifying causes of salinity in arid-region rivers: Preliminary results from the Rio Grande, southwestern USA, in Alsharhan, A.S., and Wood, W.W., eds., Water resources perspectives: Evaluation, management, and policy: Developments in Water Science, v. 50: Amsterdam, Elsevier Science, 327–334

Parcher, J. W., Woodward, D. G., Durall, R. A. (2010). A descriptive overview of the Rio Grande-Rio Bravo Watershed. *Journal of Transboundary Water Resources* 1,159–176

Raczek, I., Jochum, K. P., Hofmann, A. W. (2003). Neodymium and strontium isotope data for USGS reference materials BCR-1, BCR-2, BHVO-1, BHVO-2, AGV-1, AGV-2, GSP-1, GSP-2 and eight MPI-DING reference glasses. *Geostandards Newsletter 27*(2), 173-179.

Robinson, L., Henderson, G., Hall, L., Matthews, I. (2004). Climatic control of riverine and seawater uranium-isotope ratios. *Science* 305,851–854

Riotte, J. and Chabaux, F. (1999). (^{234} U/^{238} U) activity ratios in freshwaters as tracers of hydrological processes: the Strengbach watershed (Vosges, France). *Geochimica et Cosmochimica Acta 63*(9), 1263-1275.

Riotte, J., Chabaux, F., Benedetti, M., Dia, A., Gérard, M., Boulègue, J., Etamé, J. (2003). Uranium colloidal transport and origin of the 234 U–238 U fractionation in surface waters: new insights from Mount Cameroon.*Chemical Geology 202*(3), 365-381.

Sardinha, D. S., Bonotto, D. M., Da Conceição, F. T. (2010). Weathering rates at Alto Sorocaba basin, Brazil, using U-isotopes and major cations.*Environmental Earth Sciences 61*(5), 1025-1036.

Seager, W. R., Shafiqullah, M., Hawley, J. W., Marvin, R. (1984). New K-Ar dates from basalts and the evolution of the southern Rio Grande rift.*Geological Society of America Bulletin* 95(1), 87-99.

Semhi, K., Clauer, N., Probst, J. L. (2000). Strontium isotope compositions of river waters as records of lithology-dependent mass transfers: the Garonne river and its tributaries (SW France). *Chemical Geology 168*(3), 173-193.

Shand, P., Darbyshire, D. P. F., Love, A. J., Edmunds, W. M. (2009). Sr isotopes in natural waters: applications to source characterisation and water–rock interaction in contrasting landscapes. *Applied Geochemistry 24*(4), 574-586.

Sheng, Z. (2013). Impacts of groundwater pumping and climate variability on groundwater availability in the Rio Grande Basin. *Ecosphere 4*(1), 1-25.

Sims, K. W., Gill, J. B., Dosseto, A., Hoffmann, D. L., Lundstrom, C. C., Williams, R. W., Ball L, Tollstrup, D., Turner, S., Prytulak, J.,Glessner, J. J. (2008). An inter-laboratory assessment of the thorium isotopic composition of synthetic and rock reference materials. *Geostandards and Geoanalytical Research 32*(1), 65-91.

Szynkiewicz, A., Borrok, D. M., Ganjegunte, G. K., Skrzypek, G., Ma, L., Rearick, M. S., Perkins, G. B. (2015). Isotopic studies of the Upper and Middle Rio Grande. Part 2—Salt loads and human impacts in south New Mexico and west Texas. *Chemical Geology 411*, 336-350.

Szynkiewicz, A., Witcher, J.C., Modelska, M., Borrok, D.M., Pratt, L.M., 2011. Anthropogenic sulfate loads in the Rio Grande, New Mexico (USA). *Chemical Geology* 283(3-4), 194-209.

Suarez, D. L. (2000). Impact of Agriculture on CO_2 as Affected by Changes in Inorganic Carbon', in Lal, R., Kimble, J. M., Eswaran, H., and Stewart, B. A. (eds.), Global Climate Change and Pedogenic Carbonates, CRC/Lewis Publishers, Boca Raton, FL, 257–272.

Uralbekov, B., Burkitbayev, M., Satybaldiyev, B., Matveyeva, I., Tuzova, T., Snow, D. (2014). Spatial and temporal variability of 234U/238U activity ratios in the Shu River, Central Asia. *Environmental Earth Sciences 72*(9), 3635-3642.

United States Army Corps of Engineers (USACE). (2013). Distal Mesilla Conceptual Site Model. Available at https://www.env.nm.gov/.../RGSS_Mesilla_Conceptual_Model_Final.pdf
Seager, W.R., 1987. Caldera-like collapse at Kilbourne Hole maar, New Mexico. New Mexico *Geology* 9, 69–73.

Vigier, N., Bourdon, B., Lewin, É., Dupré, B., Turner, S., Van Calsteren, P., Subramanian, V., Allègre, C.J. (2005). Mobility of Useries nuclides during basalt weathering: an example of the Deccan Traps (India). *Chemical Geology* 219 (1–4), 69–91.

Vigier, N., Burton, K.W., Gislason, S.R., Rogers, N.W., Duchene, S., Thomas, L., Hodge, E., Schaefer, B. (2006). The relationship between riverine U-series disequilibria and erosion rates in a basaltic terrain. *Earth and Planetary Science Letters* 249, 258–273.

Yuan, F. and Miyamoto, S. (2005), Dominant processes controlling water chemistry of the Pecos River in American southwest. *Geophysical Research Letters* 32, L17406, doi:10.1029/2005GL023359.

Vitvar, T., Aggarwal, P., McDonnell, J.J. (2005). A review of isotope applications in catchment hydrology. In Isotopes in the Water Cycle: Past, Present and Future of a Developing Science, Aggarwal PK, Gat J, Froehlich K (eds). Springer, Dordrecht, 151–170

Wainwright, J. (2006) Climate and climatological variations in the Jornada Basin. In: Havstad K, Huenneke L, Schlesinger W (eds) Structure and function of the Chihuahuan Desert ecosystem. Oxford University Press, Oxford, 44–80

Walton, J., Ohlmacher, G., Utz, D., Kutianawala, M. (1999). Response of the Rio Grande and shallow ground water in the Mesilla Bolson to irrigation, climate stress, and pumping. *Environmental & Engineering Geoscience*, (1), 41-50.

Walton, J. and Ohlmacher, G. (2000). Surface and groundwater interactions: El Paso Ciudad Juarez region. Southwest Center for Environmental Research and Policy (SCERP), San Diego,

CA. Available online at http://www. scerp. org/pubs/monographs. htm [Accessed 31 March 2005].

Witcher, J.C., J.P. King, J.W. Hawley, J.F. Kennedy, J. Williams, M. Cleary, and L.R. Bothern. 2004. Sources of salinity in the Rio Grande and Mesilla Basin groundwater. New Mexico Water Resources Research Institute Technical Completion Report No. 330. Las Cruces, New Mexico: New Mexico Water Resources Research Institute.

Wood, W., Kraemer, T., Shapiro, A. (2004) Radon (^{222}Rn) in ground water of fractured rocks: a diffusion/ion exchange model. *Ground Water* 42, 552–567

Zielinski, R. A., Orem, W. H., Simmons, K. R., Bohlen, P. J. (2006). Fertilizer-derived uranium and sulfur in rangeland soil and runoff: A case study in central Florida. *Water, air, and soil pollution*, *176*(1-4), 163-183.

Zielinski, R.A., Simmons, K.R., Orem, W.H. (2000). Use of ^{234}U and ^{238}U isotopes to identify fertilizer-derived uranium in the Florida Everglades. *Applied Geochemistry* 15,369–83.

Zielinski, R.A., Asher-Bolinder, S., Meier, A.L., Johnson, C.A., Szabo, B.J. (1997). Natural or fertilizer-derived uranium in irrigation drainage: A case study in southeastern Colorado, USA. *Applied Geochemistry*, 12, 9–21.

Tables

Table 3.1: Sample site description and field measurements in the Lower Rio Grande River water during the irrigation (May-July) and non-irrigation (August-November) seasons, irrigation groundwater and city drains sampled between 2014 and 2015.

Site No./ Sampling date	Sampling Site Name	Sample Name abbreviation	Sampling season	Sample Type	Distance from EBR	Latitude	Longitude	Temp	pH	TDS_Field
30th May 2014					**(Km)**			**(^{0}C)**		**mg/L**
1	Elephant Butte state park	RG_EBR	Irrigation	River	0	33.178667°	-107.201683°	23.7	8.53	604.5
3	Percha Dam state park	RG_Percha dam	Irrigation	River	53	32.868485°	-107.304567°	21	8.18	715.0
4	Rio Grande @187	RG_NM 187/1	Irrigation	River	61.57	32.808633°	-107.303200°	21.5	8.14	721.5
5	R io Grange @391	RG_NM 391	Irrigation	River	76.07	32.693800°	-107.213900°	22.2	8.16	715.0
6	Rio Grande @154	RG_NM 154	Irrigation	River	86.07	32.667817°	-107.119117°	22.7	8.19	715.0
7	Rio Grande @185	RG_RV 185	Irrigation	River	111.87	32.516000°	-106.972450°	22.6	8.17	721.5
8	Rio Grande @ US_70	RG_US 70	Irrigation	River	144.17	32.309717°	-106.828467°	21.7	8.27	702.0
9	Rio Grande @359	RG_NM 359	Irrigation	River	149.57	32.263800°	-106.826333°	27	8.2	728.0
10	Rio Grande @28	RG_NM 28	Irrigation	River	158.94	32.206933°	-106.759750°	28	8.27	721.5
11	Rio Grande @189	RG_NM 189	Irrigation	River	173.04	32.113367°	-106.667983°	30.4	8.34	708.5
12	Rio Grande @225	RG_NM 225	Irrigation	River	185.94	31.999917°	-106.636017°	30.5	8.31	741.0
13	Rio Grande @ TX 259	RG_TX 259	Irrigation	River	197.34	31.914667°	-106.601667°	30.2	8.28	728.0
14	Rio Grande @ Racetrack	RG_TX Racetrack	Irrigation	River	213.14	31.798633°	-106.555867°	28.2	8.13	838.6
30th June 2014										
1	Elephant Butte state park	RG_EBR	Irrigation	River	0	33.179869°	-107.200637°	24.3	8.37	598.0
3	Percha Dam state park	RG_Percha dam	Irrigation	River	53	32.868515°	-107.304495°	22.6	8.17	611.0
4	Rio Grande @187	RG_187/1	Irrigation	River	61.57	32.808823°	-107.303280°	22.3	8.06	611.0
5	R io Grange @391	RG_391	Irrigation	River	76.07	32.694513°	-107.212810°	23	8.19	611.0
6	Rio Grande @154	RG_154	Irrigation	River	86.07	32.667744°	-107.119096°	23.4	8.21	611.0

7	Rio Grande @185	RG_RV_185	Irrigation	River	111.87	32.516038°	-106.972665°	24.8	8.33	617.5
8	Rio Grande @ US_70	RG_U70	Irrigation	River	144.17	32.311075°	-106.827436°	26.6	8.34	617.5
9	Rio Grande @359	RG_359	Irrigation	River	149.57	32.263850°	-106.826333°	27	8.35	624.0
10	Rio Grande @28	RG_28	Irrigation	River	158.94	32.206025°	-106.759097°	27.7	8.43	630.5
11	Rio Grande @189	RG_189	Irrigation	River	173.04	32.114031°	-106.668961°	28.1	8.45	630.5
12	Rio Grande @225	RG_225	Irrigation	River	185.94	31.999400°	-106.636021°	29.2	8.48	630.5
13	Rio Grande @ TX 259	RG_259	Irrigation	River	197.34	31.915462°	-106.602480°	29.2	8.45	630.5
14	Rio Grande @ Racetrack	RG_Racetrack	Irrigation	River	213.14	31.799177°	-106.557596°	28.8	8.46	630.5
30th July 2014										
1	Elephant Butte state park	RG_EBR	Irrigation	River	0	33.179869°	-107.200637°	28.2	8.26	591.5
2	Rio Grande near Williamsburg	RG_WB	Irrigation	River	18	33.105773°	-107.296884°	26.4	7.85	611.0
3	Percha Dam state park	RG_Percha dam	Irrigation	River	53	32.868515°	-107.304495°	26.4	8.15	617.5
4	Rio Grande @ 187	RG_187/1	Irrigation	River	61.57	32.808823°	-107.303280°	27	8.18	617.5
5	Rio Grande @ 391	RG_391	Irrigation	River	76.07	32.694513°	-107.212810°	28.2	8.24	617.5
6	Rio Grande @ 154	RG_154	Irrigation	River	86.07	32.667744°	-107.119096°	28.1	8.19	617.5
7	Rio Grande @ 185	RG_RV_185	Irrigation	River	111.87	32.516038°	-106.972665°	27.4	8.08	591.5
8	Rio Grande @ US70	RG_U70	Irrigation	River	144.17	32.311075°	-106.827436°	29	8.25	617.5
9	Rio Grande @ 359	RG_359	Irrigation	River	149.57	32.263850°	-106.826333°	28.6	8.2	630.5
10	Rio Grande @ 28	RG_28	Irrigation	River	158.94	32.206025°	-106.759097°	30.1	8.32	617.5
11	Rio Grande @ 189	RG_189	Irrigation	River	173.04	32.114031°	-106.668961°	30	8.43	630.5
12	Rio Grande @ 225	RG_225	Irrigation	River	185.94	31.999400°	-106.636021°	30.8	8.92	611.0
13	Rio Grande @ 259	RG_259	Irrigation	River	197.34	31.915462°	-106.602480°	31.1	8.48	617.5
14	Rio Grande @ Racetrack	RG_Racetrack	Irrigation	River	213.14	31.799177°	-106.557596°	31	8.5	624.5
15	Rio Grande @ 237	RG_237	Irrigation	River	215.02	31.802645°	-106.541194°	30.9	8.48	637.0
29th August 2015										
1	Elephant Butte state park	RG_EBR	Non-Irrigation	River	0	33.179869°	-107.200637°	26.8	8.52	617.5
2	Rio Grande near Williamsburg	RG_WB	Non-Irrigation	River	18	33.105773°	-107.296884°	28	8.13	1300.0
3	Percha Dam state park	RG_Percha dam	Non-Irrigation	River	53	32.868515°	-107.304495°	33.4	8.45	734.5

4	Rio Grande @ 187	RG_187/1	Non-Irrigation	River	61.57	32.808823°	-107.303280°	28.8	8.26	838.5
5	Rio Grande @ 391	RG_391	Non-Irrigation	River	76.07	32.694513°	-107.212810°	33.4	8.44	728.0
6	Rio Grande @ 154	RG_154	Non-Irrigation	River	86.07	32.667744°	-107.119096°	33.9	8.55	715.0
7	Rio Grande @ 185	RG_RV_185	Non-Irrigation	River	111.87	32.516038°	-106.972665°	31.8	8.48	630.5
8	Rio Grande @ US70	RG_U70	Non-Irrigation	River	144.17	32.311075°	-106.827436°	33.6	8.72	643.5
9	Rio Grande @ 359	RG_359	Non-Irrigation	River	149.57	32.263850°	-106.826333°	32.2	8.04	890.5
10	Rio Grande @ 28	RG_28	Non-Irrigation	River	158.94	32.206025°	-106.759097°	32.9	9	702.0
11	Rio Grande @ 189	RG_189	Non-Irrigation	River	173.04	32.114031°	-106.668961°	32.2	8.98	721.5
12	Rio Grande @ 225	RG_225	Non-Irrigation	River	185.94	31.999400°	-106.636021°	32.6	9.4	780.0
13	Rio Grande @ 259	RG_259	Non-Irrigation	River	197.34	31.915462°	-106.602480°	30.2	9.22	650.0
14	Rio Grande @ Racetrack	RG_Racetrack	Non-Irrigation	River	213.14	31.799177°	-106.557596°	29.4	8.47	682.5
15	Rio Grande @ 237	RG_237	Non-Irrigation	River	215.02	31.802645°	-106.541194°	27.8	8.11	2574.0
24th September 2014										
14	Rio Grande @ Racetrack	RG_Racetrack	Non-Irrigation	River	213.14	31.799177°	-106.557596°	26.6	8.66	591.5
15	Rio Grande @ 237	RG_237	Non-Irrigation	River	215.02	31.802645°	-106.541194°	24.6	7.99	2502.5
7th November 2014										
1	Elephant Butte	RG_EBR	Non-Irrigation	River	0	33.179869°	-107.200637°	18.2	7.96	630.5
2	Rio Grande near Williamsburg	RG_WB	Non-Irrigation	River	18	33.105773°	-107.296884°	14.8	8.15	2080.0
3	Percha Dam state park	RG_Percha dam	Non-Irrigation	River	53	32.868515°	-107.304495°	17.1	8.43	799.5
4	Rio Grande @ 187	RG_187/1	Non-Irrigation	River	61.57	32.808823°	-107.303280°	11.9	8.38	650.0
6	Rio Grande @ 154	RG_154	Non-Irrigation	River	86.07	32.667744°	-107.119096°	33.9	8.23	835.3
7	Rio Grande @ 185	RG_RV_185	Non-Irrigation	River	111.87	32.516038°	-106.972665°	16.6	8.44	715.0
9	Rio Grande @ 359	RG_359	Non-Irrigation	River	149.57	32.263850°	-106.826333°	19.9	8.61	903.5
14	Rio Grande @ Racetrack	RG_Racetrack	Non-	River	213.14	31.799177°	-106.557596°	18.9	8.56	1859.0

			Irrigation							
15	Rio Grande @ 237	RG_237	Non-Irrigation	River	215.02	31.802645°	-106.541194°	20.1	8.2	2639.3
City drains 24th September 2014										
16	Sunset drain	City drain	Non-Irrigation	City drain	206.6	31.831167°	-106.583889°	23.9	8.01	4095.0
17	Racetrack drain	City drain	Non-Irrigation	City drain	216.8	31.806150°	-106.551600°	23.6	7.88	2795.0
Irrigation Groundwater wells 26th February 2015										
18	Groundwater Well 1@ NM-391	GW1_NM391	Non-Irrigation	Ground water	77.77	32.679111°	-107.213083°	20.3	7.69	1638.0
19	Groundwater Well 2@ NM-185	GW2_NM185	Non-Irrigation	Ground water	135.17	32.391194°	-106.845278°	19.1	7.41	1599.0
20	Groundwater Well 3@ NM-28	GW3_NM28	Non-Irrigation	Ground water	159.44	32.210694°	-106.758611°	19	7.57	786.5
21	Groundwater Well 4@ NM-28	GW4_NM28	Non-Irrigation	Ground water	168.24	32.145556°	-106.721944°	18.4	7.49	1209.0
22	Groundwater Well 5@ NM-28	GW5_NM28	Non-Irrigation	Ground water	175.24	32.116222°	-106.703000°	18.8	7.52	1053.0
23	Groundwater Well 6@ NM-28	GW6_NM28	Non-Irrigation	Ground water	176.17	32.111611°	-106.696361°	18.3	7.4	1200.0

Table 3.2 : Major and minor element concentrations in the Lower Rio Grande River water during the irrigation (May-July) and non-irrigation (August-November) seasons, ground water and city drains

Site No./Sampling date	**Na**	**Ca**	**Mg**	**K**	**Si**	**Sr**	**SO_4**	**Cl**	**HCO_3**	**Br**	**NO_3**	**PO_4**	**TDS**	**Total +**	**Total -**	**Charge balance**
30th May 2014	**(mg/L)**	**(mg/L)**	**(mg/L)**	**(mg/L)**	**(mg/L)**	**(mg/L)**	**(mg/L)**	**(mg/L)**	**meq/kg**	**(mg/L)**	**(mg/L)**	**(mg/L)**	**mg/L**	**meq/L**	**meq/L**	**(%)**
1	101	68.81	15.84	10.31	6.95	0.86	191.49	80.56	2.06	0.85	N.D	N.D	603.4	9.39	8.33	6%
3	110	81.11	15.29	13.97	7.67	0.84	96.10	181.50	2.71	0.24	0.14	N.D	672.9	10.45	9.83	3%
4	111	81.89	15.07	13.72	9.29	0.84	96.42	181.36	2.58	1.39	N.D	0.19	669.2	10.50	9.72	4%
5	110	82.62	15.31	13.70	7.49	0.84	94.28	182.72	2.70	0.29	N.D	N.D	672.9	10.54	9.82	4%
6	110	79.97	14.67	13.66	7.44	0.83	94.99	182.55	2.64	2.77	N.D	0.50	669.1	10.33	9.81	3%
7	108	81.74	15.35	13.47	8.62	0.85	93.07	181.54	2.77	0.19	0.31	N.D	674.1	10.42	9.83	3%

8	106	80.63	14.63	12.83	7.30	0.88	90.83	178.51	3.16	0.14	0.14	N.D	686.0	10.20	10.08	1%
9	108	81.79	15.57	13.83	7.97	0.91	92.67	179.69	2.56	0.22	2.94	N.D	661.1	10.44	9.61	4%
10	107	81.58	15.16	13.69	7.75	0.93	92.32	178.41	2.86	0.22	0.94	N.D	673.2	10.32	9.83	2%
11	107	81.99	15.40	13.97	7.58	0.96	92.74	178.08	3.14	0.12	1.23	N.D	691.6	10.40	10.11	1%
12	113	82.89	15.69	14.63	8.04	1.02	96.77	184.31	2.49	0.29	2.35	N.D	671.7	10.74	9.74	5%
13	109	81.38	15.35	14.30	7.41	1.00	94.36	178.71	2.63	1.49		N.D	664.9	10.46	9.65	4%
14	143	79.46	14.32	14.46	9.31	0.99	127.55	199.45	3.02	0.19	0.15	1.73	775.8	11.76	11.35	2%
30th June 2014																
1	100	65.56	15.78	9.46	6.05	0.84	191.63	83.05	2.98	0.39	1.12	N.D	657.0	9.18	9.33	-1%
3	102	70.51	15.76	9.75	7.55	0.86	195.23	85.93	2.98	0.29	0.81	N.D	672.0	9.51	9.49	0%
4	101	69.65	15.55	9.66	6.58	0.85	192.43	84.84	2.93	0.33	0.94	N.D	661.6	9.42	9.34	0%
5	101	70.27	15.60	9.50	6.47	0.86	193.69	84.96	3.35	0.14	0.50	N.D	688.7	9.46	9.79	-2%
6	102	70.56	15.82	9.38	6.07	0.86	193.17	84.78	2.95	0.35	0.75	N.D	664.2	9.50	9.37	1%
7	101	70.75	15.31	9.51	6.74	0.86	194.95	85.36	3.24	0.55	N.D	N.D	683.9	9.45	9.71	-1%
8	102	70.06	15.56	9.76	6.54	0.87	194.51	86.38	3.14	0.22	0.24	N.D	679.1	9.50	9.63	-1%
9	102	71.02	15.83	9.80	6.62	0.87	194.65	86.72	3.08	0.17	N.D	N.D	676.7	9.57	9.58	0%
10	104	72.00	16.01	10.56	6.75	0.88	197.39	88.57	2.72	0.39	1.64	N.D	664.7	9.70	9.36	2%
11	104	72.02	15.68	10.17	6.52	0.88	198.99	89.38	3.27	0.43	1.06	N.D	699.5	9.68	9.95	-1%
12	105	72.00	15.76	10.23	6.55	0.88	198.22	89.08	3.13	0.32	N.D	N.D	690.7	9.75	9.77	0%
13	105	72.08	15.64	10.34	6.34	0.88	197.97	88.81	2.96	0.37	N.D	N.D	678.9	9.74	9.59	1%
14	105	71.53	15.59	10.21	6.87	0.88	198.74	89.60	3.21	0.15	N.D	N.D	695.2	9.70	9.87	-1%
30th July 2014																
1	104	61.14	15.93	9.62	6.66	0.84	191.65	85.58	2.17	0.32	0.51	N.D	610.0	9.16	8.58	3%
2	103	65.22	15.65	9.55	7.13	0.85	181.80	89.84	2.37	0.31	0.08	N.D	619.8	9.31	8.70	3%
3	103	68.49	15.85	9.54	6.44	0.85	188.78	87.70	2.69	0.56	N.D	N.D	646.3	9.46	9.10	2%
4	104	67.72	15.59	9.67	6.47	0.85	187.90	87.35	2.35	1.63	N.D	N.D	625.7	9.45	8.75	4%
5	104	68.62	15.52	10.03	9.07	0.85	186.48	86.95	2.67	0.21	N.D	N.D	646.4	9.50	9.01	3%
6	102	69.43	15.52	10.00	8.58	0.84	187.94	87.07	2.39	1.06	N.D	N.D	629.9	9.45	8.77	4%
7	96	70.41	13.04	9.93	7.16	0.85	179.09	81.83	2.44	1.09	N.D	N.D	609.3	9.05	8.49	3%

8	102	71.26	15.61	10.07	6.90	0.92	194.63	86.55	2.38	0.45	N.D	N.D	634.8	9.57	8.87	4%
9	99	75.48	16.88	10.11	6.64	0.98	217.57	83.35	2.67	0.36	0.58	N.D	674.4	9.72	9.56	1%
10	102	68.46	15.61	10.14	6.93	0.87	195.72	86.26	2.67	0.34	0.49	N.D	650.9	9.42	9.19	1%
11	106	68.86	15.66	10.46	6.76	0.86	189.37	91.06	2.51	0.31	0.48	N.D	643.6	9.62	9.03	3%
12	112	72.56	16.58	11.02	7.32	0.91	181.64	88.15	2.41	0.33	0.32	N.D	639.1	10.18	8.68	8%
13	115	74.62	16.80	11.30	9.49	0.93	187.59	90.88	2.90	1.14	N.D	N.D	686.6	10.41	9.38	5%
14	107	69.13	15.96	10.24	6.39	0.86	189.78	91.32	2.50	0.32	N.D	N.D	644.9	9.71	9.03	4%
15	109	68.16	15.59	10.37	6.43	0.86	191.80	94.38	2.48	0.16	N.D	N.D	649.0	9.70	9.14	3%
29th August 2014																
1	107	62.30	15.89	9.84	8.01	0.87	214.93	83.67	1.42	0.33	0.49	N.D	590.8	9.33	8.26	6%
2	241	110.95	20.64	19.51	6.88	1.79	185.74	418.60	2.56	0.33	11.66	0.54	1175.2	18.24	18.43	-1%
3	142	59.12	17.68	11.23	9.84	0.85	186.69	115.59	3.52	0.34	0.30	N.D	760.0	10.89	10.68	1%
4	154	99.55	22.51	12.78	8.40	1.19	242.30	141.06	3.33	0.44	0.57	N.D	888.1	13.89	12.37	6%
5	120	77.62	18.28	10.86	7.40	1.03	220.71	113.41	1.58	0.27	0.05	N.D	667.3	10.91	9.38	8%
6	122	74.81	17.80	10.94	6.72	1.00	217.76	111.55	2.26	0.41	0.88	N.D	703.1	10.82	9.95	4%
7	95	77.35	13.96	11.09	8.22	1.11	194.87	90.73	2.18	0.36	0.62	N.D	627.2	9.46	8.80	4%
8	101	68.16	16.08	11.78	6.82	0.95	207.56	103.06	1.41	0.31	0.62	N.D	603.5	9.44	8.65	4%
9	124	87.88	26.59	23.53	13.97	1.14	159.23	187.74	1.81	0.33	148.79	4.39	889.2	12.60	12.96	-1%
10	121	54.29	17.42	14.15	7.84	0.87	195.98	127.26	1.47	0.36	19.16	N.D	649.5	9.80	9.45	2%
11	140	42.20	18.58	14.14	6.30	0.86	214.15	157.41	0.73	0.38	5.36	N.D	645.6	10.12	9.72	2%
12	160	38.47	17.50	15.16	5.97	0.87	211.81	186.33	0.55	0.28	14.11	N.D	684.6	10.71	10.44	1%
13	129	43.74	14.67	11.84	3.99	0.74	204.03	133.10	0.35	0.32	0.37	N.D	564.7	9.33	8.36	5%
14	124	60.75	17.51	12.12	7.30	0.94	202.93	112.85	2.74	0.32	0.12	N.D	706.7	10.19	10.15	0%
15	683	137.80	32.16	13.43	20.97	1.96	829.46	633.94	6.59	1.27	4.18	N.D	2762.7	39.61	41.81	-3%
24th September 2014																
14	107	61.55	14.75	9.19	7.71	0.83	166.47	98.06	2.45	0.39	N.D	N.D	616.6	9.19	8.68	3%
15	660	135.61	36.38	13.22	18.73	2.03	741.38	627.51	5.90	3.65	15.03	0.64	2616.0	38.85	39.54	-1%
7th November 2014																
1	111.04	63.44	16.23	9.41	8.35	0.93	220.31	89.55	2.86	0.28	0.20	N.D	695.5	9.59	9.98	-2%

2	437.85	163.14	26.65	29.58	13.63	3.15	208.97	807.51	3.14	0.57	6.68	N.D	1891.8	30.20	30.35	0%
3	170.40	81.12	23.02	10.34	12.13	1.00	184.36	137.03	4.34	0.34	1.91	N.D	887.6	13.64	12.07	6%
4	164.18	82.36	21.29	9.79	8.17	0.95	221.95	149.13	4.18	0.08	N.D	N.D	914.2	13.27	13.00	1%
6	138.71	110.00	20.35	9.54	10.52	1.31	250.83	123.28	3.78	0.37	0.88	N.D	897.6	13.47	12.49	4%
7	108.22	85.65	17.02	9.58	7.95	1.13	185.96	104.58	4.02	0.84	N.D	N.D	766.9	10.65	10.85	-1%
9	137.17	88.72	24.75	30.22	13.84	1.19	159.83	214.00	1.33	0.32	164.04	5.09	921.2	13.23	13.50	-1%
14	426.20	159.11	39.91	14.31	5.55	2.94	824.75	394.12	2.69	1.96	2.44	N.D	2036.6	30.19	31.03	-1%
15	853.47	164.19	40.47	15.63	21.80	2.39	973.06	829.47	6.08	1.74	3.00	4.19	3282.6	49.10	49.91	-1%
City drains																
24th September 2014																
16	1306.61	200.71	46.23	11.14	20.93	2.51	1192.80	1258.78	6.02	3.35	N.D	N.D	4412.6	70.99	66.36	3%
17	768.84	156.87	40.76	11.95	20.65	2.17	877.27	716.57	6.74	2.55	N.D	N.D	3010.8	44.98	45.23	0%
Groundwater																
26th February 2015																
18	214.85	278.50	45.47	12.58	13.31	3.11	207.04	781.26	0.64	2.20	29.64	5.44	1638	27.37	27.64	0%
19	222.24	256.54	42.02	12.03	13.26	2.24	741.70	221.78	1.05	3.16	17.12	N.D	1599	26.28	23.06	7%
20	86.26	125.02	19.83	7.16	13.51	1.41	210.07	119.36	3.00	2.83	16.34	N.D	786.5	11.84	11.04	3%
21	147.89	196.72	31.57	8.14	13.79	2.06	453.80	186.85	2.42	2.93	16.01	N.D	1209	19.10	17.43	5%
22	146.78	151.73	27.27	9.25	14.41	1.69	340.04	138.59	3.38	2.51	11.89	N.D	1053	16.47	14.59	6%
23	195.31	179.47	31.28	9.81	15.18	1.65	471.36	180.37	1.53	2.92	16.05	N.D	1200	20.31	16.72	10%

Total Dissolved Solids (TDS) were calculated by adding all measured cation and anion concentrations except for ground water, which indicates field measured TDS.

Charge balances were calculated by dividing the difference between total cations and total anions (meq/L) by total ion and multiplying by 100.

Bicarbonate ion concentrations for all samples were measured by titration method except for ground water, which were calculated based on mass balances.

Description of site numbers are given in table 1

N.D refer to not detected

Table 3.3: Water types and saturation indices of major minerals that are likely to influence water chemistry

Site No./Sampling date	Gypsum	Halite	Dolomite	Calcite	Thenardite	Water type
River						
30th May 2014	log Q/K	log Q/K	log Q/K	log Q/K	log Q/K	text
1	-1.552	-6.705	2.492	0.9998	-7.564	Na-SO4
3	-1.773	-6.312	2.04	0.8259	-7.808	Na-Cl
4	-1.767	-6.31	1.933	0.7769	-7.8	Na-Cl
5	-1.776	-6.31	2.047	0.8297	-7.814	Na-Cl
6	-1.783	-6.313	2.073	0.8438	-7.811	Na-Cl
7	-1.785	-6.32	2.1	0.8524	-7.831	Na-Cl
8	-1.801	-6.334	2.35	0.9869	-7.857	Na-Cl
9	-1.787	-6.334	2.25	0.9116	-7.831	Na-Cl
10	-1.791	-6.345	2.501	1.039	-7.843	Na-Cl
11	-1.792	-6.347	2.798	1.177	-7.833	Na-Cl
12	-1.767	-6.31	2.559	1.057	-7.771	Na-Cl
13	-1.782	-6.337	2.527	1.042	-7.808	Na-Cl
14	-1.684	-6.174	2.204	0.8952	-7.458	Na-Cl
30th June 2014						
1	-1.577	-6.696	2.489	0.9858	-7.568	Na-SO4
3	-1.54	-6.672	2.066	0.7965	-7.553	Na-SO4
4	-1.547	-6.68	1.814	0.6722	-7.564	Na-SO4
5	-1.547	-6.681	2.212	0.8691	-7.561	Na-SO4
6	-1.544	-6.68	2.166	0.8433	-7.557	Na-SO4
7	-1.545	-6.682	2.511	1.018	-7.556	Na-SO4
8	-1.55	-6.675	2.568	1.035	-7.544	Na-SO4
9	-1.545	-6.675	2.597	1.048	-7.545	Na-SO4

10	-1.534	-6.661	2.678	1.087	-7.529	Na-SO4
11	-1.537	-6.657	2.869	1.185	-7.523	Na-SO4
12	-1.538	-6.654	2.93	1.211	-7.51	Na-SO4
13	-1.535	-6.656	2.824	1.16	-7.512	Na-SO4
14	-1.54	-6.653	2.89	1.193	-7.512	Na-SO4
30th July 2014						
1	-1.595	-6.671	2.117	0.7723	-7.521	Na-SO4
2	-1.589	-6.65	1.341	0.4083	-7.556	Na-SO4
3	-1.562	-6.664	2.064	0.7769	-7.549	Na-SO4
4	-1.565	-6.662	2.022	0.7556	-7.54	Na-SO4
5	-1.567	-6.667	2.289	0.8886	-7.543	Na-SO4
6	-1.556	-6.674	2.1	0.7975	-7.558	Na-SO4
7	-1.561	-6.723	1.817	0.6993	-7.623	Na-SO4
8	-1.534	-6.677	2.251	0.8743	-7.539	Na-SO4
9	-1.477	-6.712	2.278	0.8838	-7.533	Na-SO4
10	-1.551	-6.682	2.504	0.9879	-7.536	Na-SO4
11	-1.563	-6.641	2.664	1.069	-7.518	Na-SO4
12	-1.576	-6.631	3.593	1.526	-7.485	Na-SO4
13	-1.546	-6.612	2.974	1.222	-7.461	Na-SO4
14	-1.563	-6.636	2.836	1.148	-7.504	Na-SO4
15	-1.564	-6.616	2.773	1.119	-7.488	Na-SO4
29th August 2014						
1	-1.543	-6.668	2.206	0.8257	-7.453	Na-SO4
2	-1.477	-5.648	2.247	0.9068	-6.92	Na-Cl
3	-1.652	-6.42	3.068	1.199	-7.27	Na-SO4
4	-1.374	-6.302	2.774	1.127	-7.147	Na-SO4
5	-1.464	-6.5	2.491	0.9655	-7.353	Na-SO4
6	-1.491	-6.5	2.988	1.208	-7.34	Na-SO4
7	-1.502	-6.692	2.697	1.13	-7.597	Na-SO4

8	-1.526	-6.613	2.838	1.137	-7.51	Na-SO4
9	-1.574	-6.273	2.003	0.6712	-7.506	Na-Cl
10	-1.655	-6.442	3.285	1.294	-7.372	Na-Cl
11	-1.717	-6.286	2.557	0.8655	-7.205	Na-Cl
12	-1.771	-6.159	2.936	1.045	-7.1	Na-Cl
13	-1.701	-6.387	2.209	0.7579	-7.289	Na-Cl
14	-1.6	-6.483	2.772	1.072	-7.357	Na-SO4
15	-0.985	-5.067	2.947	1.196	-5.505	Na-Cl
24th September 2014						
14	-1.656	-6.597	2.913	1.191	-7.56	Na-SO4
15	-1.019	-5.077	2.584	0.9949	-5.58	Na-Cl
7th November 2014						
1	-1.532	-6.608	1.411	0.4535	-7.425	Na-SO4
2	-1.364	-5.101	2.16	0.9241	-6.444	Na-Cl
3	-1.552	-6.245	2.885	1.168	-7.175	Na-HCO3
4	-1.462	-6.211	2.532	1.028	-7.124	Na-Cl
6	-1.32	-6.414	2.983	1.259	-7.218	Na-SO4
7	-1.499	-6.552	2.742	1.176	-7.544	Na-HCO3
9	-1.576	-6.153	2.392	0.9167	-7.433	Na-Cl
14	-0.8699	-5.444	2.966	1.22	-5.887	Na-SO4
15	-0.8903	-4.851	2.907	1.185	-5.292	Na-Cl
City drains **24th September 2014**						
16	-0.8095	-4.516	2.695	1.078	1.24E-05	Na-Cl
17	-0.9287	-4.961	2.499	0.9608	3.9E-06	Na-Cl
Groundwater **26th February 2015**						
18	-1.176	-5.44	0.5184	0.09001	7.68E-08	Ca-Cl
19	-0.6841	-5.968	0.1403	-0.0954	3.14E-07	Na-SO4

20	-1.312	-6.603	1.037	0.3674	1.89E-08	Ca-SO4
21	-0.9156	-6.199	0.8957	0.2915	9.76E-08	Ca-SO4
22	-1.098	-6.323	1.148	0.3938	7.88E-08	Na-SO4
23	-0.9356	-6.093	0.2525	-0.0466	1.79E-07	Na-SO4

Table 3.4: Uranium and strontium (concentrations and activity/isotope ratios) at for selected sites along the Lower Rio Grande river and archived river, groundwater, city drains and wastewater samples.

Site No./Sampling date	**Sr**	**U**	**($^{234}U/^{238}U$)**	**$^{87}Sr/^{86}Sr$**
	ppm	**ppb**		
30th May 2014				
9	0.91	3.14	2.05	0.7109
30th June 2014				
1	0.84	3.09	1.75	0.7099
3	0.86	3.12	1.77	0.7100
4	0.85	3.08	1.78	0.7100
5	0.86	3.13	1.78	0.7102
6	0.86	3.13	1.78	0.7101
7	0.86	3.14	1.78	0.7101
8	0.87	3.16	1.77	0.7102
9	0.87	3.21	1.78	0.7102
10	0.88	3.21	1.77	0.7102
11	0.88	3.28	1.77	0.7102
12	0.88	3.31	1.77	0.7103
13	0.88	3.39	1.79	0.7103
14	0.88	3.42	1.78	0.7103
30th July 2014				

2	0.85	3.05	1.77	0.7101
9	0.98	3.34	1.69	0.7103
14	0.86	3.24	1.78	0.7101
15	0.86	3.33	1.77	0.7101
29th August 2014				
2	1.79	4.66	2.16	0.7139
9	1.14	1.82	1.75	0.7099
14	0.94	2.61	1.78	0.7103
15	1.96	5.65	1.52	0.7098
24th September 2014				
14	0.83	0.72	1.64	0.7102
15	2.03	3.67	1.53	0.7098
7th November 2014				
1	0.93	3.35	1.79	0.7098
2	3.15	4.05	2.46	0.7150
3	1.00	5.69	2.18	0.7105
4	0.95	5.87	2.06	0.7100
6	1.31	3.83	1.65	0.7120
7	1.13	0.92	1.75	0.7104
9	1.19	0.94	1.82	0.7097
14	2.94	0.55	1.67	0.7103
15	2.39	5.60	1.55	0.7097
City drains				
24th September 2014				
16	2.51	0.69	1.56	0.7097
17	2.17	3.59	1.52	0.7098
Groundwater				

26th February 2015				
18	3.11	3.31	1.61	0.7111
19	2.24	12.95	1.38	0.7105
20	1.41	1.61	2.71	0.7093
21	2.06	1.64	1.45	0.7095
22	1.69	2.36	1.28	0.7098
23	1.65	4.58	1.55	0.7104

Table 3.5: Seasonal uranium and strontium (concentrations and activity/isotope ratios) at selected sites along the Lower Rio Grande river and archived river, groundwater, city drains and wastewater samples.

Sampling site	**Site No.**	**Distance from EBR**	**Sampling period**	**Season**	**Sr**	**U**	**($^{234}U/^{238}U$)**	**$^{87}Sr/^{86}Sr$**
		(km)			**(mg/L)**	**ppb**		
Rio Grande @ Williamsburg	2	18	7/1/2014	irrigation	0.86	3.05	1.77	0.7101
Rio Grande@ Williamsburg	2	18	8/1/2014	non-irrigation	1.79	4.66	2.16	0.7139
Rio Grande @ Williamsburg	2	18	11/1/2014	non-irrigation	3.15	4.05	2.46	0.7150
Rio Grande @ 237	15	215.02	7/1/2014	irrigation	0.86	3.33	1.77	0.7101
Rio Grande @ 237	15	215.02	8/1/2014	non-irrigation	1.96	5.65	1.52	0.7098
Rio Grande @237	15	215.02	9/1/2014	non-irrigation	2.03	3.67	1.53	0.7098
Rio Grande @ 237	15	215.02	11/1/2014	non-irrigation	2.39	5.60	1.55	0.7097
Rio Grande @359	9	149.57	5/1/2014	irrigation	0.91	3.14	2.05	0.7109
Rio Grande @ 359	9	149.57	6/1/2014	irrigation	0.87	3.21	1.78	0.7102
Rio Grande @ 359	9	149.57	7/1/2014	irrigation	0.98	3.34	1.69	0.7103
Rio Grande @ 359	9	149.57	8/1/2014	non-irrigation	1.14	1.82	1.75	0.7099
Rio Grande @ 359	9	149.57	11/1/2014	non-irrigation	1.19	0.94	1.82	0.7097

Rio Grande @ Racetrack	14	213.14	5/1/2014	irrigation	0.99	3.75	1.93	0.7103
Rio Grande @ Racetrack	14	213.14	6/1/2014	irrigation	0.88	3.42	1.78	0.7103
Rio Grande @ Racetrack	14	213.14	7/1/2014	irrigation	0.86	3.24	1.78	0.7101
Rio Grande @ Racetrack	14	213.14	8/1/2014	non-irrigation	0.94	2.61	1.78	0.7103
Rio Grande @ Racetrack	14	213.14	9/1/2014	non-irrigation	0.83	0.72	1.64	0.7102
Rio Grande @ Racetrack	14	213.14	11/1/2014	non-irrigation	2.39	0.55	1.67	0.7103
Archived water samples								
Rio Grande @ Canutillo	13	197.34	11/1/2009	non-irrigation	1.42	4.54	2.06	0.7109
Rio Grande @ Canutillo	13	197.34	4/1/2010	non-irrigation	0.63	2.89	1.77	0.7105
Rio Grande @ Canutillo	13	197.34	6/15/2010	irrigation	0.54	2.70	1.73	0.7105
Rio Grande @ Canutillo	13	197.34	7/13/2010	irrigation	0.57	2.53	1.62	0.7104
Rio Grande @ Canutillo	13	197.34	7/13/2010	irrigation	0.57	2.53	1.62	0.7104
Rio Grande @ Canutillo	13	197.34	7/29/2010	irrigation	0.64	2.61	1.73	0.7105
Rio Grande @ Canutillo	13	197.34	8/18/2010	non-irrigation	0.64	2.48	1.74	0.7105
Rio Grande @ Canutillo	13	197.34	9/16/2010	non-irrigation	0.79	3.25	1.75	0.7105
Rio Grande @ Canutillo	13	197.34	11/1/2010	non-irrigation	1.26	4.79	2.04	0.7108
Rio Grande @ Canutillo	13	197.34	12/4/2010	non-irrigation	1.23	4.07	2.07	0.7108
Rio Grande @ Canutillo	13	197.34	1/18/2011	non-irrigation	1.92	2.96	2.24	0.7107
Rio Grande @ Canutillo	13	197.34	2/11/2011	non-irrigation	0.82	3.05	2.18	0.7105
Tornillo agricultural drain	54	284	12/1/2009	non-irrigation	3.30	12.04	1.31	0.7099
Tornillo agricultural drain	54	284	5/1/2010	irrigation	3.14	10.94	1.34	0.7099
Tornillo agricultural drain	54	284	9/12/2010	irrigation	3.50	8.59	1.37	0.7099
Tornillo agricultural drain	54	284	11/20/2010	non-irrigation	3.91	11.29	1.32	0.7091
Tornillo agricultural drain	54	284	2/12/2011	non-irrigation	3.92	9.52	1.32	0.7099
El Paso wastewater treatment	58	217	1/8/2011	-	3.028	15.00	1.60	0.7089
Hemway Rd 170 (Domestic well)	83	144.7	7/19/2010	-	1.642	13.04	1.18	0.7100

Hemway Rd 140 (Domestic well)	84	143.17	7/19/2010	-	0.915	3.48	1.27	0.7106
Artesian well 2 Fabens	87	275.62	12/1/2009	-	0.314	0.01	1.88	0.7091
Artesian well 1 Fabens	88	273.6	12/1/2009	-	5.464	ND	ND	0.7092
Artesian spring hot spring (TorC)	77	16	8/1/2009	-	0.094	3.40	2.66	0.7203
Vado R189	46	183.04	7/13/2010	irrigation	0.972	2.71	1.663	0.7104
Vado R189	46	183.04	6/15/2010	irrigation	0.88	2.77	1.717	0.7104
Vado R189	46	183.04	9/16/2010	non-irrigation	1.203	2.68	1.707	0.7103
Vado R189	46	183.04	8/18/2010	non-irrigation	1.065	2.17	1.713	0.7105
Vado R189	46	183.04	1/8/2011	non-irrigation	1.15	0.90	1.705	0.7106
Vado R189	46	183.04	2/11/2011	non-irrigation	1.31	0.94	1.708	0.7106
Westside Dr	47	205.86	8/11/2010	non-irrigation	1.022	4.99	1.554	0.7100
New Mexas Dr	48	209.22	8/11/2010	non-irrigation	0.915	3.82	1.577	0.7100
Faben Dr	53	275.62	12/1/2009	non-irrigation	3.07	5.11	1.528	0.7098
Montoya Dr.	50	210.57	5/13/2010	irrigation	0.74	0.69	1.535	0.7103
Montoya Dr.	50	210.57	12/17/2010	non-irrigation	0.994	0.67	1.489	0.7103

Sr concentrations and sample location numbers for all archived samples (2009-2010) were adopted from Szynkiewicz et al., 2015. Uranium activity ratios for the Rio Grande at Canitillo, hot spring at T or C , Faben well, Montaya, and Tornillo drain are reported in Szynkiewicz et al., 2015, all the other data were determined in this study**.**

ND = Not detectable

Table 3.6: Elemental concentrations of river sediment water leachates in the lower Rio Grande

Sampling Site	**Distance from EBR**	**Ca**	**Mg**	**Na**	**K**	**Sr**	**Si**	**Cl**	**SO_4**	**NO_3**	**Br**	**PO_4**
Nov 7th 2014 (Non-Irrigation season)	**(km)**	**(mg/L)**	**(mg/L)**	**(mg/L)**	**(mg/L)**	**(mg/L)**	**(mg/L)**	**(mg/L)**	**(mg/L)**	**(mg/L)**	**(mg/L)**	**(mg/L)**
391_clay river bank	76.07	18.54	2.09	27.38	4.10	0.22	5.67	1.43	25.98	0.44	ND	ND
391 middle_R_bed	76.07	22.65	2.15	15.88	4.33	0.22	5.57	ND	31.72	9.12	ND	ND

154 center of river bed (0-20cm)	86.07	40.53	6.35	20.56	4.21	0.50	4.72	5.10	95.90	1.97	ND	ND
US70_Clay_sed	144.17	26.94	5.24	24.88	6.65	0.36	7.58	8.77	29.29	0.48	0.02	ND
US70_sed_center	144.17	11.30	1.73	9.32	3.35	0.13	7.17	0.91	7.18	3.17	ND	ND
359_Riverbed	149.57	10.65	2.37	21.02	4.45	0.12	5.06	12.89	11.35	12.15	ND	ND
NM28 Surface_clay	158.94	32.69	6.52	24.07	7.13	0.40	10.12	7.39	19.59	0.08	0.04	ND
NM28_River_bed_center	158.94	14.91	2.39	13.47	4.53	0.17	6.67	5.74	8.80	8.41	ND	ND
189_River bed	173.04	7.82	1.49	7.61	1.42	0.09	2.91	1.20	6.46	4.35	ND	ND
189 clays	173.04	39.88	8.10	32.07	6.54	0.51	8.87	13.66	22.83	0.11	0.11	ND
259_Riverbed	197.34	8.52	1.28	4.28	1.34	0.09	2.68	0.55	4.64	0.31	ND	ND
259 clay samples	197.34	31.96	8.76	30.38	3.98	0.49	6.30	3.12	16.38	0.24	0.10	ND
Racetrack salt deposits_ near parking	213.14	164.55	10.08	521.18	8.84	2.28	2.47	207.15	1431.23	50.25	3.10	ND
Racetrack river B. sediment	213.14	11.07	3.22	72.84	4.40	0.17	3.15	58.11	54.77	13.15	0.12	ND
Racetrack_sed	213.14	14.32	2.56	30.15	2.55	0.17	2.57	23.22	44.13	0.24	ND	0.32
Racetract (white soils)	213.14	198.80	64.33	ND	701.34	11.74	1.25	ND	45892.67	146.39	39.09	3.45
237_Coshein Bridge	215.02	130.63	29.63	224.53	9.41	1.56	2.07	273.72	498.70	3.13	1.17	ND
237_surface_clay	215.02	516.63	176.36	1000.52	30.88	6.10	7.67	1339.72	2129.37	18.21	6.63	ND

ND= Not detected

Figures

Figure 3.1a: Location map showing the general studied area in the Lower Rio Grande valley

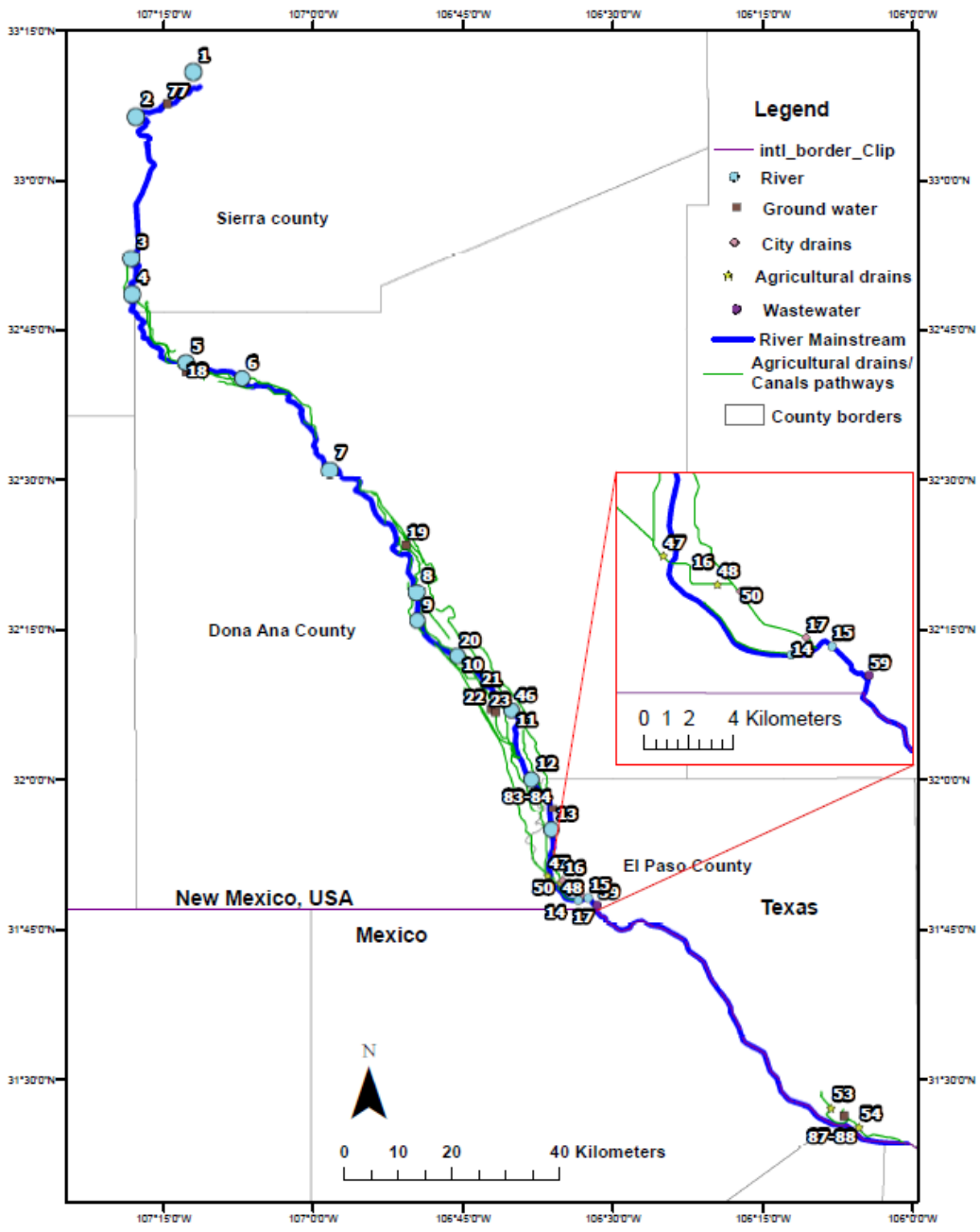

Figure 3.1b: Location map showing sampling sites in the Lower Rio Grande valley.
River water from elephant Butte (site 1) to the Rio Grande at 237(site 15), city drains (sites 16-17), ground water (sites 18-23). The map also shows sample locations for Ground water (sites 77, 83-84, 87-88), agricultural drains (sites 46-48, 50, 53-54), and wastewater (site 59) adoted from Szynkiewicz et al. (2015)

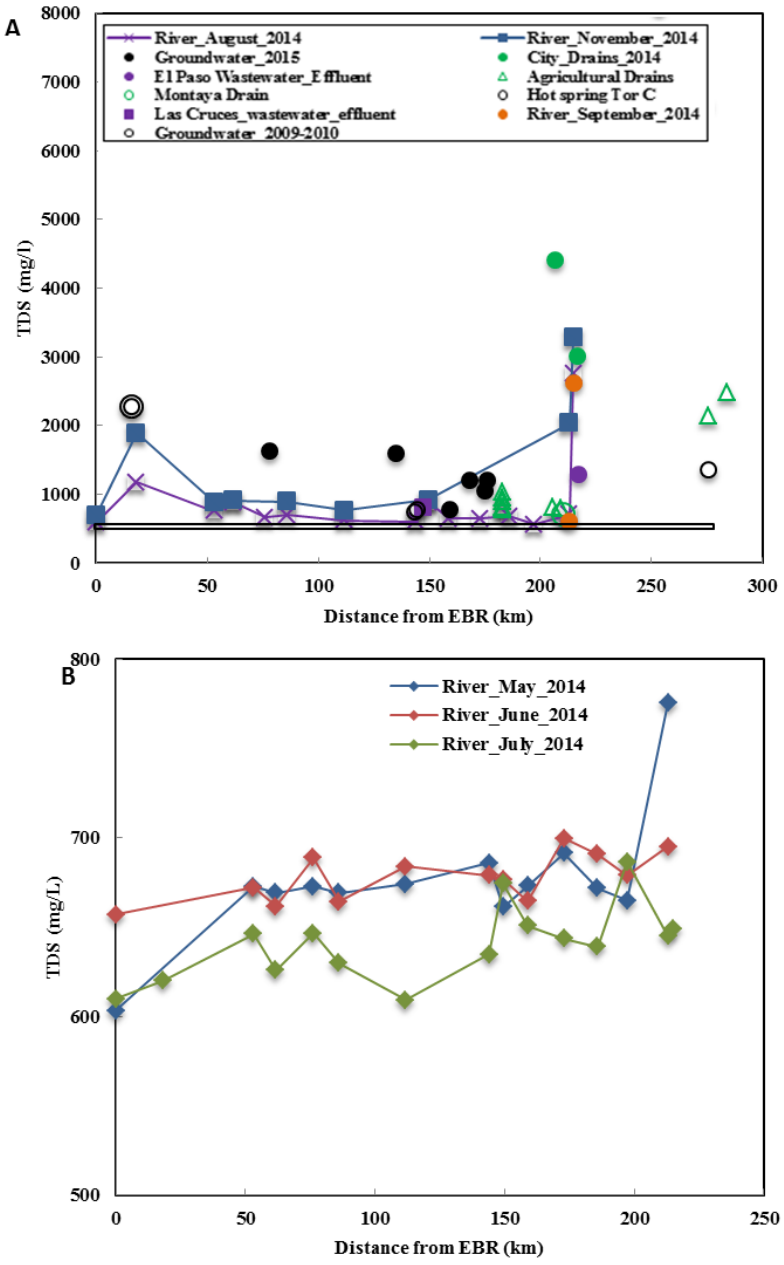

Figure 3.2: Total dissolved solids in the lower Rio Grande during the non-irrigation (A) and irrigation (B) seasons.

Black trangle in figure 3.2 A at ~600 shows a range of TDS concentrations for the irrigation season; TDS in the non-irrigation season is higher than that of the irrigation season, which slightly increases downstream. The non-irrigation season showed spike concentrations at specific sites downstream. Figure 3.2A also shows TDS concentrations for El Paso waste water effluents, Montaya drain, Tor C hot spring adopted from Szynkiewicz et al., 2015

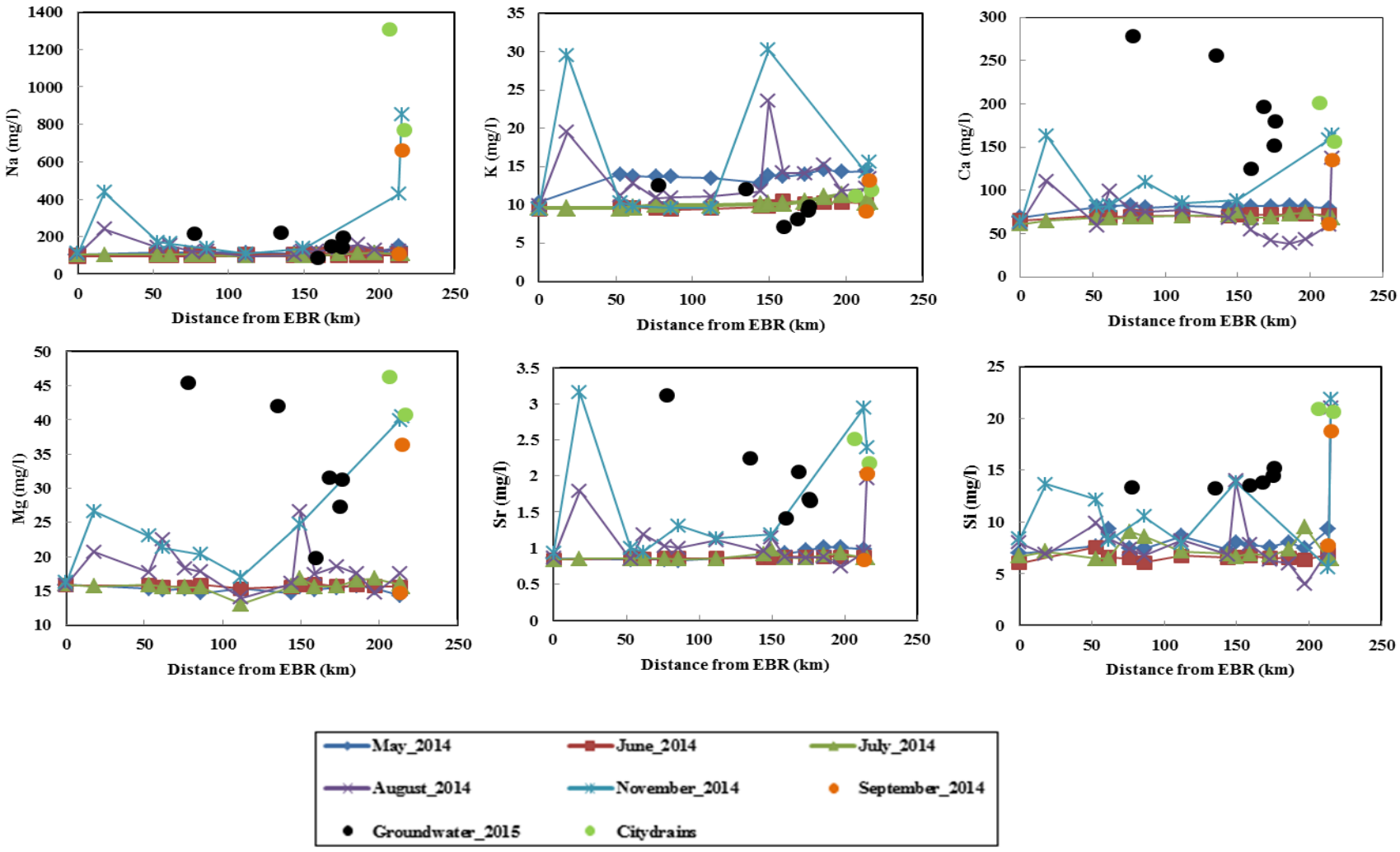
Na (mg/l)
Distance from EBR (km)
K (mg/l)
Distance from EBR (km)
Ca (mg/l)
Distance from EBR (km)
Mg (mg/l)
Distance from EBR (km)
Sr (mg/l)
Distance from EBR (km)
Si (mg/l)
Distance from EBR (km)
May_2014
June_2014
July_2014
August_2014
November_2014
September_2014
Groundwater_2015
Citydrains

Figure 3.3a: Plots showing variation of cation concentrations with distance from Elephant Butte Resevior (EBR) to El Paso, TX for river water in the non-irrigation (Aug-Nov. 2014) and irrigation (May-July 2014) seasons; concentrations of end-member groundwater and city drains are also shown.

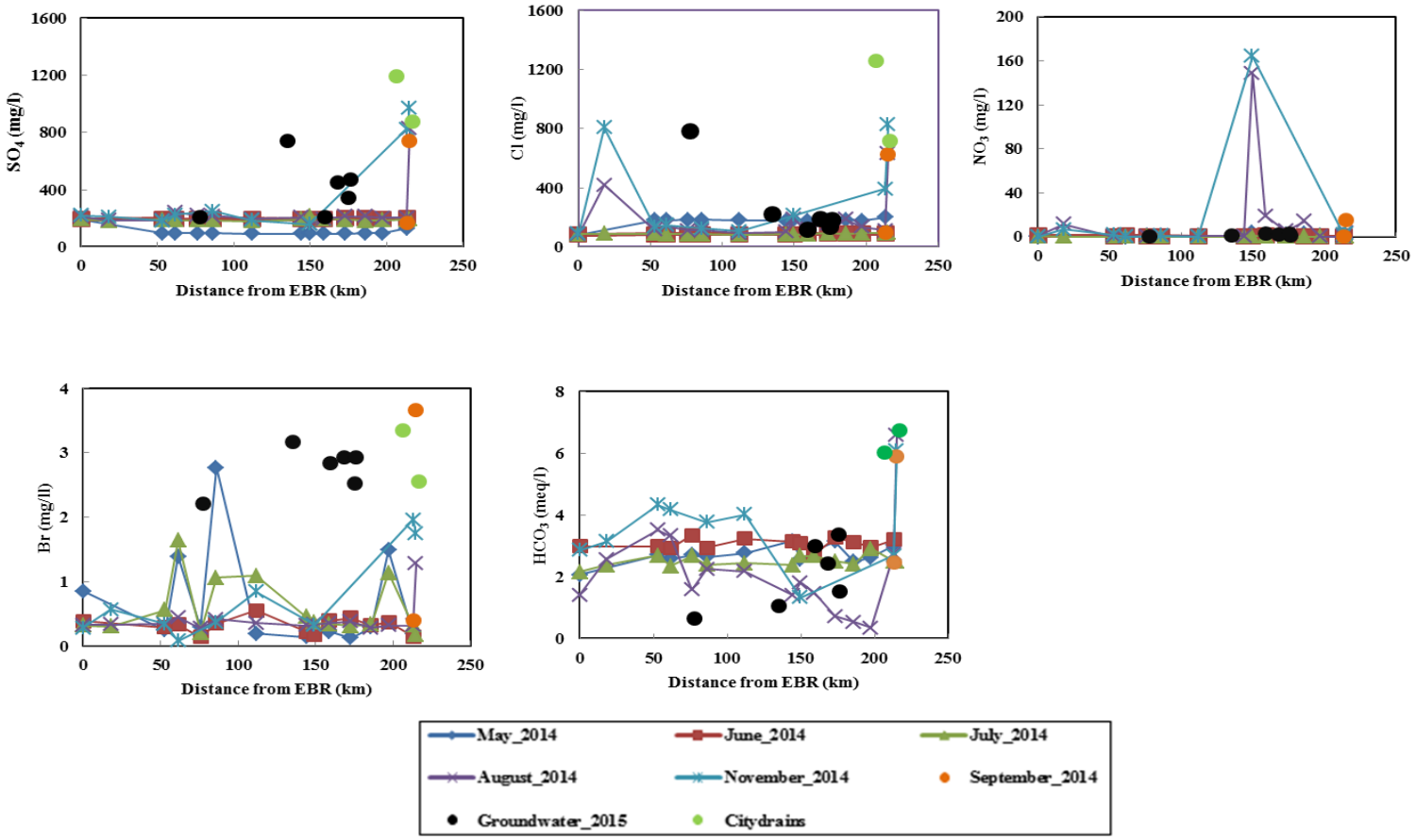

Figure 3.3b: Plots showing variation of anions concentrations with distance from Elephant Butte Resevior (EBR) to El Paso, TX for river water in the non-irrigation (Aug-Nov. 2014) and irrigation (May-July 2014) seasons; concentrations of end-member groundwater and city drains are also shown.

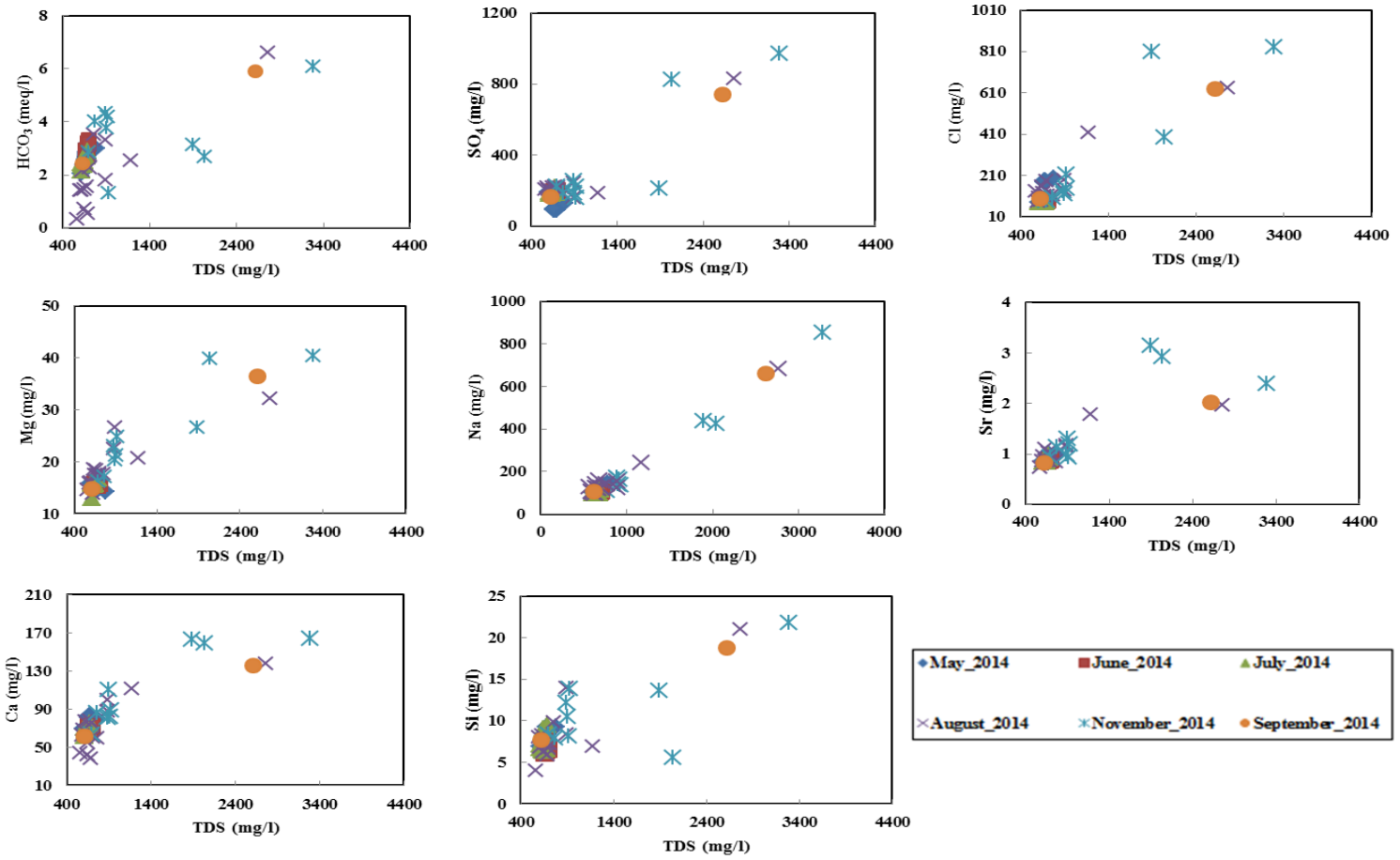

Figure 3.4: Plots showing relationship of major and minor ion concentrations with TDS for river water in the non-irrigation (Aug-Nov. 2014) and the irrigation (May-July 2014) seasons.

The ions show a positive correlation with TDS in all seasons.

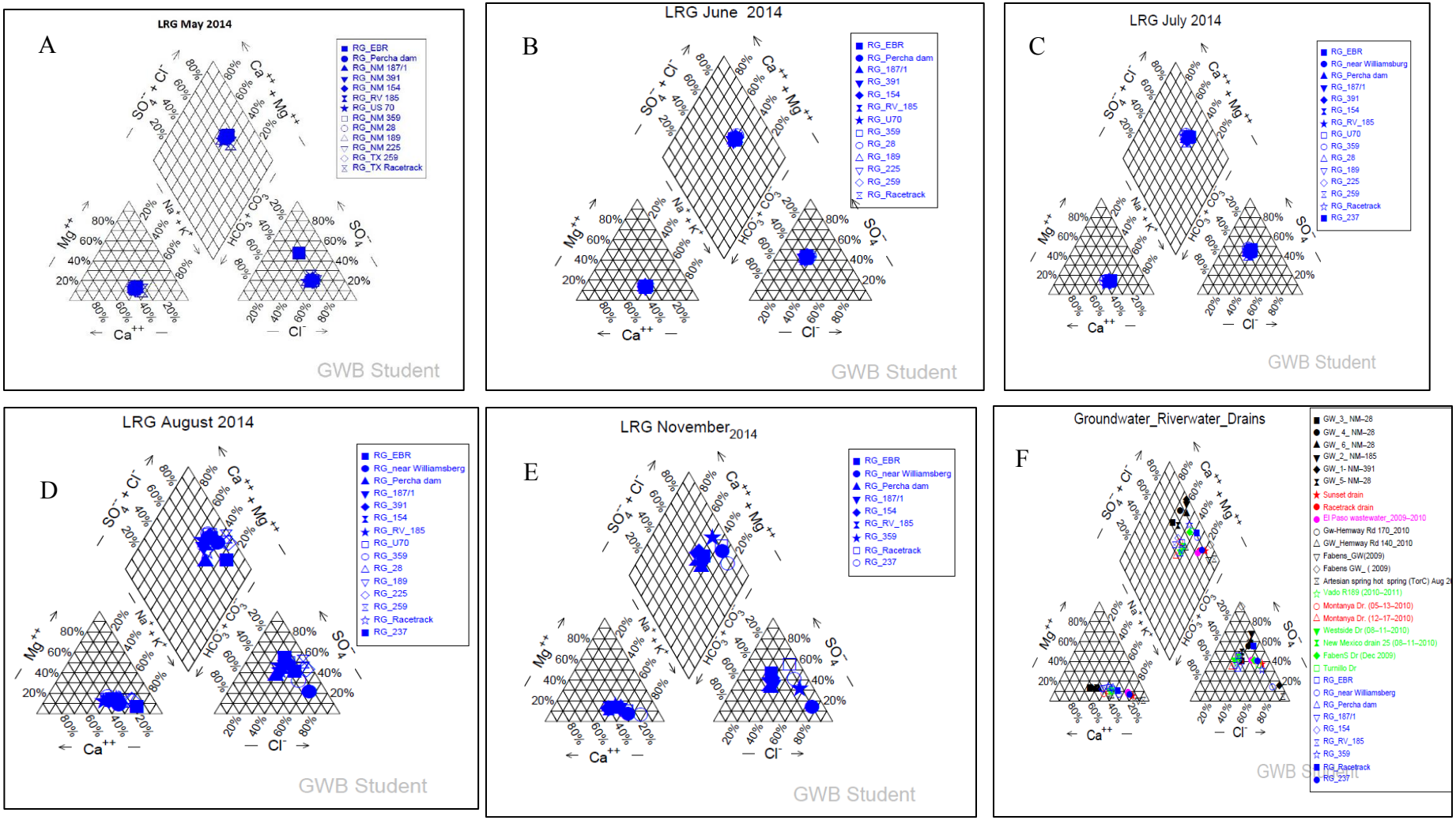

Figure 3.5: Water types for the Lower Rio Grande water during the irrigation (May, June, and July 2014; (a-c)) and non-irrigation seasons (August and November, 2014; (d-e)).

Water types of groundwater, irrigation drains, city drains, wastewater, and November river water are shown in figure 3.5 (f).

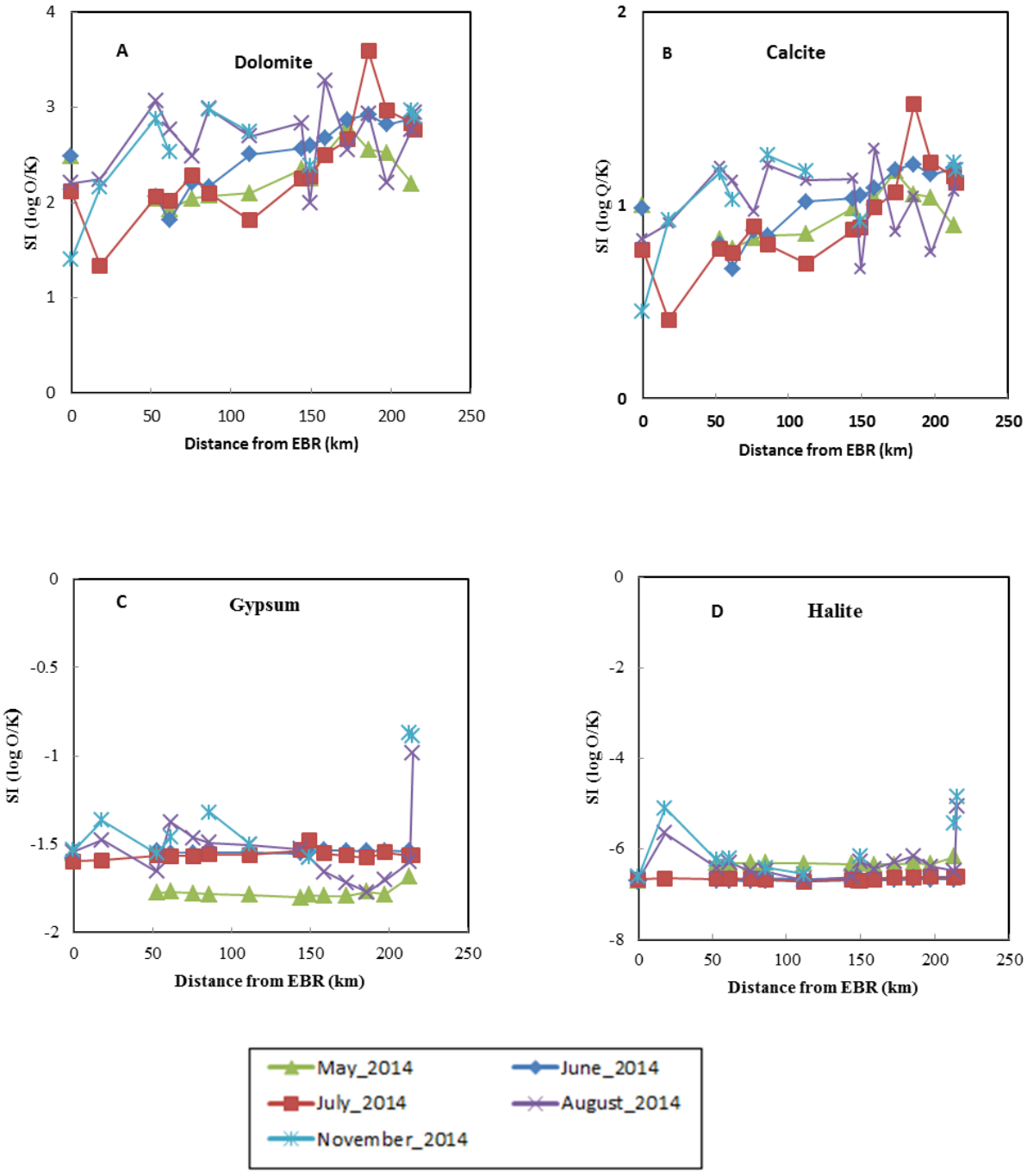

Figure 3.6: Plots showing saturation indices (SI) of (A) Dolomite, (B) Calcite, (C) Gypsum, and (D) Halite in the lower Rio Grande during the irrigation and non-irrigation seasons. Dolomite

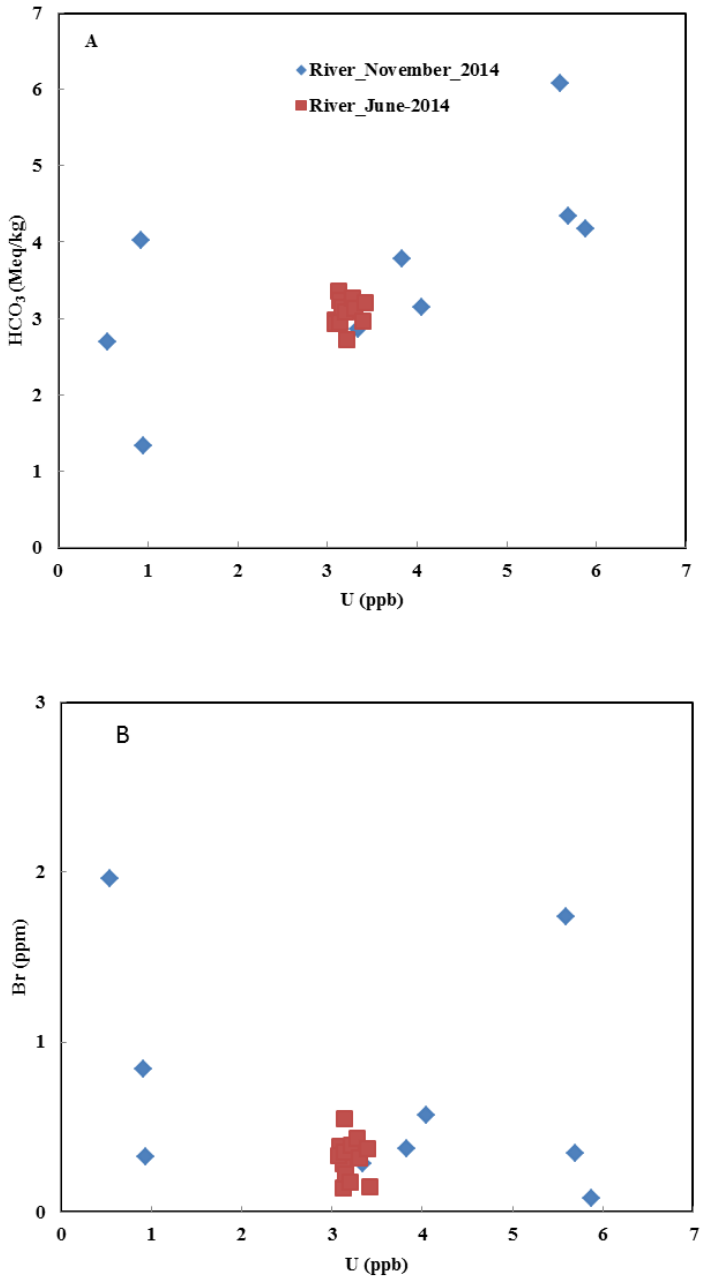

Figure 3.7: Plots showing relationship of (a) HCO3- and (b) Br with uranium concentrations for river water in the non-irrigation (Nov. 2014) and irrigation (June 2014) seasons. Bicarbonate ions indicate positive correlation while the Br indicate negative correlation with uranium in the non- irrigation season. The irrigation season shows clustered values, no correlation

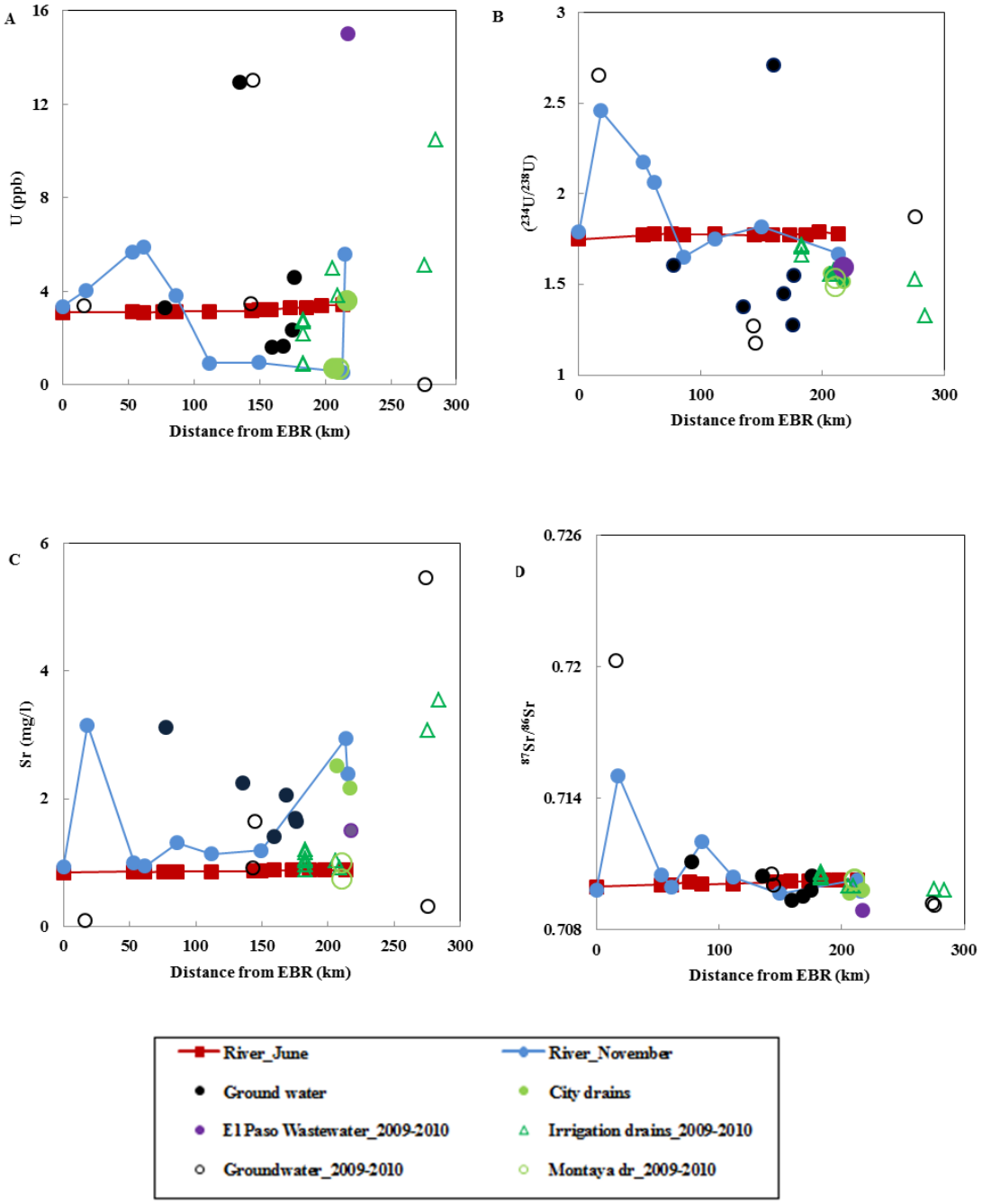

Figure 3.8: Plots of (A) uranium concentration, (B) ($^{234}U/^{238}U$), (C) Sr concentration, and (D) $^{87}Sr/^{86}Sr$ against distance in the river water, groundwater, wastewater, and drains between Elephant Butte Reservoir and El Paso, TX.

Uranium and Sr concentrations, uranium activity ratios of Tor C and Faben groundwater and Montaya drain were adopted from Szynkiewicz et al., 2015. Strontium isotopic compositions of these samples were determined in this study.

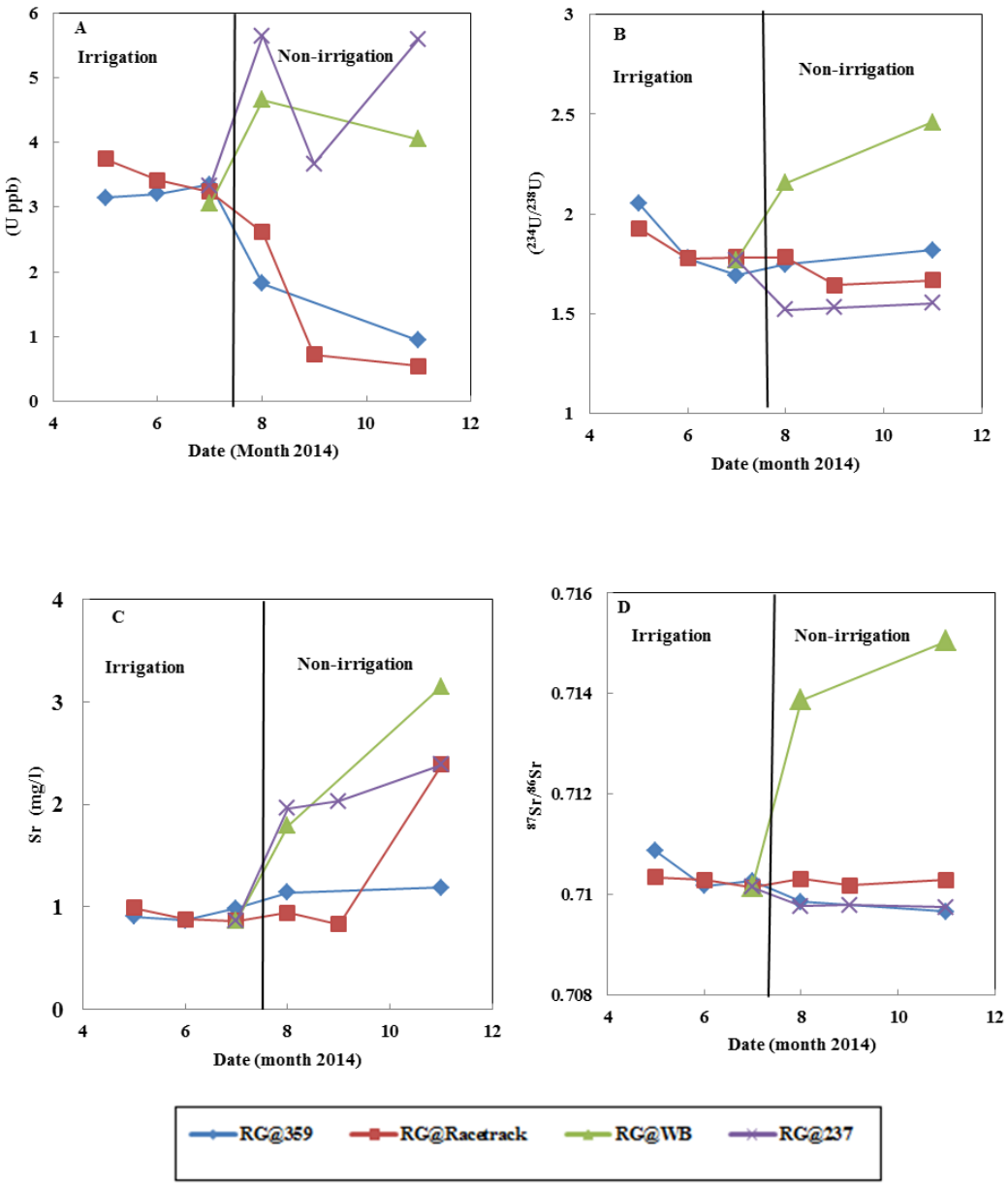

Figure 3.9: Temporal variation of [U] (a), ($^{234}U/^{238}U$) (b), [Sr] (c), and $^{87}Sr/^{86}Sr$ (d) for the Rio Grande at Williamsburg (site 2; ~18 km), Road 359 (site 9; ~150 km), Racetrack (site 14; ~213 km), and Road 237 (site 15; ~215 km).

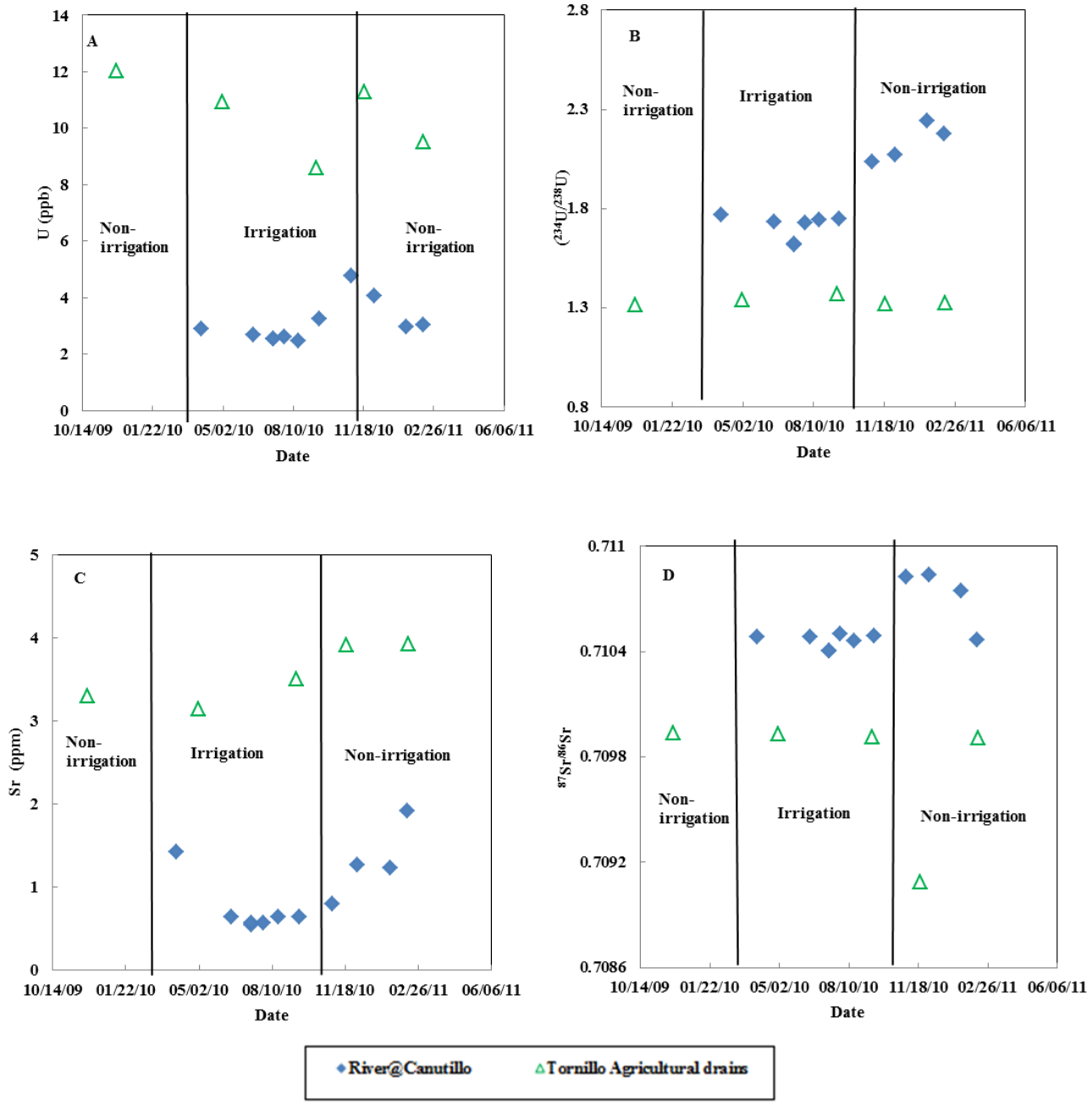

Figure 4.0: Temporal variation of [U] (a), ($^{234}U/^{238}U$) (b), [Sr] (c), and $^{87}Sr/^{86}Sr$ (d) for the Rio Grande at Canutillo (site 13) and Tornillo agricultural drains (site 54).
The agricultural drains showed high U and Sr concentrations and low ($^{234}U/^{238}U$) and $^{87}Sr/^{86}Sr$ compared to the Rio Grande at Canutillo.

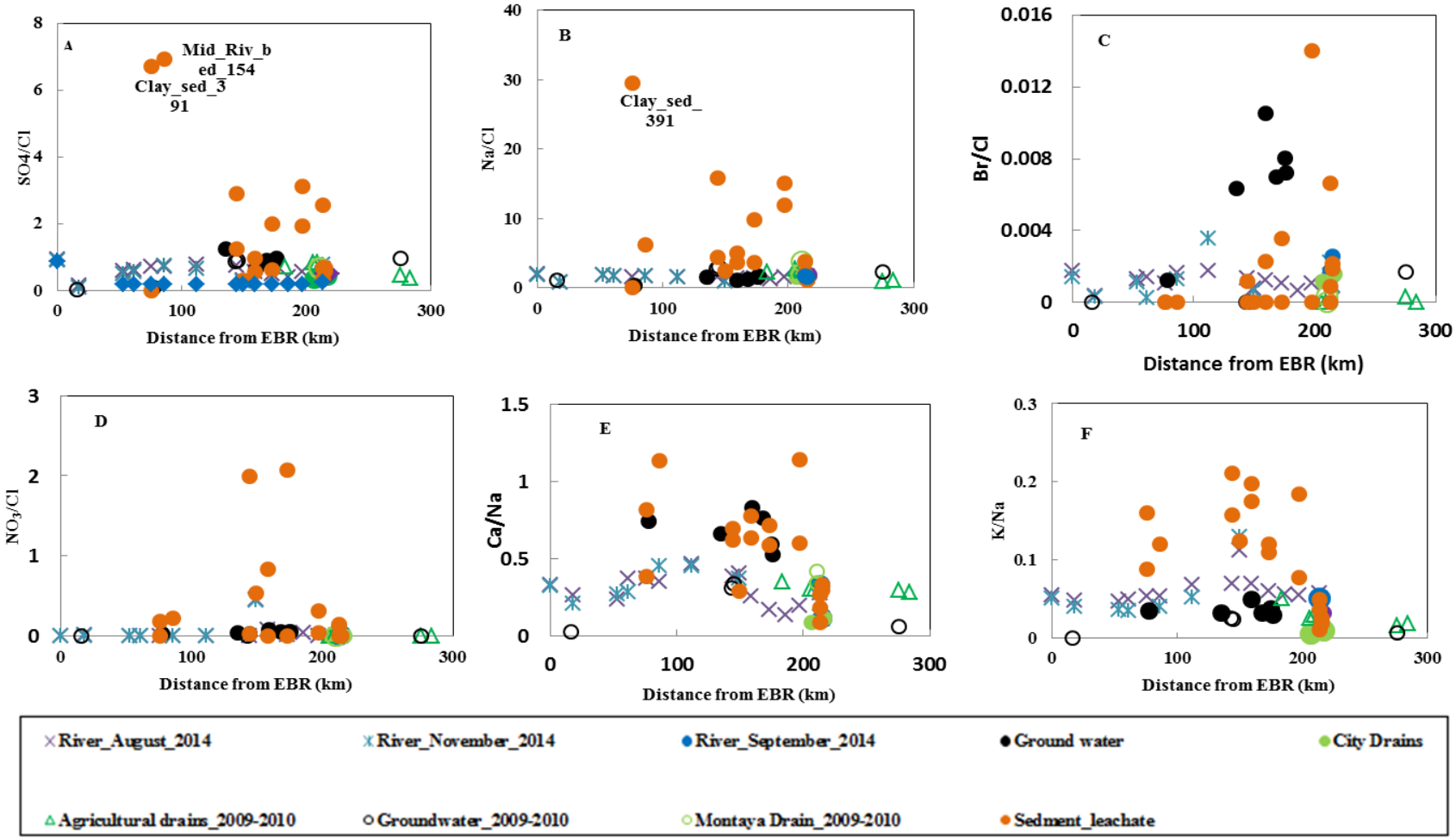

Figure 4.1: Plots indicating molar ratios of the river water in the Lower Rio Grande against distance.
Groundwater, wastewater and drain data for samples collected between 2009 and 2010 was obtained from Szynkiewicz et al., 2015.

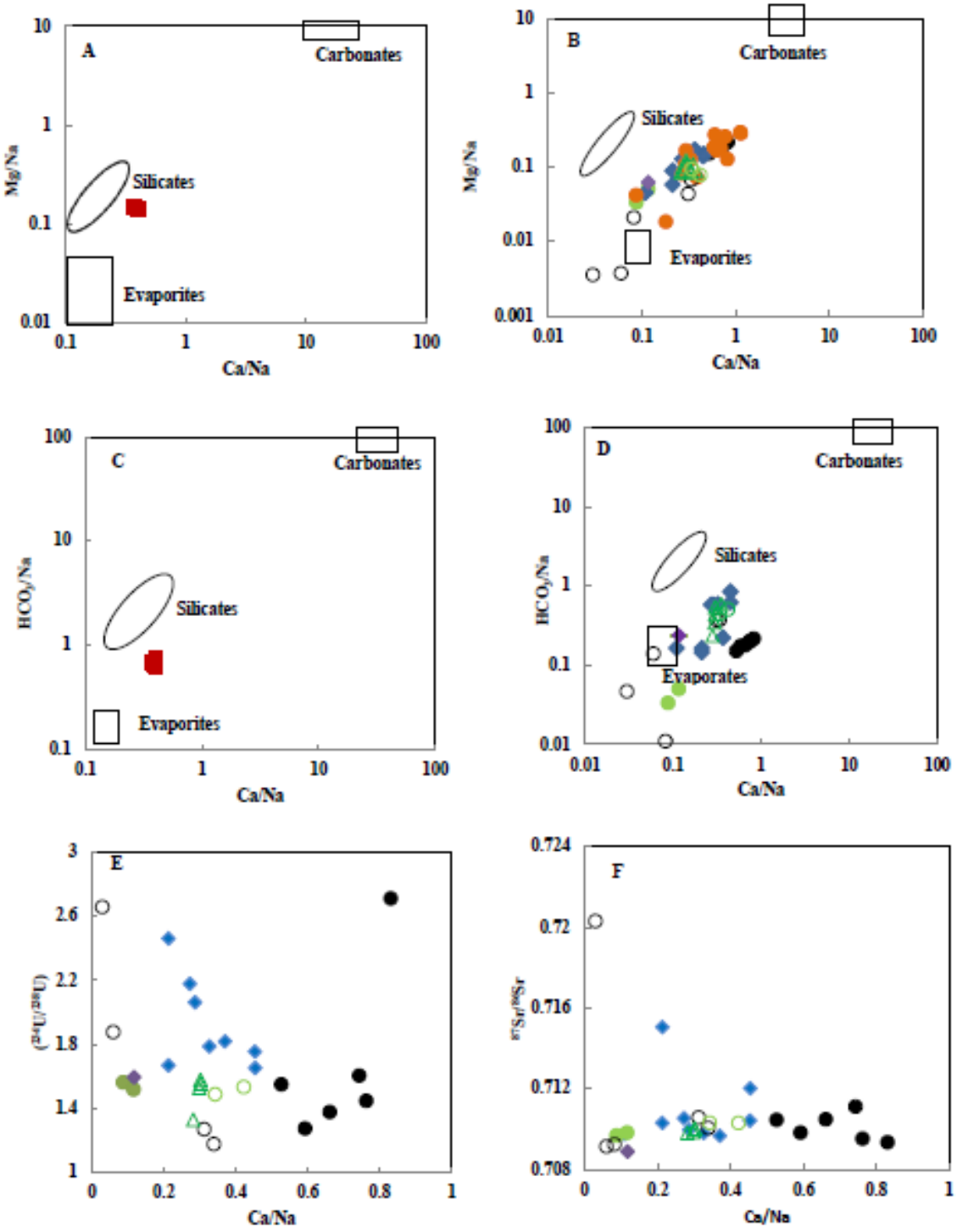
A
Carbonates
Silicates
Evaporites
Mg/Na
Ca/Na
B
Carbonates
Silicates
Evaporites
Mg/Na
Ca/Na
C
Carbonates
Silicates
Evaporites
HCO3/Na
Ca/Na
D
Carbonates
Silicates
Evaporates
HCO3/Na
Ca/Na
E
(234U/238U)
Ca/Na
F
87Sr/86Sr
Ca/Na

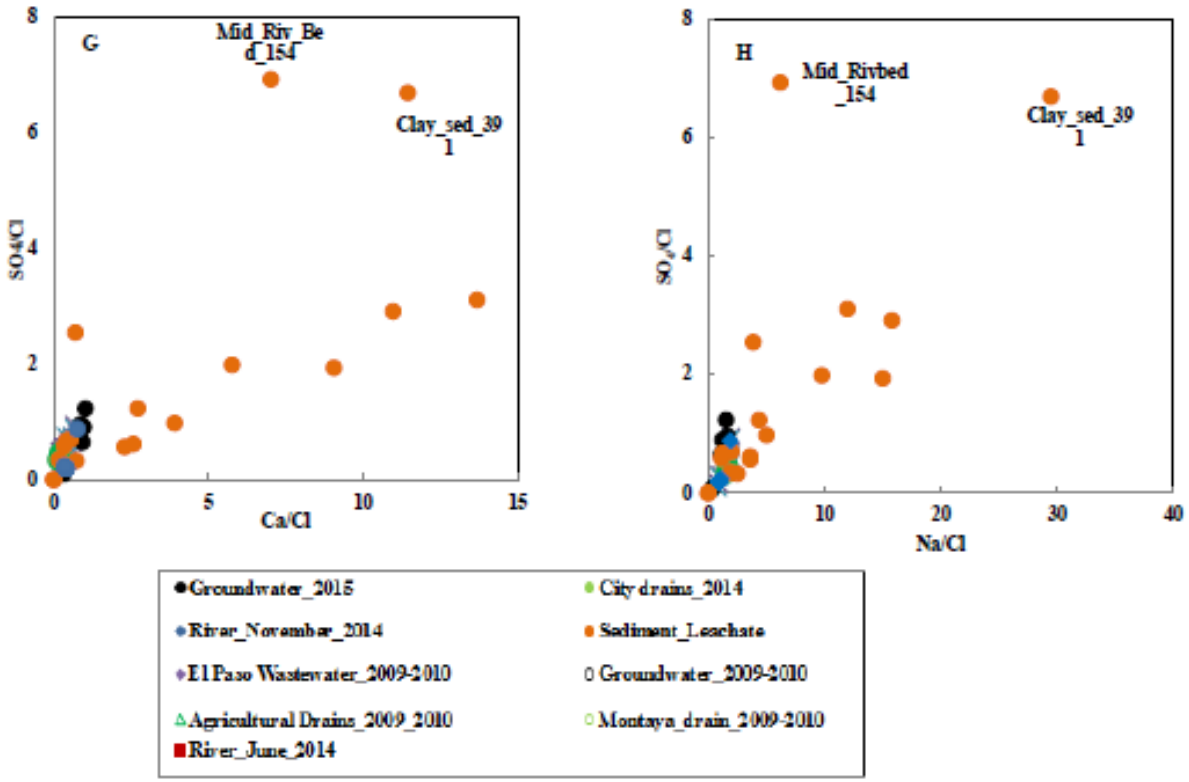

Figure 4.2: Plots indicating molar ratios of the river water, Groundwater, wastewater, and drains in the Lower Rio Grande.

A and B shows relation of Mg, HCO_3^- , and Ca normalized with Na for the irrigation season while C and D show relation of these molar ratios in river during non-irrigation, ground water, waste water , and drains. Molar ratios for end member lithology are from Gaillardet et al. (1999).

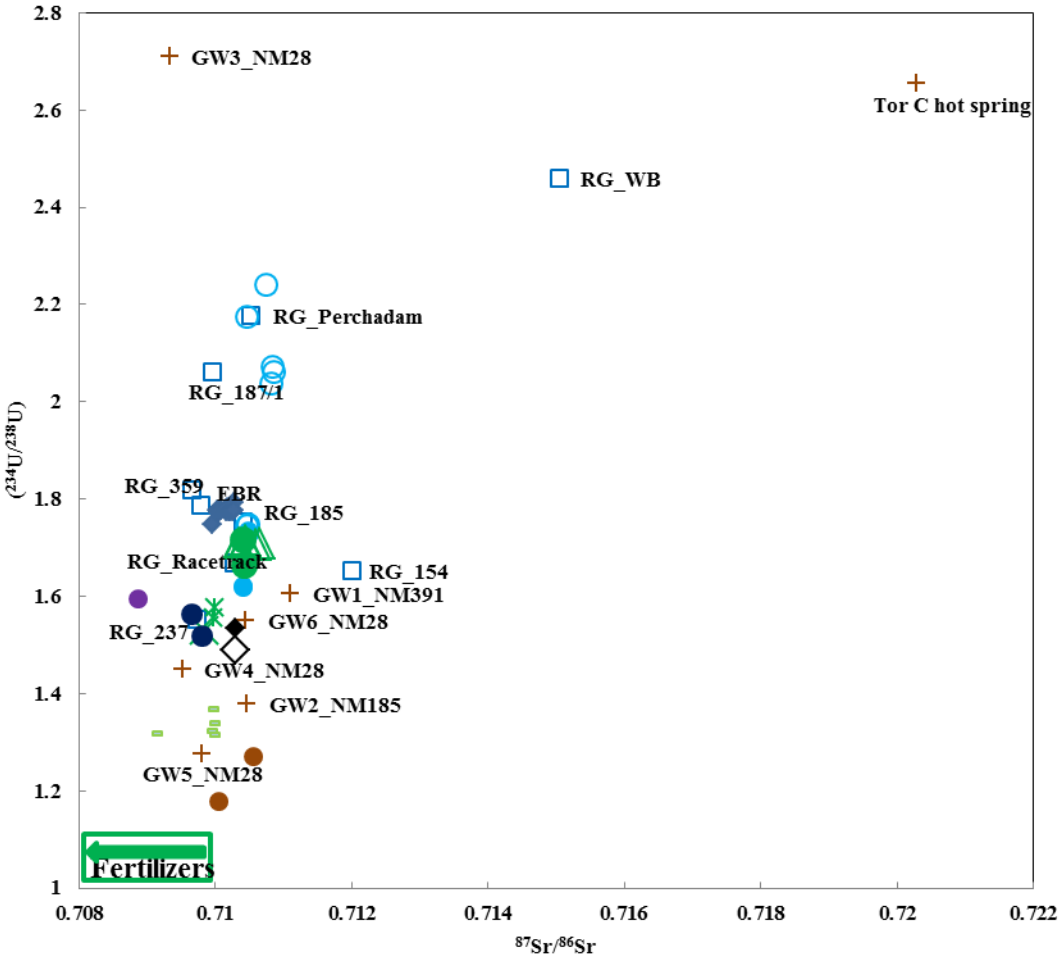

Figure 4.3: A plot of ($^{234}U/^{238}U$) versus $^{87}Sr/^{86}Sr$ ratios for lower Rio Grande water during the irrigation and non irrigation seasons, groundwater, agricultural drains, city drains, and wastewater.

Deep ground water (Tor C and GW3_NM28) and shallow groundwater in combination with agricultural drains were distinct end members.

Chapter 5

Conclusion

This study was set within the southwest USA to explore the impact of anthropogenic factors such as land use and management on carbonate fluxes thus, the carbon cycle. Current significant increasing levels of atmospheric CO_2 due to anthropogenic factors and its long-term effect on global temperatures (green house effect) have enhanced the need to understand global C cycle. Carbon sequestration mechanisms through soil organic carbon (SOC) are well understood (Lal et al., 1998c). However, more work is needed to appreciate the role of soil inorganic carbon (SIC) on the global C cycle because they form through complex mechanisms involving chemical, biological and anthropogenic factors.

Accumulation rates of pedogenic carbonate in an irrigated alfalfa cropland near El Paso, TX were compared to naturally precipitating carbonates in the Jornada Basin, NM. This study identified that high accumulation rates at alfalfa site were significantly influenced by high Ca^{2+} and DIC influxes from saline Lower Rio Grande river water and shallow groundwater used in irrigation activities. Meanwhile, low Ca^{2+} and C fluxes from dust and rainfall at the Jornada site resulted in lower precipitation rates despite thick older carbonates at depth. Due to effects of climate such as annual rainfall on carbonate formation mechanisms in natural systems, this study sought to reconstruct paleo-moisture conditions at the Jornada Basin. The moisture conditions have been decreasing through time in the Jornada Basin and its environs. Drier conditions would influence the chemistry and discharge of dryland rivers, ground water table, and soil quality and productivity over time. The Rio Grande river quality is vital to the growing population in cities along its valley because it serves important agricultural, municipal, industrial, and recreational purposes. Literature of the Rio Grande water quality is extensive but no studies have examined

its effect on managed agricultural soils along its valley. This study explored the following issues; (1) factors that affect the formation rates of pedogenic carbonates in arid and semiarid soils of southwest USA, (2) Paleo-environmental conditions of the Jornada Basin as recorded in the pedogenic carbonates, (3) Fingerprinting natural and anthropogenic salt loads into the Lower Rio Grande river.

Due to high pedogenic carbonate accumulation rates in managed irrigated soils, this study recognizes that land management activities such as irrigation gradually affect the carbon cycle by sequestering carbon in terrestrial environment. In addition, irrigation activities increase plant biomass and displace soil CO_2 to the atmosphere thus affecting carbon fluxes. Long-term carbon fluxes affect the carbon cycle and therefore climate. Climatic factors such as rainfall quantities, evapotranspiration rates, and dust influence precipitation of carbonates in soils. At the Jornada Basin NM, paleo-moisture (therefore rainfall quantities) conditions have varied between late Pleistocene and mid-Holocene. This study showed that older carbonates at soil depth in the La Mesa geomorphic surface within the Jornada Basin precipitated during high soil moisture events evidenced by low ($^{234}U/^{238}U$) and high $^{87}Sr/^{86}Sr$ ratios due to weathering processes. Low $\delta^{13}C_{OC}$ values in these carbonates support existence of C3 vegetation, which dwell in wetter environments during their formation. Younger shallower carbonates were precipitated in drier environments similar to the current climate. Past climatic changes aid in understanding and predicting future climate. With increasing desertification and projected drier climate in the southwest USA, irrigation activities would boost food security and economic status of the population growing in drylands. The dissolved load of the Rio Grande fluctuates depending on the river discharge; the river volume in turn depends on upstream snowmelts. However in the Lower Rio Grande section, the river discharge is controlled manually at the Elephant Butte

Reservoir gates, NM. In the irrigation season, the reservoir water dominates the river as evidenced from low, well mixed total dissolved solids (TDS), major ion concentrations, ($^{234}U/^{238}U$) and $^{87}Sr/^{86}Sr$ ratios. In the non-irrigation season, the river base flow, which mainly consists of deep ground water, shallow groundwater, agricultural drains, and urban effluents add high salt content spatially along the river. Deep groundwater salinity was observed a few km below the reservoir while anthropogenic salt loads mainly through agricultural drains were noticeable downstream. Fertilizer-derived salinity was clear in the river water during the irrigation season while in the non-irrigation, shallow groundwater used in irrigation add salts to the river via drains. Indeed, the salinity of the Rio Grande river has been associated with natural and anthropogenic factors (Hogan et al., 2007; Szynkiewicz et al., 2011, 2015). Clearly, salinity in the soils and water of the Lower Rio Grande is cyclical.

Several other studies including this work improve our understanding of sources of salinity and identify particular point salt loads, which would increase usable water if salts were controlled. However, salinity of the Lower Rio Grande and its effect to managed soils still remain unsolved. One common proposed strategy is to control the amount of irrigation water by practicing drip irrigation rather than flood irrigation. Water salinity management would reduce salt accumulation in irrigated desert soils and increase plant biomass thus more atmospheric C sequestration through SOC. To generate more achievable strategies to tackle soil and water salinity in the Lower Rio Grande, there is need to; (1) carry out isotopic studies to estimate Ca fluxes from irrigation water, fertilizers, and Ca-bearing minerals precipitated in pedogenic carbonates, (2) elucidate the role of biota (e.g. microbes, plant root respiration) on SIC pool at the studied soil profiles, (3) Use additional isotopic tools to clearly identify the mixed salinity puzzle at some sites (e.g. along the Rio Grande river near El Paso, TX).

This study has quantified and compared accumulation rates of carbonates in natural soils verses managed irrigated soils within southwest USA. The carbon data contributes to the database of the ongoing SIC pool quantification studies and improves our understanding on the effect of land use management practices on global C cycle. The paleo-climatic information recorded in carbonates provides clues to climate modelers on future climate changes and its effect on water budgets. The study has also identified specific salinity end-members at specific sites along the Lower Rio Grande that affect the general water quality.

References

Hogan, J. F., Phillips, F. M., Mills, S. K., Hendrickx, J. M., Ruiz, J., Chesley, J. T., Asmerom, Y. (2007). Geologic origins of salinization in a semi-arid river: The role of sedimentary basin brines. *Geology 35*(12), 1063-1066.

Lal, R., Kimble, J.M., Follet, R., Cole,C.V (1998c). The potential of U.S. cropland to sequester C and mitigate the Greenhouse effect. Ann Arbor Press, Chelsea, MI. 128

Szynkiewicz, A., Borrok, D. M., Ganjegunte, G. K., Skrzypek, G., Ma, L., Rearick, M. S., Perkins, G. B. (2015). Isotopic studies of the Upper and Middle Rio Grande. Part 2—Salt loads and human impacts in south New Mexico and west Texas. *Chemical Geology 411*, 336-350.

Szynkiewicz, A., Witcher, J.C., Modelska, M., Borrok, D.M., Pratt, L.M., 2011. Anthropogenic sulfate loads in the Rio Grande, New Mexico (USA). *Chemical Geology* 283(3-4), 194-209.

Appendix I

Tables and Figures

Table A1: Measured ($^{234}U/^{238}U$), ($^{230}Th/^{238}U$), ($^{232}Th/^{238}U$) activity ratios for bulk soil and caliche samples, acid leachate and residue, water suspended and residual samples for Alfalfa and Jornada profiles

Correlation coefficients (R2) for Osmond isochron [($^{230}Th/^{238}U$) and ($^{234}U/^{238}U$) vs ($^{232}Th/^{238}U$)] and Rosholt isochron [($^{230}Th/^{232}Th$) and ($^{234}U/^{232}Th$) vs ($^{238}U/^{232}Th$)] plots are also shown.

ample Name	Sample type	($^{234}U/^{238}U$)	±	($^{230}Th/^{238}U$)	±	($^{232}Th/^{238}U$)	±	R^2 ($^{230}Th/^{238}U$ vs $^{232}Th/^{238}U$)	R^2 ($^{234}U/^{238}U$ vs $^{232}Th/^{238}U$)	R^2 ($^{230}Th/^{232}Th$ vs $^{238}U/^{232}Th$)	R^2 ($^{234}U/^{232}Th$ vs $^{238}U/^{232}Th$)
Alfalfa (0-3 cm)	Bulk soil	1.009	0.005	1.211	0.019	1.145	0.014	0.88	0.95	0.65	1
	HCl_L	1.290	0.006	0.652	0.010	0.464	0.006				
	HCl_R	0.969	0.005	1.306	0.021	1.227	0.015				
	H_2O_S	1.037	0.005	1.542	0.025	1.224	0.015				
	H_2O_R	1.003	0.005	1.154	0.018	1.117	0.013				
Alfalfa (10-13 cm)	Bulk soil	1.001	0.005	1.034	0.017	1.240	0.015	0.95	0.9	0.5	1
	HCl_L	1.346	0.007	0.461	0.007	0.436	0.005				
	HCl_R	0.957	0.005	1.151	0.018	1.222	0.015				
	H_2O_S	1.021	0.005	1.281	0.020	1.306	0.016				
	H_2O_R	1.000	0.005	1.020	0.016	1.054	0.013				
Alfalfa (20-23 cm)	Bulk soil	1.011	0.005	1.079	0.017	1.074	0.013	0.95	0.86	0.58	0.99
	HCl_L	1.300	0.006	0.689	0.011	0.620	0.007				
	HCl_R	0.974	0.005	1.162	0.019	1.169	0.014				
	H_2O_S	1.039	0.005	1.309	0.021	1.269	0.015				
	H_2O_R	1.003	0.005	1.053	0.017	1.142	0.014				
Alfalfa (30-33 cm)	Bulk soil	1.001	0.005	1.083	0.017	1.078	0.013	0.99	0.52	0.74	0.99
	HCl_L	1.308	0.007	0.639	0.010	0.575	0.007				
	HCl_R	0.964	0.701	1.344	0.021	1.333	0.016				
	H_2O_S	1.031	0.224	1.970	0.032	1.931	0.023				

	H_2O_R	0.991	0.882	1.498	0.024	1.569	0.019				
Alfalfa (40-43 cm)	Bulk soil	1.003	0.005	1.045	0.017	1.028	0.012	0.99	0.93	0.98	1
	HCl_L	1.440	0.007	0.111	0.002	0.085	0.001				
	HCl_R	0.950	0.005	1.163	0.019	1.194	0.014				
	H_2O_S	1.060	0.005	1.185	0.019	1.167	0.014				
	H_2O_R	0.991	0.005	1.008	0.016	1.017	0.012				
Alfalfa (50-53 cm)	Bulk soil	0.989	0.005	0.747	0.012	1.018	0.012	0.99	0.66	0.89	1
	HCl_L	1.223	0.006	0.293	0.005	0.369	0.004				
	HCl_R	0.954	0.005	0.927	0.015	1.312	0.016				
	H_2O_S	1.042	0.005	1.135	0.018	1.548	0.019				
	H_2O_R	0.977	0.005	1.074	0.017	1.501	0.018				
Alfalfa (60-63 cm)	Bulk soil	0.968	0.005	1.001	0.016	1.055	0.013	0.98	0.19	0.82	0.91
	HCl_L	1.125	0.006	0.869	0.014	0.866	0.010				
	HCl_R	0.950	0.005	1.043	0.017	1.097	0.013				
	H_2O_S	1.027	0.005	1.203	0.019	1.324	0.016				
	H_2O_R	0.968	0.005	0.989	0.016	1.084	0.013				
JPT 1 (0-10 cm)	Bulk soil	0.954	0.005	1.233	0.020	1.503	0.018	0.71	0.85	0.64	0.99
	HCl_L	1.152	0.006	0.909	0.015	0.757	0.009				
	HCl_R	0.940	0.005	1.356	0.022	1.366	0.016				
	H_2O_S	0.965	0.005	1.511	0.024	1.416	0.017				
	H_2O_R	0.965	0.005	1.182	0.019	1.179	0.014				
JPT 1 (10-15 cm)	Bulk soil	0.967	0.005	1.208	0.019	1.029	0.012	0.99	0.01	0.06	0.99
	HCl_L	1.159	0.006	1.071	0.017	0.918	0.011				
	HCl_R	0.988	0.005	1.308	0.021	1.199	0.014				
	H_2O_S	0.976	0.005	0.378	0.006	0.346	0.004				
	H_2O_R	1.001	0.005	4.729	0.076	4.794	0.058				
JPT 1 (10-15 cm)	Bulk soil	1.004	0.005	1.204	0.019	1.068	0.013	0.94	0.91	0.9	1
	HCl_L	1.226	0.006	0.852	0.014	0.594	0.007				

	HCl_R	0.965	0.005	1.309	0.021	1.170	0.014				
	H_2O_S	1.034	0.005	1.385	0.022	1.176	0.014				
	H_2O_R	0.995	0.005	1.176	0.019	1.092	0.013				
JPT 1(25-30 cm)	Bulk soil	1.003	0.005	1.192	0.019	1.076	0.013	0.98	0.87	0.88	1
	HCl_L	1.233	0.006	0.643	0.010	0.476	0.006				
	HCl_R	0.977	0.005	1.244	0.020	1.116	0.013				
	H_2O_S	1.042	0.005	1.361	0.022	1.176	0.014				
	H_2O_R	0.988	0.005	1.128	0.018	1.051	0.013				
JPT 1 (40 cm)	Bulk carbonate sub 1	1.003	0.005	0.891	0.014	0.654	0.008	0.28	0.14	0.98	0.97
	Bulk carbonate sub 2	1.233	0.006	0.901	0.014	0.724	0.009				
	Bulk carbonate sub 3	0.977	0.005	0.938	0.015	1.029	0.012				
	Bulk carbonate sub 4	1.042	0.005	0.901	0.014	0.596	0.007				
	Bulk carbonate sub 5	0.988	0.005	0.968	0.015	0.756	0.009				
JPT 2 (0-7 cm)	Bulk soil	0.962	0.005	1.535	0.025	1.463	0.018	0.07	0.46	0.15	0.82
	HCl_L	1.216	0.006	1.289	0.021	1.173	0.014				
	HCl_R	0.967	0.005	1.167	0.019	1.517	0.018				
	H_2O_S	0.963	0.005	1.614	0.026	1.395	0.017				
	H_2O_R	0.954	0.005	1.169	0.019	1.242	0.015				
JPT 2 (7-10 cm)	Bulk soil	0.970	0.005	1.185	0.019	1.173	0.014	0.91	0.88	0.87	1
	HCl_L	1.223	0.006	0.828	0.013	0.610	0.007				
	HCl_R	0.943	0.005	1.237	0.020	1.222	0.015				
	H_2O_S	0.993	0.005	1.399	0.022	1.255	0.015				
	H_2O_R	0.960	0.005	1.111	0.018	1.071	0.013				
JPT 2 (27-30 cm)	Bulk soil	0.994	0.005	1.183	0.019	1.022	0.012	0.97	0.85	0.87	0.99

	HCl_L	1.207	0.006	0.802	0.013	0.601	0.007				
	HCl_R	0.969	0.005	1.248	0.020	1.130	0.014				
	H_2O_S	1.023	0.005	1.347	0.022	1.132	0.014				
	H_2O_R	0.988	0.005	1.138	0.018	0.978	0.012				
JPT 2 (37-40 cm)	Bulk soil	0.994	0.005	1.176	0.019	1.246	0.015	0.72	0.85	0.83	0.99
	HCl_L	1.207	0.006	0.990	0.016	0.769	0.009				
	HCl_R	0.969	0.005	1.202	0.019	1.139	0.014				
	H_2O_S	1.023	0.005	1.319	0.021	1.200	0.014				
	H_2O_R	0.988	0.005	1.146	0.018	1.129	0.014				
JPT 2 (48 cm)	Bulk carbonate sub 1	1.323	0.007	0.659	0.011	0.885	0.011	0.17	0.01	0.82	0.97
	Bulk carbonate sub 2	1.330	0.007	0.709	0.011	0.527	0.006				
	Bulk carbonate sub 3	1.283	0.006	0.798	0.013	0.682	0.008				
	Bulk carbonate sub 4	1.237	0.006	0.855	0.014	0.610	0.007				
	Bulk carbonate sub 5	1.319	0.007	0.734	0.012	0.571	0.007				

Figure A1; U-series 2D Rosholt [(^{230}Th/^{232}Th) and (^{234}U/^{232}Th) vs (^{238}U/^{232}Th)] and Osmond [(^{230}Th/^{238}U) and (^{234}U/^{238}U) vs (^{232}Th/^{238}U)] isochron plots of coeval samples for alfalfa and Jornada profiles
Coeval samples include the Bulk (black diamond), HCl_R (red diamond), HCl_L (red unfilled diamond), H_2O_R (blue diamond), and H2O _S (blue unfilled diamond)

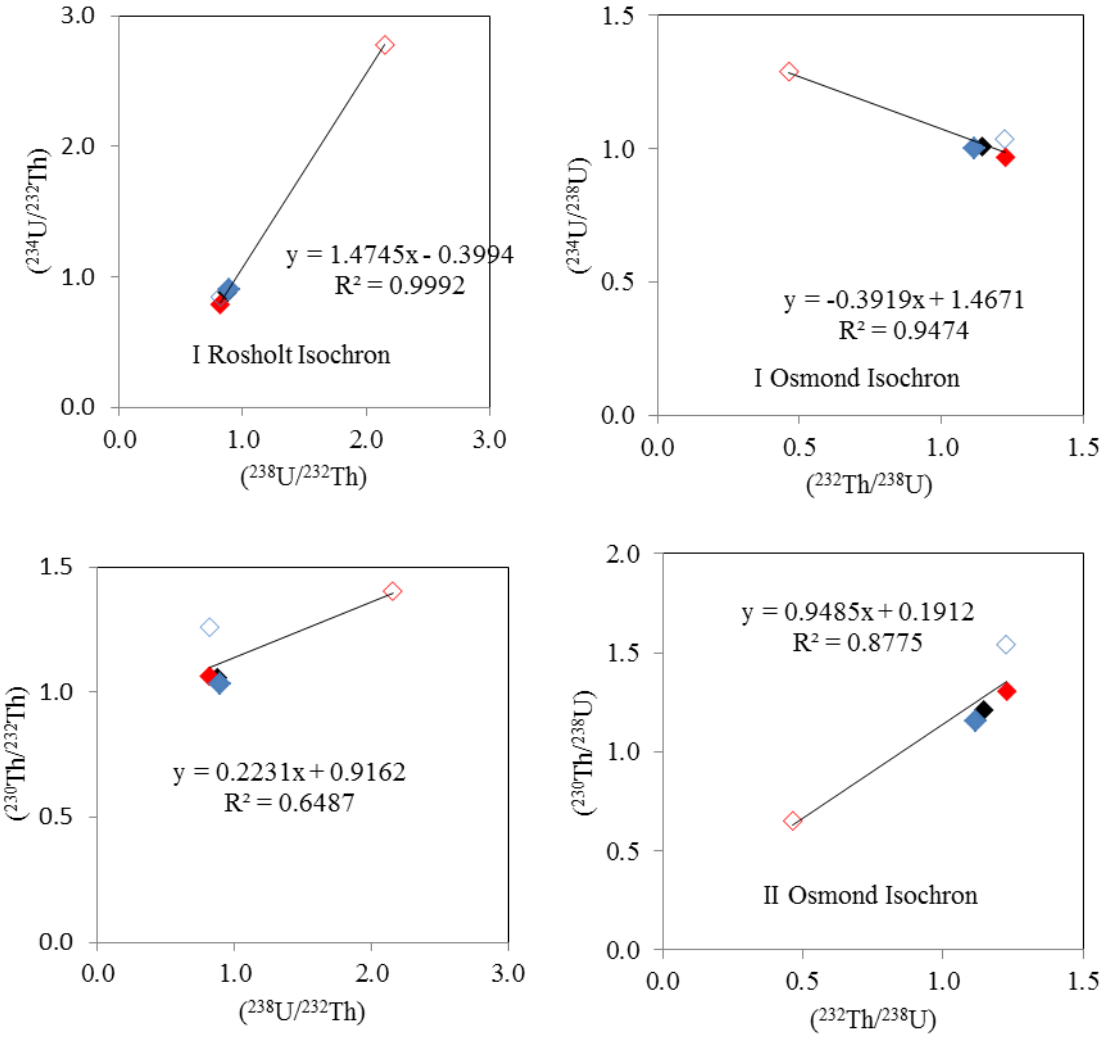

Figure A1a; 2D Rosholt and Osmond isochron plots of coeval samples [Bulk (black diamond), HCl_R (red diamond), HCl_L (red unfilled diamond), H_2O_R (blue diamond), H2O _S (blue unfilled diamond) for alfalfa 0-3 cm sample.

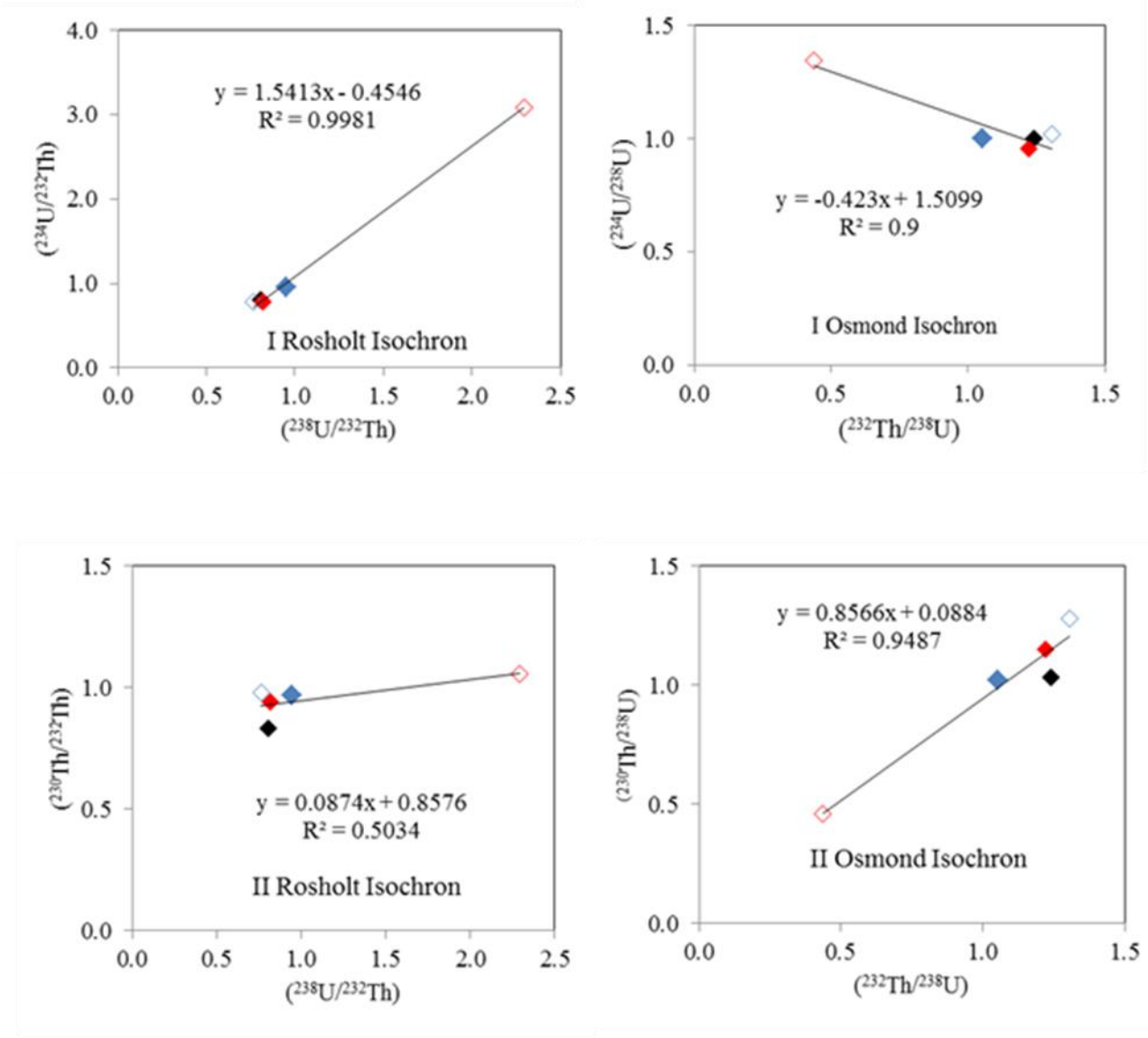

Figure A1 b; 2D Rosholt and Osmond isochron plots of coeval samples [Bulk (black diamond), HCl_R (red diamond), HCl_L (red unfilled diamond), H_2O_R (blue diamond), H2O _S (blue unfilled diamond) for alfalfa 10-13 cm sample

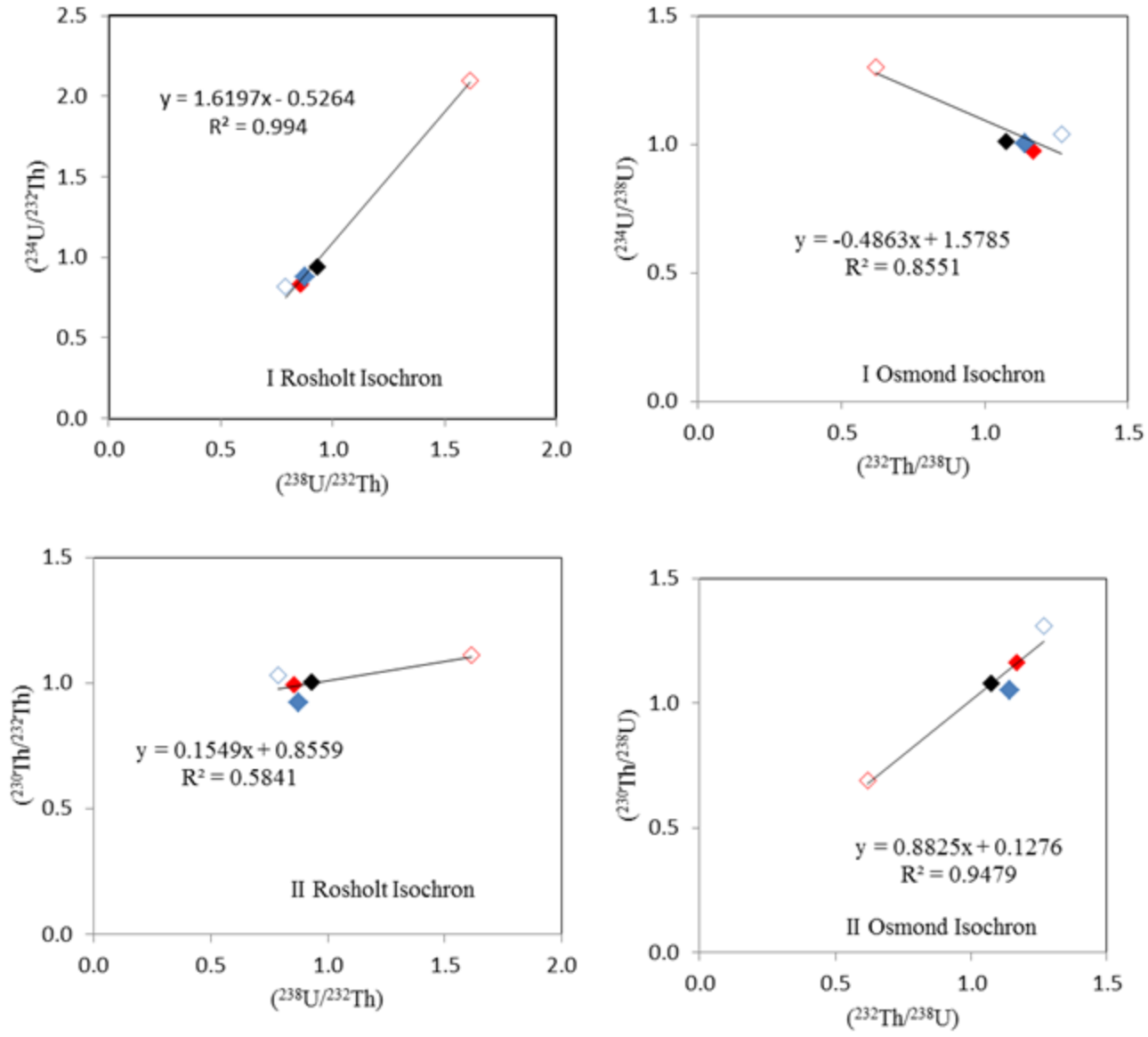

Figure A1c; 2D Rosholt and Osmond isochron plots of coeval samples [Bulk (black diamond), HCl_R (red diamond), HCl_L (red unfilled diamond), H_2O_R (blue diamond), H2O _S (blue unfilled diamond) for alfalfa 20-23 cm sample

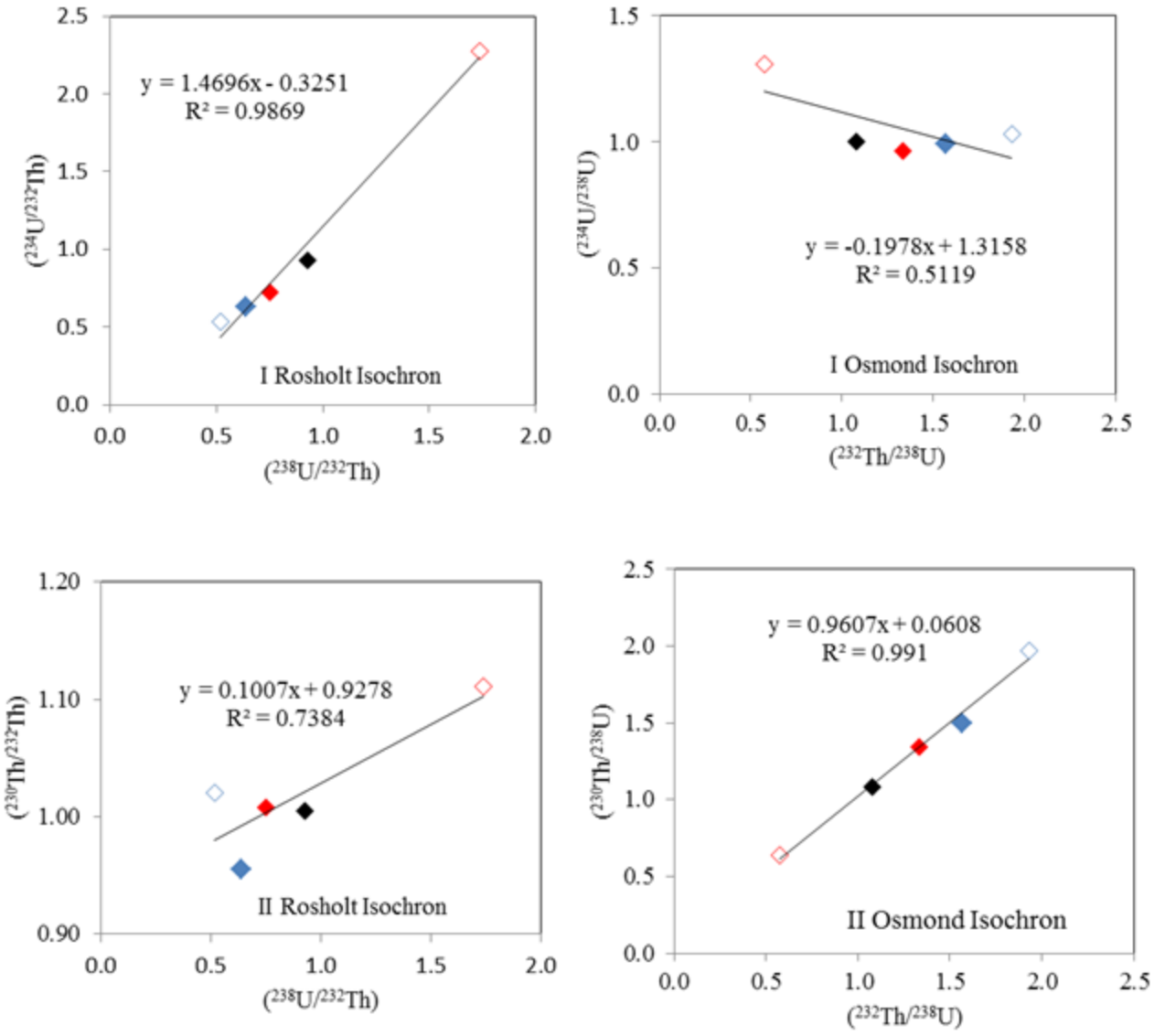

Figure A1d; 2D Rosholt and Osmond isochron plots of coeval samples [Bulk (black diamond), HCl_R (red diamond), HCl_L (red unfilled diamond), H_2O_R (blue diamond), H2O _S (blue unfilled diamond) for alfalfa 30-33 cm sample

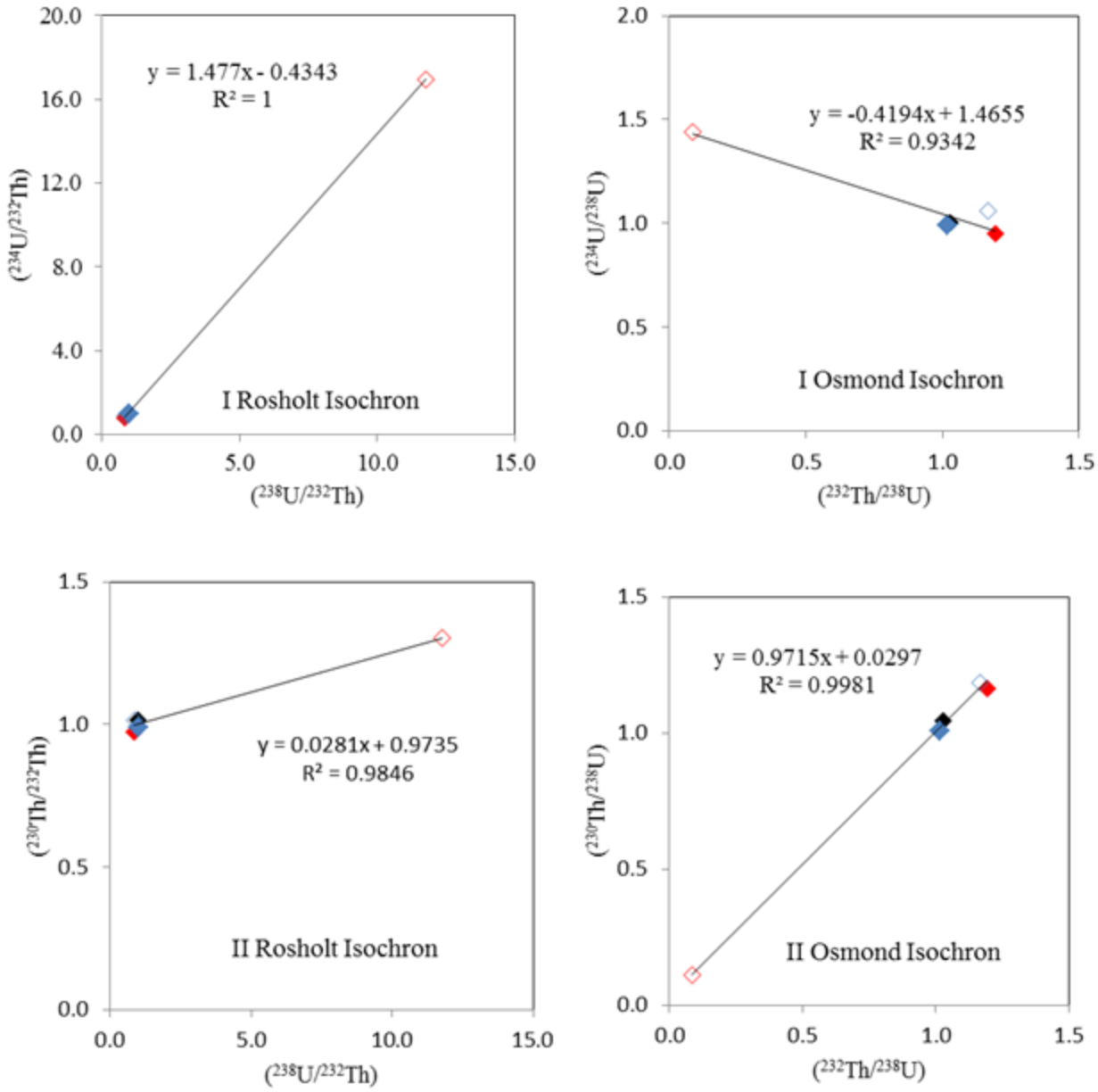

Figure A1.e; 2D Rosholt and Osmond isochron plots of coeval samples [Bulk (black diamond), HCl_R (red diamond), HCl_L (red unfilled diamond), H_2O_R (blue diamond), H2O _S (blue unfilled diamond) for alfalfa 40-43 cm sample

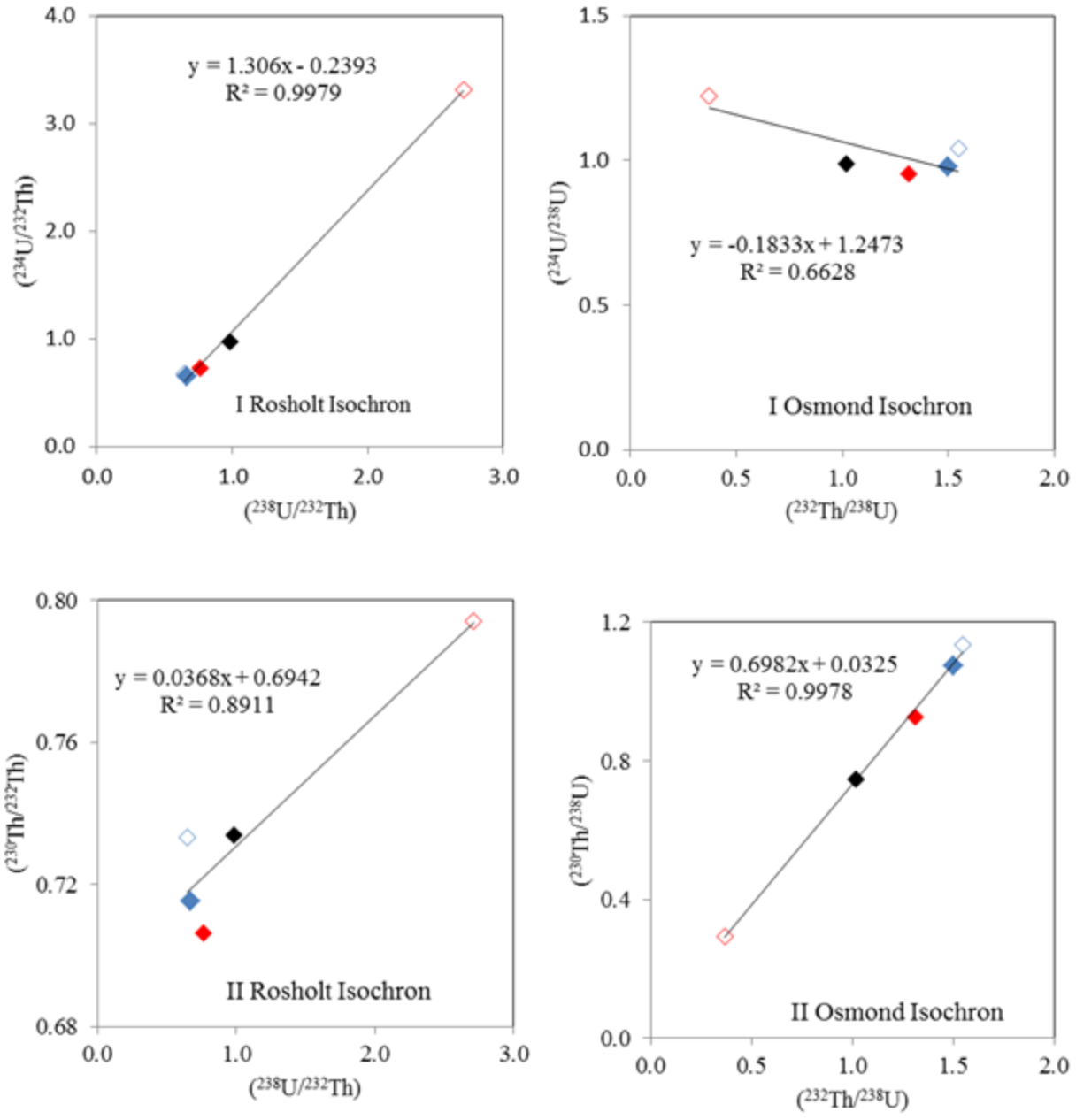

Figure A1f; 2D Rosholt and Osmond isochron plots of coeval samples [Bulk (black diamond), HCl_R (red diamond), HCl_L (red unfilled diamond), H_2O_R (blue diamond), H2O _S (blue unfilled diamond) for alfalfa 50-53 cm sample

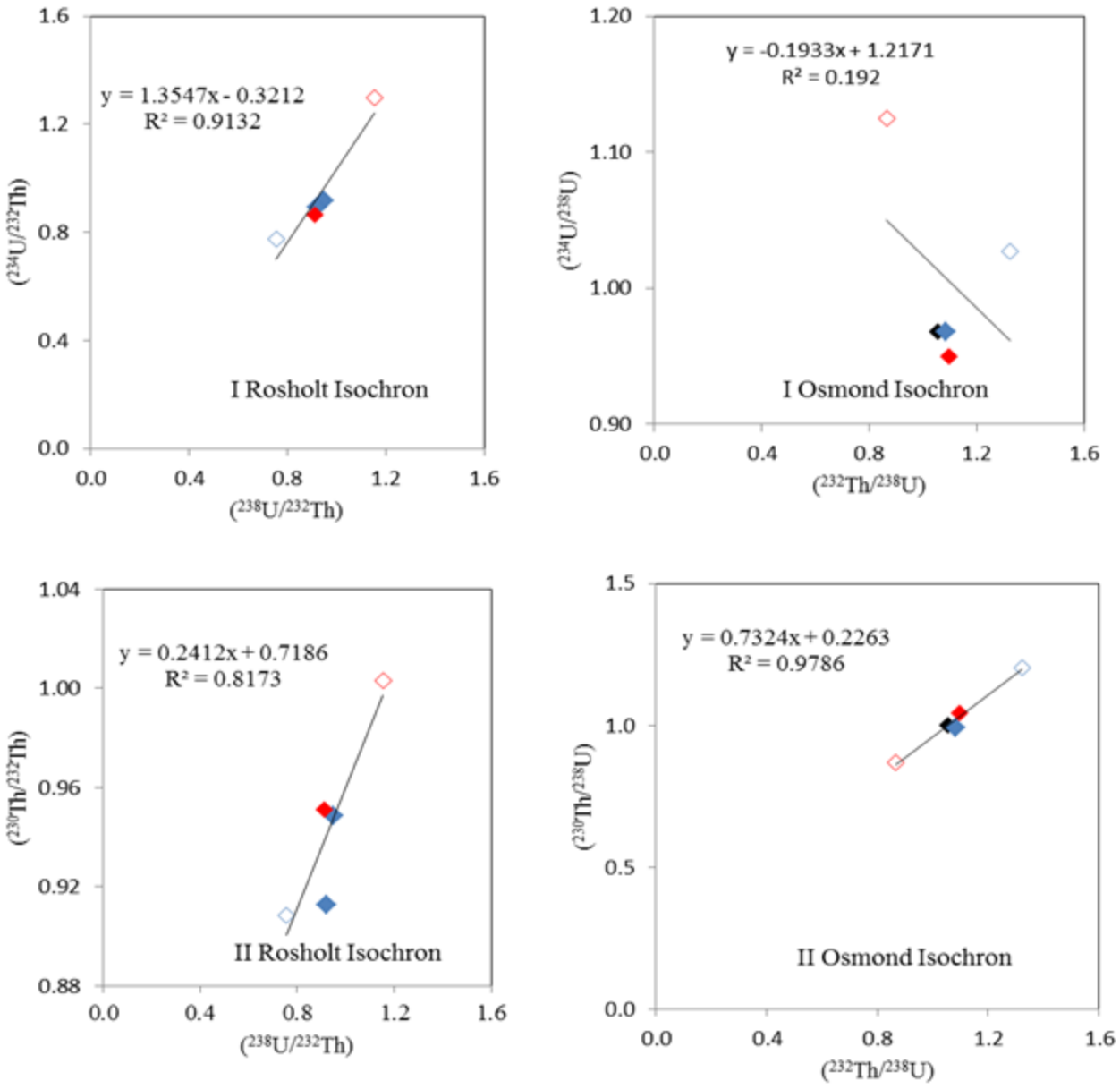

Figure A1g; 2D Rosholt and Osmond isochron plots of coeval samples [Bulk (black diamond), HCl_R (red diamond), HCl_L (red unfilled diamond), H_2O_R (blue diamond), H2O _S (blue unfilled diamond) for alfalfa 60-63 cm sample

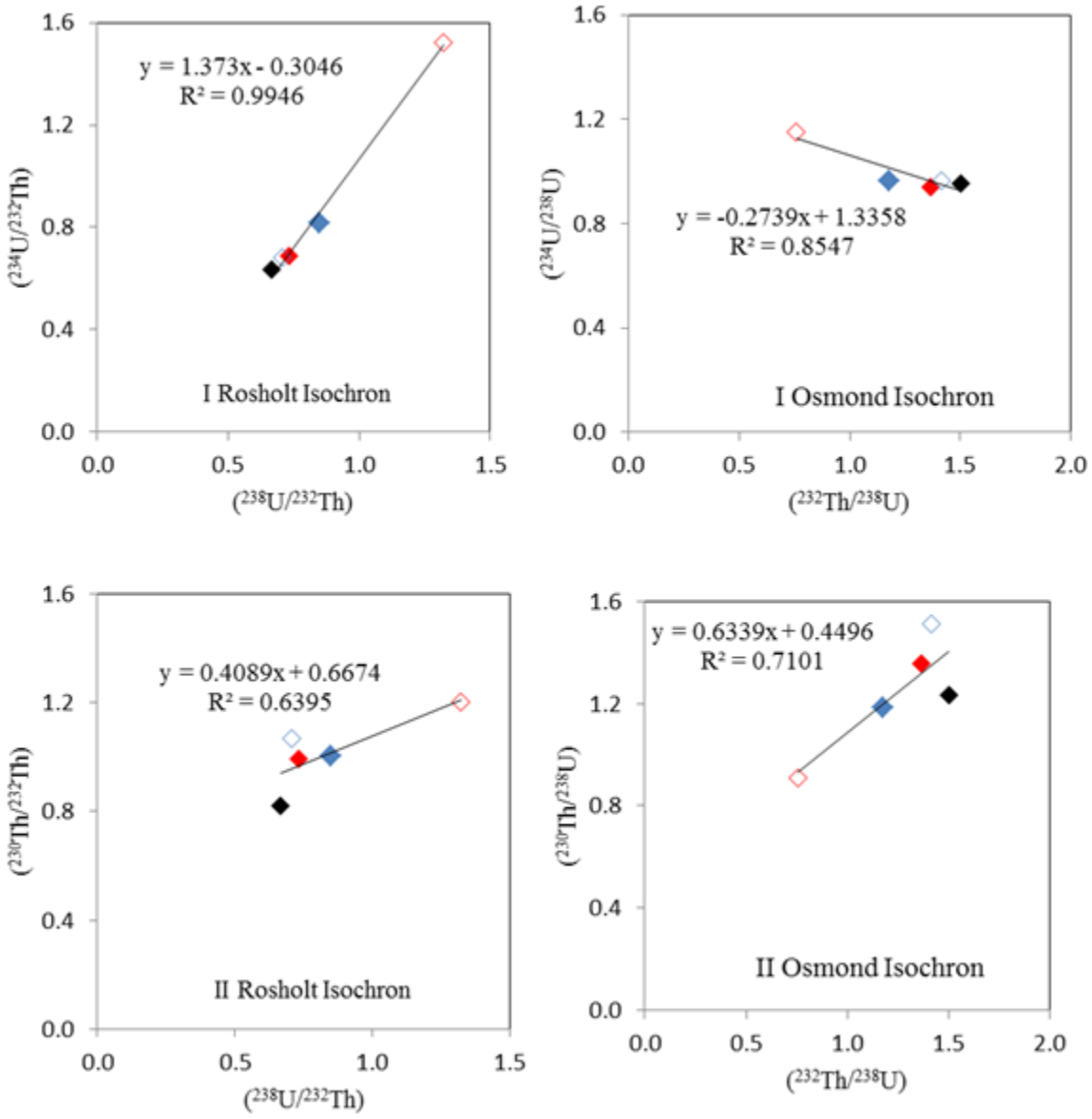

Figure A1h; 2D Rosholt and Osmond isochron plots of coeval samples [Bulk (black diamond), HCl_R (red diamond), HCl_L (red unfilled diamond), H_2O_R (blue diamond), H2O _S (blue unfilled diamond) for Jornada pit 1 (JPT1) 0-10 cm sample

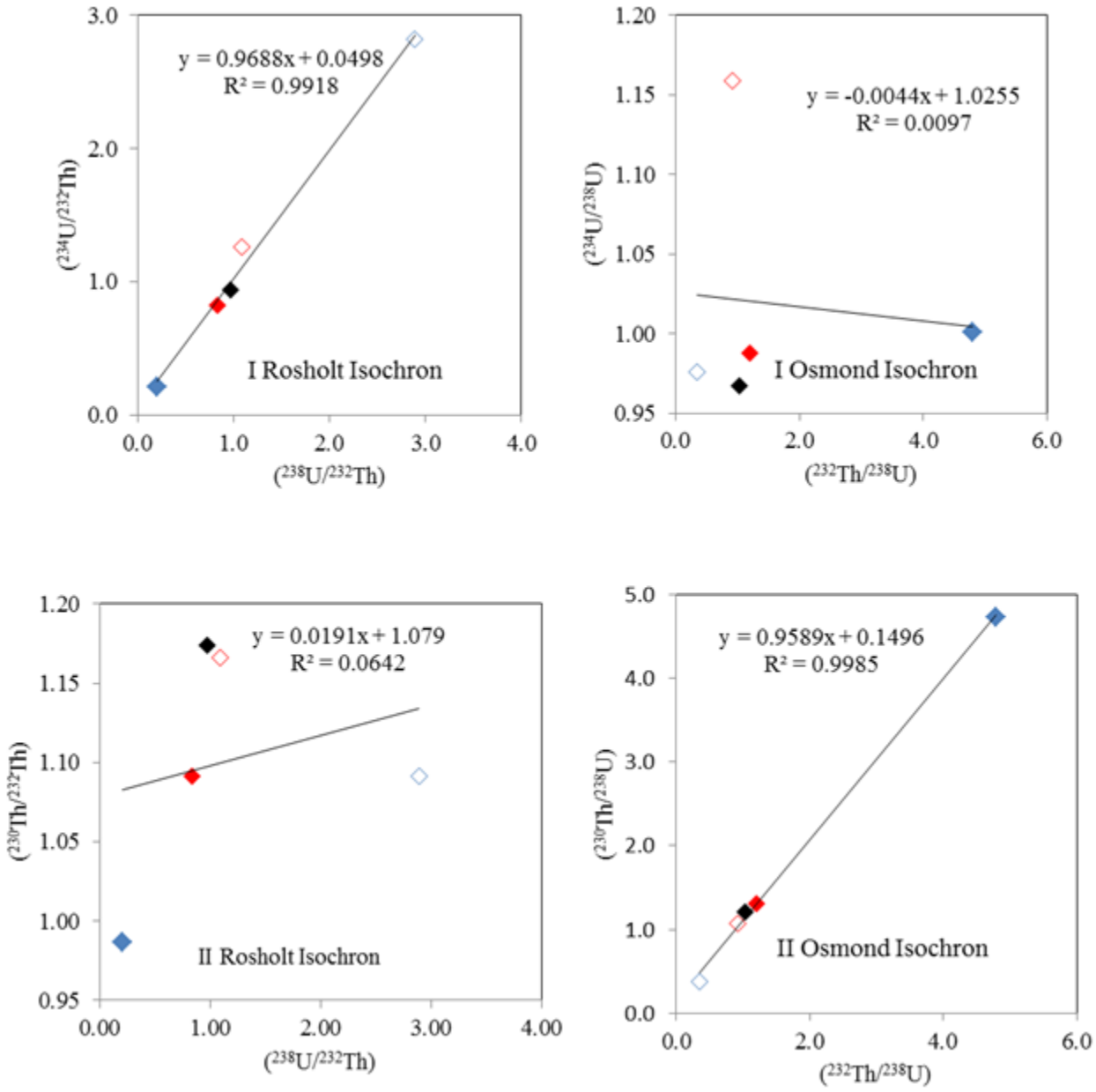

Figure A1i; 2D Rosholt and Osmond isochron plots of coeval samples [Bulk (black diamond), HCl_R (red diamond), HCl_L (red unfilled diamond), H_2O_R (blue diamond), H2O _S (blue unfilled diamond) for Jornada pit 1 (JPT1) 10-15 cm sample

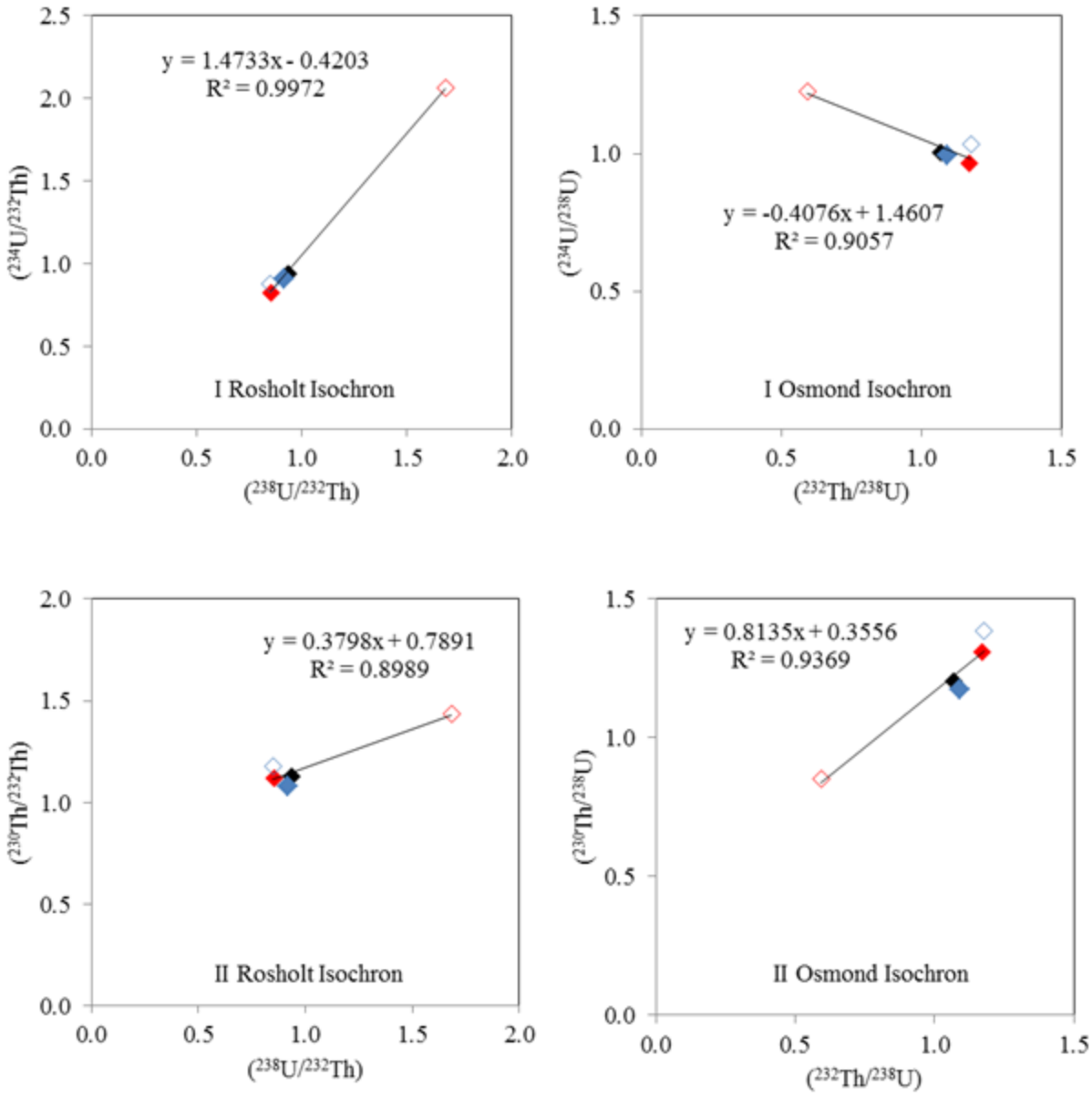

Figure A1j; 2D Rosholt and Osmond isochron plots of coeval samples [Bulk (black diamond), HCl_R (red diamond), HCl_L (red unfilled diamond), H_2O_R (blue diamond), H2O _S (blue unfilled diamond) for Jornada pit 1 (JPT1) 15-20 cm sample

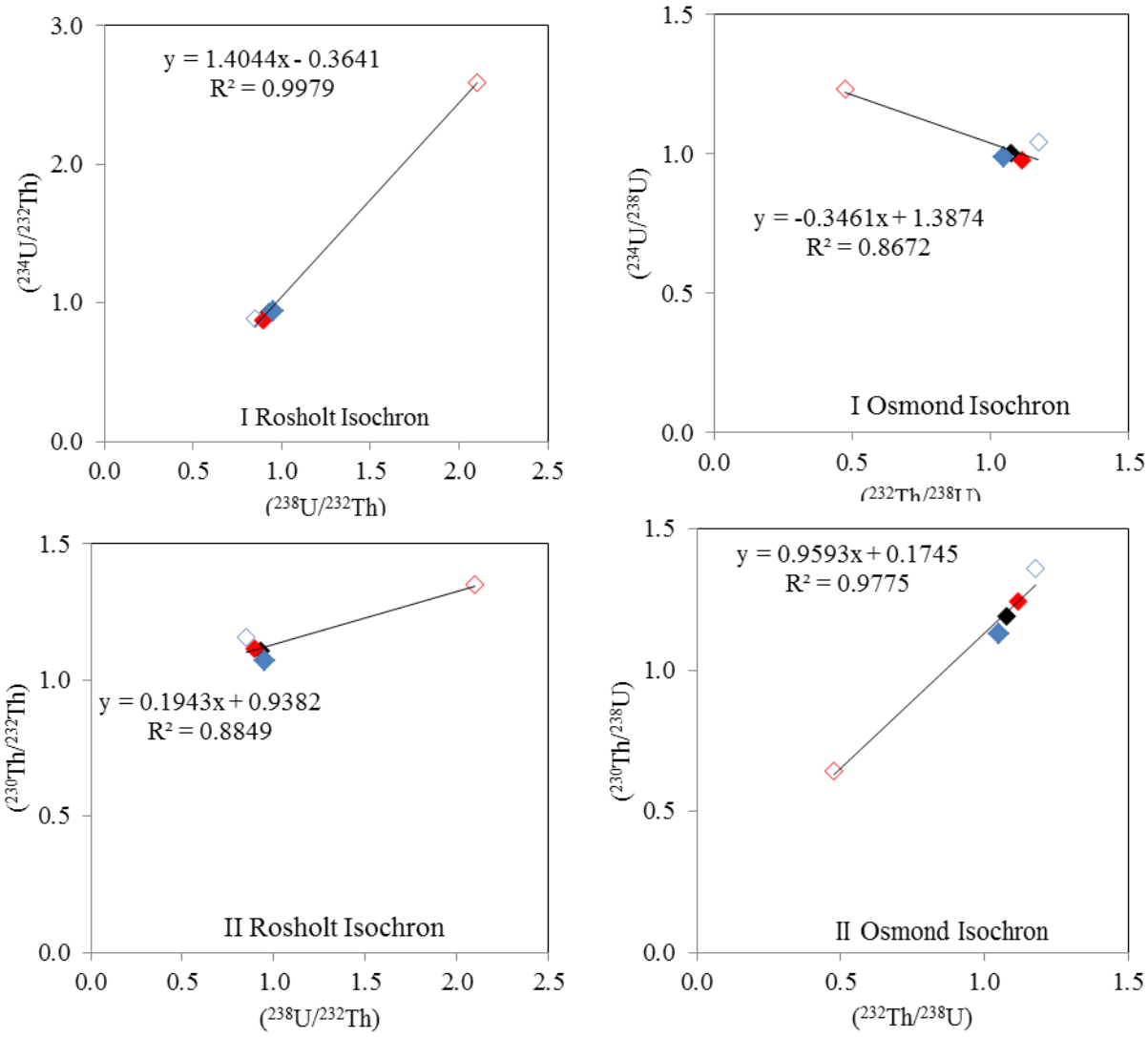

Figure A1k; 2D Rosholt and Osmond isochron plots of coeval samples [Bulk (black diamond), HCl_R (red diamond), HCl_L (red unfilled diamond), H_2O_R (blue diamond), H2O _S (blue unfilled diamond) for Jornada pit 1 (JPT1) 25-30 cm sample

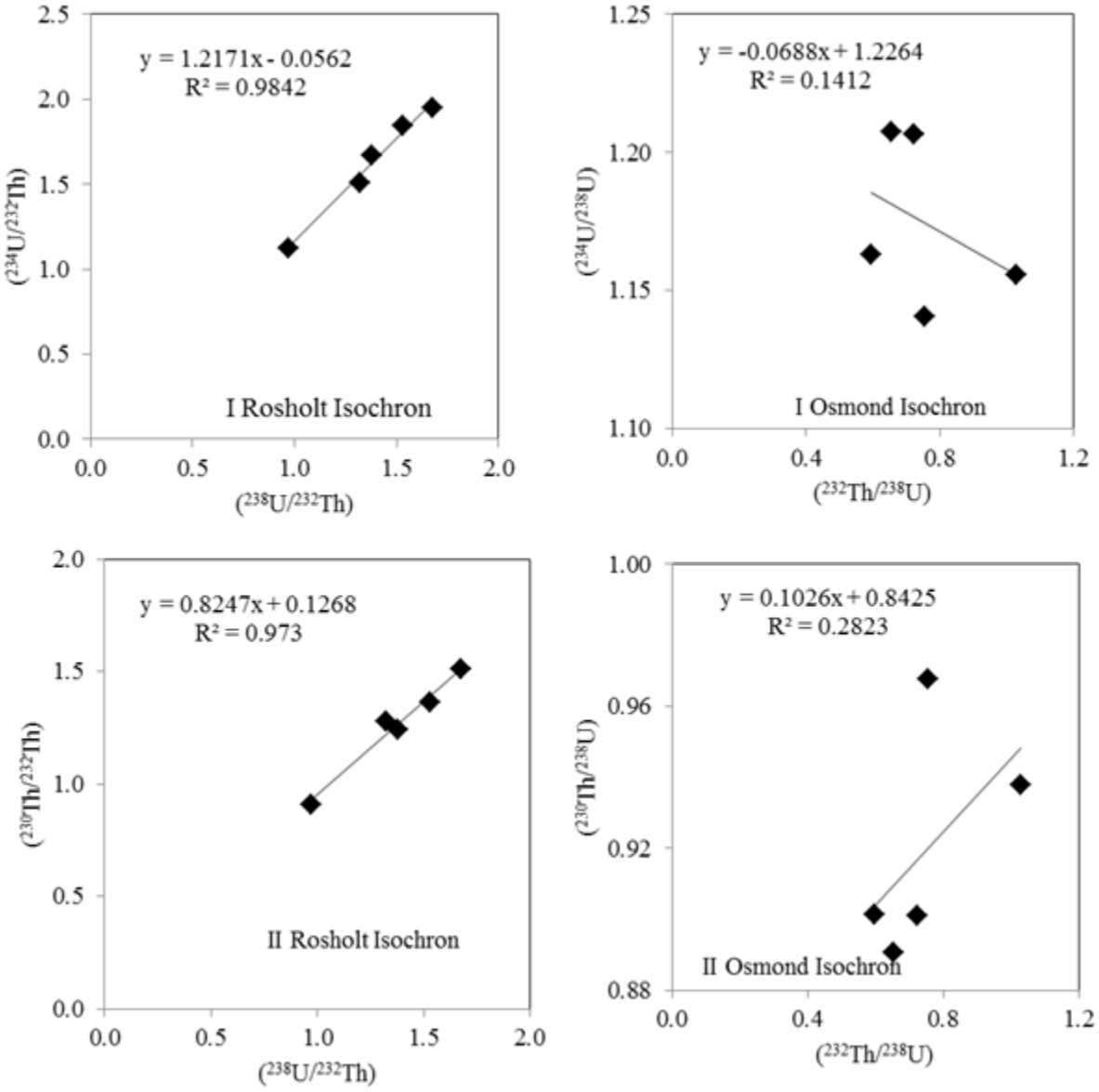

Figure A1l; 2D Rosholt and Osmond isochron plots of coeval samples all bulk (black diamond) for Jornada pit 1 (JPT1) 40 cm sample

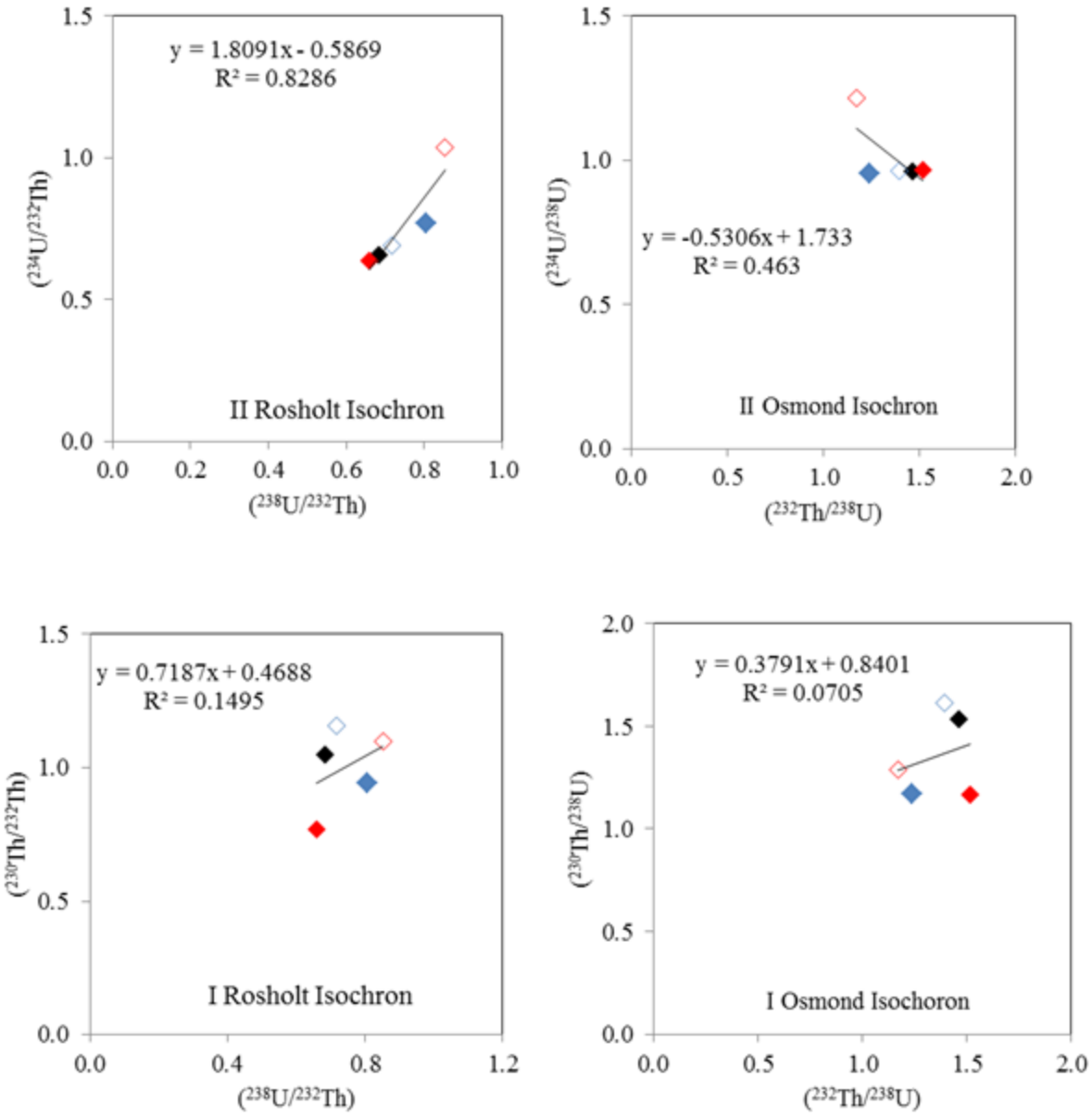

Figure A1m; 2D Rosholt and Osmond isochron plots of coeval samples [Bulk (black diamond), HCl_R (red diamond), HCl_L (red unfilled diamond), H_2O_R (blue diamond), H2O _S (blue unfilled diamond) for Jornada pit 2 (JPT2) at 0-7 cm sample

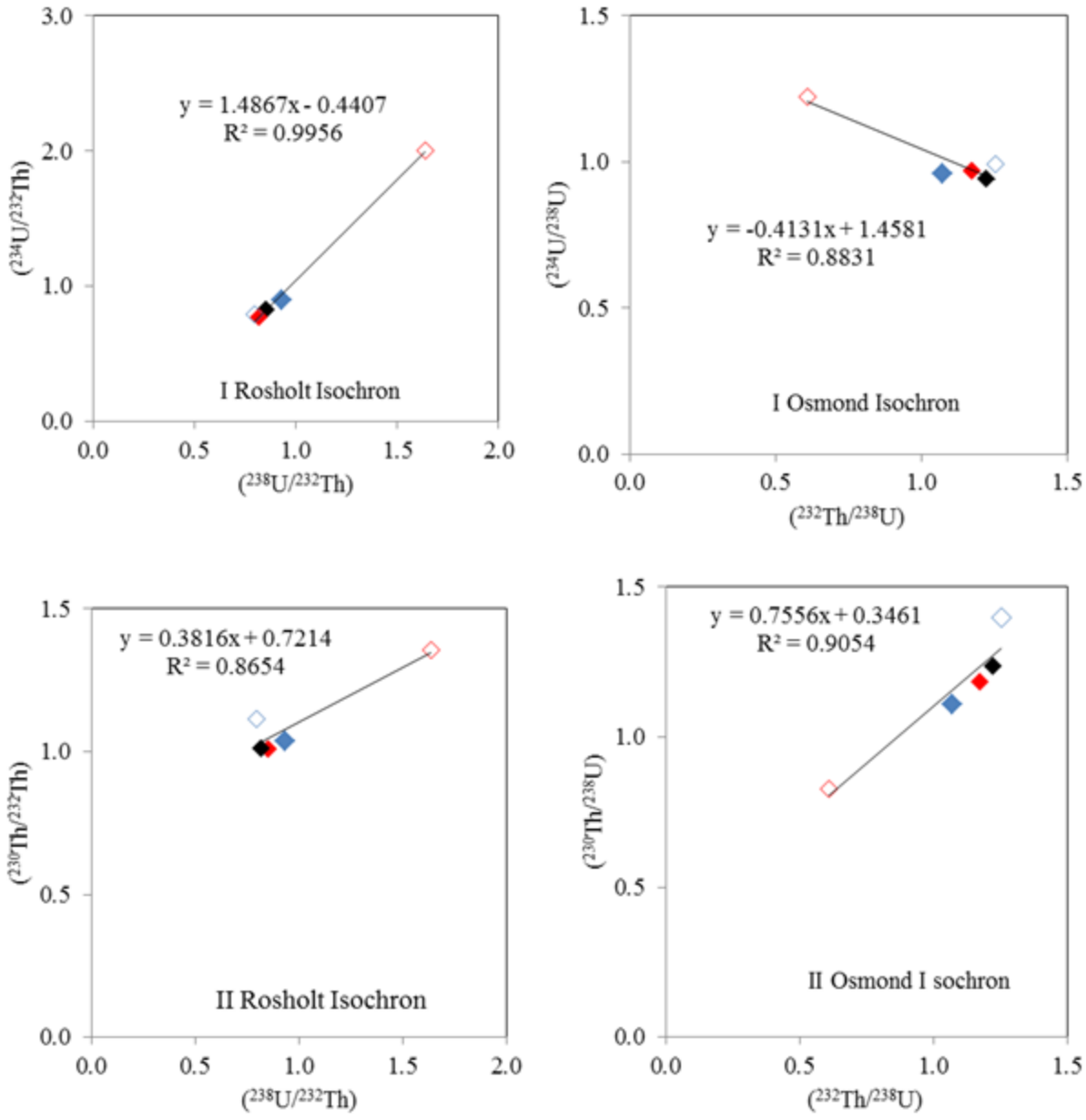

Figure A1n; 2D Rosholt and Osmond isochron plots of coeval samples [Bulk (black diamond), HCl_R (red diamond), HCl_L (red unfilled diamond), H_2O_R (blue diamond), H2O _S (blue unfilled diamond) for Jornada pit 2 (JPT2) at 7-10 cm sample

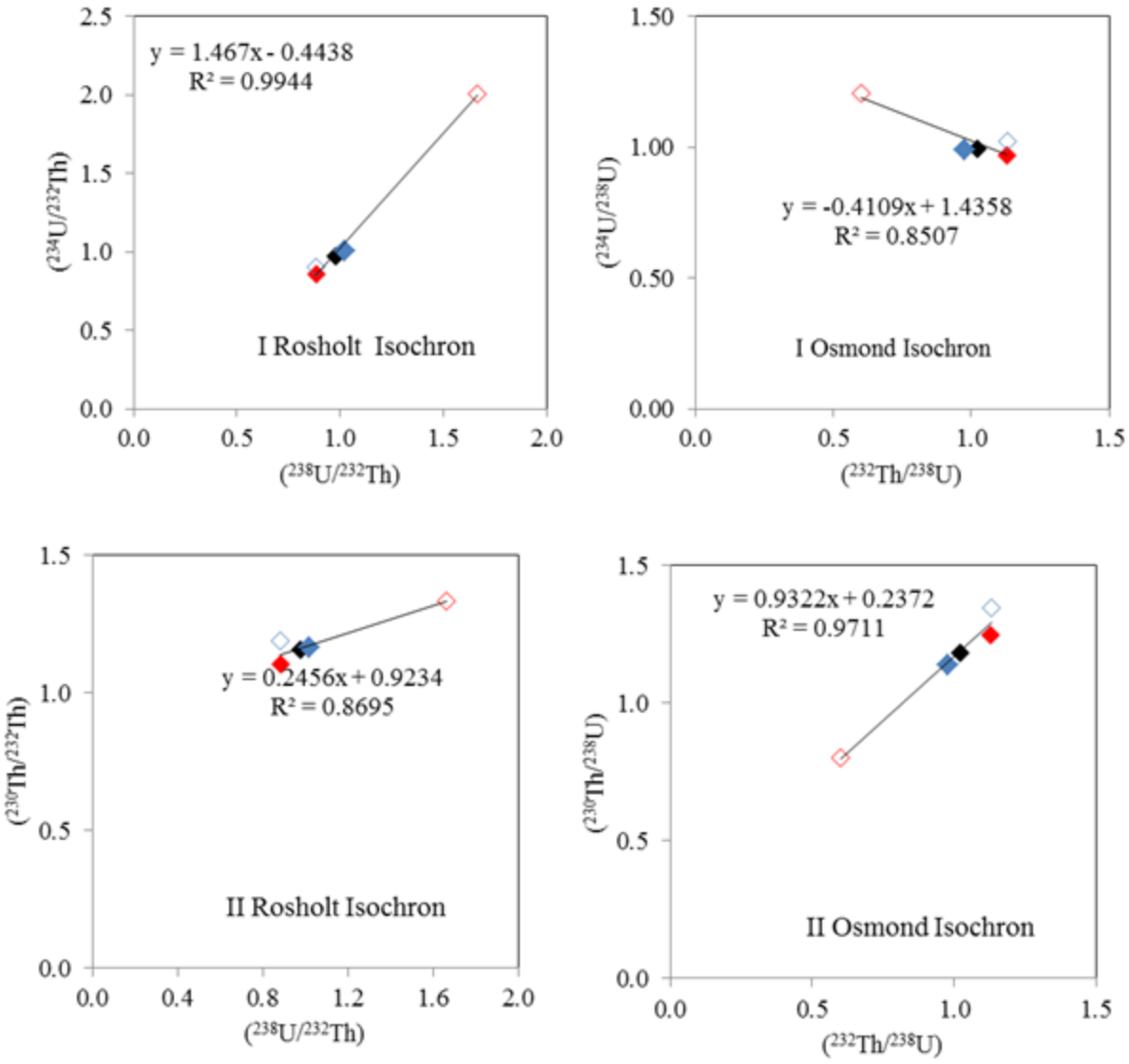

Figure A1o; 2D Rosholt and Osmond isochron plots of coeval samples [Bulk (black diamond), HCl_R (red diamond), HCl_L (red unfilled diamond), H_2O_R (blue diamond), H2O _S (blue unfilled diamond) for Jornada pit 2 (JPT2) at 27-30 cm sample

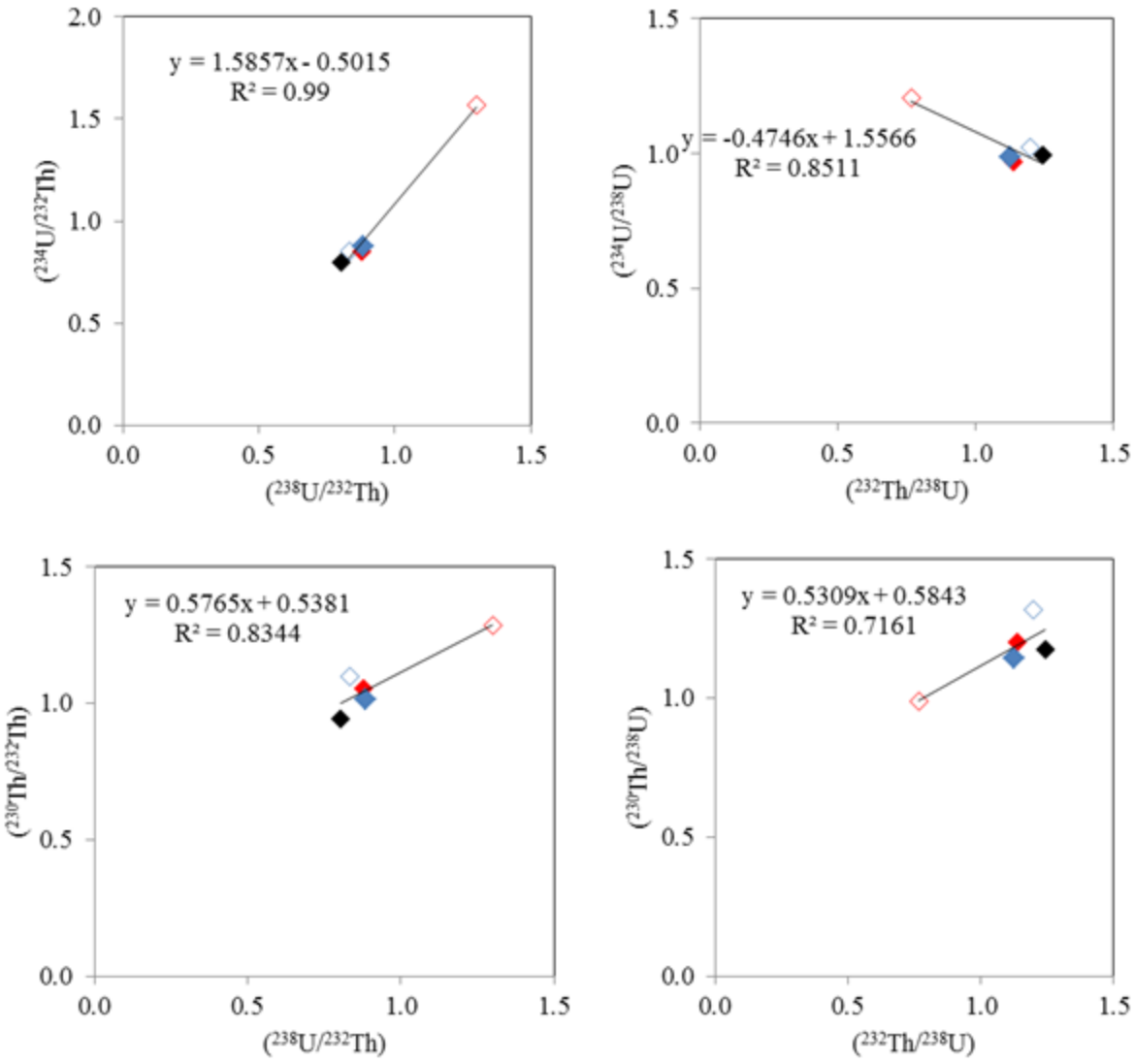

Figure A1p; 2D Rosholt and Osmond isochron plots of coeval samples [Bulk (black diamond), HCl_R (red diamond), HCl_L (red unfilled diamond), H_2O_R (blue diamond), H2O _S (blue unfilled diamond) for Jornada pit 2 (JPT2) at 37-40 cm sample

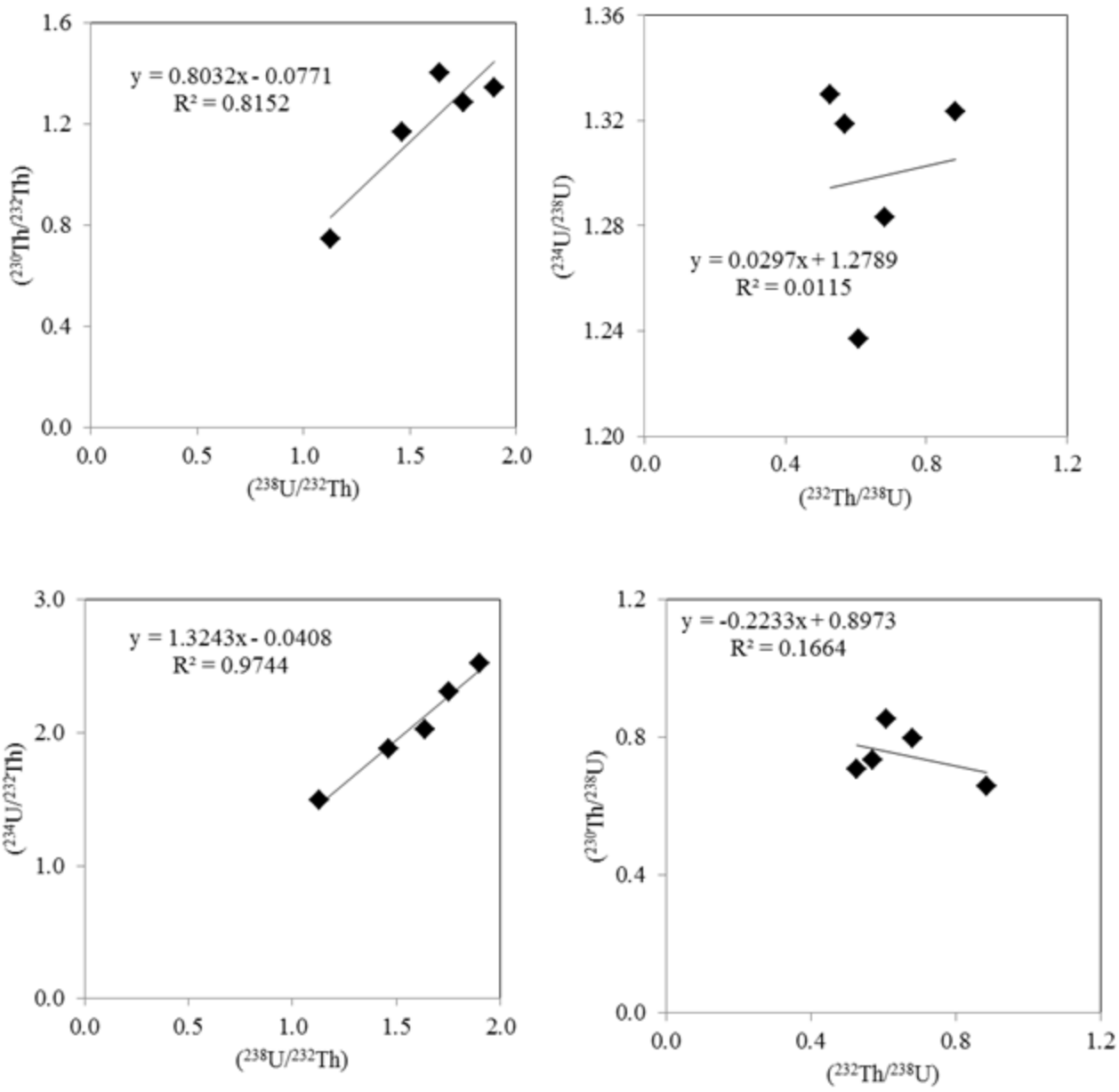

Figure A1q; 2D Rosholt and Osmond isochron plots of coeval samples all bulk (black diamond) for Jornada pit 2 (JPT2) at 48 cm sample.

Appendix II

Tables and Figures

Table A2: Measured U and Th concentrations and activity ratios for three subsamples (bulk, acid residues and leachates) and 3D Osmond -derived ages.

Subsample ID	^{238}U	±2σ	^{232}Th	±2σ	$^{230}Th/^{232}Th$	error	$^{230}Th/^{238}U$		$^{234}U/^{238}U$		$^{232}Th/^{238}U$		Age (ka)	±2σ	$(^{234}U/^{238}U)_0$	±2σ
H1 Bulk	1.585	0.016	6.017	0.060	0.620	0.006	0.770	0.012	0.911	0.005	1.242	0.015	No age			
H1 HCl R	0.956	0.010	4.227	0.042	0.917	0.009	1.327	0.021	0.915	0.005	1.447	0.017				
H1 HCl L	0.043	0.000	0.173	0.002	0.897	0.009	1.192	0.019	1.098	0.005	1.328	0.016				
H1 Bulk	1.585	0.016	6.017	0.060	0.620	0.006	0.770	0.012	0.911	0.005	1.242	0.015	-73	230	0.93	0.48
H1AcOH R	0.684	0.007	4.301	0.043	0.886	0.009	1.825	0.029	0.913	0.005	2.059	0.025				
H1 AcOH L	0.055	0.001	0.284	0.003	0.840	0.008	1.426	0.023	0.997	0.005	1.697	0.020				
H2A Bulk	0.989	0.010	2.547	0.025	0.887	0.009	0.747	0.012	1.192	0.006	0.843	0.010	22	12	1.69	0.14
H2A HCl R	0.719	0.007	2.837	0.028	0.734	0.007	0.949	0.015	1.005	0.005	1.292	0.016				
H2A HCl L	0.393	0.004	0.411	0.004	1.411	0.014	0.484	0.008	1.483	0.007	0.343	0.004				
H2A Bulk	0.989	0.010	2.547	0.025	0.887	0.009	0.747	0.012	1.192	0.006	0.843	0.010	18	22	1.77	0.27
H2A AcOH R	0.692	0.007	2.052	0.021	0.945	0.009	0.916	0.015	1.015	0.005	0.970	0.012				
H2A AcOH L	0.352	0.004	0.343	0.003	1.473	0.015	0.470	0.008	1.500	0.007	0.319	0.004				
H2C Bulk	1.421	0.014	1.849	0.018	1.188	0.012	0.506	0.008	1.365	0.007	0.426	0.005	12.42	0.45	1.5994	0.0079
H2C HCl R	0.488	0.005	1.390	0.014	0.953	0.010	0.889	0.014	1.120	0.006	0.932	0.011				
H2C HCl L	0.900	0.009	0.360	0.004	2.080	0.021	0.273	0.004	1.516	0.008	0.131	0.002				
H2C Bulk	1.421	0.014	1.849	0.018	1.188	0.012	0.506	0.008	1.365	0.007	0.426	0.005	8.1	6.8	1.6	0.14

H2C AcOH R	0.729	0.007	1.688	0.017	1.223	0.012	0.926	0.015	1.133	0.006	0.758	0.009				
H2C AcOH L	0.352	0.004	0.343	0.003	1.473	0.015	0.231	0.004	1.515	0.008	0.113	0.001				
H3A Bulk	2.068	0.021	2.394	0.024	2.636	0.026	0.999	0.016	1.016	0.005	0.379	0.005	507	2400	1.9	5.8
H3A HCl R	1.026	0.010	1.706	0.017	1.679	0.017	0.914	0.015	0.955	0.005	0.544	0.007				
H3A HCl L	0.920	0.009	0.805	0.008	3.826	0.038	1.096	0.018	1.080	0.005	0.287	0.003				
H3A Bulk	2.068	0.021	2.394	0.024	2.636	0.026	0.999	0.016	1.016	0.005	0.379	0.005	448	940	1.5	1.4
H3A AcOH R	1.203	0.012	1.833	0.018	1.917	0.019	0.956	0.015	0.987	0.005	0.499	0.006				
H3A AcOH L	0.831	0.008	0.571	0.006	4.838	0.048	1.088	0.017	1.080	0.005	0.225	0.003				
H3C Bulk	1.667	0.017	2.864	0.017	1.738	0.017	0.978	0.016	0.980	0.005	0.562	0.007	305	460	2.6	2.1
H3C HCl R	0.884	0.009	1.647	0.017	1.447	0.014	0.882	0.014	0.884	0.004	0.610	0.007				
H3C HCl L	0.771	0.008	1.065	0.017	2.480	0.025	1.122	0.018	1.094	0.005	0.452	0.005				
H3C Bulk	1.667	0.017	2.864	0.017	1.738	0.017	0.978	0.016	0.980	0.005	0.562	0.007	68	92	1.26	0.31
H3C AcOH R	0.910	0.009	1.857	0.017	1.348	0.013	0.900	0.014	0.883	0.004	0.668	0.008				
H3C AcOH L	1.154	0.012	0.806	0.017	3.014	0.030	0.689	0.011	1.097	0.005	0.229	0.003				

Table A3: Summary of reliable ages and initial uranium activity ratios used on paleoclimatic interpretation.

Sample	**sample treatment; Sub-sample No.**	**Detrital corrected method**	**Corrected age (ka)**	**$(^{234}U/^{238}U)_0$**
H2C	TDS;1	SS	8.67±0.1	1.35±0.007
H2C	TDS;3	2D_Osmond-type_derived	58±24	1.38±0.09
H2C	L/R;5	2D_Osmond-type_derived	10.9±4.4	1.60±0.02
H2C	L/R;5	3D-osmond-type	10±3.2	1.6±0.064
H2B	TDS;1	SS	5.94±0.07	1.21±0.006
H2B	TDS;3	2D_Osmond-type_derived	56.1±7.5	1.54±0.09
H2A	L/R;5	3D-osmond-type	20±10	1.73±0.12
H3C	TDS;1	SS	131.3±2.9	1.11±0.007
H3C	TDS;3	2D_Osmond-type_derived	194±37	1.21±0.09
H3C	L/R;5	2D_Osmond-type_derived	87±41	1.33±0.1
H3B	TDS;1	SS	145.7±3.6	0.95±0.008
H3A	TDS;1	SS	99.8±1.9	0.99±0.007
H4C	TDS;1	SS	20.59±0.3	1.21±0.006
H4C	TDS;3	2D_Osmond-type_derived	116.2±7.3	1.58±0.05
H4B	TDS;1	SS	71.6±1.1	1.18±0.007
H4A	TDS;1	SS	48.53±0.7	1.15±0.006

Figure A2; U-series 2D Rosholt [(^{230}Th/^{232}Th) and (^{234}U/^{232}Th) vs (^{238}U/^{232}Th)] and Osmond [(^{230}Th/^{238}U) and (^{234}U/^{238}U) vs (^{232}Th/^{238}U)] isochron plots of three coeval samples [all Bulk (blue squares) for caliche samples of the La Mesa Geomorphic surface Jornada Basin

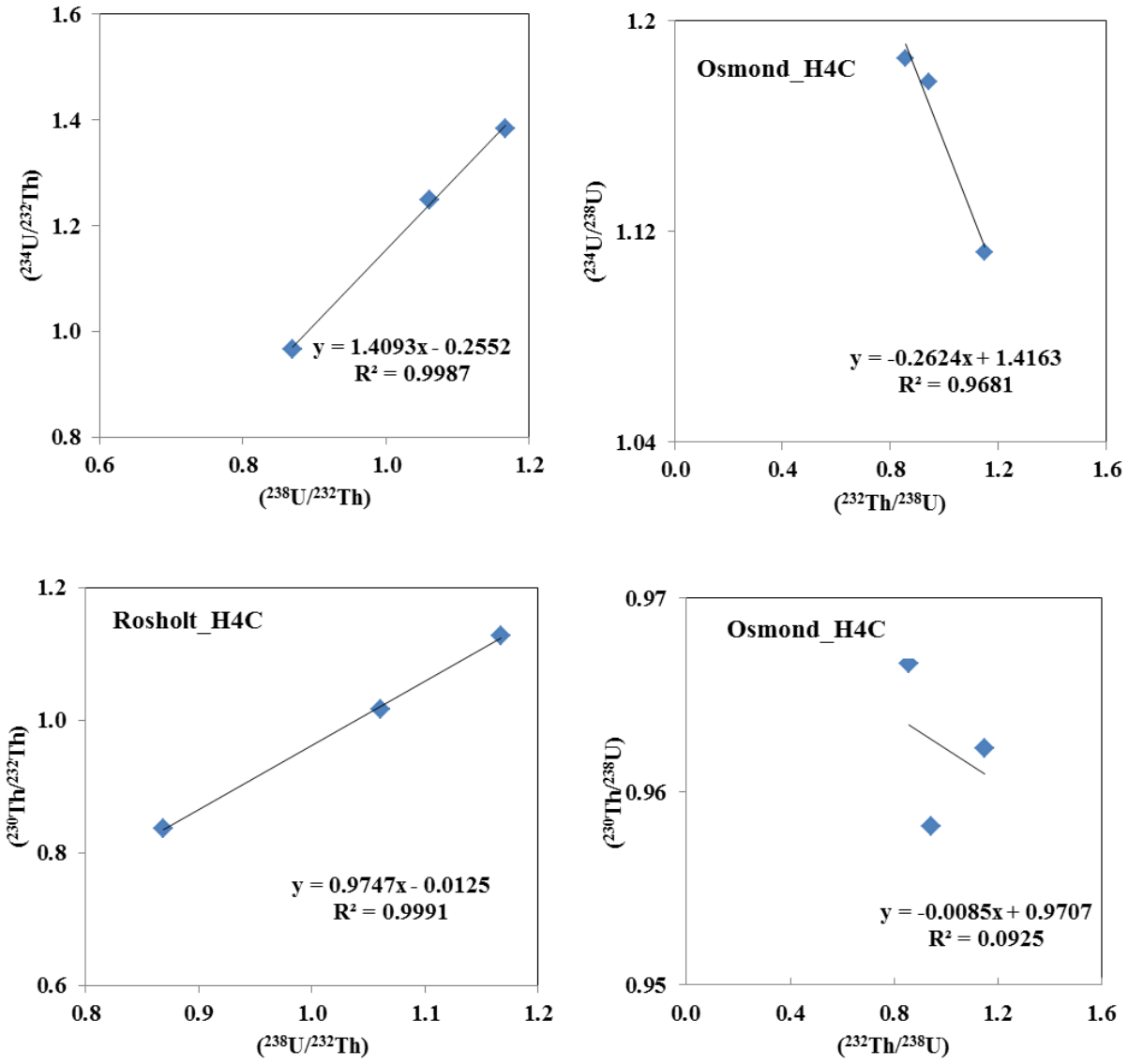

Figure A2 (a): 2D Rosholt and Osmond isochron plots of coeval samples all bulk (blue squares) for the H4C caliche sample

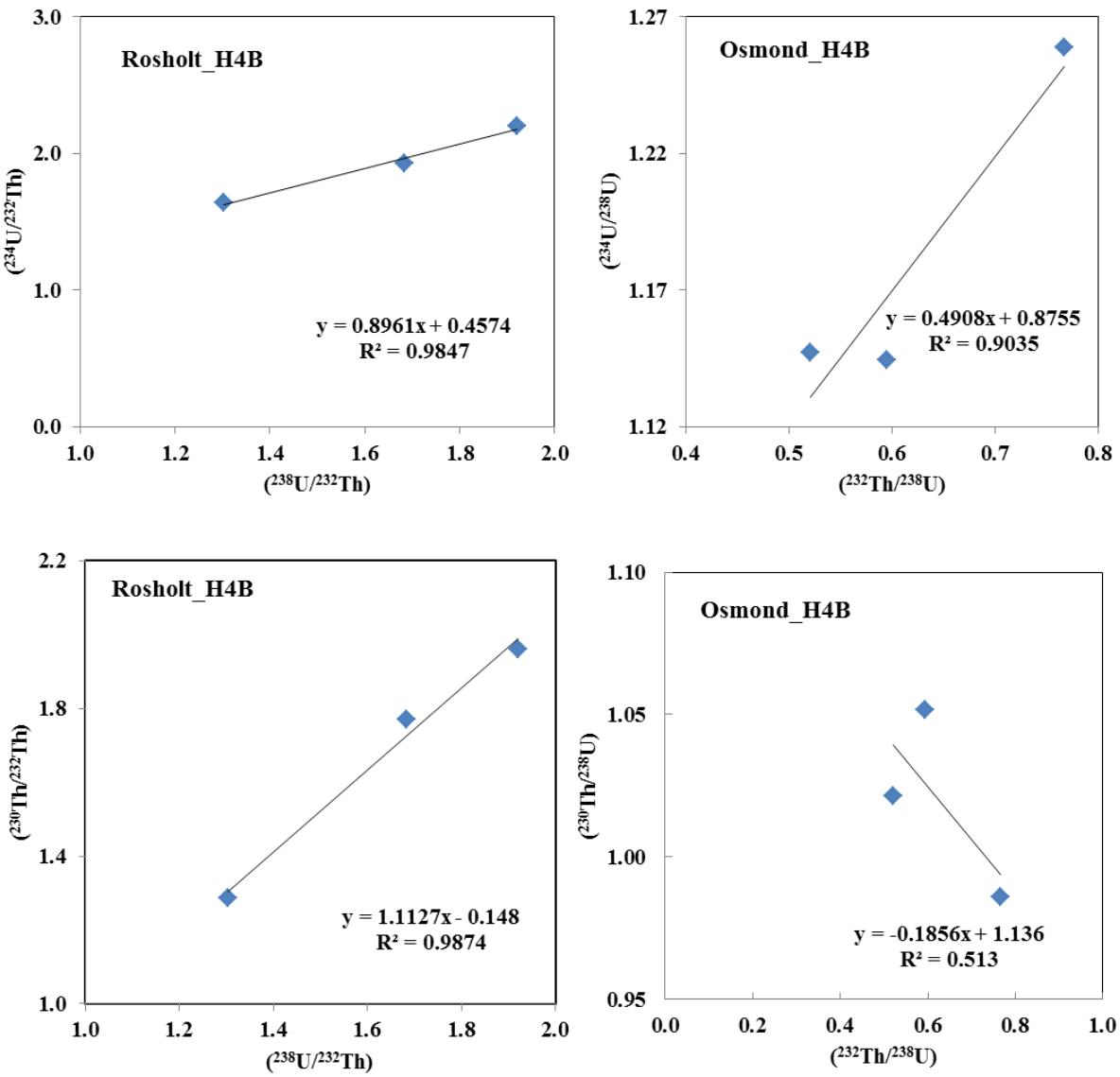

Figure A2 (b): 2D Rosholt and Osmond isochron plots of coeval samples all bulk (blue squares) for the H4B caliche sample

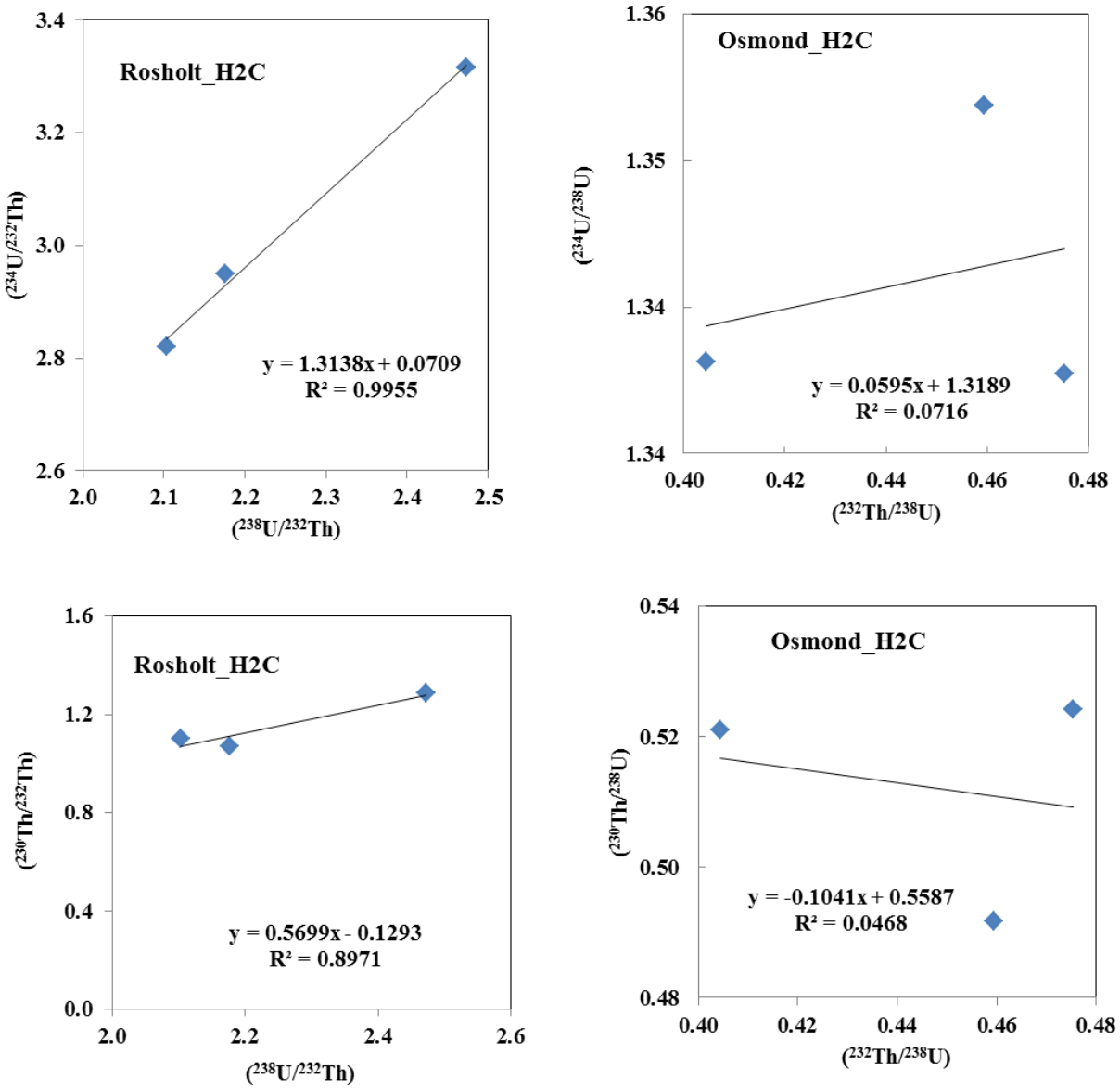

Figure A2 (c): 2D Rosholt and Osmond isochron plots of coeval samples all bulk (blue squares) for the H2C caliche sample

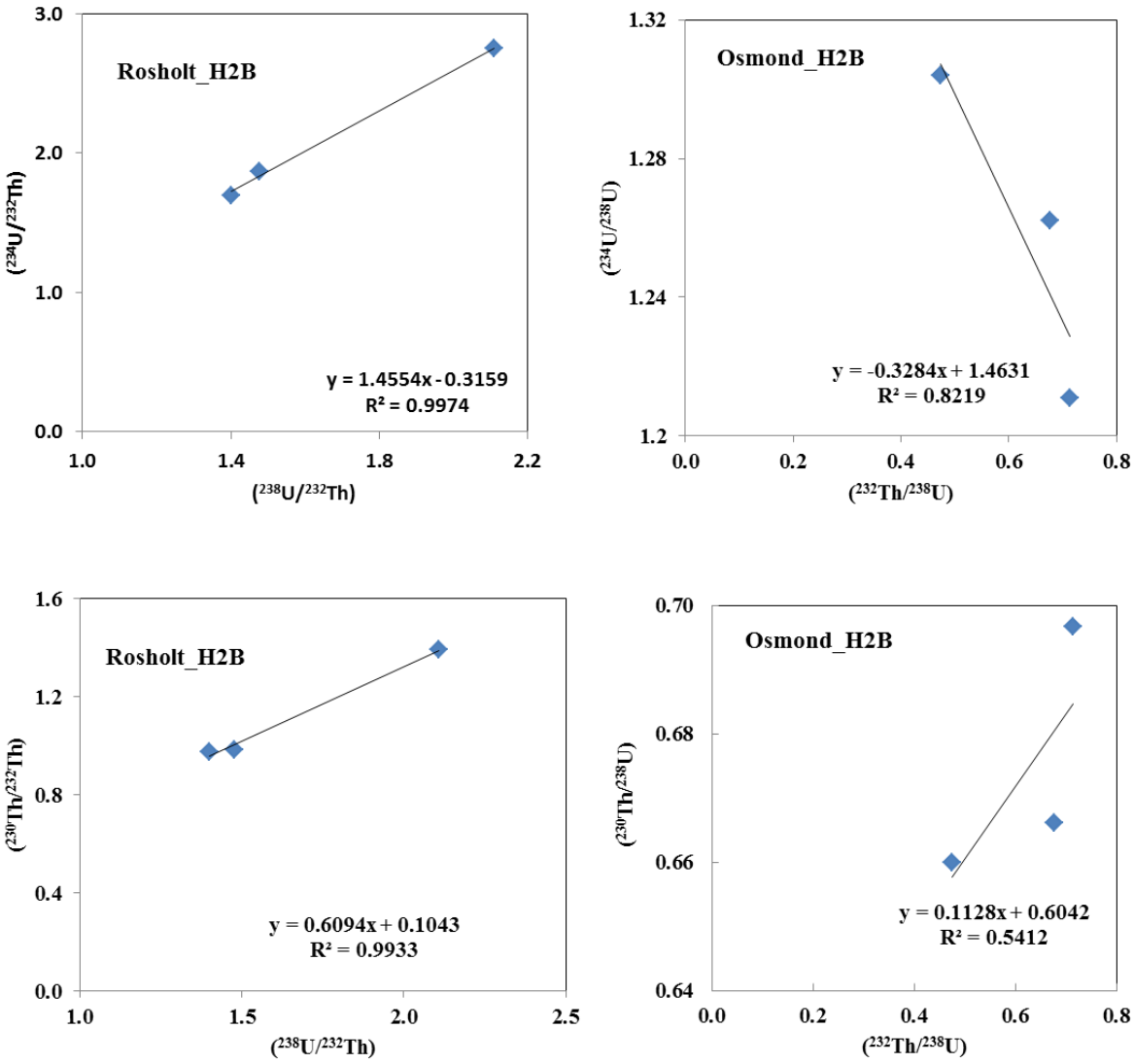

Figure A2 (d): 2D Rosholt and Osmond isochron plots of coeval samples all bulk (blue squares) for the H2B caliche sample

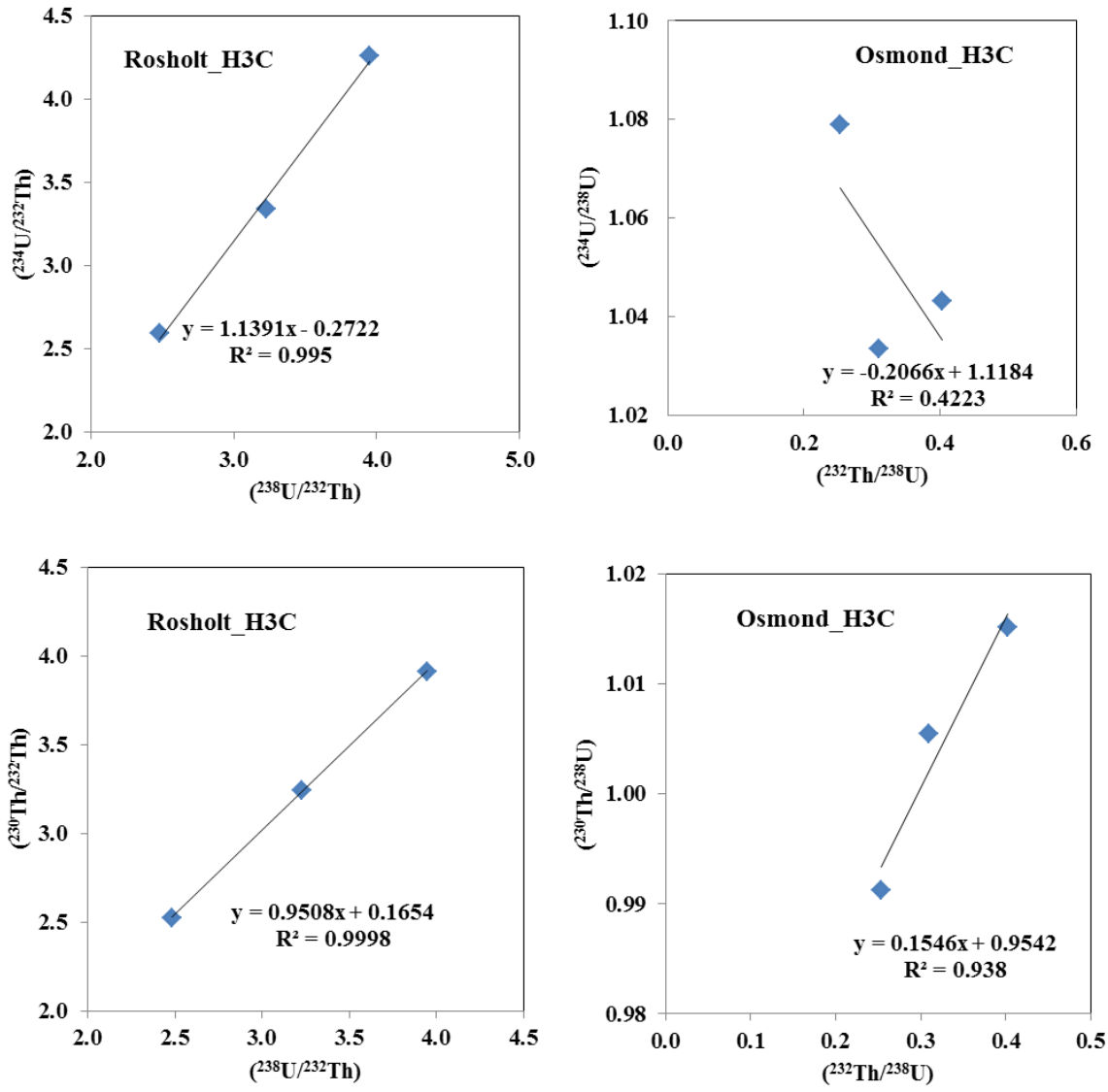

Figure A2 (e): 2D Rosholt and Osmond isochron plots of coeval samples all bulk (blue squares) for the H3C caliche sample

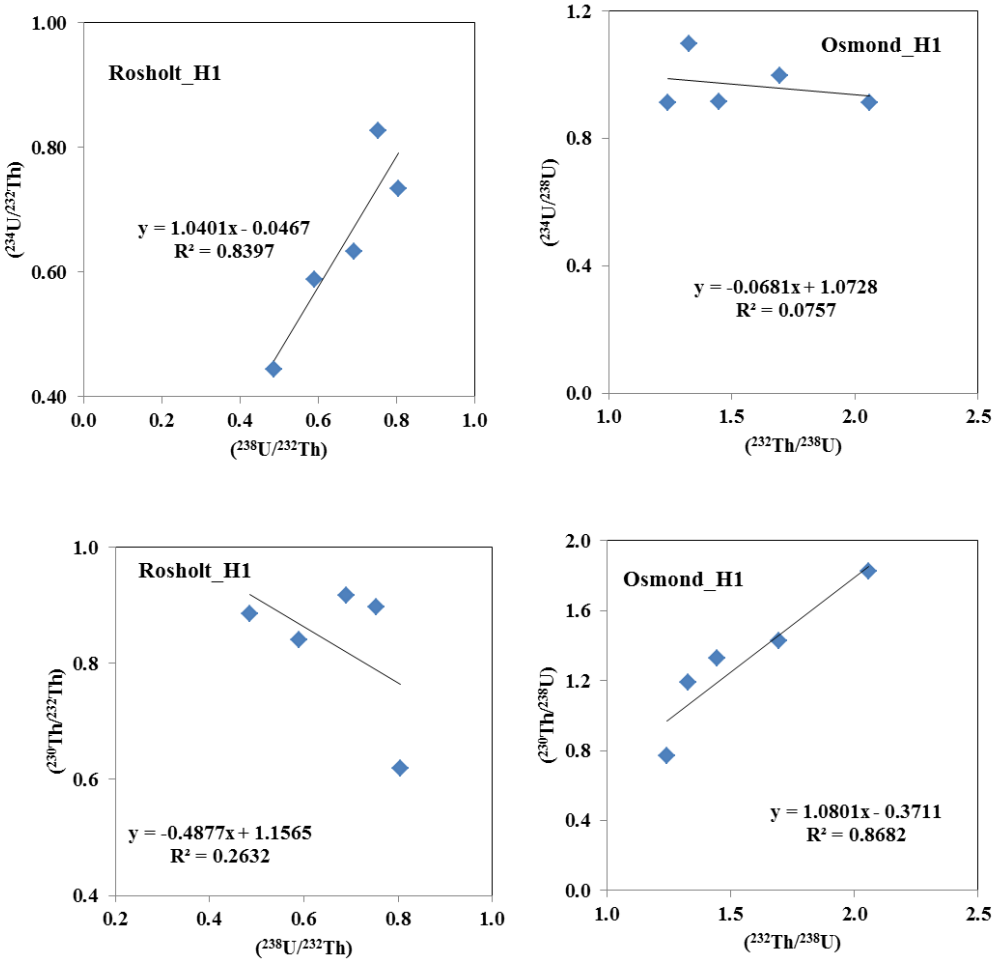

Figure A2 (f); 2D Rosholt and Osmond isochron plots of five coeval samples [Bulk, HCl_R , HCl_L AcOH_R , AcOH_L H1 soil sample

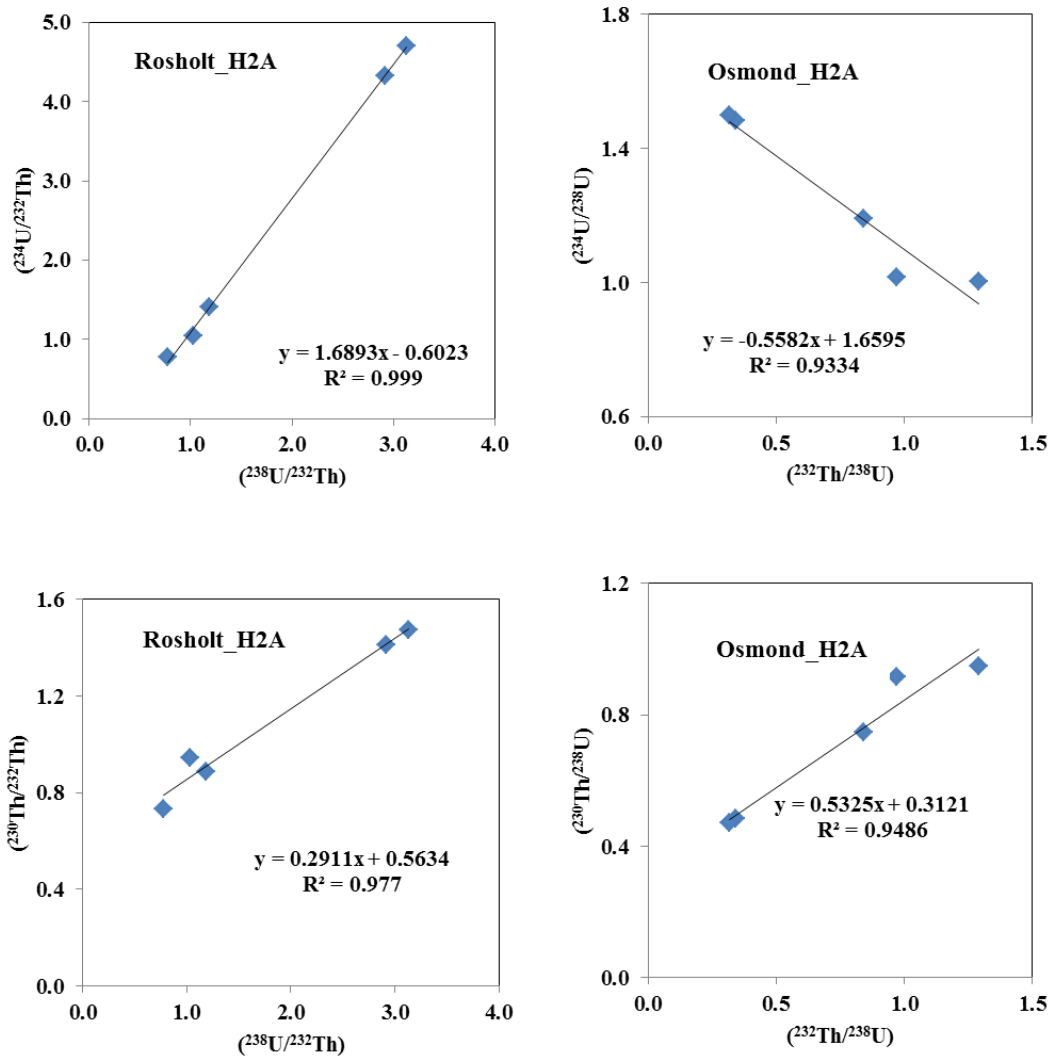

Figure A2 (g); 2D Rosholt and Osmond isochron plots of five coeval samples [Bulk, HCl_R , HCl_L AcOH_R , AcOH_L of H2A caliche sample

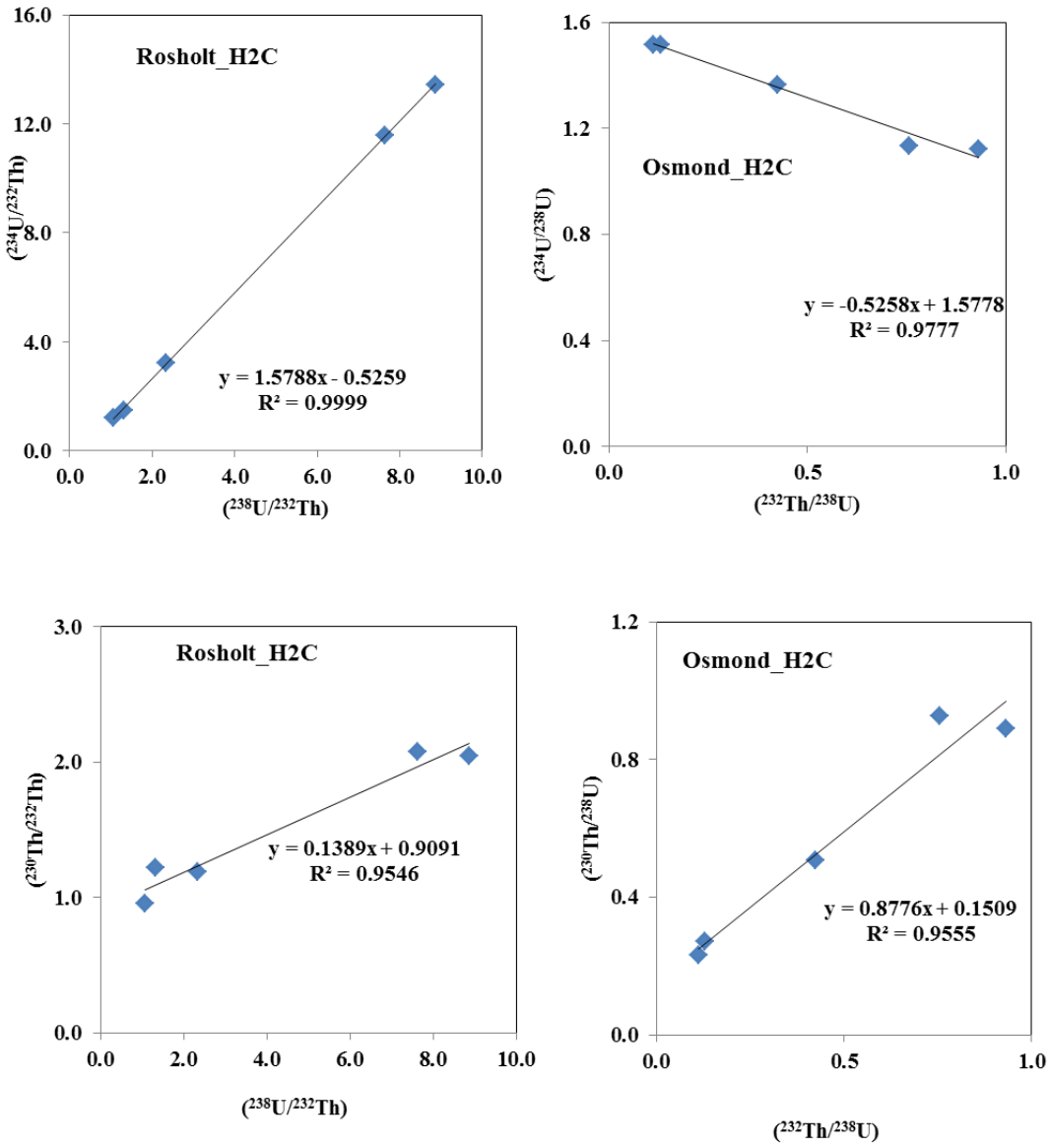

Figure A2 (h); 2D Rosholt and Osmond isochron plots of five coeval samples [Bulk, HCl_R , HCl_L AcOH_R , AcOH_L of H2C caliche sample

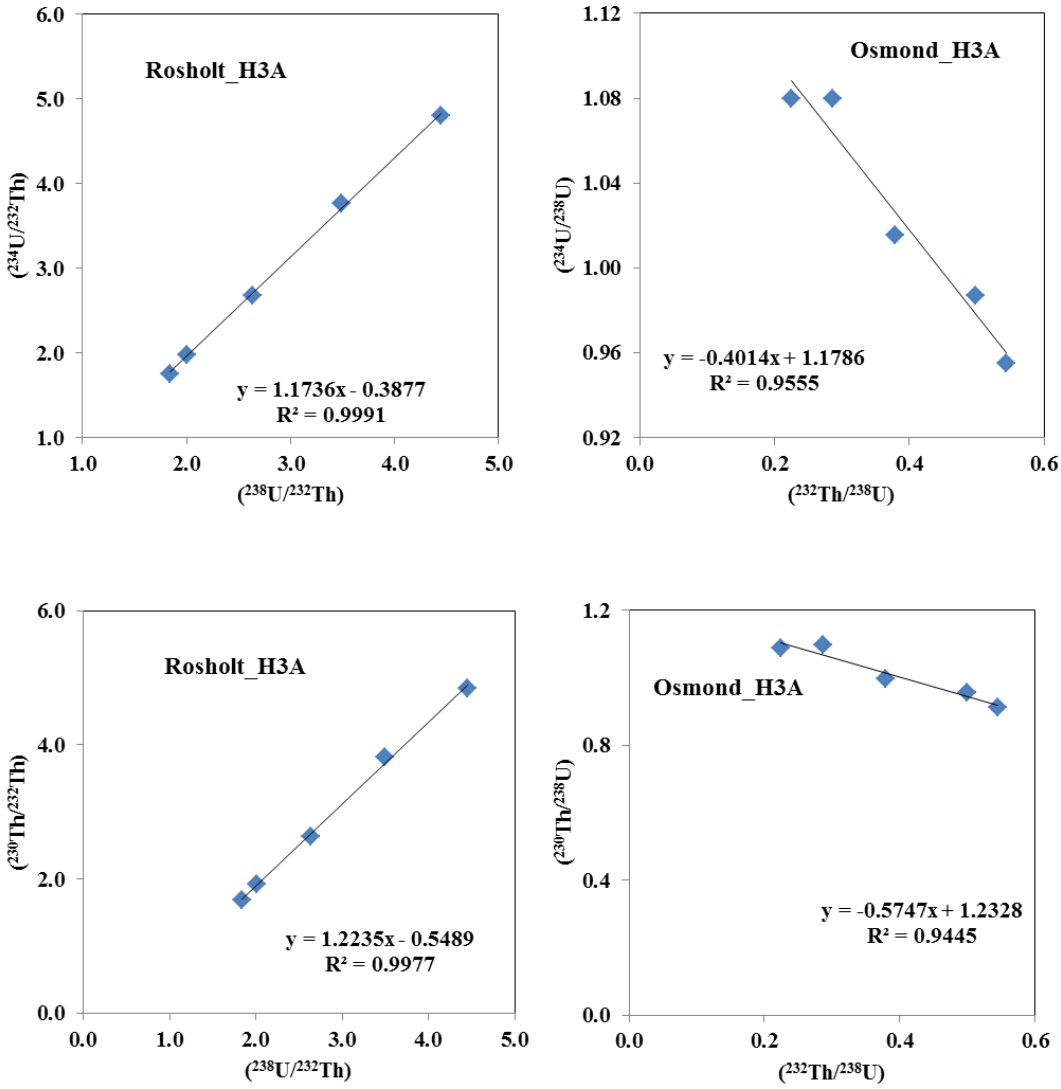

Figure A2 (i); 2D Rosholt and Osmond isochron plots of five coeval samples [Bulk, HCl_R , HCl_L AcOH_R , AcOH_L of H3A caliche sample

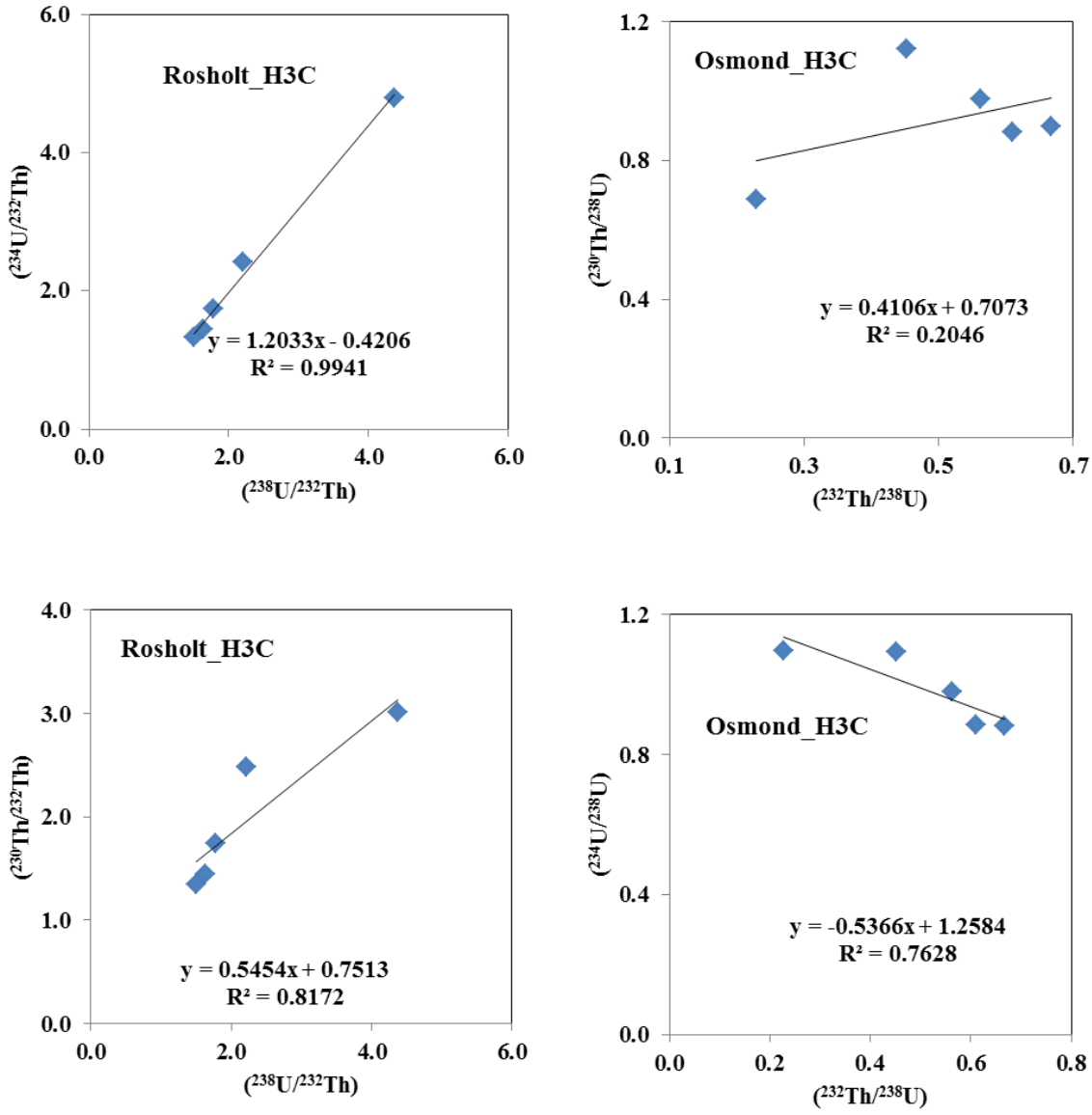

Figure A2 (j); 2D Rosholt and Osmond isochron plots of five coeval samples [Bulk, HCl_R , HCl_L AcOH_R , AcOH_L of H3C caliche sample

Curriculum Vita

Syprose Kemunto Nyachoti is daughter of Justus Nyachoti Menge and Sabina Moraa Nyachoti born in Nyamira, Kenya. She is the first generation to obtain PhD degree in her family. Syprose earned her Bachelor of Science degree in Chemistry in 2005 and Master of Science degree in Chemistry in 2009 from Moi University and Kenyatta University, Kenya respectively. After graduation with a bachelor's degree, she worked as an assistant lecturer in the Chemistry Department at Gusii Institute of Technology, Kisii. In 2007, she enrolled for a master's degree at Kenyatta University before working with the Ministry of Environment, Mines and Geological Department (2008-2010) and the Kenya Plant Health and Inspectorate Services (2010) in Kenya as a chemist. In 2011, she began her doctorate degree at the University of Texas at El Paso, U.S.A.

She has presented her research in several meetings including American Geophysical Union (AGU). She has been the recipient of the Vernon and Joy Hunt, and Hunt and Rowling scholarships. While pursuing her degree, she worked as a Research Associate and Teaching Assistant for the Department of Geological Sciences. She participated in several extracurricular and community outreach activities such as organizing campus visit of first graders, and summer camp training of children between 8 and 14 years at El Paso Botanical Garden in El Paso, TX. She also served as secretary of Society of Exploration Geophysicists (SEG) UTEP chapter in 2013. Her dissertation: *Application of uranium and strontium isotopes as salinity and paleo-environmental conditions tracers: insight from the Rio Grande River and pedogenic carbonates in dryland soils of southwest, USA* was supervised by Dr. Lin Ma.

Permanent address: P.O BOX 254-40202

Keroka, Kenya

This dissertation was typed by Syprose Nyachoti